LARS INFORMATION NOTE 033169

BI-DIRECTIONAL SCATTERING CHARACTERISTICS OF HEALTHY, GREEN SOYBEAN AND CORN LEAVES IN VIVO

HARRY T. BREECE, III
ROGER A. HOLMES

The Laboratory for Applications of Remote Sensing
Purdue University
West Lafayette, Indiana

BI-DIRECTIONAL SCATTERING CHARACTERISTICS OF HEALTHY, GREEN SOYBEAN AND CORN LEAVES IN VIVO

Harry T. Breece, III
Roger A. Holmes

TR-EE 69-11

April, 1969

LARS Information Note 033169

School of Electrical Engineering
Purdue University
Lafayette, Indiana 47907

Sponsored by NASA Grant No. NGR 15-005-028
U.S. Department of Agriculture Contracts 12-14-100-8307(20), 12-14-100-8926(20), 12-14-100-9502(20), and 12-14-100-9549(20)
Purdue University Laboratory for Agricultural Remote Sensing
Joint Services Electronics Program, N00014-67-A-0226

TABLE OF CONTENTS

page

LIST OF TABLES

LIST OF FIGURES

Figure | Page

Figure

Figure | Page

Figure | Page

Figure | Page

Figure Page

Figure

Figure

Page

Figure

Page

ABSTRACT

Measurements were made to determine the bi-directional scattering characteristics of living, green soybean and corn leaves in the range from 375 nm to 1μm.

A goniometer was constructed to study bi-directional scattering on the leaves of potted soybean and corn plants. The leaf sample was held in a plane and light of a selected wavelength was incident at a given angle. A detector was then moved around the sample at a constant radius resulting in a polar plot of scattered radiant power as a function of observation angle for a given angle of incidence and wavelength.

The results show strong specular components of reflection in addition to diffuse components for both soybean and corn leaves. Both soybean and corn leaves have a diffuse transmission component along with a definite refractive component.

The results describe a simple four layer bi-directional scattering model for a soybean leaf. This model has a rough surface with isotropy relative to the midvein.

The results for a corn leaf describe a simple three layer bi-directional scattering model. This model has a rough surface with a definite anisotropy relative to the midvein.

The results are two-dimensional polar graphs. Measurements were carried out which indicate the extension of these results to three dimensions.

INTRODUCTION

This work consists of experiments performed on living, healthy, normal soybean and corn leaves in order to investigate their bi-directional radiation scattering characteristics in the visible and near infrared wavelength ranges.

A green leaf surface is illuminated with a monochromatic beam of light and the reflected and transmitted radiation is collected at various locations around the leaf by means of a detector.

This bi-directional scattering characteristic suggests a mathematical scattering model for the living soybean leaves and living corn leaves.

Corn and soybeans were investigated because of their agricultural value and because of the structural differences between the two leaves. The glossy surface corn leaf with a surface parallel groove structure and the mat surface soybean leaf with a fan-out surface appearance, they also have cell layer structure differences.

PREVIOUS RESEARCH

Early Green Leaf Bi-Directional Scattering Measurements

Research in the field of bi-directional leaf scattering has been extremely limited. The work done in this area was usually a small part of a project concerned with green leaf absorption characteristics and photosynthesis. This small amount of work is probably due to the fact that studies of absorption and photosynthesis usually deal with chlorophyll extracts in solution, rather than the living plant leaf. That is, the green leaf is physically chopped into small pieces and chemically separated into the desired components.

In 1933, Seybold [10] used two methods to study bi-directional leaf scattering. The first method was a photographic technique where he used normal incidence at 540 nm with a strip of film formed in a circle around the irradiated leaf sample. The density reading for the exposed film results in a bi-directional scattering plot. Results are given for Fiscus elastica, Sagittaria montevedensis, Tropaeolum majus and Prunus laurocerasus leaves. Both diffuse and specular components of reflection are shown. The transmission characteristic has both diffuse and refracted components.

In Seybold's second method a photoelectric detector was mounted so that it could be moved in a circle around the irradiated leaf sample. Normal incidence at about 540 nm was used. Results are given for Aesculus Hippocastanum, Pelargonium zonale, Fiscus elastica, Prunus laurocerasus and Tussilago Farfara leaves. The results show specular and diffuse reflection components. The transmission curve has both diffuse and refracted components.

Dinger [5] in 1941, used an RCA 929 phototube detector to measure bi-directional leaf reflection and transmission for Fiscus elastica, maize, pansy and coleus leaves. He used normal incidence and an unknown wavelength. The Fiscus elastica leaf had an appreciable amount of specular reflection for top normal incidence but the bottom normal incidence reflection was nearly diffuse. The transmission was nearly diffuse for the Fiscus elastica leaf.

The reflection from the top and bottom surfaces of the maize, pansy and coleus leaves for normal incidence approached a diffuse scattering characteristic. The transmission curves for the maize, pansy and coleus leaves at normal incidence had a directional refractive characteristic along with a diffuse component.

Dinger's work was concerned with leaf radiation absorption properties and he worked with chlorophyll solutions and leaf extracts as well as plant leaves. He concluded that in a study of leaf absorption of light the leaf structure cannot be ignored.

In 1960, Shul'gin [11] did work on bi-directional reflection for normal incidence and a wavelength band from 400 nm to 600 nm determined by means of a filter. He assumed axial symmetry about a normal to the leaf surface. Results are given for eight leaves with a xeromorphic structure, nine succulent leaves and nine leaves of mesophytes. For the different leaves studied for normal incidence a general conclusion is that reflection of radiant energy from leaves does not obey Lambert's law for diffuse reflection.

In 1961, Shul'gin [12] experimented on bi-directional reflection for angles of incidence of 20°, 45° and 60° and a source assumed to be in the band from 400 nm to 600 nm as in his previous work. The apparatus

was a goniophotometer employing a plane-polarized light source. Shul'gin assumed axial symmetry about a normal to the leaf surface. Reflection curves for incidence angles of 20°, 45°, and 60° are given for Cineraria hybrida and Gesneria cardinalis leaves, which are mesophytes, and for Laurocerrasus officinalis and Camellia japonica leaves, which are xeromorphic leaves of evergreens. The reflection results for these four leaves show a strong specular reflection component which increases with increasing angle of incidence.

Some literature on hemispherical reflectance and transmittance using an intact leaf or sample cut from a leaf is available. This work uses the integrating sphere spectrophotometer; the reflectance is not bi-directional but is an integration of the total scattering from a sample surface at nearly normal incidence. These data are sources for absorption properties of green leaves. Gates, et. al. [7] have given a good summary of the work done in the field of the spectral properties of plants. They present a brief discussion of leaf morphology and then discuss past and present spectral measurements.

Coulson [4] reports on experiments with green grass turf and the degree of polarization for this sample as a function of angle for several wavelengths in the visible and near infrared. This work, however, is not a single leaf study but is done for an area of turf containing many blades of grass at various angles with respect to the incident beam.

In 1968, the Laboratory for Agricultural Remote Sensing at Purdue University [9] reported a statistical experiment carried out with soybean leaves and corn leaves. A Beckman DK-2A integrating sphere spectroreflectometer was used to measure reflectance on leaves from

three periods during the growing season. These periods were early in the growing season, middle of the growing season and late in the growing season. Spectra were taken over the range from 0.5 μm to 2.6 μm. The experiment studied a 50 mm^2 square area not including the midvein.

Table 1 gives the results of this statistical soybean leaf experiment for the range of wavelengths which are of interest to the bi-directional scattering experiment. The table gives the mean percent reflectance and standard deviation for each wavelength. The results for normal incidence on the integrating sphere instrument show that the mean reflectance is almost the same for the early and middle periods. The standard deviations are almost the same for the early and middle periods for all wavelengths. The mean reflectance is greater for the late period than for the two earlier periods. The standard deviations for the late period are also much larger than those for the two earlier periods. During the late period the leaves are browning and beginning to shed while in the early and middle periods the leaves are green. These results on soybean leaf reflectance indicate that scattering experiments conducted during the early and middle periods of the growing season can be expected to have consistent results from leaf to leaf.

Table 2 gives the results of the statistical corn leaf experiment for much of the range of wavelengths which are of interest to the bi-directional scattering experiment. The table gives the mean percent reflectance and standard deviation for each wavelength. The results for normal incidence on the integrating sphere instrument show that the mean reflectance is almost the same for the early and middle periods. The standard deviations are almost the same for the early and middle periods. The mean reflectance is greater for the late period than for the two

SOYBEAN SAMPLES

Wavelength μm	Early 45 Samples Mean Percent Reflectance	Stand. Dev.	Middle 108 Samples Mean Percent Reflectance	Stand. Dev.	Late 97 Samples Mean Percent Reflectance	Stand. Dev.
0.51	11.9	0.8	11.0	0.8	17.3	4.8
0.53	13.3	1.1	12.1	0.9	23.2	6.9
0.55	12.8	1.0	11.7	0.9	25.5	8.7
0.57	11.4	0.7	10.4	0.8	26.0	10.7
0.59	10.0	0.6	9.3	0.7	26.4	12.3
0.61	9.1	0.4	8.5	0.7	26.6	13.6
0.63	8.5	0.3	8.0	0.7	26.5	14.6
0.65	8.6	0.4	8.1	0.6	25.1	15.4
0.67	11.7	0.8	10.9	0.8	26.6	15.5
0.69	20.1	1.2	19.3	1.1	36.2	12.2
0.71	32.5	1.6	32.0	1.3	45.9	5.9
0.73	43.2	1.8	43.3	1.5	50.9	3.7
0.75	49.1	1.7	45.3	1.5	52.8	3.8
0.77	51.3	1.6	51.6	1.6	53.7	3.6
0.79	51.7	1.5	52.1	1.6	54.3	3.3
0.81	51.8	1.5	52.2	1.6	54.6	3.2
0.83	51.8	1.6	52.2	1.7	54.9	3.1
0.85	51.8	1.5	52.3	1.7	55.3	3.1
0.87	51.8	1.5	52.3	1.7	55.6	3.0
0.89	51.7	1.5	52.3	1.7	55.9	3.1
0.91	51.6	1.5	52.2	1.7	56.1	3.2
0.93	51.3	1.5	52.0	1.7	56.1	3.4
0.95	51.1	1.5	51.7	1.7	56.0	3.6
0.97	51.1	1.5	51.7	1.7	56.2	3.7
0.99	51.2	1.5	51.8	1.7	56.5	3.8
1.01	51.3	1.5	52.0	1.7	56.8	3.8
1.03	51.4	1.6	52.2	1.7	56.8	4.6
1.05	51.4	1.6	52.3	1.8	57.1	3.9

TABLE 1. SOYBEAN LEAF REFLECTANCE [9]

CORN SAMPLES

Wavelength μm	Early 172 Samples Mean Percent Reflectance	Stand. Dev.	Middle 184 Samples Mean Percent Reflectance	Stand. Dev.	Late 108 Samples Mean Percent Reflectance	Stand. Dev.
0.51	13.5	1.1	13.5	1.3	17.0	5.3
0.53	15.0	1.2	14.9	1.5	20.6	5.4
0.55	14.7	1.2	14.4	1.4	21.1	6.3
0.57	13.3	1.1	12.9	1.3	19.5	7.4
0.59	11.9	1.0	11.6	1.1	18.3	8.5
0.61	10.9	0.9	10.6	1.0	17.4	9.4
0.63	10.1	0.8	9.8	0.8	16.5	10.3
0.65	10.1	0.8	9.6	0.7	14.9	11.3
0.67	12.3	1.1	12.0	1.0	15.7	11.7
0.69	19.2	1.3	19.2	1.6	24.8	10.4
0.71	29.5	1.3	30.0	2.0	37.7	7.4
0.73	39.0	1.3	39.8	2.1	46.6	4.7
0.75	44.8	1.2	45.1	2.1	49.9	4.0
0.77	47.2	1.3	47.1	2.0	50.8	4.2
0.79	47.7	1.4	47.5	2.0	51.1	4.3
0.81	47.8	1.4	47.5	2.0	51.3	4.5
0.83	47.8	1.4	47.5	2.0	51.4	4.6
0.85	48.0	3.8	47.5	2.0	51.6	4.8
0.87	47.7	1.4	47.4	2.0	51.6	4.8
0.89	47.6	1.4	47.4	2.0	51.7	4.9
0.91	47.3	1.4	47.2	2.0	51.7	4.9
0.93	47.0	1.4	46.9	2.0	51.4	4.9
0.95	46.9	3.4	46.6	1.9	51.1	5.0
0.97	46.6	1.4	46.5	1.9	51.0	5.2
0.99	46.7	1.4	46.7	1.9	51.4	5.1
1.01	47.0	1.4	46.9	2.0	51.2	5.1
1.03	47.1	1.4	47.0	2.0	51.8	5.1
1.05	47.1	1.4	47.0	1.9	51.8	5.0

TABLE 2. CORN LEAF REFLECTANCE [9]

earlier periods at all wavelengths. The standard deviations for the late period are also much larger than those for the two earlier periods. During the late period the leaves are beginning to turn brown while in the early and middle periods the leaves are green. These results on corn leaf reflectance indicate that scattering experiments conducted during the early and middle periods of the growing season can be expected to have consistent results from leaf to leaf.

Feasibility Study

Preliminary experiments were performed in order to establish basic trends of the bi-directional scattering data and expected levels of signal and noise. These experiments provided the necessary experience in goniometric problems to design a permanent scattering facility. Leaves on tobacco, philodendron and salal plants were used in this feasibility study because of the structural differences among these leaves and the good adaptation of these plants to life in the laboratory.

In the first experiment, a tungsten lamp source was used. The incident light was focused onto the top surface of the green leaf sample and the scattered radiation was measured at various angles around the leaf sample in the principal plane with the distance from the illuminated area to the detector remaining constant. The detector employed was an RCA 7102 photomultiplier tube (S-1 response). This was not a spectral experiment but contained wavelengths in the 400 nm to 1.1 μm range as determined by the S-1 photomultiplier tube response and the tungsten lamp characteristic. Figure 1A shows the bi-directional scattering for a salal leaf for an incidence angle of 60° from the normal to the sample

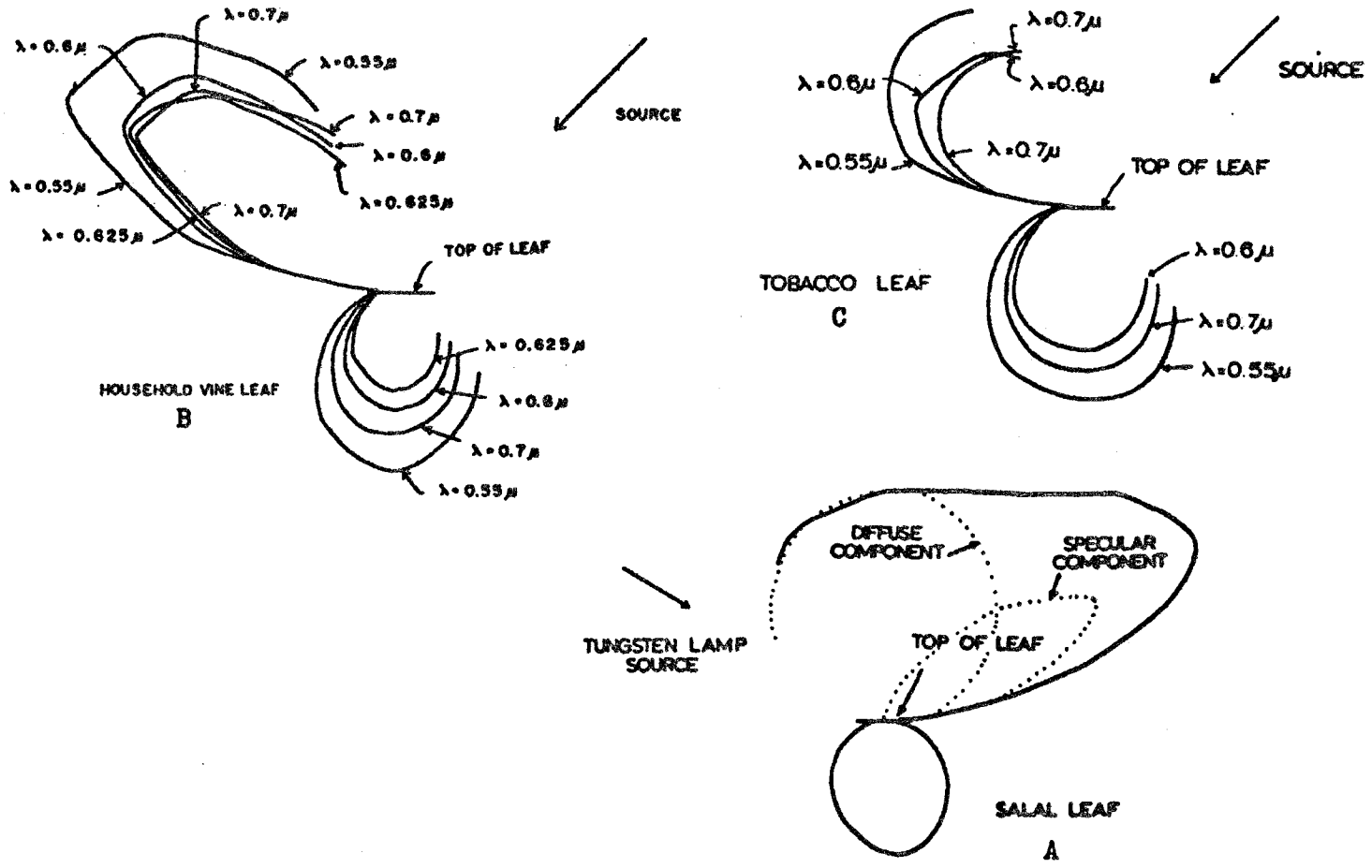

Figure 1. Feasibility Experiment Results.

plane and top incidence for the tungsten lamp source. The transmission characteristic is diffuse in nature but has an additional directional refractive character. The reflection characteristic has both specular and diffuse components. This curve is presented to show the functional forms of these characteristics.

A second experiment was performed much the same as the first, except that a monochromatic source was used. The responsivity of the entire system without the sample is determined by the product of a tungsten lamp radiance characteristic, the transmission characteristic of a Bausch and Lomb 500 mm monochromator and the sensitivity of an S-1 photo-cathode. The monochromator dispersion was 9.9 nm and had a degree of polarization of 44.2% at 550 nm with the axis of polarization parallel to the exit slit. A sheet polarizer was used to give a source degree of polarization of 97.5% at 550 nm with the polarization axis parallel to the exit slit. Figure 2 is a photograph of the monochromatic source feasibility experiment as seen from behind the detector with a tobacco leaf sample.

A relative calibration of the data in this monochromatic source experiment was obtained in order to compare results for different wavelengths.

The monochromatic source experiment was carried out on both tobacco leaves and household vine (philodendron) leaves. The household vine leaf surface has a glossy appearance while the tobacco leaf surface is more mat-like. Figure 1B shows the bi-directional scattering characteristic for a living household vine leaf with top incidence at 45° from the sample normal for 550 nm, 600 nm, 625 nm and 700 nm. This characteristic shows a strong fairly sharp specular reflection component with

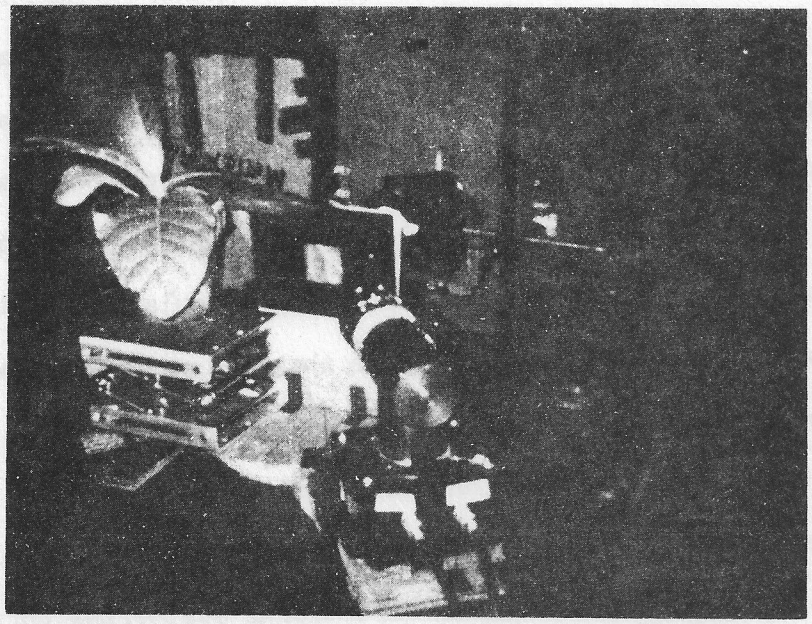

Figure 2. Feasibility Experiment

a near diffuse transmission. The transmission spectrum shows the expected absorption of blue and red by the green leaf sample, while the specular reflection spectrum does not have this high degree of absorption in the blue and red. This indicated a possibility for separating the surface effects from the internal leaf absorption effects, since the reflection curves cross over for angles smaller than the specular angle to show stronger red and blue absorption characteristics again.

Figure 1C shows the bi-directional scattering characteristic for a living tobacco leaf with top incidence at 45° from the sample normal for 550 nm, 600 nm and 700 nm. This characteristic has a large reflection component at the specular angle but has a larger angular spread than the vine leaf. The transmission spectrum shows blue and red absorption. The reflection spectrum at the specular angle does not have this high degree of absorption in the blue and red. The reflection curves cross over for angles smaller than the specular angle to show stronger red and blue absorption characteristics.

These representative results from the feasibility study are presented to show the form of the bi-directional scattering curves for several green leaves.

Limited polarization studies were performed using tobacco leaves and household vine leaves. The incident light was polarized with a degree of polarization of 97.5% with the axis of polarization parallel to the exit slit and parallel to the sample plane. A polarization analyzer was mounted at the detector aperture. The polarization data were taken at 550 nm.

The results show that the degree of polarization is reduced after the radiation is scattered by the green leaf sample, however, the

direction of the axis of polarization remains parallel to the exit slit and parallel to the sample plane.

For the household vine leaf at normal incidence to the top surface, the degree of polarization was reduced from the source value of 97.5% to about 42.8% for transmission along a normal to the sample plane. The degree of polarization was further reduced to 33.3% for a transmission collection angle of 30° from the sample normal. For a 45° angle of incidence to the top surface and a data reflection collection angle of 60° from the leaf normal, the degree of polarization was reduced from the source value of 97.5% to 72%.

For the tobacco leaf at normal incidence, the degree of polarization was reduced from the source value of 97.5% to about 62.2% for transmission along a normal to the sample plane. For a 45° angle of incidence to the top surface and a data reflection collection angle of 60° from the leaf normal, the degree of polarization was reduced from the source value of 97.5% to 60%.

These experiments were performed to establish the character of the bi-directional scattering results and the feasibility of bi-directional leaf scattering studies in vivo. The general character of the reflection measurements is a diffuse component and a specular component. The transmission curves have primarily a diffuse character with a slight amount of refraction. The specular reflection is at least partially a surface effect indicating a possible top incidence green leaf mathematical scattering model of two layers; the first layer contributes specular reflection and refraction, and the second layer gives both diffuse transmission and diffuse reflection. It will be shown later in the thesis

that three or four layer models are necessary to describe leaf studies using both top and bottom incidence.

These experiments provided information about source intensities and physical dimensions necessary to have the sufficient sensitivity to ensure adequate signal-to-noise ratio over the wavelengths considered. Experience was gained in physical layout design to minimize the effect of stray light. The experiments also gave information as to the nature of the data indicating intervals for taking data and data processing as well as a procedure or format for taking the data.

A following section describes the apparatus used for performing bi-directional scattering measurements on living plant leaves.

GONIOMETRY OF RADIATION SCATTERING

In the bi-directional scattering experiment, the leaf sample is held in a plane and light is incident upon this plane illuminating a small area of the leaf. The detector is located at various data collection angles to measure the scattering characteristics. Figure 3 is a description of the coordinate system used in the experiment.

The source and detector are always in the hx plane. The source location in the hx plane is given by θ_{source} which is measured counterclockwise from the +x axis. The detector location in the hx plane is given by $\theta_{detector}$ which is measured clockwise from the +x axis.

The sample is in the hv' plane. The intersection of the sample plane and the plane of the source beam and detector is the h axis. The orientation of the sample plane is designated by the angle θ_{tilt} which is measured counterclockwise in the vx plane. The normal to the sample plane is the x' axis. The angle of incidence is measured relative to the sample normal $\theta_{inc} = f(\theta_{source}, \theta_{tilt})$ and the data collection angle is also measured relative to the sample normal $\theta_{coll} = g(\theta_{detector}, \theta_{tilt})$.

The vast majority of measurements made in this experiment were carried out with $\theta_{tilt} = 0^{\circ}$. Figure 4 shows the coordinate system for this case.

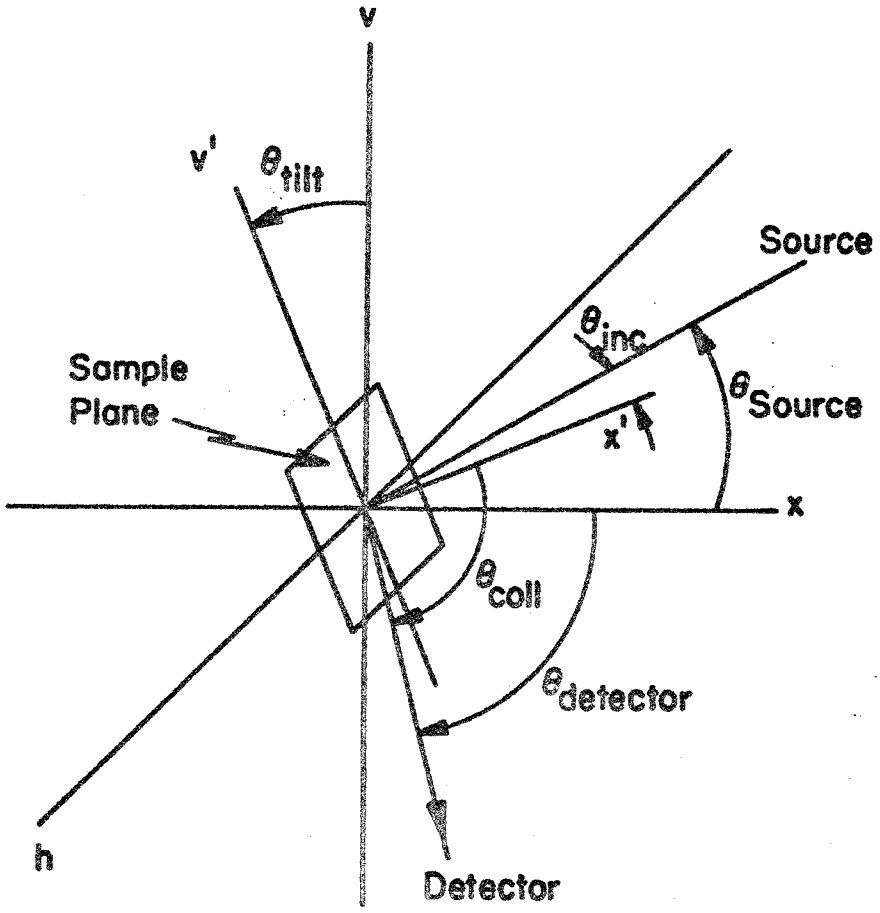

Figure 3. Laboratory Coordinate System for Incident and Scattered Elementary Beams

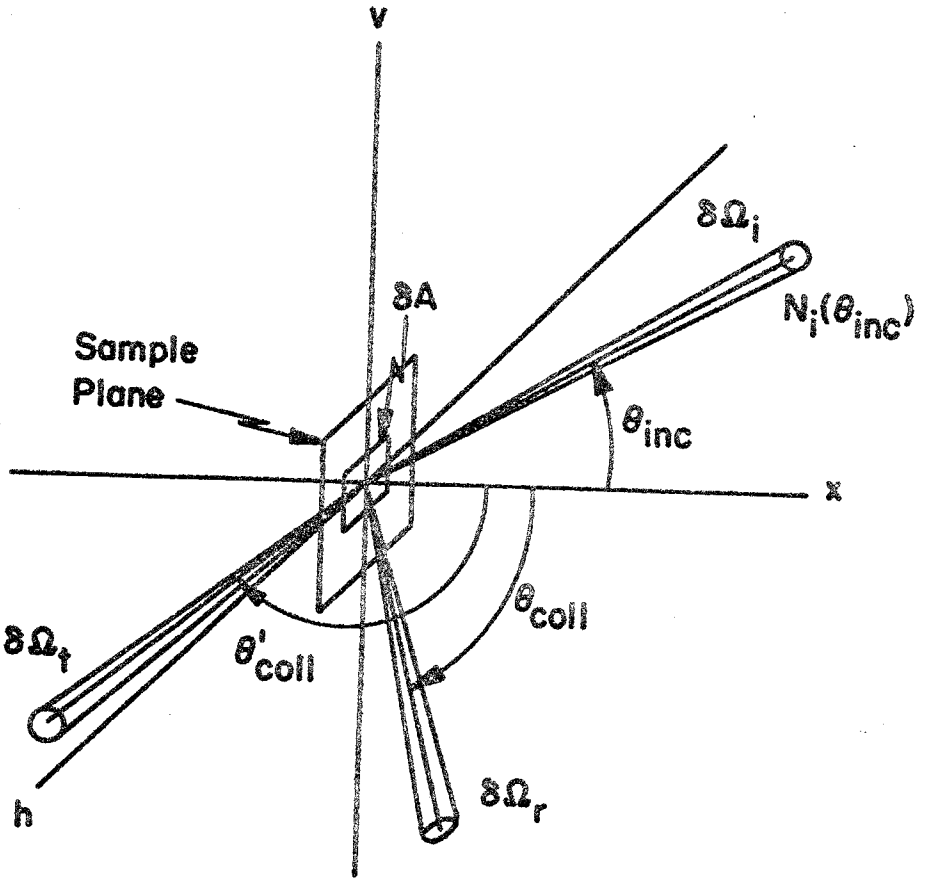

Figure 4. Geometry of Incident and Scattered Elementary Beams for Experimental Scattering Measurements.

Incident Radiant Power

The radiant power incident on a particular element δA of the sample surface through an elementary beam of solid angle $\delta\Omega_i$ from the direction (θ_{inc}) is given by

$$\delta P_i(\theta_{inc}) = N_i(\theta_{inc}) \cos \theta_{inc} \delta A \delta\Omega_i \delta\lambda$$

where $N_i(\theta_{inc})$ is the radiance of the source.

The normal incident beam area is held constant for the experiment.

$$\cos \theta_{inc} \ \delta A = \text{constant}$$

The source parameters $N_i(\theta_{inc})$ and $\delta\Omega_i$ are also constant for any given wavelength increment, $\delta\lambda$.

Thus $\delta P_i(\theta_{inc})$ = constant for a given $\delta\lambda$.

The incident irradiance, $\delta H_i(\theta_{inc})$, however, is not constant for this experiment for a given $\delta\lambda$, as seen from

$$\delta H_i(\theta_{inc}) = N_i(\theta_{inc}) \cos \theta_{inc} \ \delta\Omega_i$$

The incident irradiance is a function of $\cos \theta_{inc}$.

Reflected Radiant Power

The radiance of the surface element, δA, of the leaf sample due to reflection of radiation from this incident elementary beam in the direction of θ_{coll} is proportional to the irradiance of δA,

$$\delta N_r(\theta_{coll}) = \rho'(\theta_{inc}, \theta_{coll}) \delta H_i(\theta_{inc})$$

This equation defines

$$\rho'(\theta_{inc}, \theta_{coll}), \text{ called}$$

the "bi-directional reflection-distribution function" [8].

The reflected radiant power for $\delta\lambda$ is

$$\delta P_r(\theta_{coll}) = \delta N_r(\theta_{coll}) \cos \theta_{coll} \, \delta A \delta \Omega_r \delta\lambda$$

which can be written in terms of the irradiance and bi-directional reflection distribution function as

$$\delta P_r(\theta_{coll}) = \rho'(\theta_{inc}, \theta_{coll}) \delta H_i(\theta_{inc}) \cos \theta_{coll} \, \delta A \delta \Omega_r \delta\lambda$$

Noting further that

$$\delta H_i(\theta_{inc}) \delta A \delta\lambda = \delta P_i(\theta_{inc})$$

the reflected radiant power is

$$\delta P_r(\theta_{coll}) = \rho'(\theta_{inc}, \theta_{coll}) \delta P_i(\theta_{inc}) \cos \theta_{coll} \, \delta \Omega_r$$

The experimental output from the post-detector electronics is a voltage proportional to the power falling on the detector aperture.

A calibration measurement is made before the leaf sample is introduced into the system. For this calibration measurement the incident beam falls directly on the detector aperture. The calibration voltage, E_i, is directly proportional to the incident radiant power for the wavelength interval $\delta\lambda$ and angle of incidence, θ_{inc}.

$$E_i \propto \delta P_i(\theta_{inc})$$

A discussion of the apparatus and procedure in the next chapter gives details on this calibration voltage and the calibration procedure.

The reflection scattering measurement voltage, E_r, is directly proportional to the reflected radiant power for the wavelength interval $\delta\lambda$ and angles θ_{inc} and θ_{coll}.

$$E_r \propto \delta P_r(\theta_{coll})$$

The signal processing circuitry output is proportional to the ratio of the voltage E_r to the voltage E_i. This ratio is proportional to the ratio of the reflected radiant power to the incident radiant power for a given $\delta\lambda$,

$$\frac{E_r}{E_i} = k \frac{\delta P_r}{\delta P_i}$$

The constant k accounts for optical and electronic system responses and calibration aperture size.

This measurement result then is

$$\frac{E_r}{E_i} = k\rho'(\theta_{inc}, \theta_{coll})\cos\theta_{coll}\, \delta\Omega_r$$

The graph of $\frac{E_r}{E_i}$ versus θ_{coll} is a polar plot of $k'\rho'(\theta_{inc}, \theta_{coll})\cos\theta_{coll}$ as a function of data collection angle, θ_{coll}, for a particular incident angle, θ_{inc}, for $\delta\lambda$. The factor $k' = k\delta\Omega_r$ is constant since the solid angle of observation, $\delta\Omega_r$, is constant. This plot describes the bi-directional reflection-distribution function for the sample surface over the interval $\delta\lambda$.

For a Lambertian surface, the bi-directional reflection-distribution function is a constant and the result is proportional to cos θ_{coll}. This is illustrated in Figure 5.

Transmitted Radiant Power

The radiance of the surface element, δA, of the leaf sample due to transmission of radiation from this incident elementary beam in the direction of θ'_{coll} is proportional to the irradiance of δA,

$$\delta N_t(\theta_{coll}) = \tau'(\theta'_{inc}, \theta_{coll})\delta H_i(\theta_{inc})$$

where $\tau'(\theta_{inc}, \theta'_{coll})$, is defined here to be the bi-directional transmission-distribution function.

The sample thickness is small enough to assume $\delta A_{top} = \delta A_{bottom} = \delta A$ so that δA is the same for the transmission analysis as for the reflection analysis. The transmitted radiant power for $\delta\lambda$ is

$$\delta P_t(\theta'_{coll}) = \delta N_t(\theta'_{coll})\cos(\pi - \theta'_{coll})\delta A\delta\Omega_t\delta\lambda$$

which can be written in terms of the irradiance and bi-directional transmission-distribution function as

$$\delta P_t(\theta'_{coll}) = \tau'(\theta_{inc}, \theta'_{coll})\delta H_i(\theta_{inc})\cos(\pi - \theta'_{coll})\delta A\delta\Omega_t\delta\lambda$$

Again,

$$\delta H_i(\theta_{inc})\delta A\delta\lambda = \delta P_i(\theta_{inc})$$

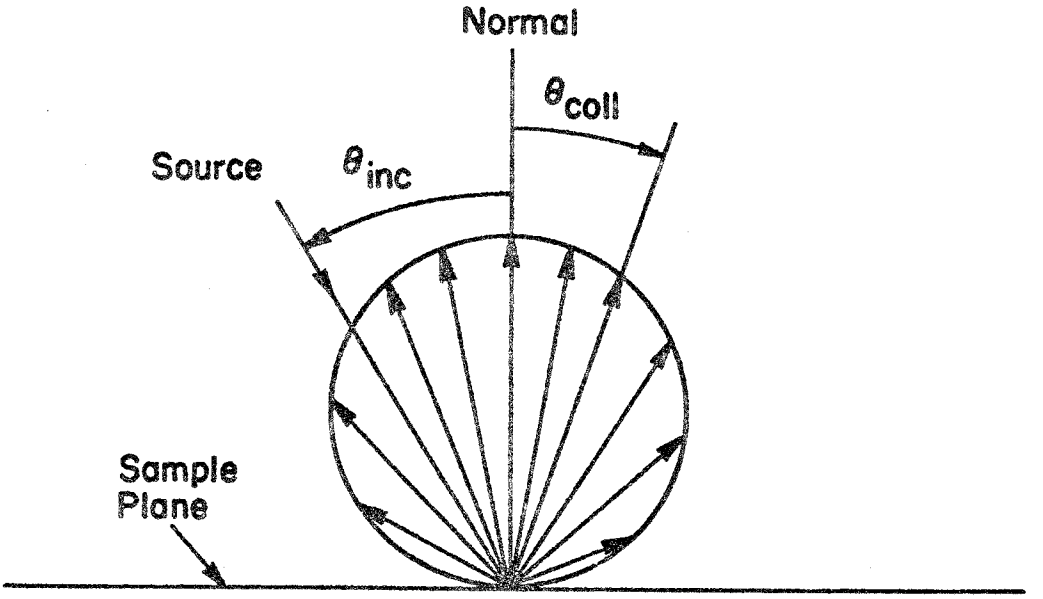

Figure 5. Polar Plot of E_r/E_i for a Lambertian Surface.

so the transmitted radiant power is

$$\delta P_t(\theta'_{coll}) = \tau'(\theta_{inc}, \theta_{coll}) \delta P_i(\theta_{inc}) \cos(\pi - \theta'_{coll}) \delta\Omega_t$$

The experimental output from the post-detector electronics is a voltage proportional to the power falling on the detector aperture.

The calibration voltage, E_i, is the same as described for the reflection measurement.

$$E_i \propto \delta P_i(\theta_{inc})$$

The transmission scattering measurement voltage, E_t, is directly proportional to the transmitted radiant power for the wavelength interval $\delta\lambda$ and angles θ_{inc} and θ'_{coll}.

$$E_t \propto \delta P_t(\theta'_{coll})$$

The signal processing circuitry output is proportional to the ratio of the voltage E_t to the voltage E_i. This ratio is proportional to the ratio of the transmitted radiant power to the incident radiant power.

$$\frac{E_t}{E_i} = k \frac{\delta P_t}{\delta P_i} \quad \text{for } \delta\lambda$$

The constant k accounts for optical and electronic system responses and calibration aperture size and is equal to that used in the reflection discussion.

This measurement result then is

$$\frac{E_t}{E_i} = k\tau'(\theta_{inc}, \theta'_{coll}) \cos(\pi - \theta'_{coll}) \delta\Omega_t$$

The graph of $\frac{E_t}{E_i}$ versus θ_{coll} is a polar plot of

$$k'\tau'(\theta_{inc}, \theta'_{coll})\cos(\pi - \theta'_{coll})$$

as a function of data collection angle, θ'_{coll}, for a particular incident angle, θ_{inc}, for $\delta\lambda$. The factor $k' = k\delta\Omega_t$ is constant since the solid angle of observation, $\delta\Omega_t$, is constant. This plot describes the bi-directional transmission-distribution function for the sample surface over the interval $\delta\lambda$.

The constant k' is the same as that for the reflection analysis since the same detector is used for transmission and reflection measurements and is a constant radius from the sample.

$$\delta\Omega_r = \delta\Omega_t$$

For Lambertian transmission, the bi-directional transmission-distribution function is a constant and the result is proportional to $\cos \theta'_{coll}$. This is illustrated in Figure 6.

The experimental result is proportional to the product of the bi-directional reflection-distribution function and $\cos \theta_{coll}$ or to the product of the bi-directional transmission-distribution function and $\cos(\pi - \theta_{coll})$. This result is composed of many data points each taken over the solid angle $\delta\Omega_r$ and plotted as a function of θ_{coll} for a particular θ_{inc}. Thus the bi-directional scattering plots describe the scattering characteristics of the leaf samples as a function of incidence angle and data collection angle for a particular wavelength interval $\delta\lambda$.

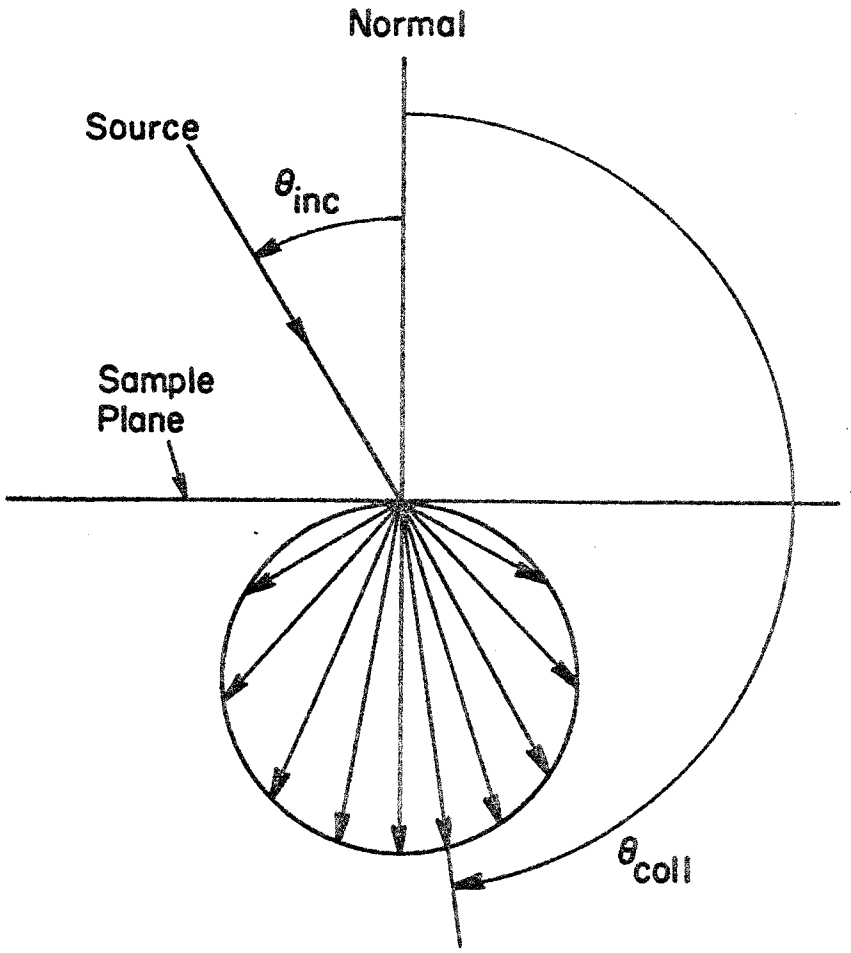

Figure 6. Polar Plot of E_t/E_i for Lambertian Transmission.

The following chapter gives a discussion of the practical details for calibration and scattering measurements and formation of the resultant ratio.

APPARATUS AND PROCEDURE

Optical and Mechanical Apparatus

The green leaf bi-directional scattering measurements are conducted in a dark chamber with monochromatic light impinging upon the leaf through an opening in the chamber wall with the detector located inside the chamber.

The plant stem extends up through an opening in the chamber floor into the chamber and the leaf is held in a sample holder, with the light impinging upon a small portion of it. Various incidence angles are available as well as a 360° trip by the detector around the sample to measure both reflection and transmission.

This arrangement assumes that the detector is measuring scattered light of the same wavelength as the light impinging on the sample. This is acceptable if fluorescence can be neglected. When dissolved in organic solvents, chlorophyll has a red fluorescence. About 25% to 30% of the incident light quanta may return as fluorescence from chlorophyll solutions. However, in the living plant, chlorophyll is only about one-tenth as efficient a fluorescing material as it is in solution [7].

The maximum fluorescence intensity is at a wavelength slightly longer than the red peak of the chlorophyll absorption curve and the fluroescence intensity rapidly falls to zero on the short wavelength side of this peak. On the long wavelength side there is a slowly decreasing tail extending toward the near infrared with a secondary minor maximum at about 730 nm. The amount of light emitted from the

leaf as fluorescence is negligible since it amounts to a few percent at most [7].

Thus the assumption that the detector measures scattered light of the same wavelength as the source is valid.

The leaf sample is held in an approximate plane between two sheets of 1/4" hardware cloth. This permits the leaf to transpire freely and minimizes leaf bruising. Figure 7 shows the sample holder. The hardware cloth is held by an aluminum frame with a 2 13/16" square opening which is fastened to holding posts by rods on ball bearings. This permits tilting of the leaf from the vertical within the restraints of the leaf stem with the angle of tilt indicated on the protractor scale at the left of the sample holder in the photograph of Figure 7.

The sample holder is mounted on a 6 1/2" diameter aluminum cylinder with a 1/2" lip which rests inside a second concentric aluminum cylinder. The second cylinder is a reference cylinder and is stationary with the sample holder cylinder free for manual rotation within to allow various angles of the leaf sample about the axis of the concentric cylinders. Figure 8 shows this arrangement.

The sample holder construction and mounting is such that the center of the illuminated area of the sample is always on the axis of the concentric cylinders. The incident angle is measured counter-clockwise from the normal to the sample surface and is designated θ_{inc}, as shown in Figure 4.

The sample holder hardware cloth is coated with 3-M black velvet flat black paint and the sample holder frame is covered with black velvelour cloth. The mounting cylinder lip is covered with black

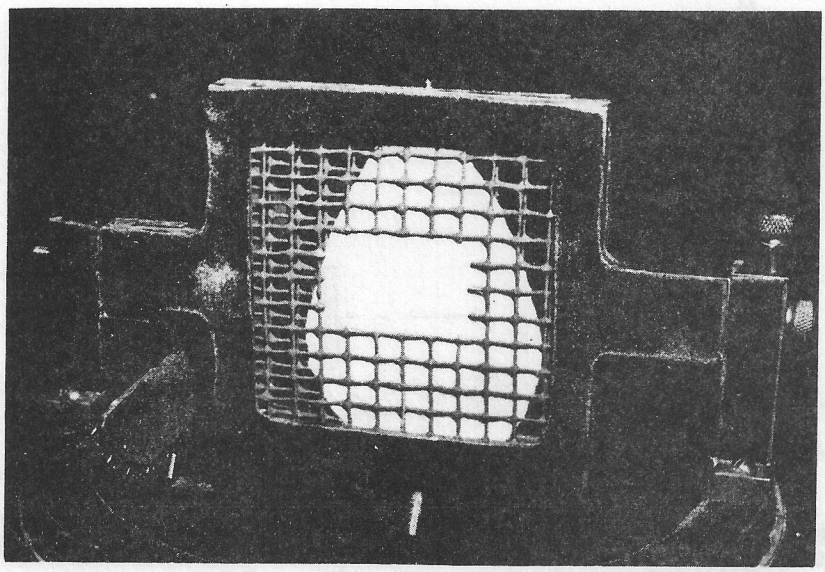

Figure 7. Sample Holder.

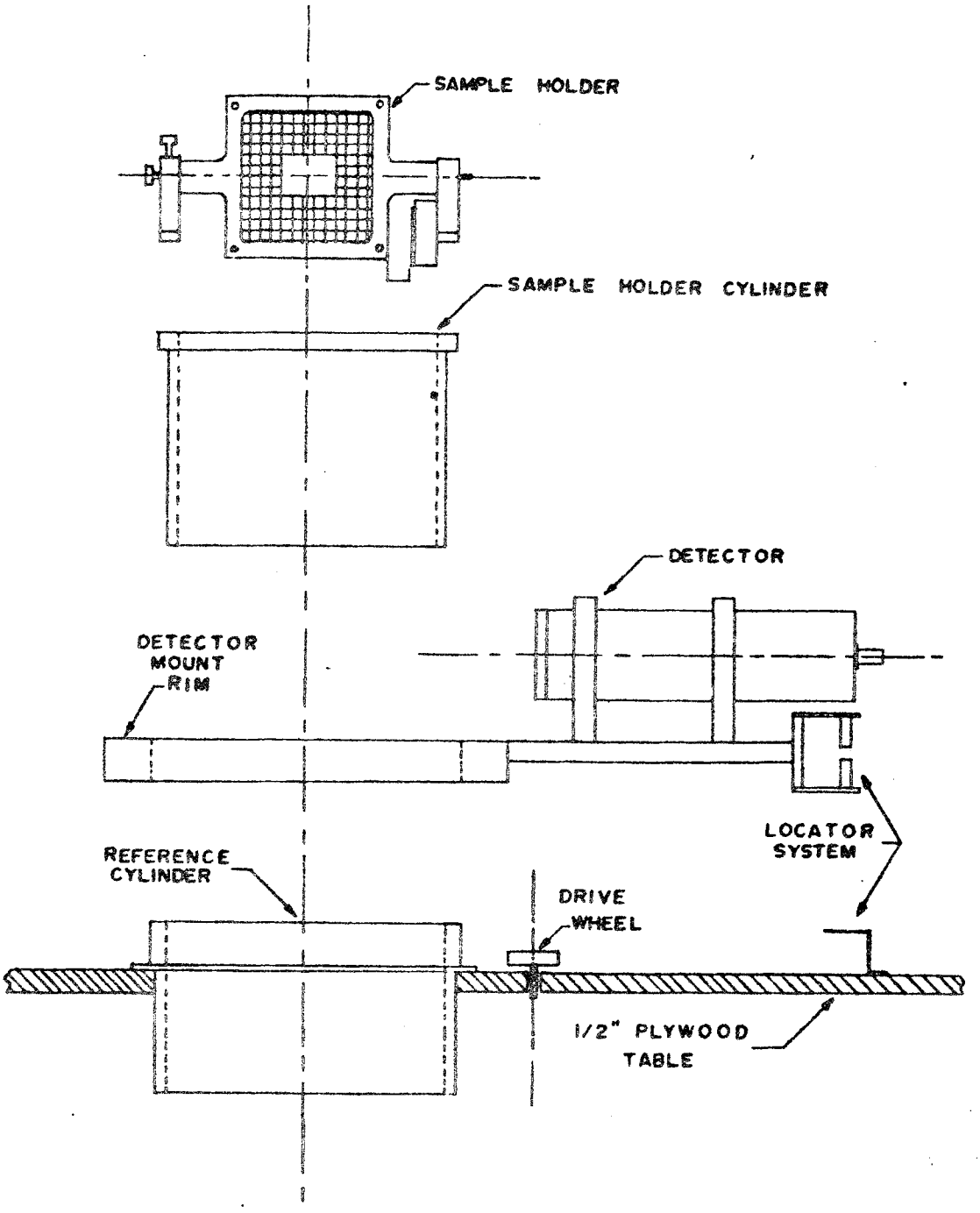

Figure 8. Bi-Directional Scattering Measurement Apparatus.

velvelour cloth. This paint and cloth covering technique greatly reduces the effect of radiation scattering from the apparatus.

The reference cylinder is 7" in diameter with a 1/4" lip and is mounted on the measurement chamber floor with three leveling screws and fastened to the surface with three hold-down screws. The stem of the plant extends through the sample holder cylinder to the potted plant which is located below the plane of the experiment. This cylinder is lined with black velvelour cloth to reduce the amount of light entering through the cylinder from below.

The sample holder is located near the center of the floor of the scattering measurement chamber. The chamber is a 41" x 48" x 24" box lined with black flock paper. The light source is located outside the chamber with the incident light focused through a small opening in the box wall onto the surface of the leaf sample by means of the monochromator quartz-flourite lens. The photomultiplier tube detector is located inside the measurement chamber. Figure 9 is a photograph of the measurement chamber.

The detector is mounted on an aluminum arm which is fastened to a one inch thick aluminum rim that is concentric with the other two aluminum cylinders. The detector rim has a bearing surface on the 1/4" lip on the stationary reference cylinder. This allows the detector to be moved in a circle of constant radius around the sample. The detector mount rim is driven by a 10 r.p.m. motor with a rubber wheel friction drive. Figure 9 shows this detector arrangement.

The angle of incidence is determined by the position of the sample holder cylinder and the detector makes the 360° excursion around the sample collecting both reflected and transmitted radiation.

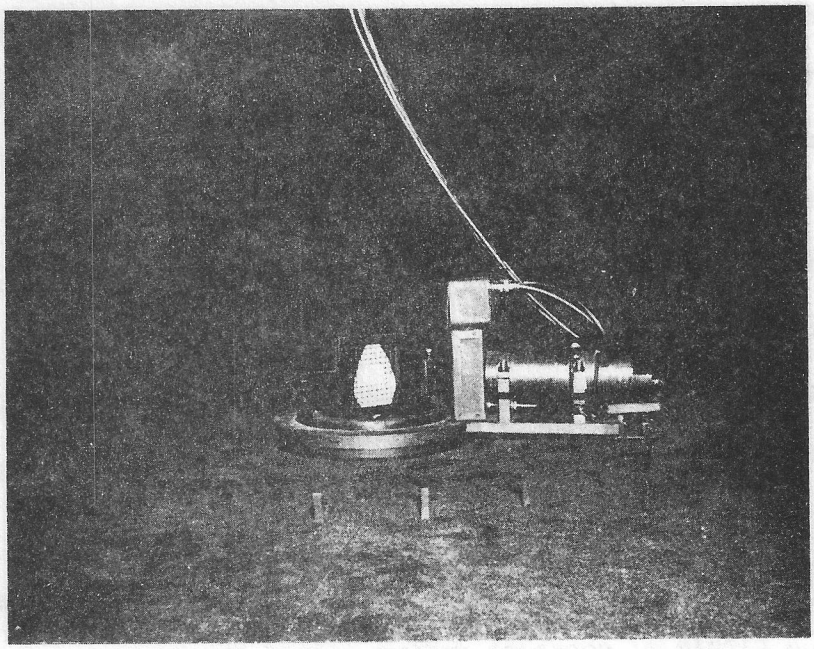

Figure 9. Scattering Measurement Chamber.

Figure 9 shows both the 931A (S-4 response) and the 7102 (S-1 response) photomultiplier tubes on the detector arm.

The 7102 photomultiplier tube is an end on looking tube and is mounted in a flat black brass tube which is lined with black velvelour cloth and mounted horizontally on the detector arm. The mount is equipped with threaded rings on the front in which to mount aperture plates. The 931A photomultiplier tube is a side looking tube and is mounted in a flat black rectangular aluminum box just in front of the 7102 mount. This box is lined with black velvelour cloth.

The 931A mounting box has slots on the front in which to mount aperture plates. The 931A tube is removed when the 7102 is in use. The distance from either detector aperture to the sample can be varied by an adjustment on the detector arm.

The metal parts in the chamber near and on line of sight with the leaf are covered with black velvelour cloth and wires and other surfaces are covered with flat black paint and 3M black paint. Each side of the chamber has a 22" wide access opening covered with a black velvelour cloth curtain. Black photographic focusing clothes are draped over the exterior of the chamber in order to further minimize light leaks.

A silicon solar cell and a small lamp are mounted on the detector arm behind the detectors. Each is mounted in a small flat black brass tube and a small lens is mounted at the opening of the lamp tube. The system is well baffled to prevent introduction of stray light to the scattering experiment. The mounting is such that the lamp beam is directed vertically upward into the silicon cell brass tube. The cell has a voltage across it when the lamp is on. Flat black brass horizontal optical interrupt tabs are mounted in a circle around the sample at 15

degree intervals. Figure 9 shows this optical interrupt location system. As the silicon cell and lamp system light path is interrupted by a tab, a dark signal pulse is developed across the cell. This provides the location signal for obtaining and analyzing the scattering data. This optical interrupt location system is adjusted for data collection with a clockwise detector revolution.

Appendix A includes mechanical diagrams for the parts of the bi-directional leaf scattering apparatus located inside the measurement chamber. In addition to individual part drawings an assembly drawing and an exploded isometric view are included to further explain the apparatus construction.

The measurement chamber is built on a frame of slotted steel angle which supports a 1/2" thick plywood table surface. The chamber occupies about one-half of the frame while the other half is used for the light source facilities. The leaf scattering apparatus is located in a relatively light-tight screen room. Figure 10 shows the apparatus frame in the screen room. The screen room is 160" x 120" x 92" with the 96" x 48" x 48" frame inside.

The source in the foreground of Figure 10 is a Bausch and Lomb High Intensity Monochromator with tungsten lamp, plug-in gratings and quartz-flourite achromatic condenser lens. The monochromator output is slightly polarized. There is an 11.5% average degree of polarization over the range from 550 nm to 700 nm (maximum 15.7% at 700 nm) with the polarization axis parallel to the exit slit.

The visible grating (350 nm to 800 nm) has a 6.4 nm/mm exit slit dispersion and the low infrared grating (0.70 μm to 1.6 μm) has a 12.8 nm/mm exit slit dispersion. Corning glass color filters are used for

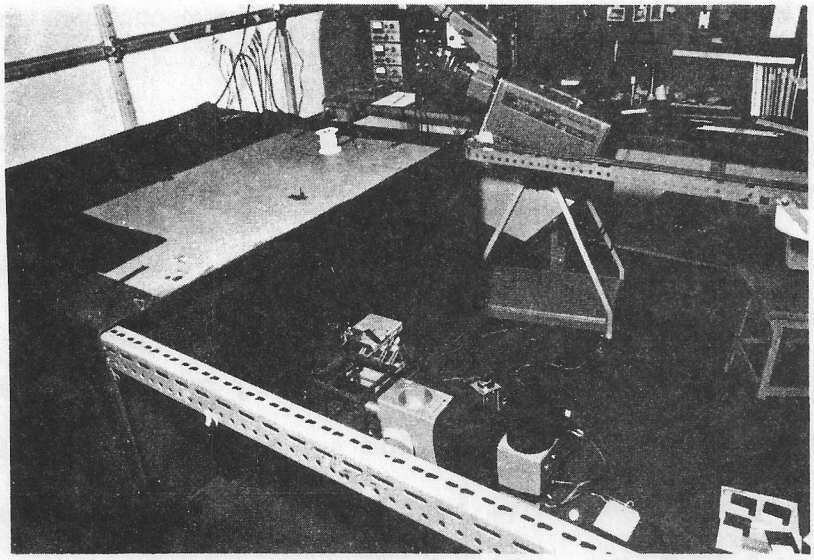

Figure 10. Apparatus Frame.

order filtering. Glass CS 0-54 for the range from 350 nm to 560 nm, CS 3-69 for the range from 560 nm to 800 nm, and CS 2-58 for the range from 700 nm to 1200 nm. A 1 mm x 1 mm exit slit is used for the infrared grating giving a dispersion of 12.8 nm for the low infrared range. A 2 mm x 2 mm exit slit is used for the visible grating giving a dispersion of 12.8 nm for the visible range. Thus the monochromator beam has a 12.8 nm dispersion for the entire range of the experiment.

Supplementary slits were constructed from brass and razor blades in order to provide the square image since the monochromator slits are vertical for line images.

The quartz-flourite achromatic condenser lens at the monochromator exit slit focuses the light through the opening in the chamber wall onto the leaf surface. This incident light is chopped at about 100 Hz. The 47 watt tungsten quartz-iodine lamp is supplied by a dc source operated with a constant voltage transformer, to reduce possibilities of source intensity variations. This source provides a collimated beam.

The incident power level is low enough to avoid apparent deviation from a normal leaf state. Visual inspection does not detect any damage to the leaves during the bi-directional scattering measurement.

Various angles of incidence are obtained with the stationary light source by rotating the sample holder cylinder within the stationary reference cylinder. The detector causes about a 30° shadow as it passes in the path of the incident beam. Incidence angles up to about 70° can be obtained before the sample holder shadow interferes for a 1/4" square normal incident beam area and about 65° for a 1/2" square normal incident beam area.

The apparatus is designed so that the detector field of view is large enough to view the entire illuminated sample area. A field of view of 14° is needed for the 931A tube aperture for 1/2" square normal incident beam area and up to 60° angle of incidence. A field of view of 6° is needed for the 7102 tube aperture for 1/4" square normal incident beam area and up to 60° angle of incidence.

The 931A actual field of view is 100°. It has a 5/16" width cathode and a 1/8" square aperture. The 7102 actual field of view is 108°. It has a 1.24" diameter cathode and a 3/16" square aperture. Thus the entire illuminated sample area is seen by the detector.

There is a spread in the collection angle due to the finite sizes of the illuminated sample area and the aperture size together with their distance of separation. The field of view and collection angle spread information is given in terms of two dimensions. This is done since the source and detector are in the same plane and most all of the data is taken with the plane of the leaf sample perpendicular to this plane thus providing a constant vertical dimension on the illuminated area.

For the infrared range, the normal illuminated area is 1/4" square with a 3/16" square detector aperture at a distance of 5.5" from detector to sample. Figure 11 is a plot of the variation of collection angle as a function of collection angle for constant angle of incidence. The worst case is about $\pm 2.7^{\circ}$ for an incidence angle of 60°.

For the visible range, the normal illuminated area is 1/2" square with a 1/8" square detector aperture at a distance of 4 1/16" from detector to sample. Figure 12 is a plot of the variation of collection

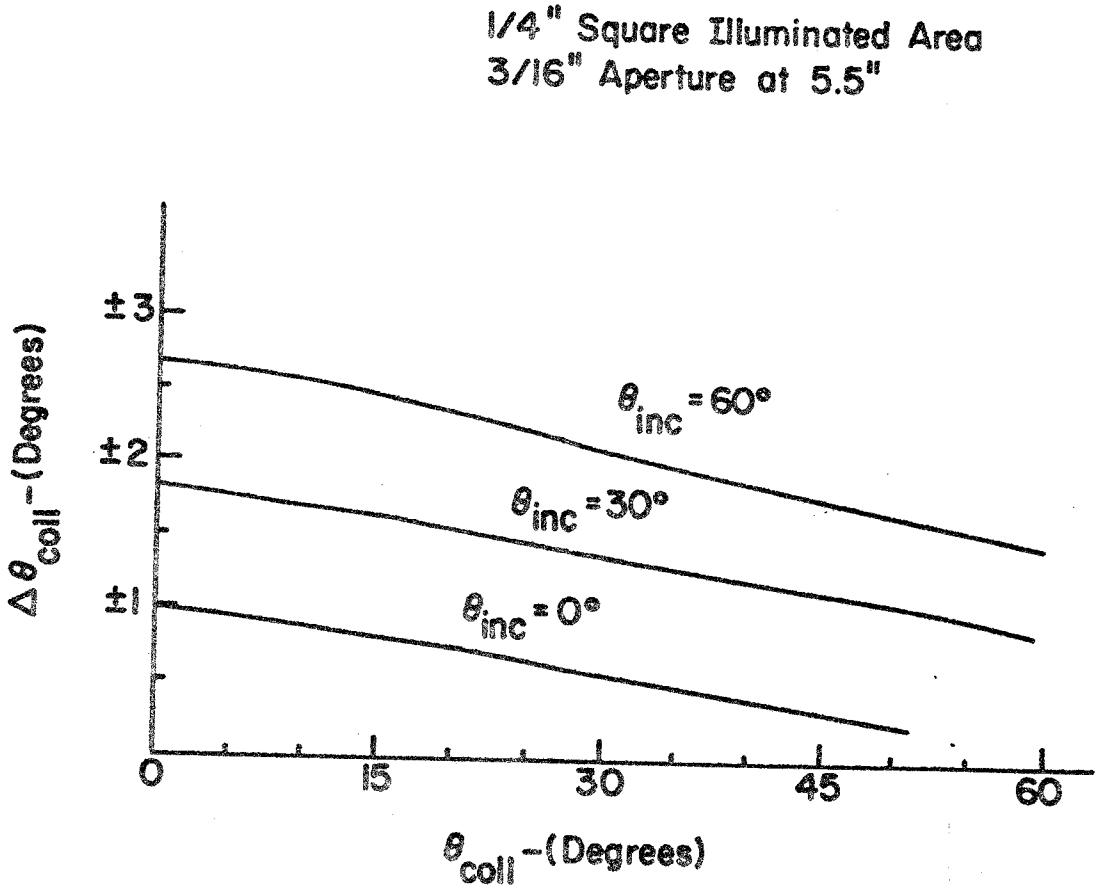

Figure 11. Variation in Collection Angle, 1/4" Square Illuminated Area.

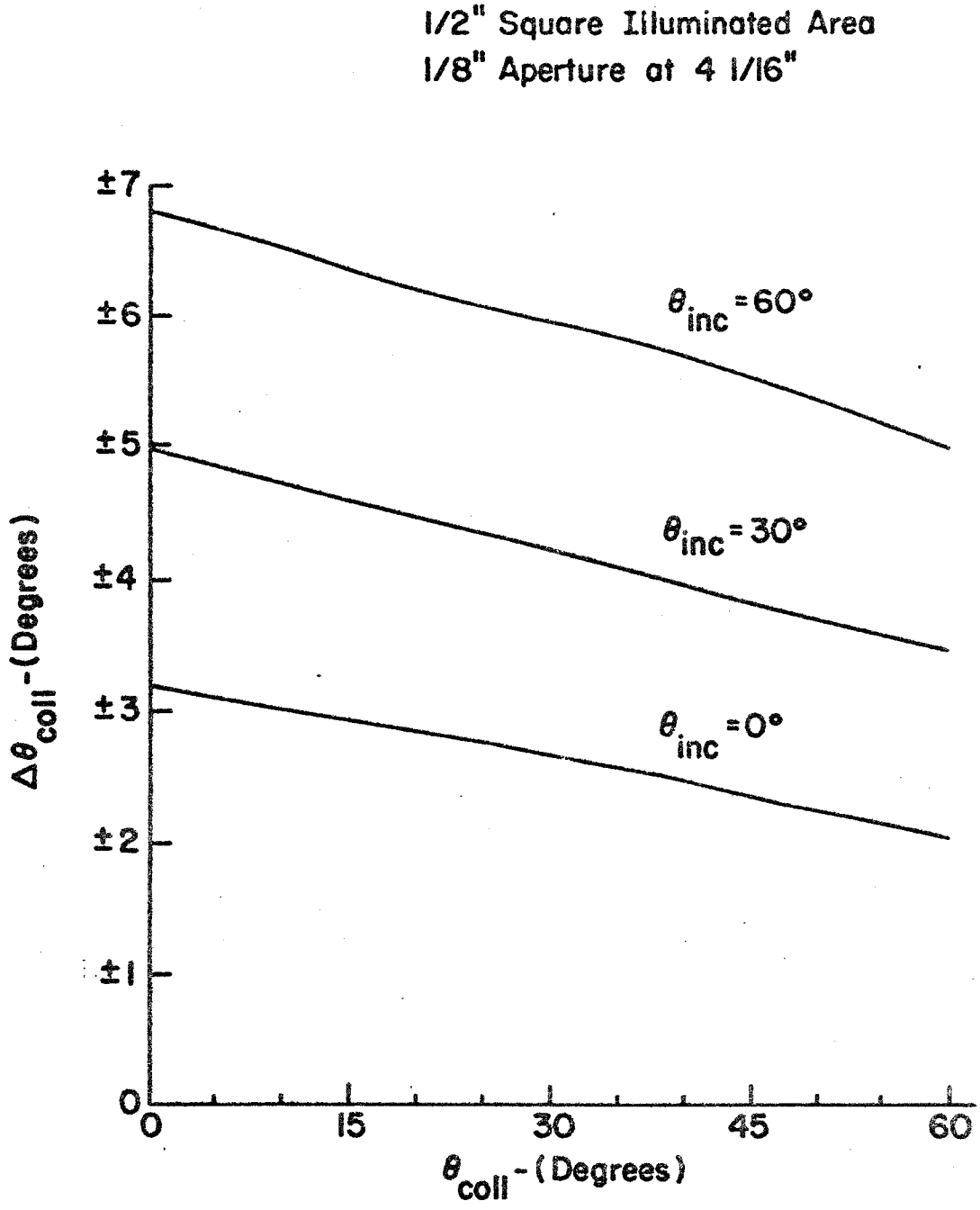

Figure 12. Variation in Collection Angle, 1/2" Square Illuminated Area.

angle as a function of collection angle for constant angle of incidence. The worst case is $\pm$ 6.8° for an incidence angle of 60°.

The scattering data is collected at intervals of 15°, thus even for the worst case situation, the data for one collection angle does not overlap with the next data collection point 15° away.

The screen room lights are off and the door is closed during data gathering runs so that possibilities of stray light problems are very small.

Pin-hole calibration apertures are used for the initial calibration run. Both the 7102 and 931A use a pin-hole calibration aperture 11.8 mils in diameter. The monochromator output is incident on the detector surface through the calibration aperture. This provides a relative correction curve for the scattering data. This is discussed in detail in the following section.

While presented in two-dimensional form, the data are part of a three-dimensional data plot. The detector aperture covers small sites on the surface of an imaginary scattering data sphere. For the 7102 tube with the 3/16" square aperture, the number of sites is about 10740. For the 931A tube with the 1/8" square aperture, the number of sites is about 12880. These numbers are area ratios but give an idea of the three-dimensional data problem. The two-dimensional data presented here can be considered as a slice or section of the three-dimensional scattering plot.

Signal Processing Circuitry

The signal processing circuitry provides a dc output voltage which is directly proportional to the amplitude of the detector square wave signal. The circuit will plot the bi-directional scattering distribution function data in polar form and plot spectra on a linear scale versus wavelength. These plots are stored on a storage oscilloscope screen and recorded photographically.

Figure 13 is the block diagram for the signal processing circuitry. Detailed circuit diagrams are given in Appendix B. The photomultiplier voltage divider circuit is built into the photomultiplier tube socket. Coaxial cables with BNC connectors are used to bring the high voltage into the chamber for the photomultiplier tube and to take the signal out of the chamber. These cables are shown in the scattering measurement chamber photograph in Figure 9.

The photomultiplier output signal is processed by a synchronous demodulator circuit which has a dc output voltage directly proportional to the peak square wave input signal. The input is ac coupled to a high impedance amplifier. The input is ac coupled because of the dc voltage produced by the photomultiplier tube dark current. A mechanical chopper is used as the demodulator. This permits detection of milli-volt level signals and allows for the large dynamic range requirement of several hundred to one. Figure 14 is a plot of the demodulator system linearity. The mechanical chopper is driven at the chopper wheel frequency to provide synchronous demodulation. A filter follows the mechanical chopper.

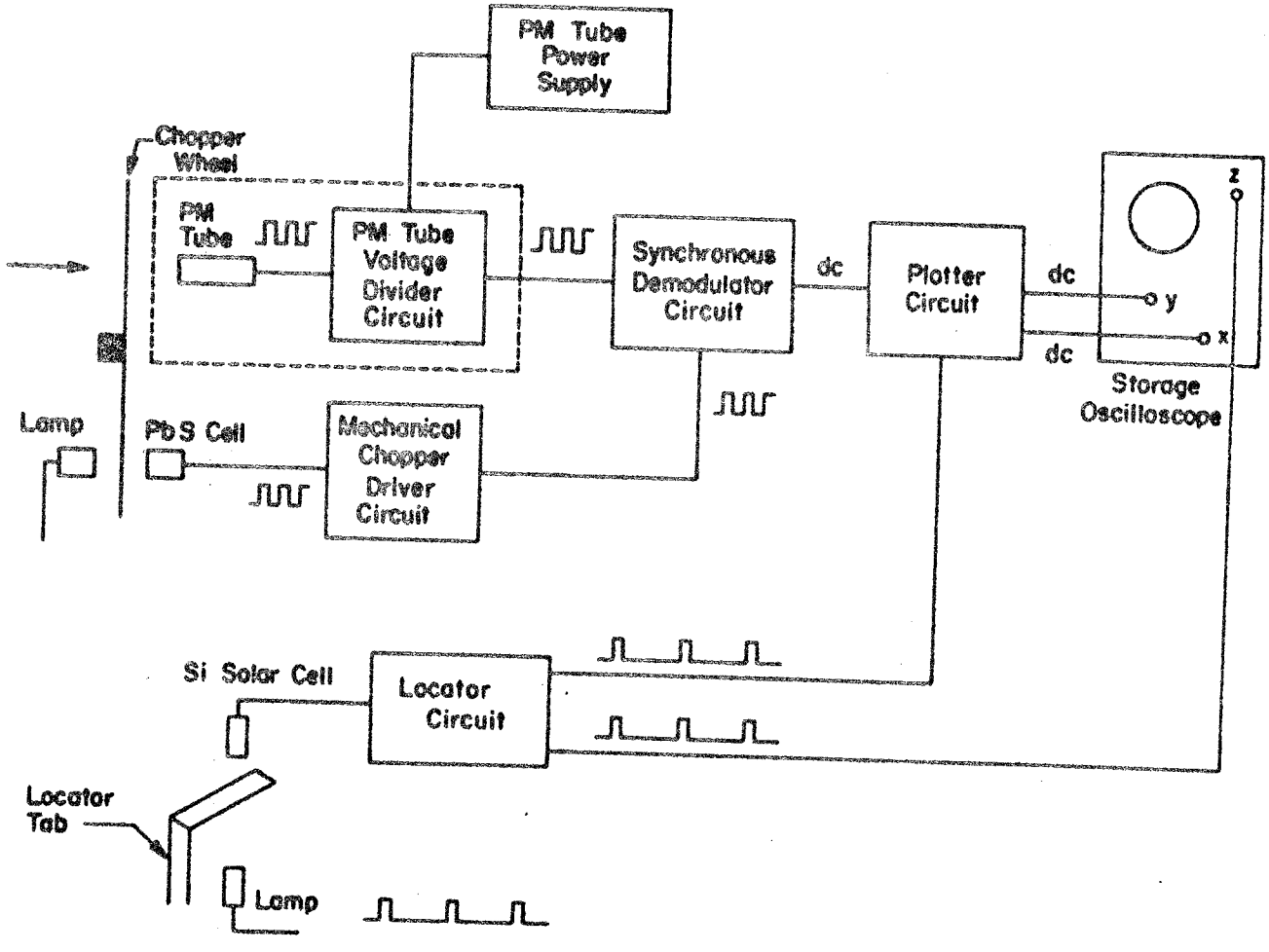

Figure 13. Signal Processing Circuitry Block Diagram.

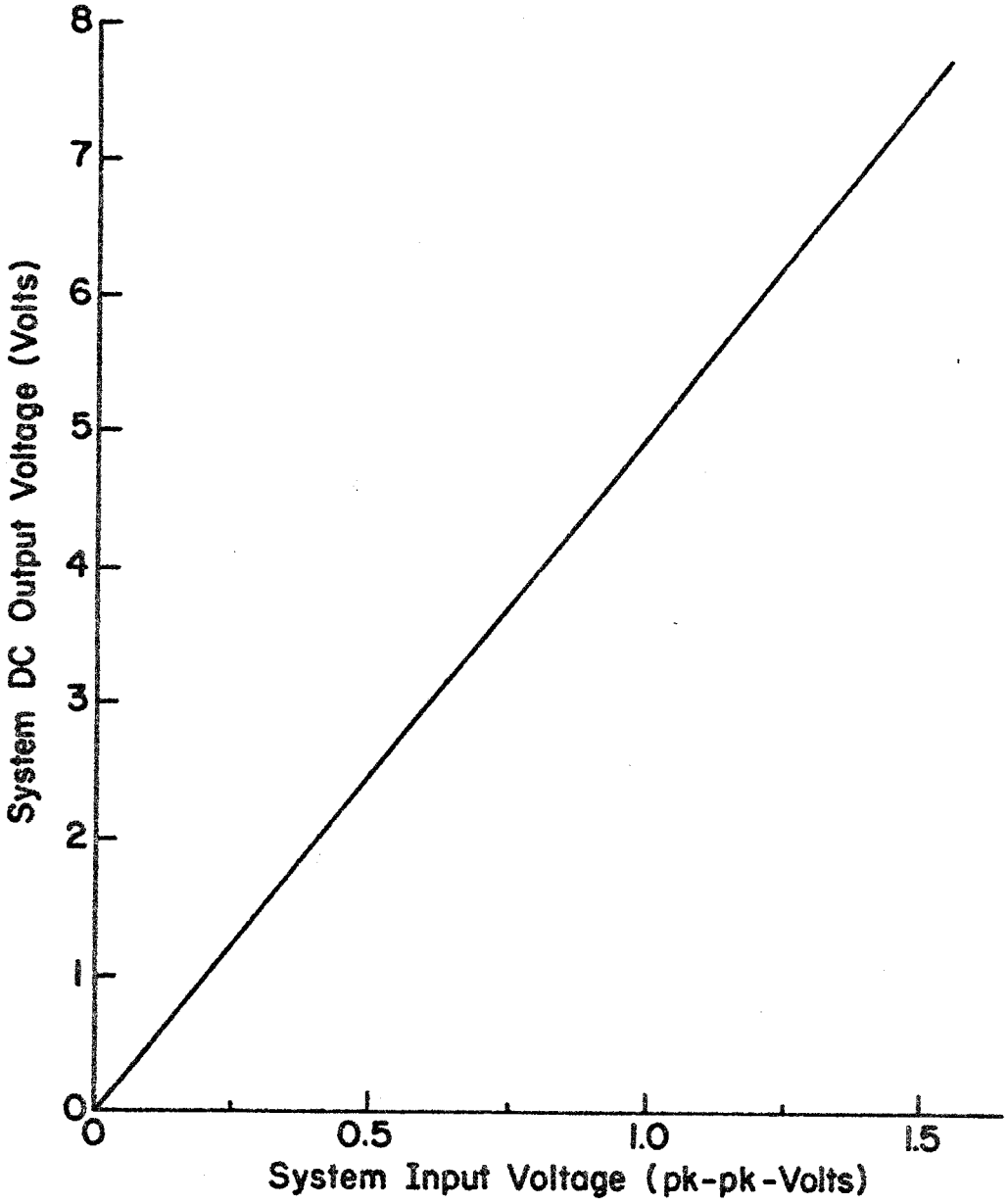

Figure 14. Detector System Linearity.

This output filter is critical in that it must reduce the noise while providing as small a delay as possible. This design gives a collection angle delay of $\theta_d = 0.13^\circ$ for a 60 second photomultiplier excursion around the leaf sample.

The mechanical chopper is driven by a signal obtained from a lead-sulphide cell and small lamp combination located at the monochromator chopper wheel. The lamp is mounted in a flat black brass tube with a lens over the end and the PbS cell is mounted in a flat black brass tube. This arrangement is shown in the photograph of Figure 15. The PbS cell and lamp assembly is mounted on a lab jack. The chopper wheel interrupts the light from the lamp producing a voltage at the chopper wheel frequency. The physical position of this system at the chopper wheel is adjusted by means of the lab jack and is the demodulator phase adjustment since this signal is used to drive the mechanical chopper.

The detector output signal is connected to the signal plotter circuit. The first stage is a wavelength normalization circuit. This consists of a buffer amplifier and a 10-turn precision potentiometer which is set for the wavelength normalization factor, K_λ. This normalization factor is defined and explained in the next section. The second stage consists of two amplifiers with the same gain; one connected for a negative output and the other connected for a positive output. Each of these amplifiers is connected to an identical parallel string of precision resistor voltage dividers. Each voltage divider in the string is designed to multiply the signal by a sine or cosine function of the collection angles from 0° to 360° taken at 15° intervals. The use of the positive signal for one voltage divider string and the negative signal for the other voltage divider string covers all four quadrants

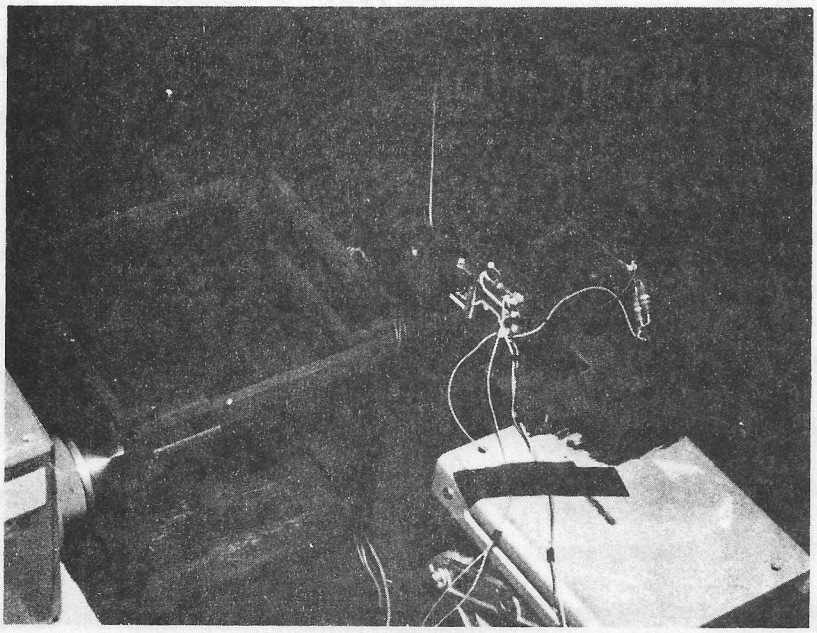

Figure 15. Chopper Wheel.

in order to plot information over the range of angles from 0° to 360°. These voltage divider circuits convert the data from polar coordinates to the rectangular coordinate system inherent in oscilloscope deflection plates. The outputs from the voltage divider circuits are connected to a rotary switch. The rotary switch is operated by the locator circuit which also modulates the Z axis. This is done in such a way that the leading edge of the locator tab pulse modulates the Z axis of the oscilloscope and then switches the rotary switch to the next position. The rotary switch is connected to the outputs of the voltage divider strings so that it selects the x and y signals necessary to plot the information is sequence from 0° to 360° at 15° intervals.

This data is stored on a 564 Tektronix storage oscilloscope screen one point at a time. The oscilloscope uses two 3A72 pre-amplifiers with input impedance of 1 meg. Ω and 47 pf.

A tape recorder could also be used for data recording when running experimental measurements with similar parameters on many samples. The optical locator signal should be recorded and can be used as a digitizing trigger signal.

This detector system results in a mechanical delay of 0.63° for the value of collection angle. The 564 oscilloscope stores the data which is recorded photographically following the data run. This gives 24 data points at intervals of 15° around the full circle.

The system adds only a small delay to the collection angle. The electronic delay of 0.13° and the mechanical delay of 0.63° are balanced somewhat by adjustment of the optical interrupt locator system. The optical collection angle spread is the only significant collection angle spread.

In addition to the polar plot capability the system can also plot spectra on a linear scale. The intensity information is plotted on the y axis of the oscilloscope and the wavelength is plotted on the x axis of the oscilloscope. A 10-turn potentiometer is used with a fixed dc voltage to give a wavelength scale. A manual oscilloscope z axis intensity dotting switch is used to record these points one at a time. A remote selection switch and additional potentiometer allow this to be done at the monochromator location as well as at the control panel.

Figure 16 is a photograph of the control panel area. The control panel is in the center of the photograph. The 564 storage oscilloscope is in the right of the photograph. A 35 mm data recording camera is mounted at the oscilloscope screen. At the left just in front of the power supply stack is the ac control box. This box contains the drive motor and chopper motor switches.

Data Processing

This section describes the procedure used to process the scattering data. At the beginning of each data run, a calibration measurement was performed. The monochromatic source beam was incident upon the photomultiplier tube through a calibration aperture. The system output is a voltage, E_i. This voltage is directly proportional to the incident radiant power at a given wavelength as follows,

$$E_i = R_\lambda^i \, \delta P_i$$

This measurement is made for all wavelengths of interest for that particular data run. The responsivity, R_λ^i, is directly proportional to

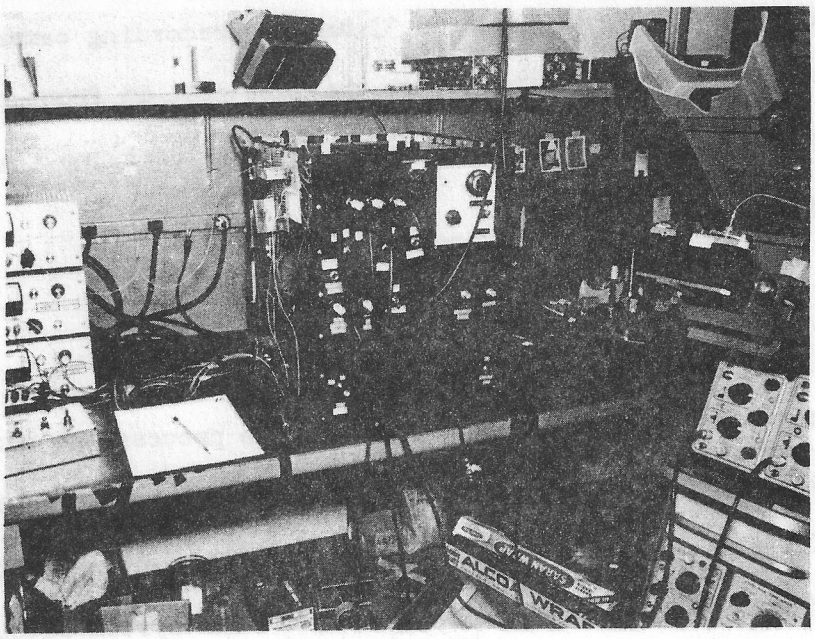

Figure 16. Control Panel.

the fixed electronic circuit gain, the photomultiplier tube quantum efficiency, the photomultiplier tube electronic gain and a transmission filter characteristic.

$$R_\lambda^i = \text{Constant}\left(\begin{matrix}\text{FIXED}\\ \text{ELECTRONIC}\\ \text{GAIN}\end{matrix}\right)\left(\text{Q.E.}(x,y)\right)\left(\begin{matrix}\text{PMT}\\ \text{GAIN}\end{matrix}\right)\left(T_{\text{FILTER}}\right)$$

Let R_{xy} be the photomultiplier sensitivity where $R_{xy} = (\text{Q.E.}(x,y))\left(\begin{matrix}\text{PMT}\\ \text{GAIN}\end{matrix}\right)$. This quantity is a function of the location on the surface of the photocathode which is illuminated.

Rewriting,

$$E_i = \text{CONSTANT}(\text{F.E.G})\left(R_{xy}\right)\left(T_{\text{FILTER}}\right)\ \delta P_i$$

A table of E_i versus λ is constructed from the data. A constant K_λ^s is calculated according to the following equation and given on the table versus λ.

$$K_{\lambda m}^s = \frac{\alpha_m T_{\text{FILTER}}}{E_{im}}$$

The subscript m denotes the m^{th} data run and the accompanying m^{th} calibration run. The m^{th} data run is the series of measurements made on one particular leaf sample. The constant α_m is used to adjust the numbers for $K_{\lambda m}^s$ so that they are all in the range from 0 to 1 for a later potentiometer setting. This factor, α_m, is constant for the m^{th} run.

The data run is begun after the $K_{\lambda m}^s$ factors are computed and listed as functions of wavelength. The green leaf sample is installed and the measurement aperture plate is placed at the photomultiplier tube photocathode. For a given wavelength, angle of incidence and data collection

angle, the system output for the scattering measurement is a voltage, E_s. This voltage is directly proportional to the scattered radiant power at the given collection angle for the specified wavelength as follows,

$$E_s = R^s_\lambda \, \delta P_s$$

The responsivity, R^s_λ, is directly proportional to the fixed electronic circuit gain, a potentiometer setting ($K^s_{\lambda m}$), the photomultiplier tube quantum efficiency and the photomultiplier tube electronic gain.

$$R^s_\lambda = \text{CONSTANT}\left(\begin{matrix}\text{FIXED}\\ \text{ELECTRONIC}\\ \text{GAIN}\end{matrix}\right)\left(K^s_{\lambda m}\text{POT}\right)\left(\text{Q.E.}(x',y')\right)\left(\begin{matrix}\text{PMT}\\ \text{GAIN}\end{matrix}\right)$$

Let $R_{x'y'}$ be the photomultiplier sensitivity where

$$R_{x'y'} = \left(\text{Q.E.}(x'y')\right)\left(\begin{matrix}\text{PMT}\\ \text{GAIN}\end{matrix}\right)$$

This quantity is a function of the location on the surface of the photocathode which is illuminated.

Rewriting,

$$E_{smj} = \text{CONSTANT(FEG)}\left(K^s_{\lambda m}\text{POT}\right)\left(R_{x'y'}\right)\, \delta P_{smj}$$

The subscripts mj are added to the output voltage to denote the m^{th} data run and the j^{th} measurement made during that data run. This voltage, E_{smj}, is the quantity which is recorded on the storage oscilloscope screen.

Substituting for the potentiometer setting, $K^s_{\lambda m}\text{POT}$,

$$E_{smj} = \text{CONSTANT(FEG)}\left(\frac{\alpha_m T_{filter}}{E_{im}}\right)\left(R_{x'y'}\right)\, \delta P_{smj}$$

Further substituting for E_{im},

$$E_{smj} = \frac{\text{CONSTANT(FEG)}\left(\alpha_m T_{filter}\right)\left(R_{x'y'}\right)\delta P_{smj}}{\text{CONSTANT(FEG)}\left(T_{filter}\right)\left(R_{xy}\right)\delta P_i}$$

Simplifying,

$$E_{smj} = \alpha_m \left(\frac{R_{x'y'}}{R_{xy}}\right)\frac{\delta P_{smj}}{\delta P_i}$$

This measured quantity, E_{smj}, is directly proportional to the ratio of the scattered radiant power, δP_{smj}, to the incident radiant power, δP_i.

This data is modified by two factors as it is retrieved from the film storage for presentation. This is done by an optical multiplication of the curve as outlined in the data recording section to follow. This result is E'_{smj},

$$E'_{smj} = \alpha'_m \beta_m E_{smj}$$

The factor, β_m, is used to allow for the use of two different beam areas. This factor is either one or four, in order to keep the product, $\beta_m(A_{beam})$, constant, where A_{beam} is the normal incident beam area. The factor, α'_m, is used to normalize the scale factors, so that the product of α'_m and α_m is the same constant for any data run, m.

$$\alpha'_m = \text{constant}\ \frac{1}{\alpha_m}$$

This result is,

$$E'_{smj} = \text{CONSTANT}\left(\frac{R_{x'y'}}{R_{xy}}\right)\frac{\delta P_{smj}}{\delta P_i}$$

and according to the results of the chapter on goniometry, is equal to the product of the bi-directional transmission distribution function and $\cos(\pi - \theta_{coll})$ within a constant or the product of the bi-directional reflection distribution function and $\cos\theta_{coll}$ to within a constant. These relative quantities will be referred to, in general here, as scattering distribution functions.

Comparison of two different measurements can be done as follows,

$$\frac{E'_{smj}}{E'_{sqk}} = \frac{\text{CONSTANT}\left(\frac{R_{x'y'}}{R_{xy}}\right)\frac{\delta P_{smj}}{\delta P_i}}{\text{CONSTANT}\left(\frac{R_{x'y'}}{R_{xy}}\right)\frac{\delta P_{sqk}}{\delta P_i}}$$

This reduces to,

$$\frac{E'_{smj}}{E'_{sqk}} = \frac{\delta P_{smj}/\delta P_i}{\delta P_{sqk}/\delta P_i}$$

This result is a direct comparison of the scattering distribution function for two different measurements.

This is also approximately the case for comparison of results for different photomultiplier tubes since the ratio $R_{x'y'}/R_{xy}$ can be assumed to be almost one using the following information.

There is a variation of the relative sensitivity of a photomultipler tube as a function of position of incidence on the cathode surface. This

is due to variation in the sensitivity in the cathode itself and to cathode-to-first-dynode electron optics.

Christensen and Ames measured this variation for a type 7200 photomultiplier tube [3]. The general trend is that the variation of relative sensitivity as a function of position on the cathode surface is smooth.

In the bi-directional scattering measurements, the calibration aperture and the measurement aperture are concentric with each one being small relative to the overall cathode. Since the calibration aperture is very small, it is a good assumption that the sensitivity for the calibration aperture at (x,y) is equal to the average sensitivity for the measurement aperture at (x',y'). This implies that only gradient terms, and not curvature or higher order terms would be predominant in a Taylor expansion of R(x',y') about x,y.

Thus to a first approximation

$$R_{x'y'}/R_{xy} = 1$$

The polar bi-directional scattering plots are given using a relative scale for $[\rho'\cos\theta_{coll}]$ versus θ_{coll} and $[\tau'\cos(\pi - \theta_{coll})]$ versus θ_{coll}. In order to convert these data to absolute units multiply the reading from the polar graph measured in units per centimeter by 3.77×10^{-4}. The units are then reciprocal steradians for ρ' and τ'.

Data Collection Procedure

Data collection begins with a calibration run after the electronic system and oscilloscope have been calibrated. The sample holder is empty so that the incident light passes through the sample holder falling

on the photomultiplier tube calibration aperture. The pin-hole calibration aperture is used for the calibration run. A No. 7-98 glass color filter is used at the light source giving approximately 20% neutral transmission. The proper wavelength band order filter is used also at the light source. A curve of radiant power output versus wavelength is the result of this calibration.

Polar plots of the scattering distribution function versus collection angle are obtained for constant wavelength and incident angle. The wavelength is set on the monochromator dial and the angle of incidence is set by rotating the sample holder cylinder to the proper position. The collection angles are measured relative to the surface normal at the surface where the incident light is impinging. These angles are measured clockwise from this sample surface normal. The initial photomultiplier tube position is slightly counterclockwise from the 270° collection angle. The rotary switch is re-set to position number one. Next the room is darkened and the photomultiplier power supply is turned on. The photomultiplier tube drive motor is turned on for clockwise travel and the data is recorded on the Tektronix 564 storage oscilloscope. The end of the run is a manual operation. The final step in the run is to photograph the polar plot of the scattering data from the storage oscilloscope screen. Figure 17 shows a data curve on the oscilloscope screen. The detector position, rotary switch and oscilloscope are then reset for the next data run.

At the end of the group of data runs before the sample is removed, a photograph of the leaf in the sample holder is taken. This records leaf condition and locates the leaf area under investigation.

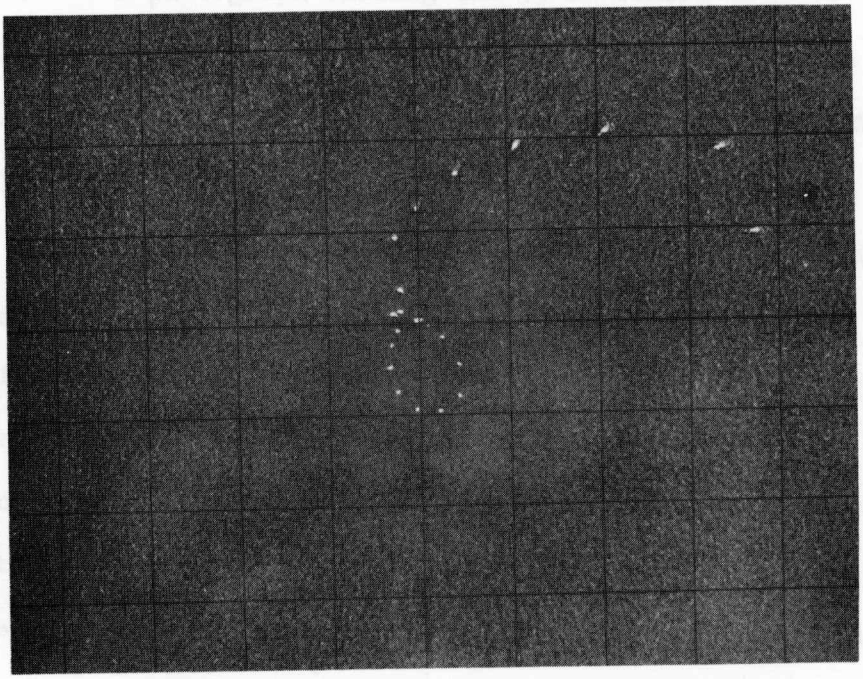

Figure 17. Data on Storage Oscilloscope Screen.

Data Recording System

The scattering data is recorded photographically from the 564 storage oscilloscope screen. A 35 mm camera mount was constructed to fit onto the C-12 Tektronix oscilloscope camera frame. A quick change design also permits use of the polaroid oscilloscope camera.

The oscilloscope screen centimeter graticle provides a reference for the collected data for comparison and study.

Figure 18 is a photograph showing the 35 mm camera mounted on the Tektronix 564 storage oscilloscope. A Nikon F 35 mm camera with a Micro-Nikkor Auto 1:3.5 55 mm lens is used to record the scattering data.

Kodak Plus-X negative film (ASA 125) is used for all of the data recording. Kodak D-11 high contrast developer is used in processing the data negatives. The leaf sample photographs are recorded on the same roll of film with the scattering data.

Data is retrieved from the negative data film rolls using a film strip projector with a 5" f/3.5 lens. The system is used to plot directional scattering curves for different wavelengths with constant incident angle on the same page for comparison. Figure 19 shows this data retrieval system. The projector is mounted on a photographic copy stand so that various magnifications can be achieved easily. This is a simple optical analog multiplier for curve scaling for comparison plotting. The negative film works well for the data storage in this system.

The centimeter lines on the oscilloscope screen graticle are the reference lines for data retrieval and curve scaling.

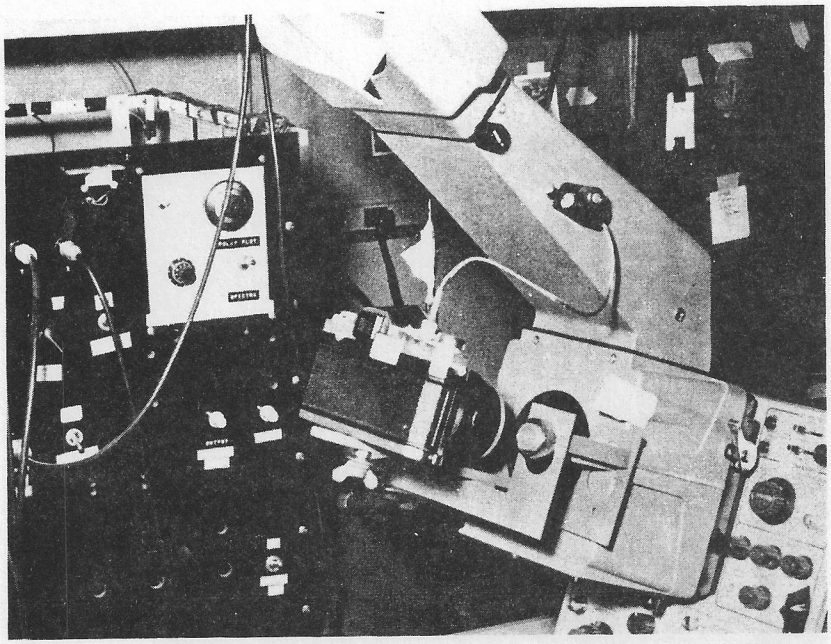

Figure 18. 35 mm Oscilloscope Camera.

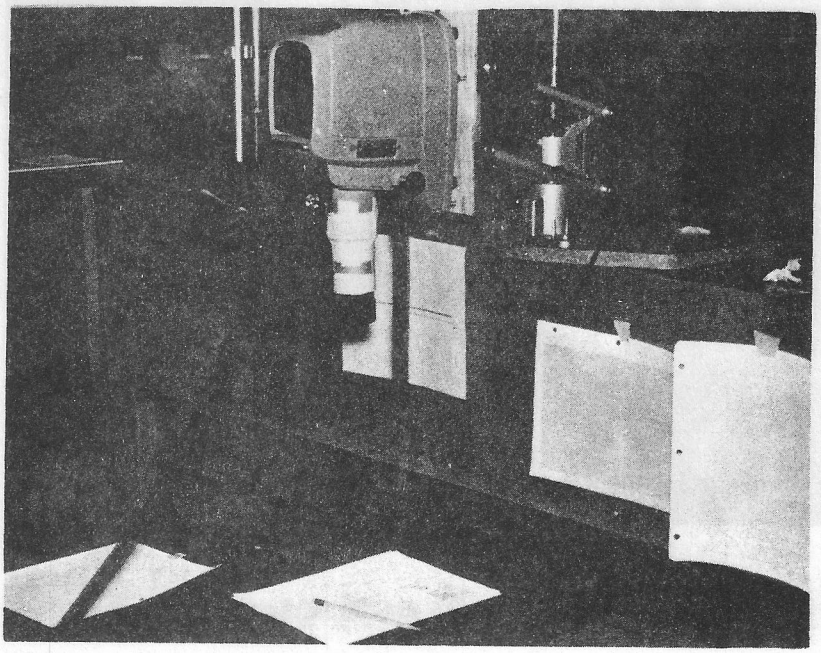

Figure 19. Data Retrieval System.

SOYBEAN LEAF BI-DIRECTIONAL SCATTERING MEASUREMENTS

Procedure

Bi-directional scattering characteristic curves were taken on healthy, living soybean leaves over the range from 375 nm to 1000 nm: from 375 nm to 700 nm at 25 nm intervals and from 750 nm to 1000 nm at 50 nm intervals. These wavelength intervals were determined from the results of a preliminary experiment which obtained the spectra for several fixed reflection and transmission collection angles at several particular angles of incidence.

The soybean leaf is a dicotyledon with a typical dorsiventral structure. The mesophyll consists of palisade tissue on the ventral or top side and spongy tissue on the dorsal or bottom side of the leaf. The palisade tissue consists of several layers of densely arranged, long cylindrical palisade cells. The spongy tissue is lacunose (many intercellular spaces) with large intercellular spaces and spongy parenchyma cells having irregular shapes.

The epiderma of the soybean leaf are continuous layers of cells except for stomata structures. Trichomes, hairlike structures, originate from some of the epidermal cells.

The chlorophyll contining cells are in the mesophyll layers of the leaf. Figure 20 is a photograph of a soybean leaf cross-section.

Figure 21 is a photograph of several of the soybean plants used in this scattering experiment. These plants were grown one plant to each six inch diameter pot in the greenhouse. The leaves used received adequate lighting and were not shaded. The soybean leaves used had an

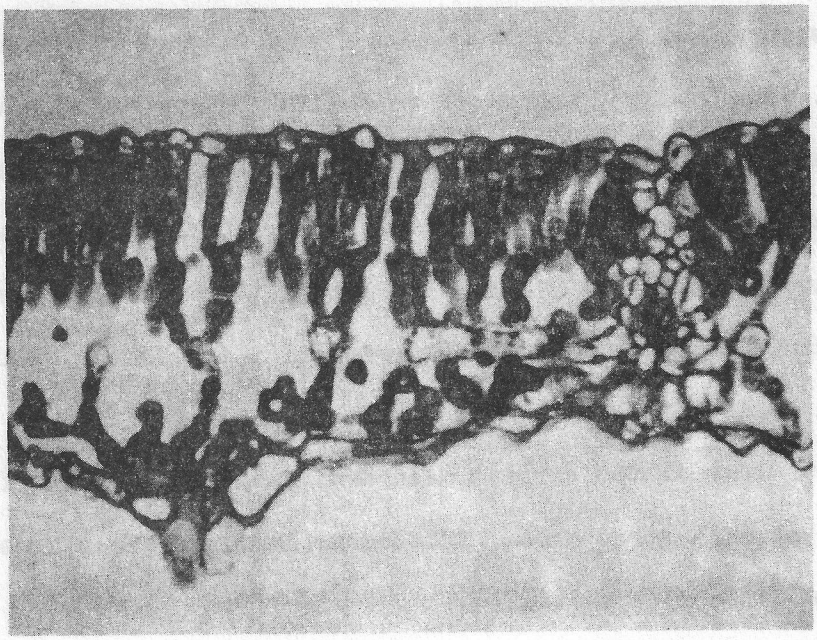

Figure 20. Soybean Leaf Cross Section.

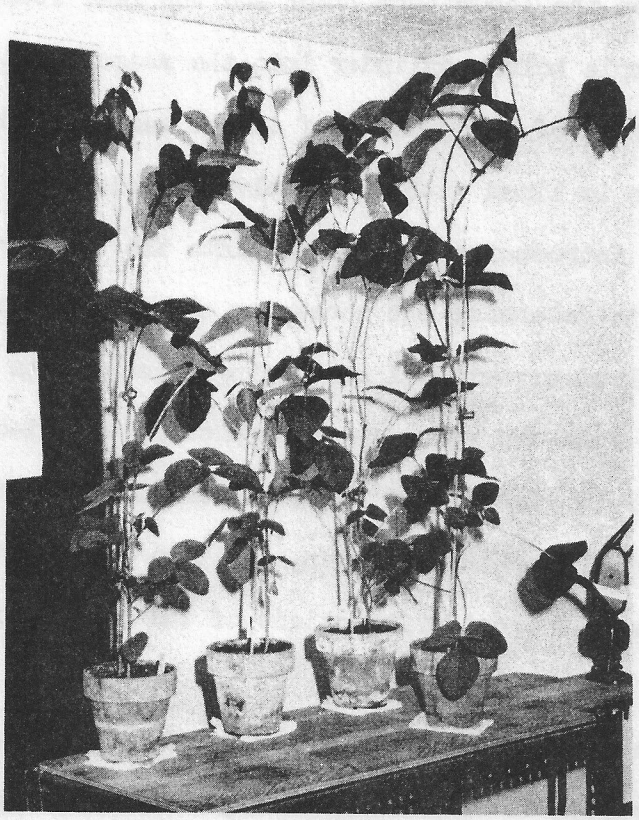

Figure 21. Soybean Plants.

average length of five inches to five and a half inches and an average width of three and a half inches to four inches. The average soybean plant height was 54 inches. The data were taken on soybean leaf sample areas not including the midvein.

Figure 22 shows a soybean plant with one of its leaves under study. The pot rests on the laboratory floor and the leaf stem extends up through the sample holder cylinder into the measurement chamber. Figure 23 is a photograph of a soybean leaf in the sample holder. The sample holder cylinder is lined with black velvelour cloth to reduce the possibility of introducing stray light into the chamber from below.

In order to determine the necessary coordinates for a full set of two-dimensional bi-directional scattering measurements experiments were carried out to find the symmetry properties in the bi-directional scattering characteristics for soybean leaves. This study compared results for top and bottom surfaces, positive and negative data collection angles and different orientations of the midvein in a given sample plane.

The midvein orientation is called vertical orientation when the midvein is parallel to the v axis of Figure 4 and is called horizontal orientation when the midvein is parallel to the h axis of Figure 4.

The bi-directional scattering results for the top and bottom leaf surfaces were different in magnitude and slightly different in functional form indicating that measurements must be carried out for both top and bottom soybean leaf surfaces.

The results for $+\theta_{inc}$ and for $-\theta_{inc}$ have the same functional form and magnitudes within 5% of one another showing that measurements may be carried out at either $+\theta_{inc}$ or $-\theta_{inc}$.

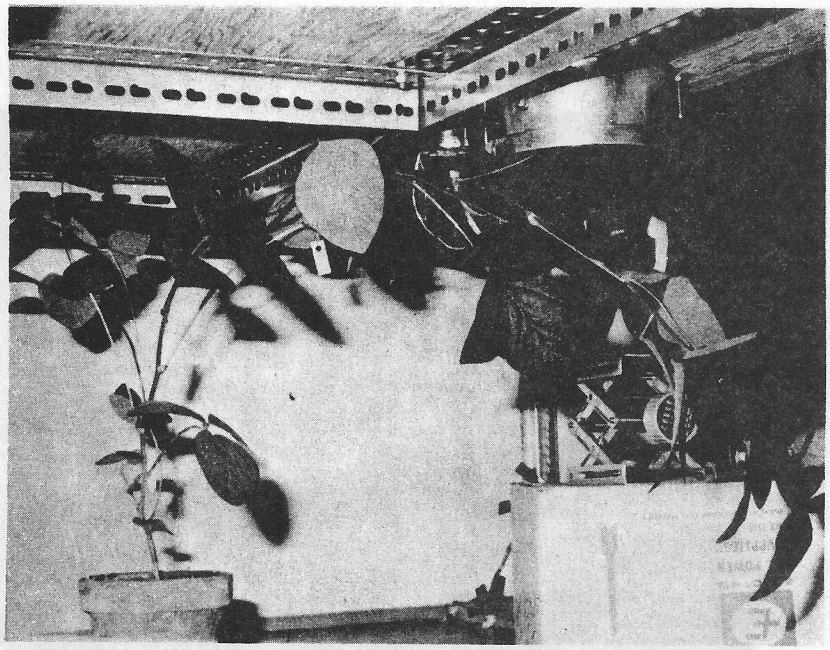

Figure 22. Soybean Plant Positioned under Measurement Chamber.

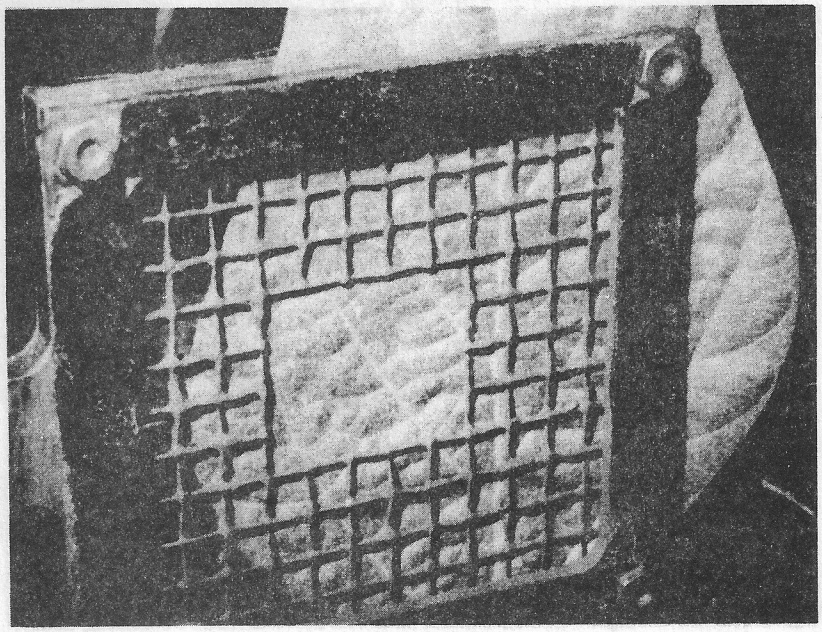

Figure 23. Soybean Leaf in Sample Holder.

A C_∞ rotational symmetry for the sample plane about a normal to that plane is found to exist for both top and bottom soybean leaf surfaces. Thus any midvein orientation may be used for the measurements.

Since a large amount of time was required to make the extensive full set of bi-directional scattering measurements, it was not feasible to make the full set of measurements on one soybean leaf. Thus some of the measurements were made at some of the conditions on one leaf and then at other conditions on another leaf, etc. until it had taken five different leaves in order to take data for all of the different measurement conditions. The data were taken on one leaf from each of three plants and two leaves from a fourth plant.

Since several leaves were used in order to make measurements at all of the conditions for a full set, an experiment was carried out on soybean leaves to determine the consistency of bi-directional scattering measurements among several leaves for a particular fixed set of conditions. Two leaves on one plant and three leaves on a second plant were used for this consistency experiment.

In this consistency experiment polar bi-directional scattering plots were taken on both the top and bottom leaf surfaces. Incidence angles of 0° and 45° (with $\theta_{tilt} = 0^\circ$) were used with wavelengths of 500 nm and 550 nm. These wavelengths were selected in order to determine variation among polar plots for the highly absorbing blue region and for the highly reflecting green region for different leaves.

The polar plots for each set of measurement conditions had nearly the same functional form for both reflection and transmission. Thus one point on each curve was selected for comparison. The transmission curves were compared by using the magnitude of the radius vector for the

transmission curve at $\theta_{coll} = 180^{\circ}$, which is along a normal to the leaf plane. The reflection curves were compared by using the magnitude of the radius vector for the reflection curve at $\theta_{coll} = 45^{\circ}$.

The mean value of the radius vectors for the five leaves was calculated for each particular set of conditions and coordinates. The standard deviation about each of these mean values was calculated and this information is presented in Table 3. The unit for measuring the radius vectors from the polar plots is consistent throughout being 1 unit per 1/2 inch for a relative scattering unit scale of 20.

Using this information, the use of several different soybean leaves to produce data for a composite scattering model was judged to be an acceptable plan.

The wavelength range of the experiment was divided into smaller ranges so that for a particular incident surface an effort could be made to complete measurements at each incidence angle on the same leaf in the same data run. The polar plots have a leaf identification as outlined in the following scattering data section.

Soybean data collection angles are measured clockwise from the normal to the surface of incidence while the incidence angles are measured counter-clockwise from this normal. The tilt angle is 0° for this experiment so the source angle symbol is θ_{inc} as shown in Figure 4.

Soybean Leaf Bi-Directional Scattering Data

The following ten figures are the polar bi-directional scattering plots for living, healthy soybean leaves. Figures 24 through 28 are the results for top incidence and Figures 29 through 33 are the results

SOYBEAN LEAVES

5 Samples

λ	θ_{inc}	θ_{coll}	Incident Surface	Mean Value of Radius Vector	Standard Deviation
500 nm	0°	180°	Top	3.516	0.445
550 nm	0°	180°	Top	16.360	2.542
500 nm	45°	180°	Top	1.378	0.234
550 nm	45°	180°	Top	10.970	1.810
500 nm	0°	45°	Top	4.275	0.470
550 nm	0°	45°	Top	7.470	1.128
500 nm	45°	45°	Top	11.556	2.455
550 nm	45°	45°	Top	14.300	3.055
500 nm	0°	180°	Bottom	3.460	0.498
550 nm	0°	180°	Bottom	16.410	2.240
500 nm	45°	180°	Bottom	1.302	0.147
550 nm	45°	180°	Bottom	10.150	1.445
500 nm	0°	45°	Bottom	7.13	1.063
550 nm	0°	45°	Bottom	12.10	1.860
500 nm	45°	45°	Bottom	15.71	2.460
550 nm	45°	45°	Bottom	21.49	3.920

TABLE 3. SOYBEAN LEAF CONSISTENCY EXPERIMENT

Figure 24. Soybean Leaf Relative $[\rho' \cos\theta_{coll}]$ and Relative $[\tau' \cos(\pi - \theta_{coll})]$ versus θ_{coll} for Top Incidence at $\theta_{inc} = 0^{\circ}$.

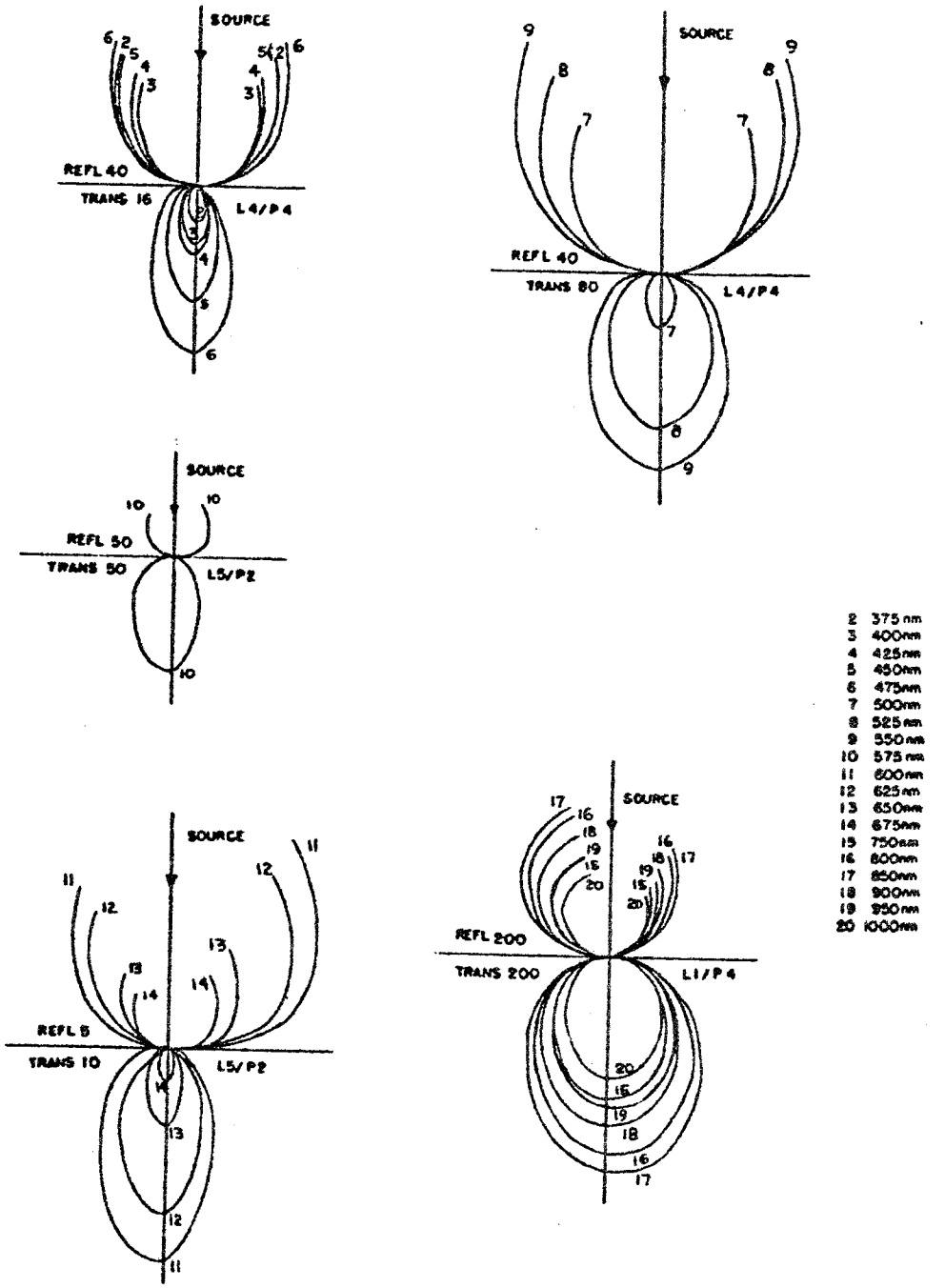
SOURCE
REFL 40
TRANS 16
L4/P4
SOURCE
REFL 40
TRANS 80
L4/P4
SOURCE
REFL 50
TRANS 50
L5/P2
SOURCE
REFL 5
TRANS 10
L5/P2
SOURCE
REFL 200
TRANS 200
L1/P4
2 375 nm
3 400nm
4 425nm
5 450nm
6 475nm
7 500nm
8 525nm
9 550nm
10 575nm
11 600nm
12 625nm
13 650nm
14 675nm
15 750nm
16 800nm
17 850nm
18 900nm
19 950nm
20 1000nm

Figure 24.

Figure 25. Soybean Leaf Relative $[\rho'\cos\theta_{coll}]$ and Relative $[\tau'\cos(\pi - \theta_{coll})]$ versus θ_{coll} for Top Incidence at $\theta_{inc} = 15^{o}$.

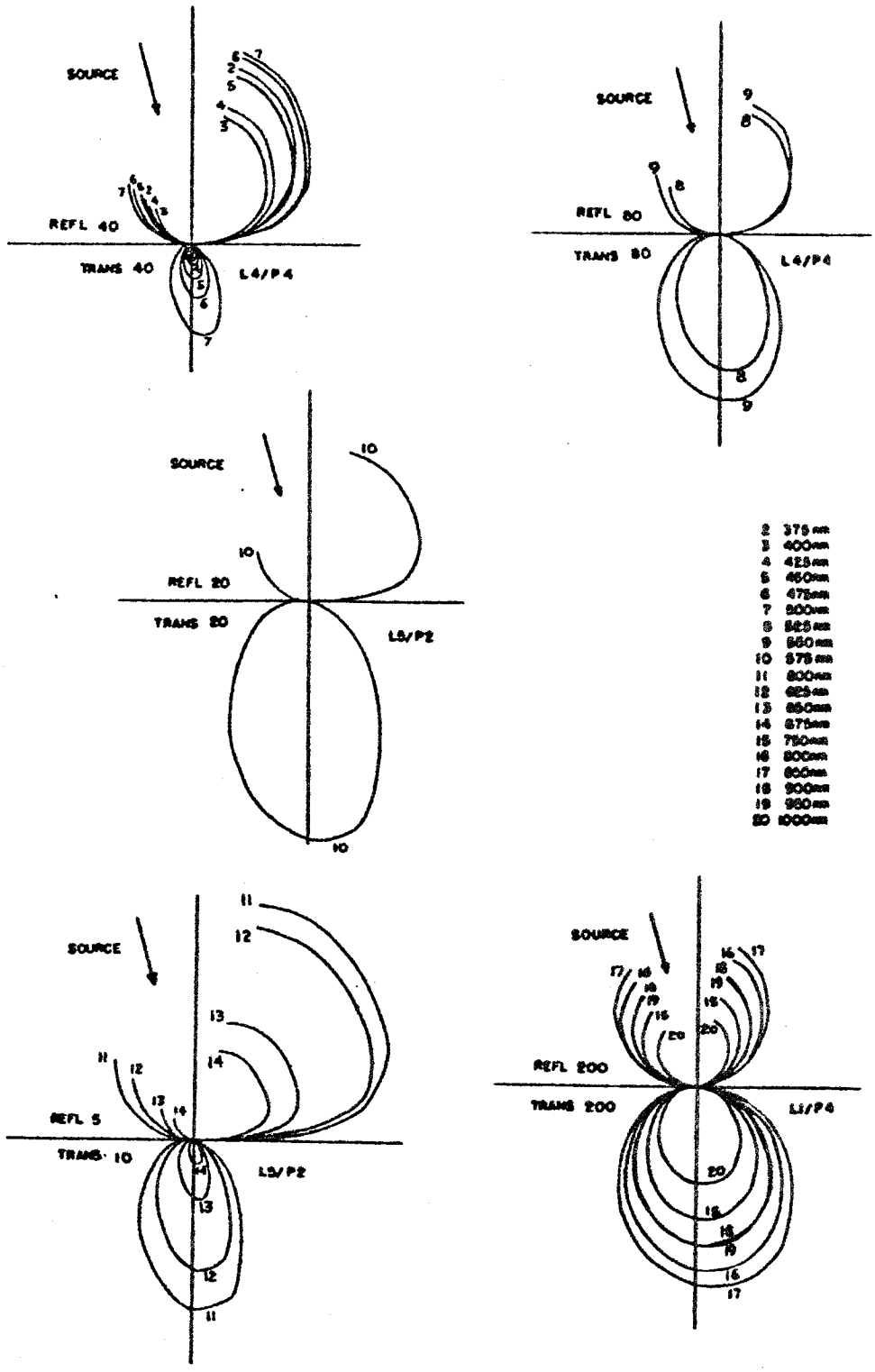
SOURCE
REFL 40
TRANS 40
L4/P4
SOURCE
REFL 80
TRANS 80
L4/P4
SOURCE
REFL 20
TRANS 20
L5/P2
2 375 nm
3 400nm
4 425 nm
5 450nm
6 475nm
7 500nm
8 525 nm
9 550 nm
10 575 nm
11 600nm
12 625 nm
13 650nm
14 675nm
15 700nm
16 800nm
17 850nm
18 900nm
19 950 nm
20 1000nm
SOURCE
REFL 5
TRANS 10
L5/P2
SOURCE
REFL 200
TRANS 200
L1/P4

Figure 25.

Figure 26. Soybean Leaf Relative $[\rho' \cos \theta_{coll}]$ and Relative $[\tau' \cos(\pi - \theta_{coll})]$ versus θ_{coll} for Top Incidence at $\theta_{inc} = 30^{o}$.

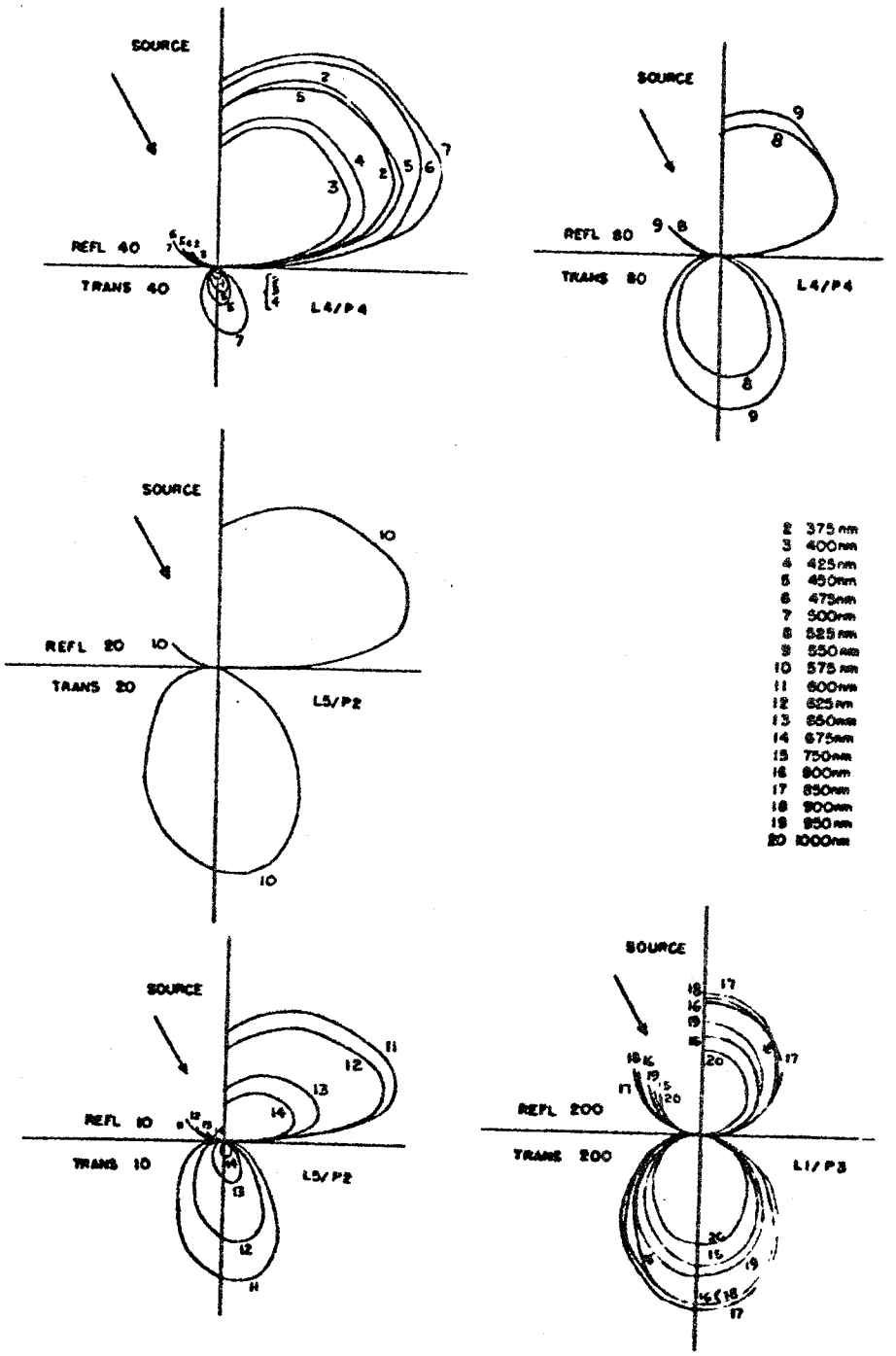
SOURCE
REFL 40
TRANS 40
L4/P4
SOURCE
REFL 80
TRANS 80
L4/P4
SOURCE
REFL 20
TRANS 20
L5/P2
2 375nm
3 400nm
4 425nm
5 450nm
6 475nm
7 500nm
8 525nm
9 550nm
10 575nm
11 600nm
12 625nm
13 650nm
14 675nm
15 750nm
16 800nm
17 850nm
18 900nm
19 950nm
20 1000nm
SOURCE
REFL 10
TRANS 10
L5/P2
SOURCE
REFL 200
TRANS 200
L1/P3

Figure 26.

Figure 27. Soybean Leaf Relative $[\rho' \cos\theta_{coll}]$ and Relative $[\tau' \cos(\pi - \theta_{coll})]$ versus θ_{coll} for Top Incidence at $\theta_{inc} = 45^{o}$.

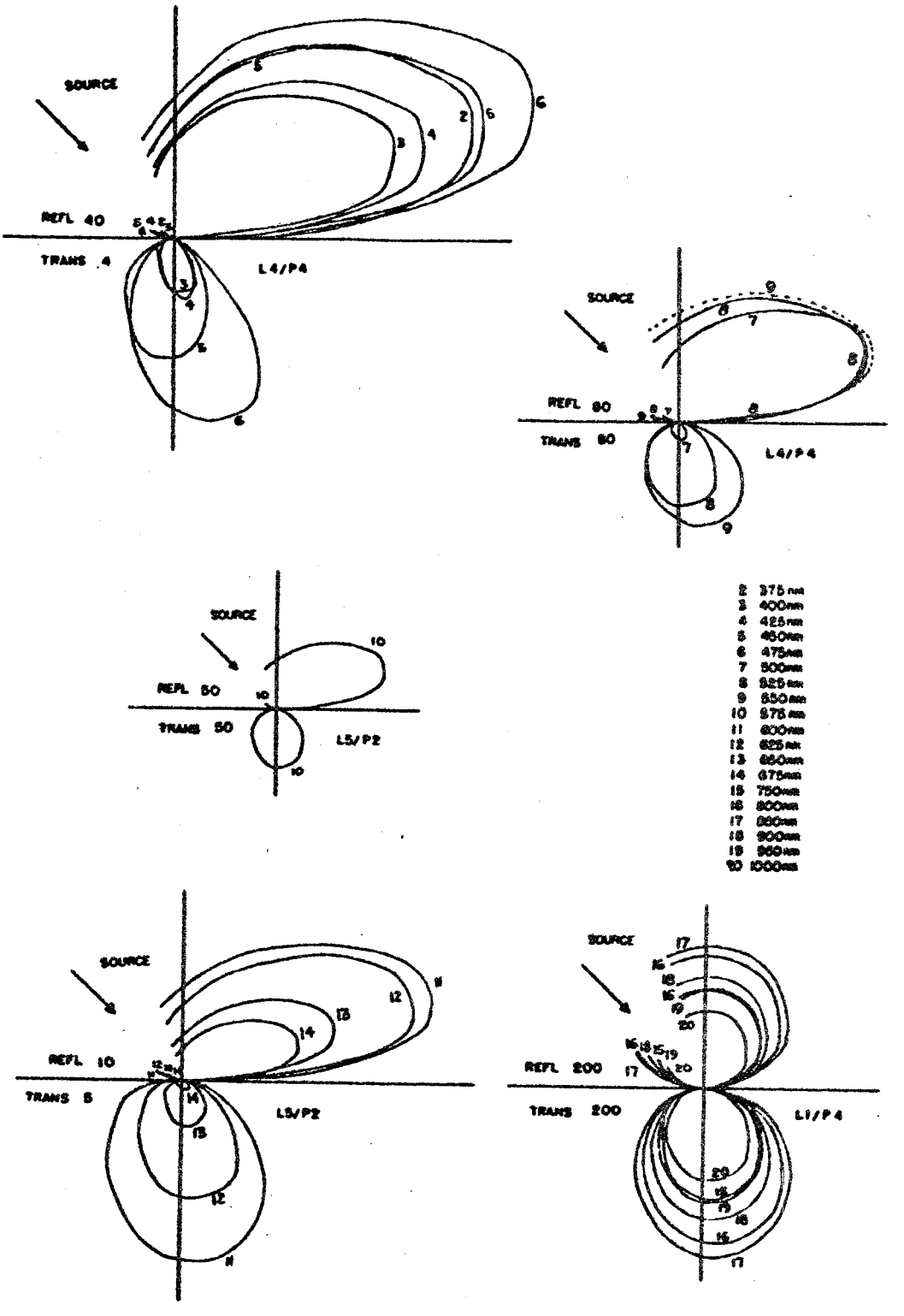
SOURCE
REFL 40
TRANS .4
L4/P4
SOURCE
REFL 80
TRANS 80
L4/P4
SOURCE
REFL 50
TRANS 50
L5/P2
2 375 nm
3 400nm
4 425nm
5 450nm
6 475nm
7 500nm
8 525nm
9 550nm
10 575nm
11 600nm
12 625nm
13 650nm
14 675nm
15 750nm
16 800nm
17 850nm
18 900nm
19 950nm
20 1000nm
SOURCE
REFL 10
TRANS 5
L5/P2
SOURCE
REFL 200
TRANS 200
L1/P4

Figure 27.

Figure 28. Soybean Leaf Relative $[\rho'\cos\theta_{coll}]$ and Relative $[\tau'\cos(\pi - \theta_{coll})]$ versus θ_{coll} for Top Incidence at $\theta_{inc} = 60^{\circ}$.

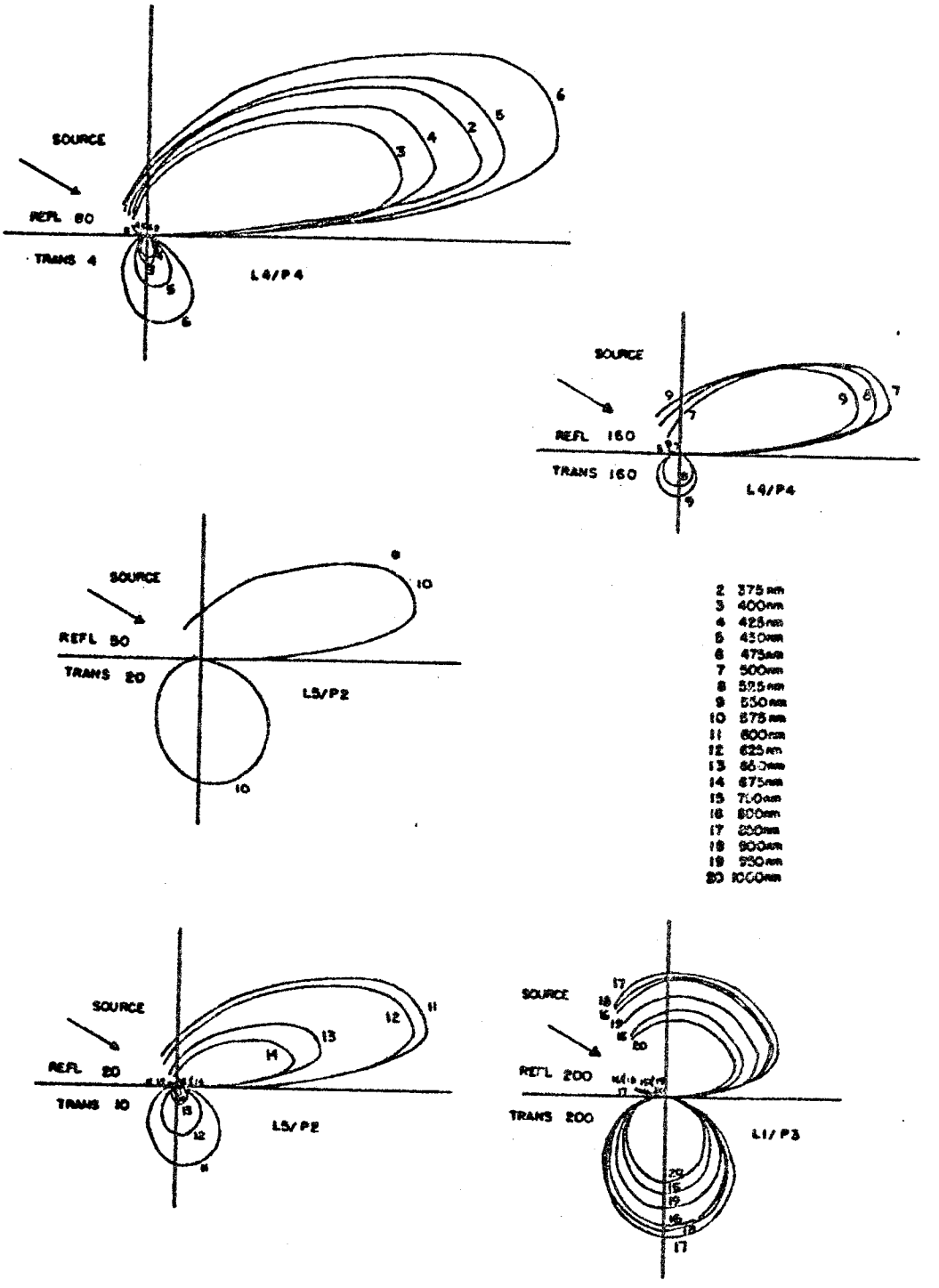
SOURCE
REFL 80
TRANS 4
L4/P4
SOURCE
REFL 160
TRANS 160
L4/P4
SOURCE
REFL 80
TRANS 20
L5/P2
2 375 nm
3 400nm
4 425nm
5 450nm
6 475nm
7 500nm
8 525nm
9 550nm
10 575nm
11 600nm
12 625nm
13 650nm
14 675nm
15 700nm
16 800nm
17 850nm
18 900nm
19 950nm
20 1000nm
SOURCE
REFL 20
TRANS 10
L5/P2
SOURCE
REFL 200
TRANS 200
L1/P3

Figure 28.

Figure 29. Soybean Leaf Relative $[\rho'\cos\theta_{coll}]$ and Relative $[\tau'\cos(\pi - \theta_{coll})]$ versus θ_{coll} for Bottom Incidence at $\theta_{inc} = 0^{o}$.

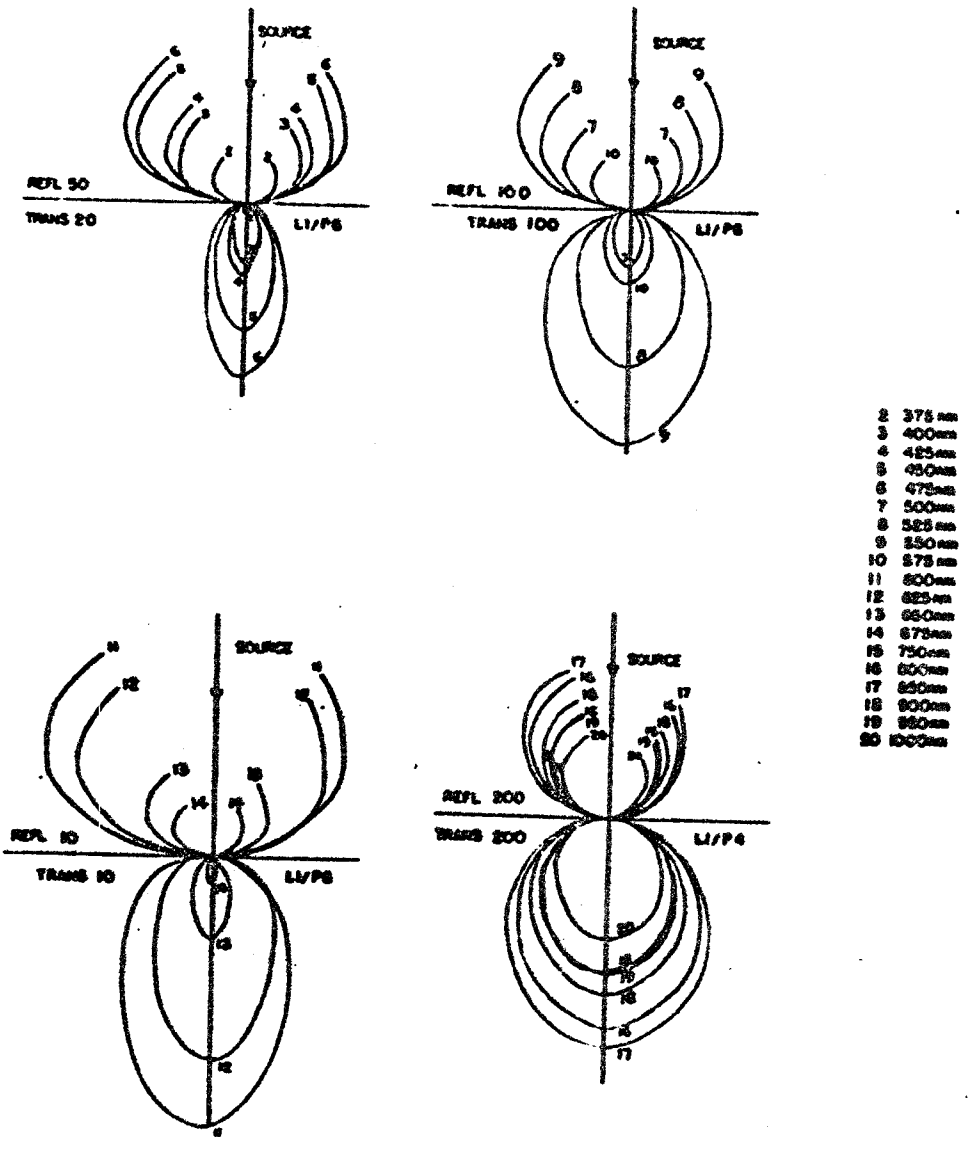
SOURCE
REFL 50
TRANS 20
LI/P6
SOURCE
REFL 100
TRANS 100
LI/P6
SOURCE
REFL 10
TRANS 10
LI/P6
SOURCE
REFL 200
TRANS 200
LI/P6
2 375 nm
3 400nm
4 425nm
5 450nm
6 475nm
7 500nm
8 525nm
9 550nm
10 575nm
11 600nm
12 625nm
13 650nm
14 675nm
15 700nm
16 800nm
17 850nm
18 900nm
19 950nm
20 1000nm

Figure 29.

Figure 30. Soybean Leaf Relative $[\rho' \cos\theta_{coll}]$ and Relative $[\tau' \cos(\pi - \theta_{coll})]$ versus θ_{coll} for Bottom Incidence at $\theta_{inc} = 15^{o}$.

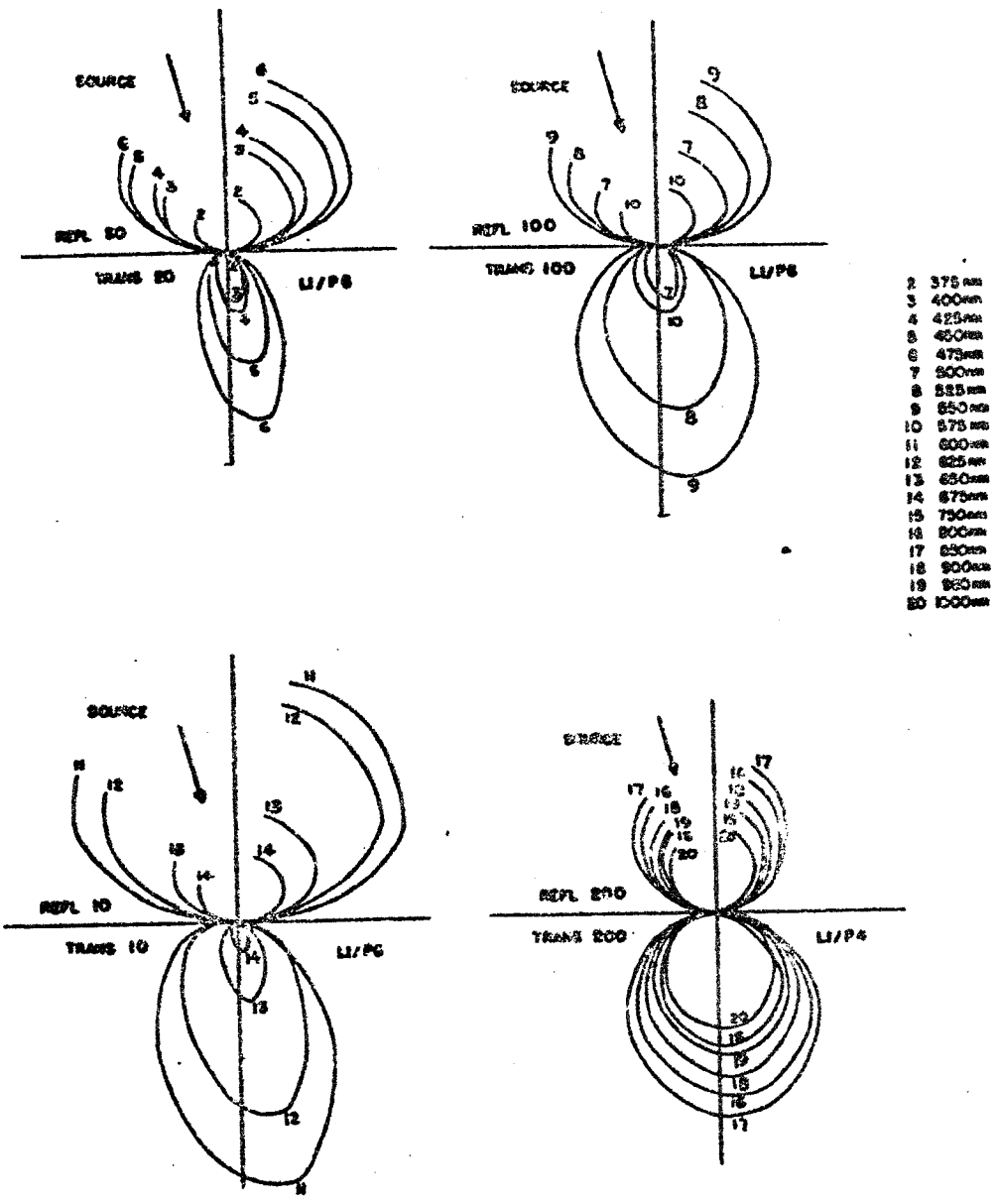
SOURCE
REFL 50
TRANS 50
LI/P6
SOURCE
REFL 100
TRANS 100
LI/P6
2 375 nm
3 400nm
4 425nm
5 450nm
6 475nm
7 500nm
8 525 nm
9 550 nm
10 575 nm
11 600 nm
12 625 nm
13 650nm
14 675nm
15 750nm
16 800nm
17 850nm
18 900nm
19 950 nm
20 1000nm
SOURCE
REFL 10
TRANS 10
LI/P6
SOURCE
REFL 200
TRANS 200
LI/P4

Figure 30.

Figure 31. Soybean Leaf Relative $[\rho' \cos\theta_{coll}]$ and Relative $[\tau' \cos(\pi - \theta_{coll})]$ versus θ_{coll} for Bottom Incidence at $\theta_{inc} = 30^{\circ}$.

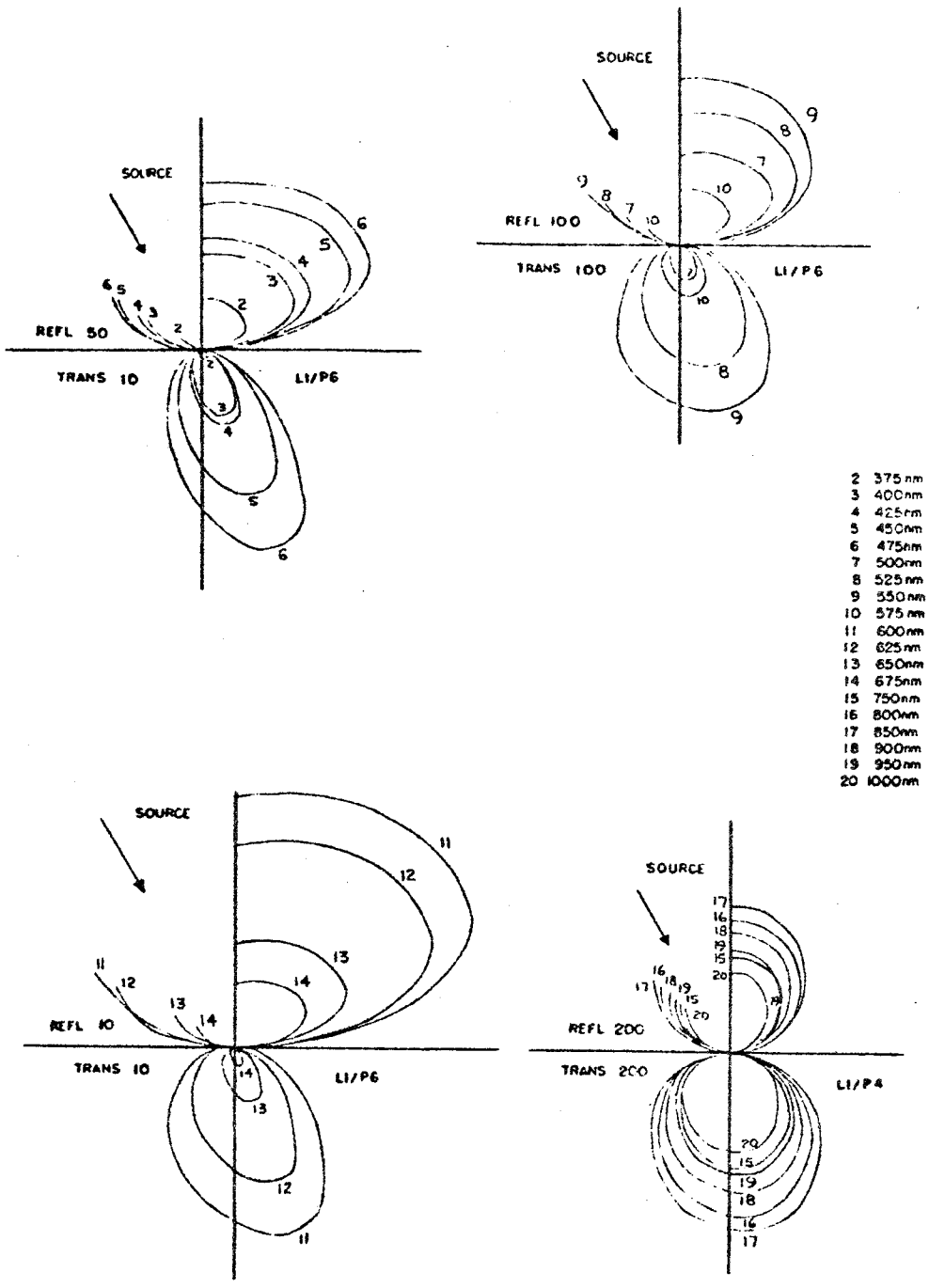
SOURCE
REFL 50
TRANS 10
LI/P6
SOURCE
REFL 100
TRANS 100
LI/P6
2 375nm
3 400nm
4 425nm
5 450nm
6 475nm
7 500nm
8 525nm
9 550nm
10 575nm
11 600nm
12 625nm
13 650nm
14 675nm
15 750nm
16 800nm
17 850nm
18 900nm
19 950nm
20 1000nm
SOURCE
REFL 10
TRANS 10
LI/P6
SOURCE
REFL 200
TRANS 200
LI/P4

Figure 31.

Figure 32. Soybean Leaf Relative $[\sigma'\cos\theta_{coll}]$ and Relative $[\tau'\cos(\pi-\theta_{coll})]$ versus θ_{coll} for Bottom Incidence at $\theta_{inc} = 45^{\circ}$.

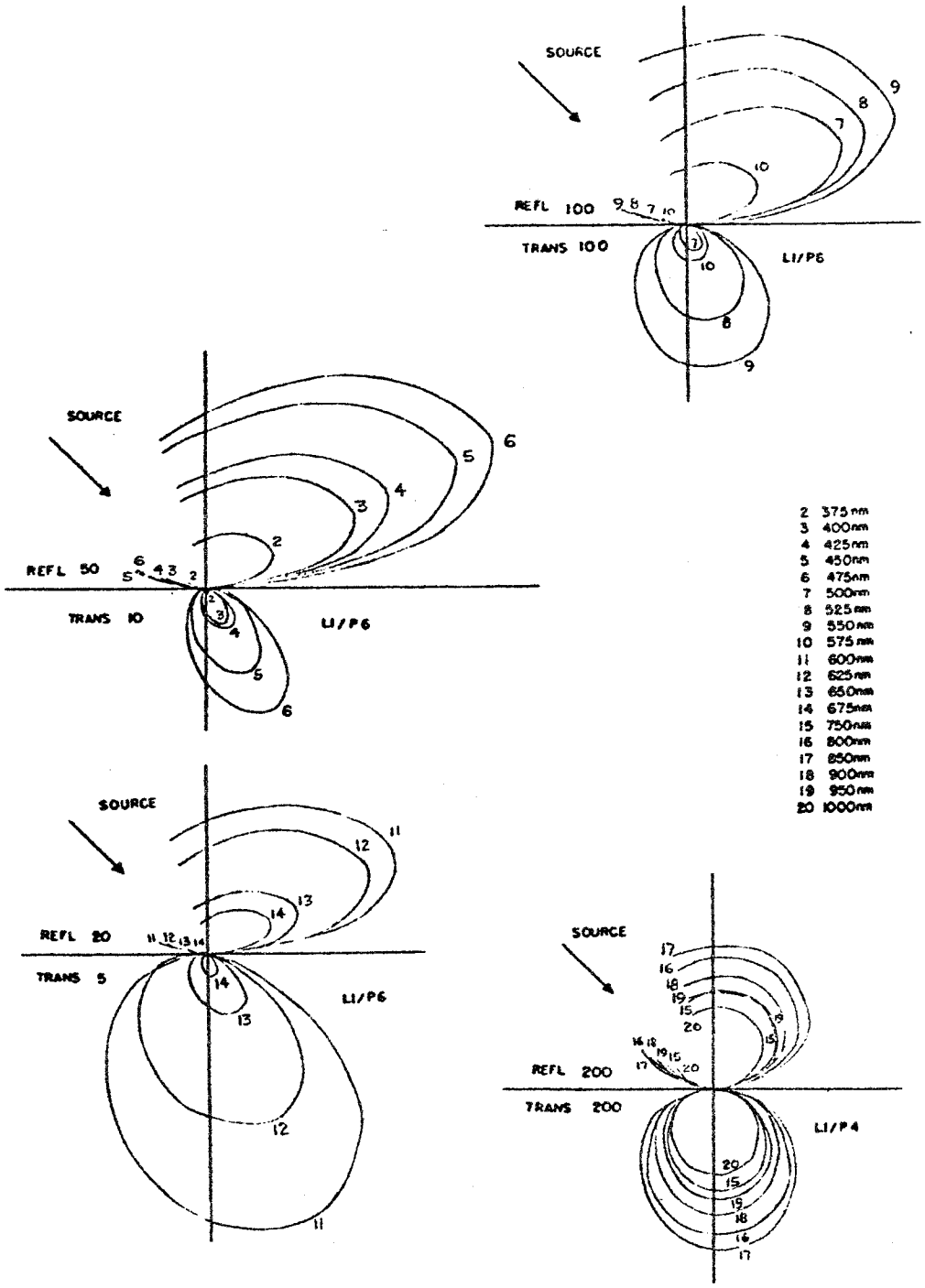
SOURCE
REFL 100
TRANS 100
LI/P6
SOURCE
REFL 50
TRANS 10
LI/P6
SOURCE
REFL 20
TRANS 5
LI/P6
SOURCE
REFL 200
TRANS 200
LI/P4
2 375nm
3 400nm
4 425nm
5 450nm
6 475nm
7 500nm
8 525nm
9 550nm
10 575nm
11 600nm
12 625nm
13 650nm
14 675nm
15 750nm
16 800nm
17 850nm
18 900nm
19 950nm
20 1000nm

Figure 32.

Figure 33. Soybean Leaf Relative [$\sigma'\cos\theta_{coll}$] and Relative [$\tau'\cos(\pi - \theta_{coll})$] versus θ_{coll} for Bottom Incidence at $\theta_{inc} = 60^{\circ}$.

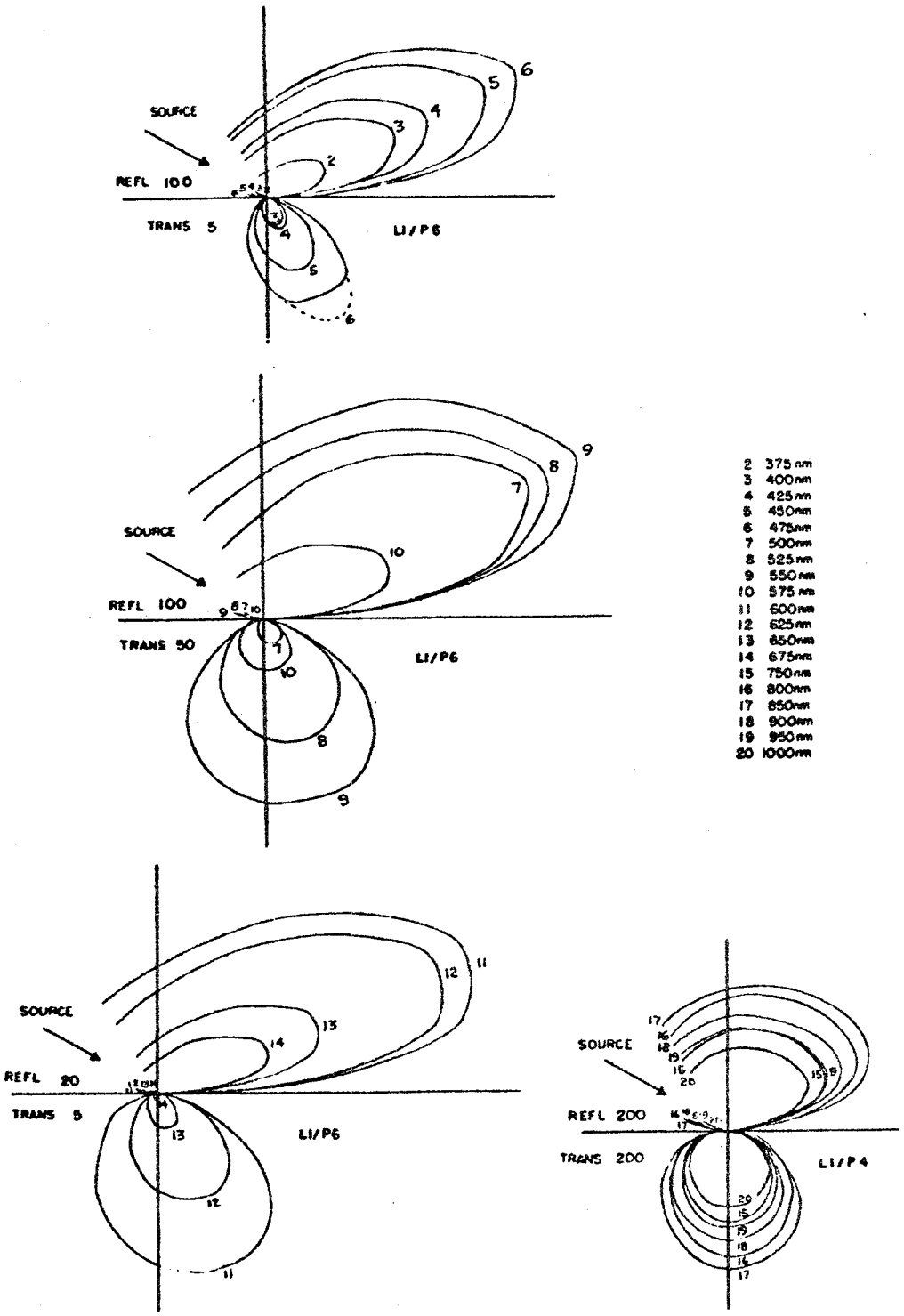
SOURCE
REFL 100
TRANS 5
LI/P6
SOURCE
REFL 100
TRANS 50
LI/P6
SOURCE
REFL 20
TRANS 5
LI/P6
SOURCE
REFL 200
TRANS 200
LI/P4
2 375 nm
3 400nm
4 425nm
5 450nm
6 475nm
7 500nm
8 525nm
9 550nm
10 575nm
11 600nm
12 625nm
13 650nm
14 675nm
15 750nm
16 800nm
17 850nm
18 900nm
19 950nm
20 1000nm

Figure 33.

for bottom incidence. This is a collection of 190 bi-directional scattering curves, representing 4560 individual data points.

The radial dimension on these bi-directional scattering plots is given in relative scattering units. These are the relative values of the scattering distribution function for a given collection angle and wavelength. The data curves which were obtained as described in the data processing section of the chapter on apparatus and procedure were all multiplied by a constant scale factor in order that the scales for presentation be larger than unity. The use of these relative units allows the selection of any linear scale to study the results. For example, a scale of 40 could be 40 relative scattering units per centimeter if centimeters are used consistently for study and comparison. The scale is given on the plot along with its use for reflection or transmission. The symbol REFL 40 designates a reflection scale of 40 relative scattering units per unit length and the symbol TRANS 16 designates a transmission scale of 16 relative scattering units per unit length. This is used since for several wavelength bands it is necessary to use different scales for reflection and transmission for data presentation. The procedure for converting these data to absolute units is given in the Apparatus and Procedures chapter.

Dashed lines are used where portions of two of the curves were estimated from results on other leaves from additional data runs and solid lines represent actual collected scattering data. The soybean leaf and plant designation is given for each scattering plot. For example, L5/P2 is used to designate leaf number 5 on plant number 2. A legend is given on each page to identify the wavelength at which the data were taken.

It was difficult to restrain the soybean leaf to a plane since it has a rough surface and a natural tendency to wrinkle, which caused several slight variations in the symmetry of the results. However, the effect is minor; for the most part the leaves could be fairly well restrained to a plane.

Scattering distribution functions versus wavelength for various collection angles are taken directly from the polar scattering plots. Figures 34 through 38 give the spectra for top incidence and Figures 39 through 43 gives the spectra for bottom incidence. The transmission curves are for a 180° collection angle which is along a normal to the leaf surface. This is a good measure of the transmission even though the functional forms vary for different incidence angles. The reflection curves are plotted for the specular angle except for normal incidence where a 45° collection angle is used. The unit is consistent throughout being 1 unit per 1/2 inch for a relative scattering unit scale of 20.

Results from several leaves are used to plot these spectra. The polar plots identify the leaf and the particular wavelength range.

Plots of the scattering distribution functions versus angle of incidence were constructed from these spectra for 450 nm, 550 nm, 650 nm, and 850 nm. These representative wavelengths were chosen in order to show these results for highly absorbing regions as well as for highly reflecting and transmitting regions. The curves for top and bottom incidence are plotted on the same graph for comparison. Different leaves are used for top and bottom curves and different leaves are sometimes used for each wavelength range. The polar plots identify the leaves used for each set of conditions. Figures 44 and 45 give the

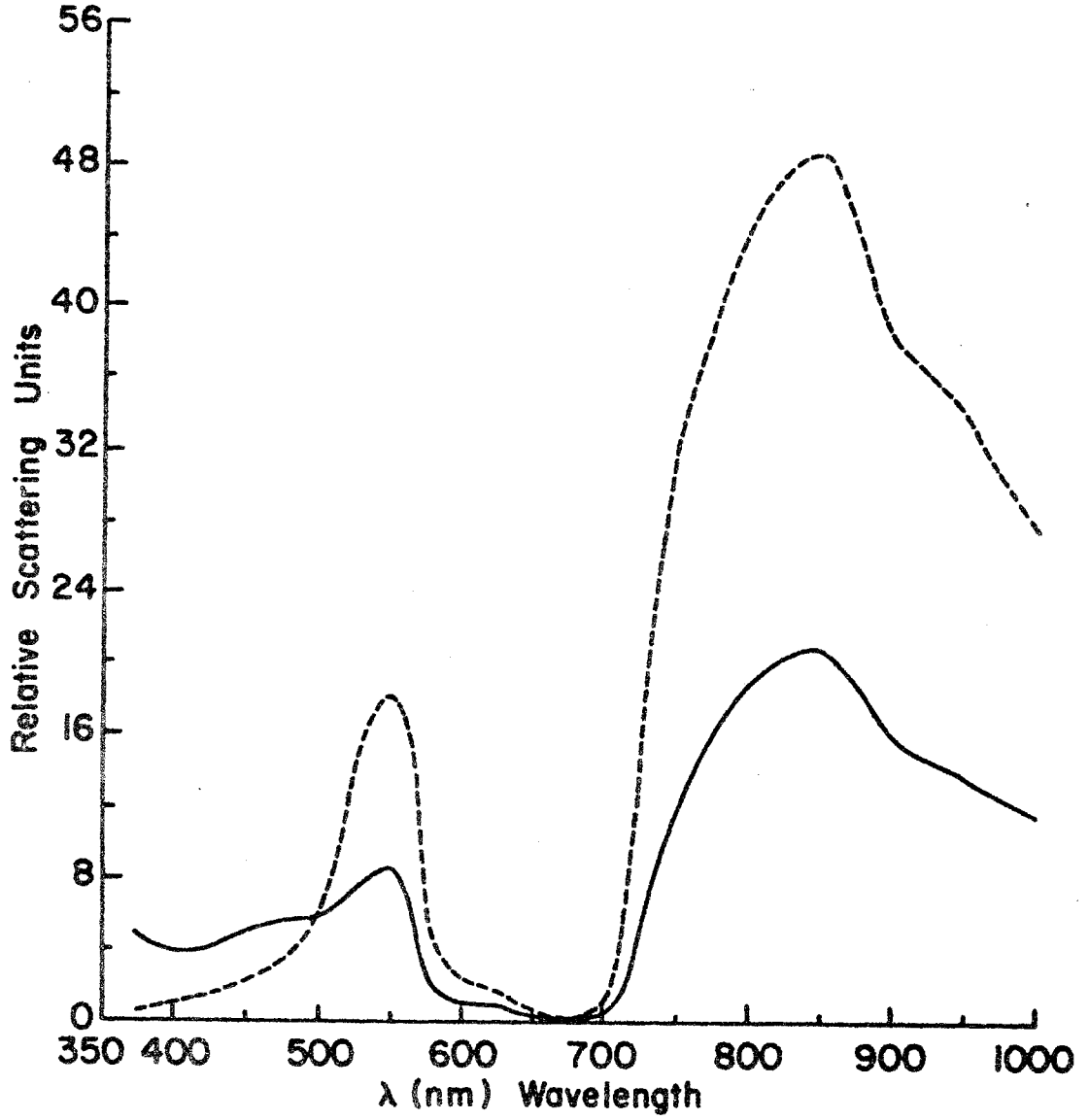

Figure 34. Soybean Leaf Relative $[\rho'\cos\theta_{coll}]$(_____) at $\theta_{coll} = 45^{\circ}$ and Relative $[\tau'\cos(\pi - \theta_{coll})]$(———) at $\theta_{coll} = 180^{\circ}$ versus λ for Top Incidence at $\theta_{inc} = 0^{\circ}$.

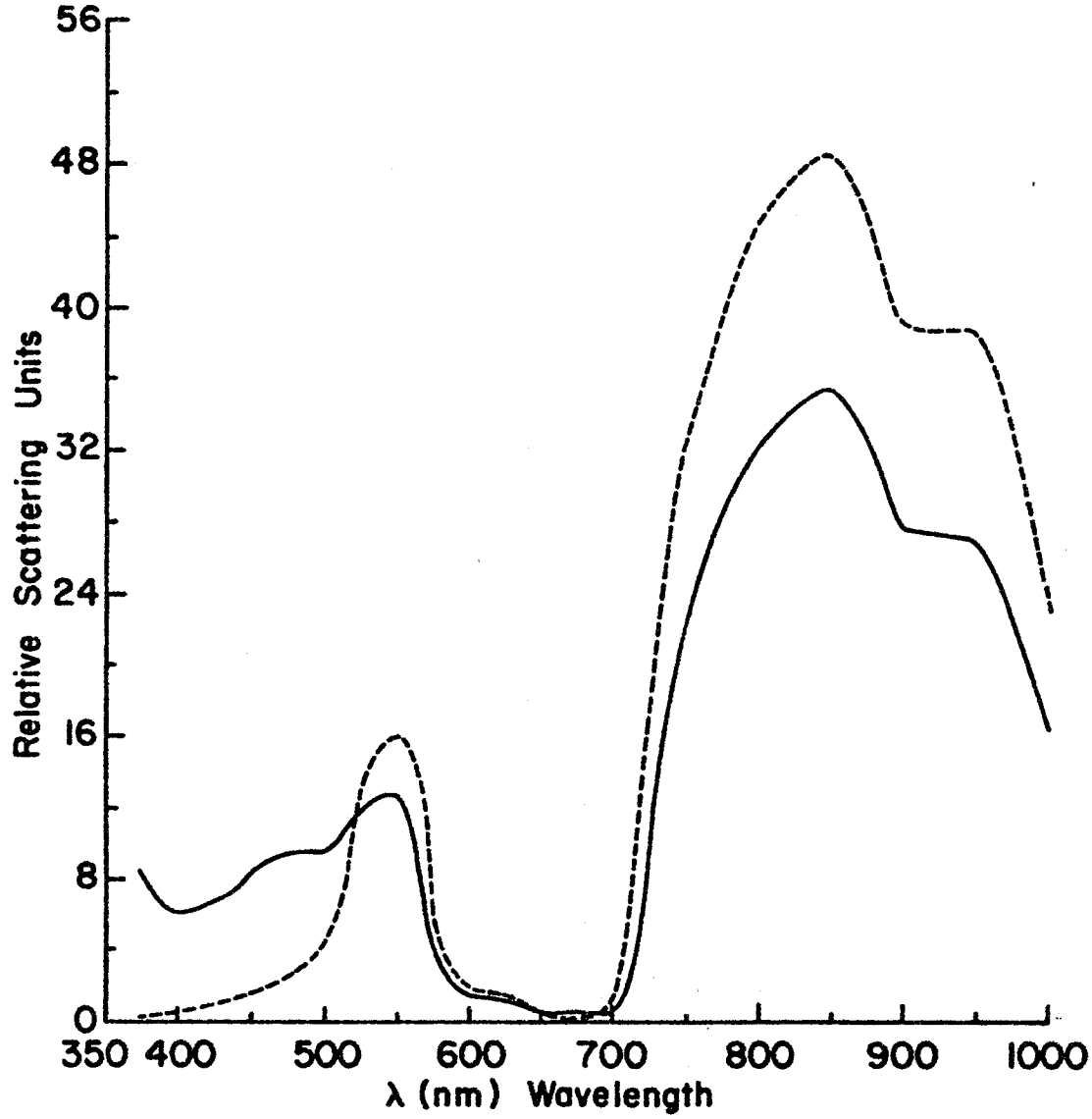

Figure 35. Soybean Leaf Relative $[\rho'\cos\theta_{coll}]$(_____) at $\theta_{coll} = 15^{\circ}$ and Relative $[\tau'\cos(\pi - \theta_{coll})]$(------) at $\theta_{coll} = 180^{\circ}$ versus λ for Top Incidence at $\theta_{inc} = 15^{\circ}$.

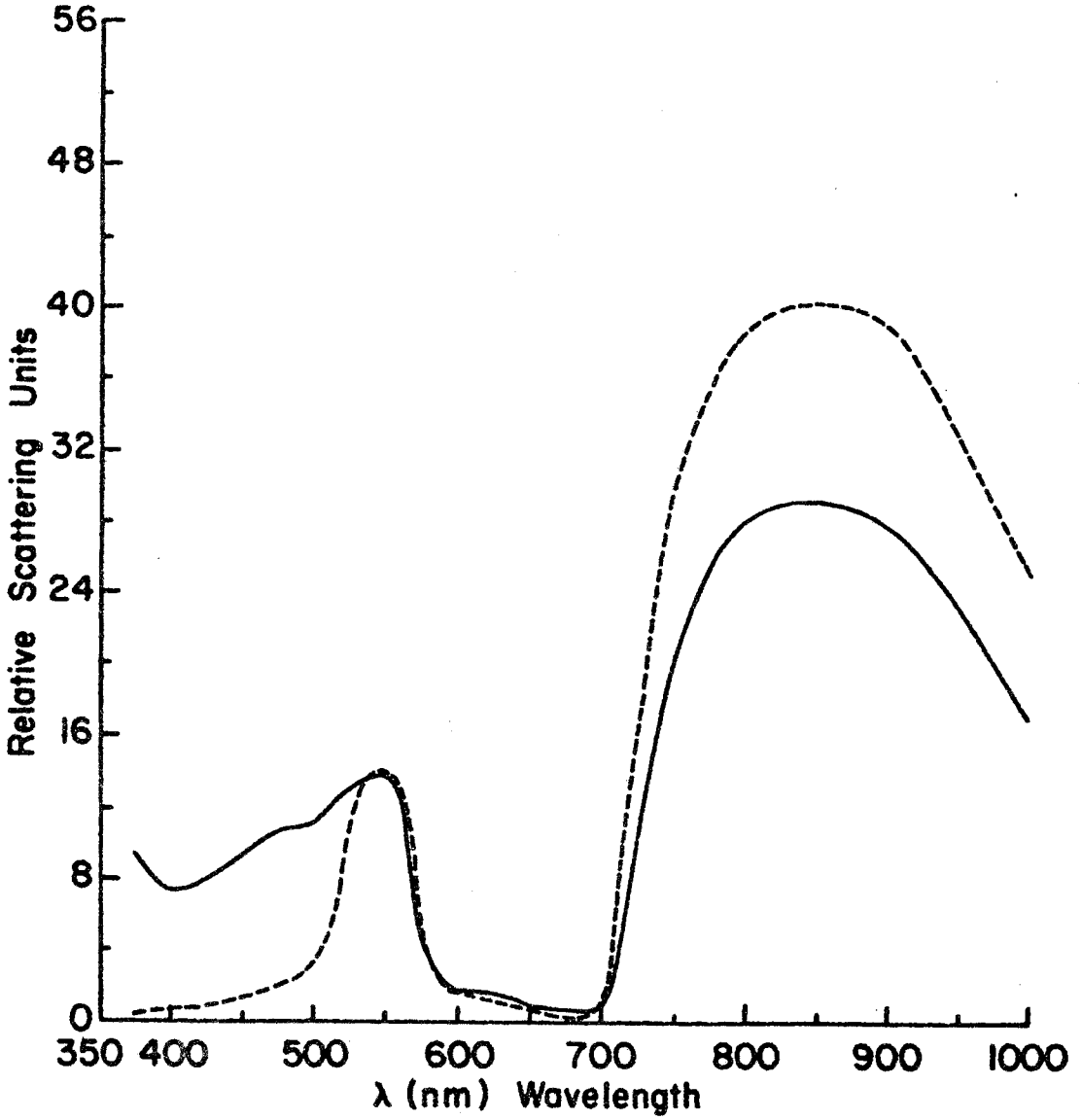

Figure 36. Soybean Leaf Relative $[\rho'\cos\theta_{coll}](\_\_\_\_)$ at $\theta_{coll} = 30^{\circ}$ and Relative $[\tau'\cos(\pi - \theta_{coll})](----)$ at $\theta_{coll} = 180^{\circ}$ versus λ for Top Incidence at $\theta_{inc} = 30^{\circ}$.

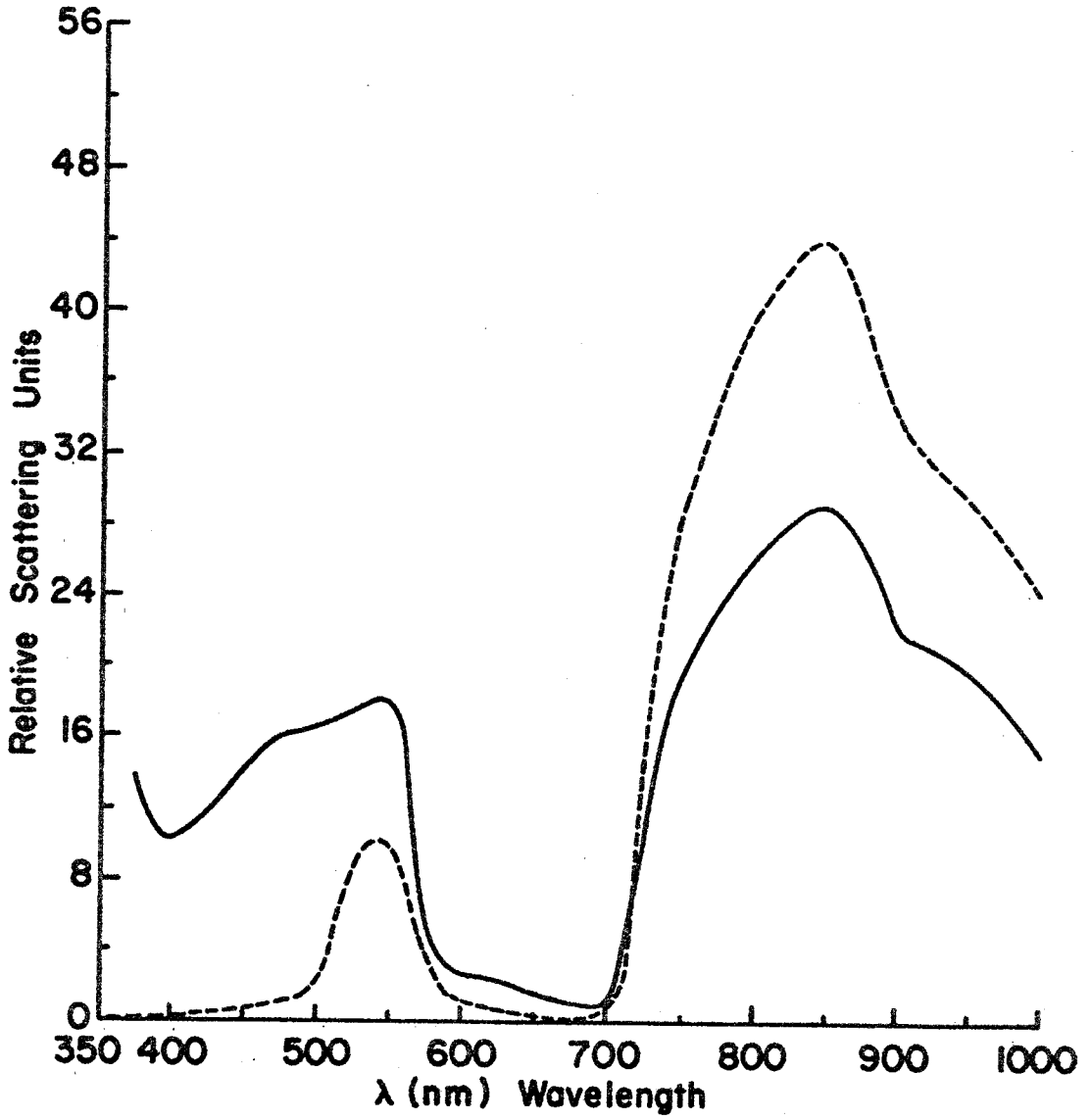

Figure 37. Soybean Leaf Relative $[\rho'\cos\theta_{coll}]$(_____) at $\theta_{coll} = 45^{\circ}$ and Relative $[\tau'\cos(\pi - \theta_{coll})]$(– – – –) at $\theta_{coll} = 180^{\circ}$ versus λ for Top Incidence at $\theta_{inc} = 45^{\circ}$.

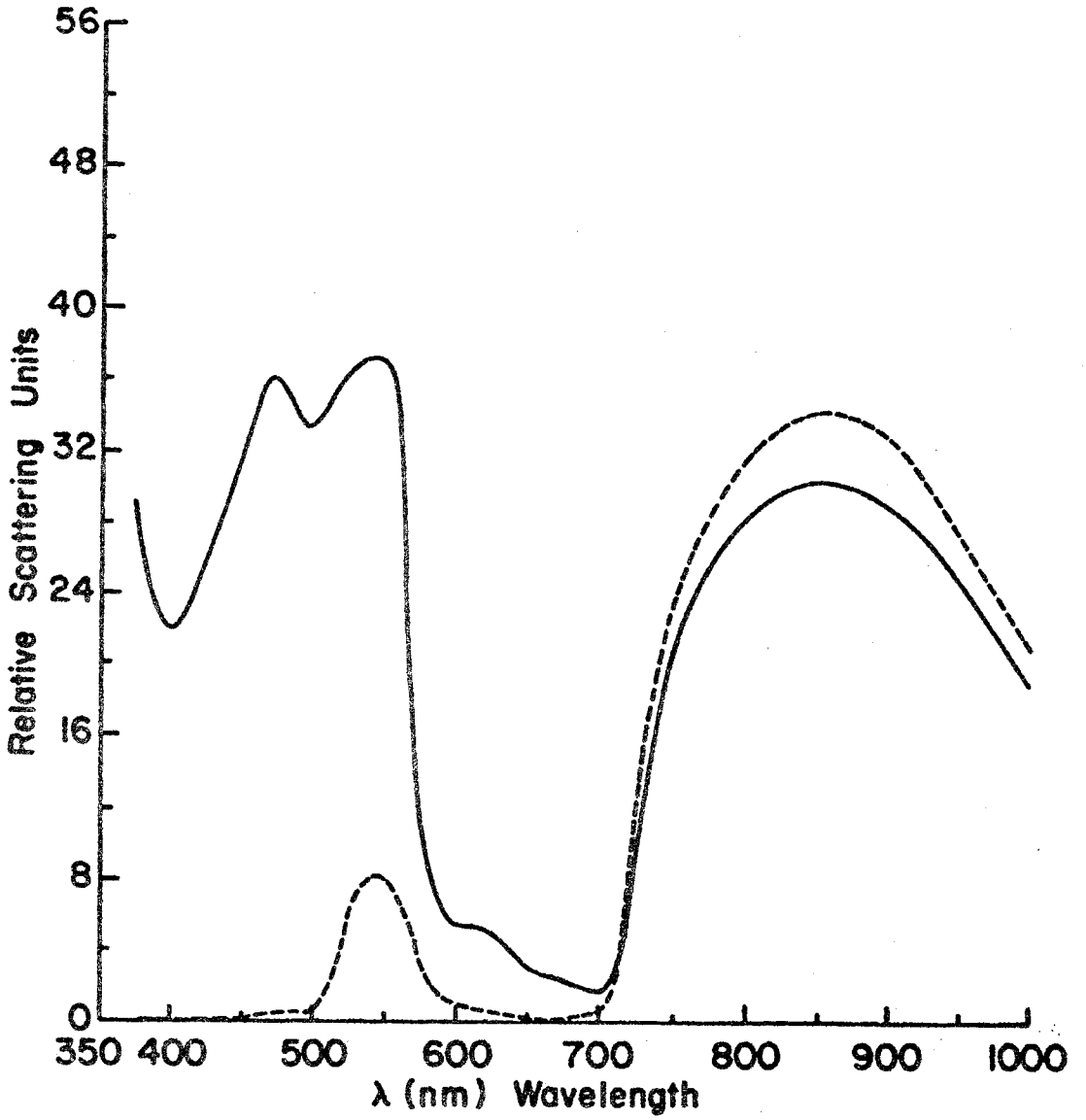

Figure 38. Soybean Leaf Relative $[\rho'\cos\theta_{coll}]$(_____) at $\theta_{coll} = 60^{\circ}$ and Relative $[\tau'\cos(\pi - \theta_{coll})]$(——) at $\theta_{coll} = 180^{\circ}$ versus λ for Top Incidence at $\theta_{inc} = 60^{\circ}$.

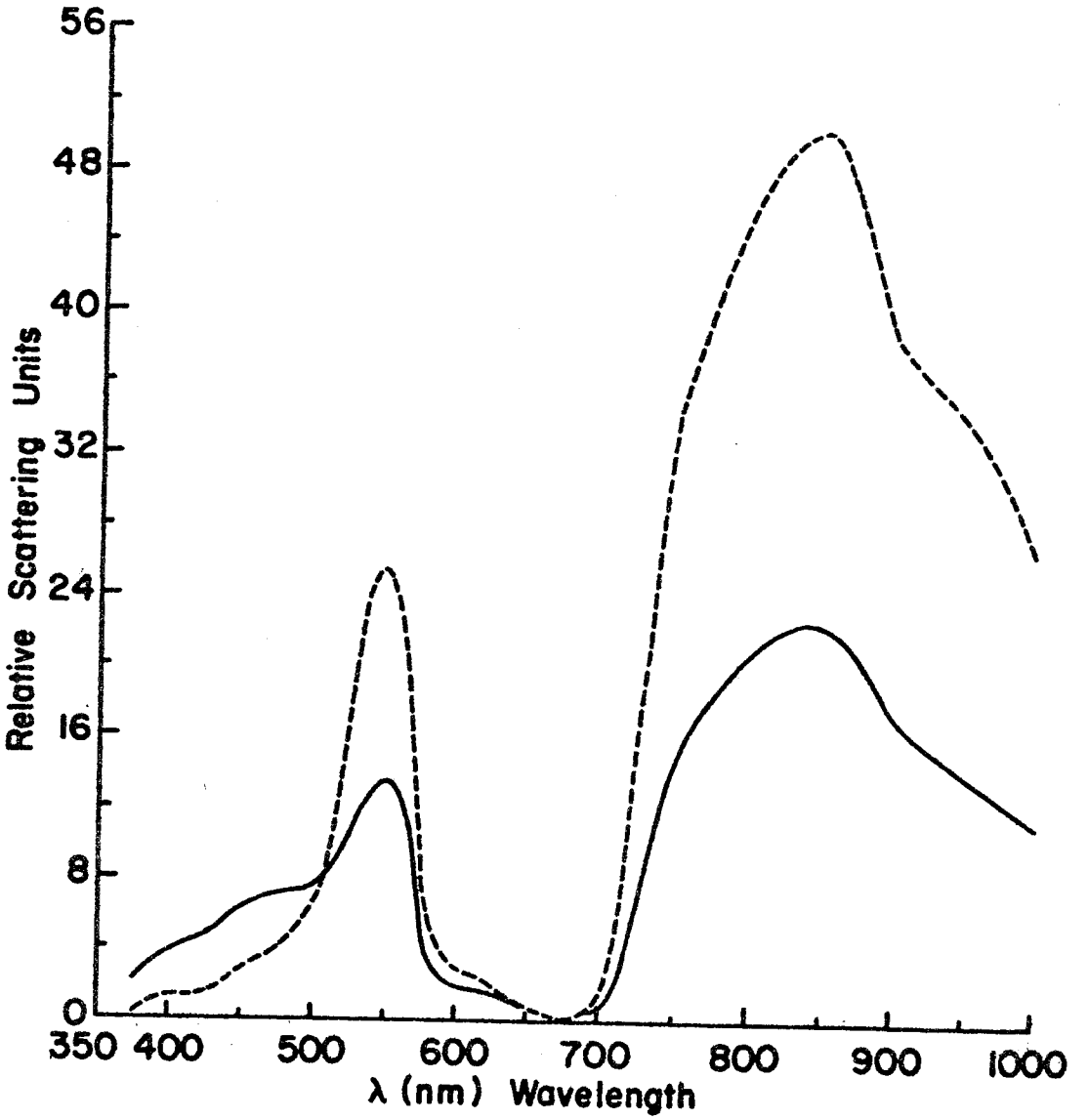

Figure 39. Soybean Leaf Relative $[\rho'\cos\theta_{coll}]$(_____) at $\theta_{coll} = 45^{o}$ and Relative $[\tau'\cos(\pi - \theta_{coll})]$(– – – –) at $\theta_{coll} = 180^{o}$ versus λ for Bottom Incidence at $\theta_{inc} = 0^{o}$.

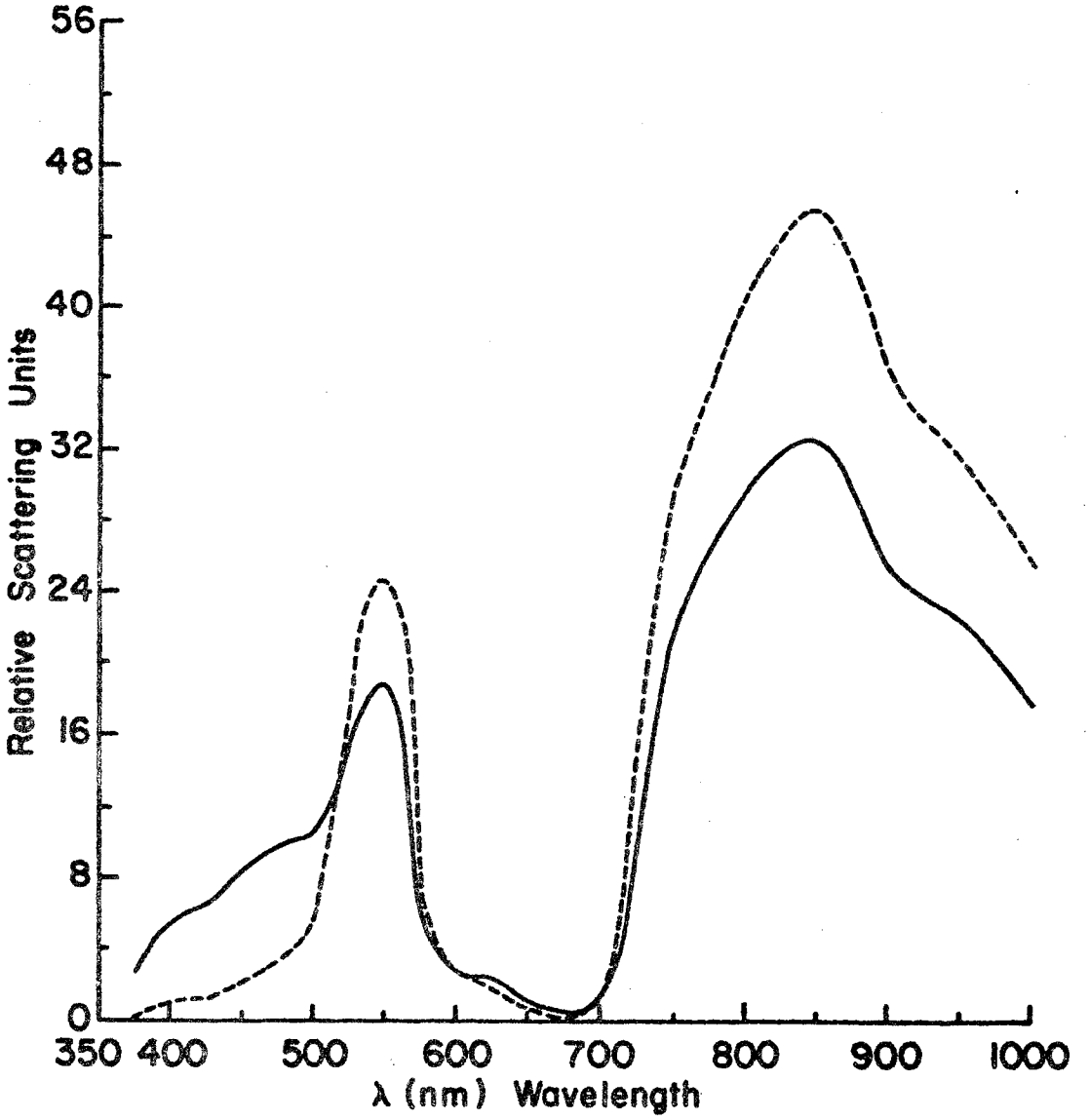

Figure 40. Soybean Leaf Relative $[\rho'\cos\theta_{coll}]$(_____) at $\theta_{coll} = 15^{o}$ and Relative $[\tau'\cos(\pi - \theta_{coll})]$(– – – –) at $\theta_{coll} = 180^{o}$ versus λ for Bottom Incidence at $\theta_{inc} = 15^{o}$.

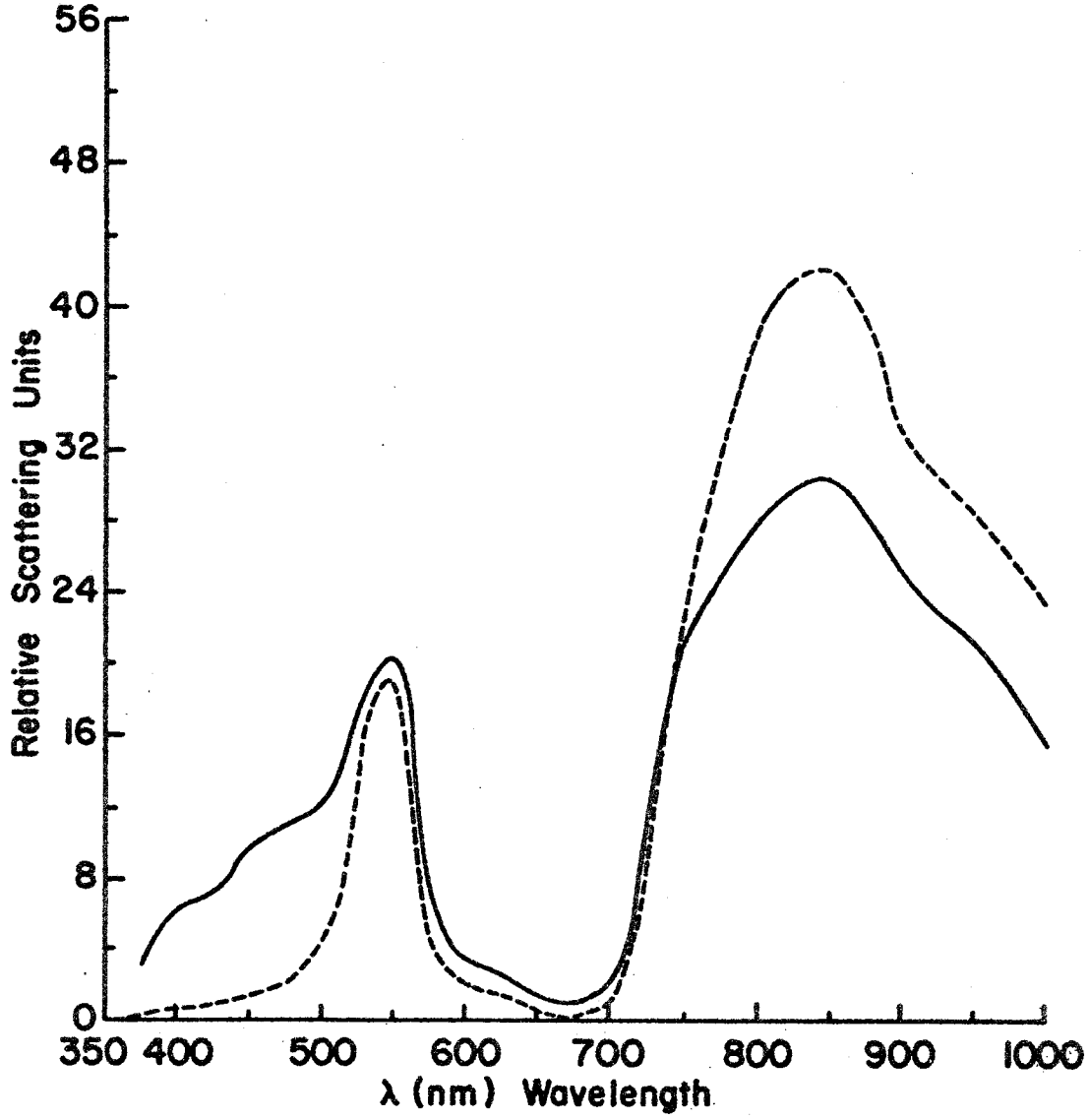

Figure 41. Soybean Leaf Relative $[\rho'\cos\theta_{coll}](\_\_\_\_\_)$ at $\theta_{coll} = 30^{\circ}$ and Relative $[\tau'\cos(\pi - \theta_{coll})](\text{———})$ at $\theta_{coll} = 180^{\circ}$ versus λ for Bottom Incidence at $\theta_{inc} = 30^{\circ}$.

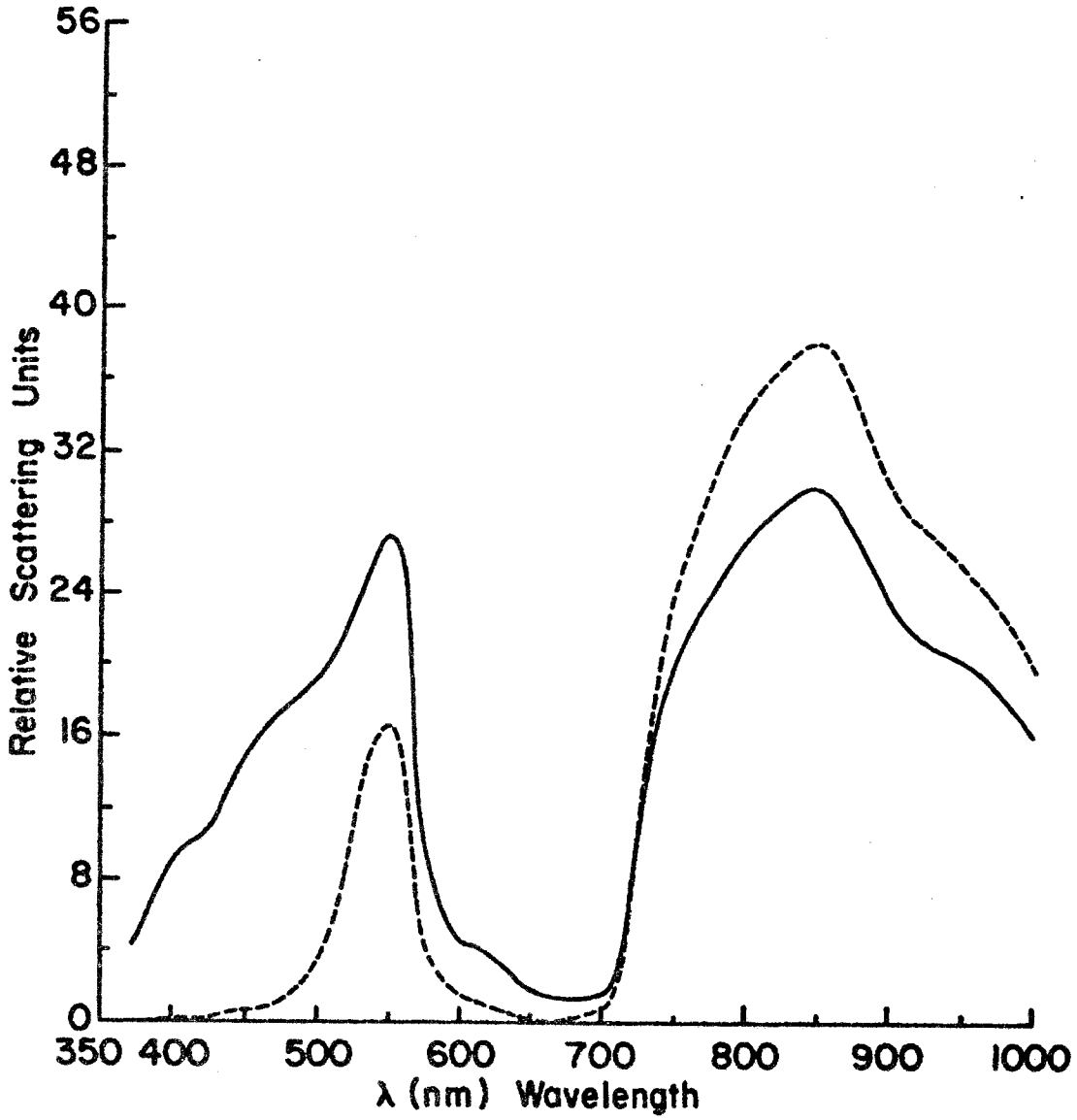

Figure 42. Soybean Leaf Relative $[\rho'\cos\theta_{coll}]$(_____) at $\theta_{coll} = 45^{\circ}$ and Relative $[\tau'\cos(\pi - \theta_{coll})]$(———) at $\theta_{coll} = 180^{\circ}$ versus λ for Bottom Incidence at $\theta_{inc} = 45^{\circ}$.

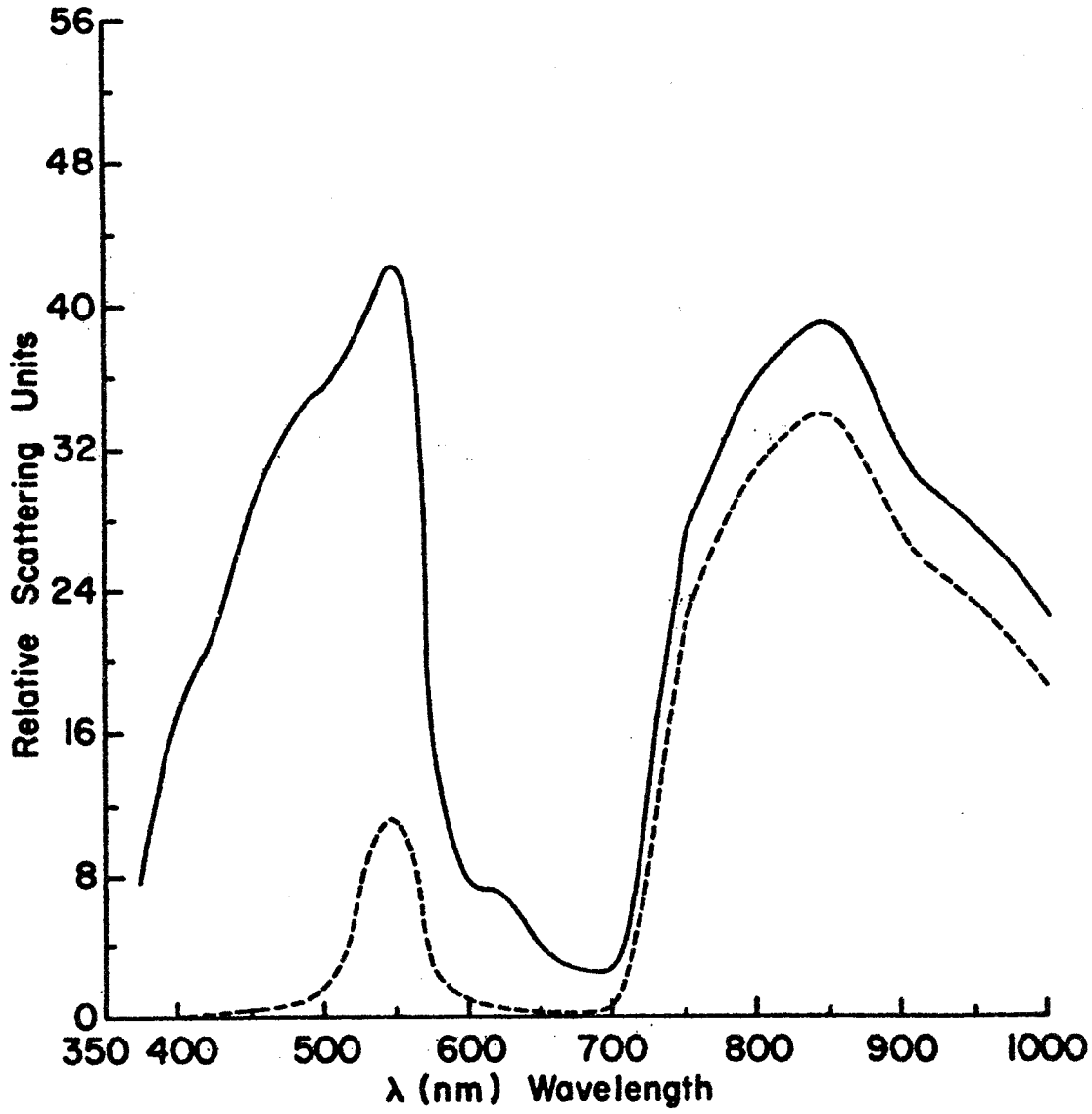

Figure 43. Soybean Leaf Relative $[\rho'\cos\theta_{coll}]$(_____) at $\theta_{coll} = 60^{\circ}$ and Relative $[\tau'\cos(\pi - \theta_{coll})]$(– – – –) at $\theta_{coll} = 180^{\circ}$ versus λ for Bottom Incidence at $\theta_{inc} = 60^{\circ}$.

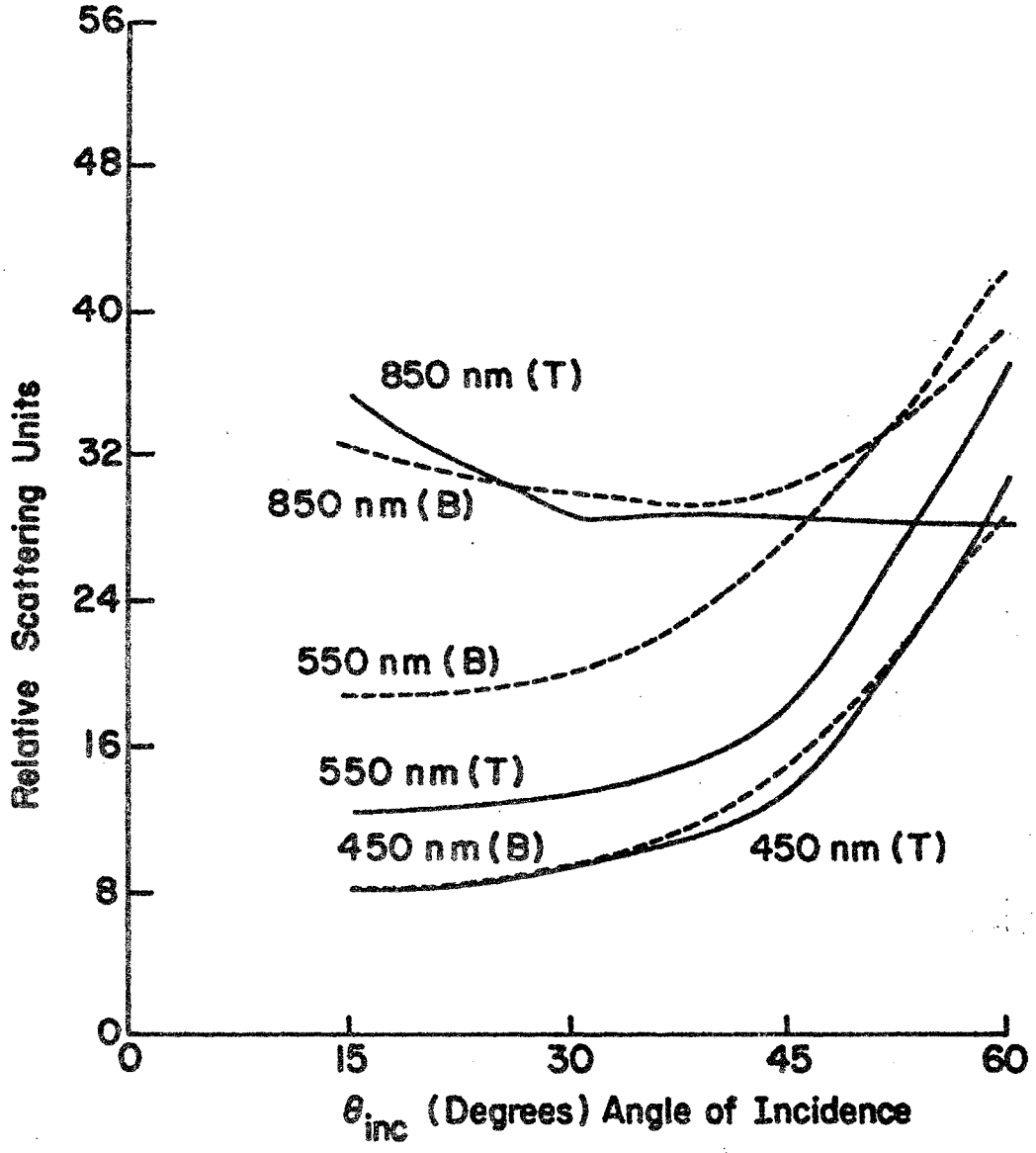

Figure 44. Soybean Leaf Relative [$\rho' \cos \theta_{coll}$] at the specular collection angle versus θ_{inc} for Top Incidence (_____) and Bottom Incidence (– – –) at 450 nm, 550 nm, and 850 nm.

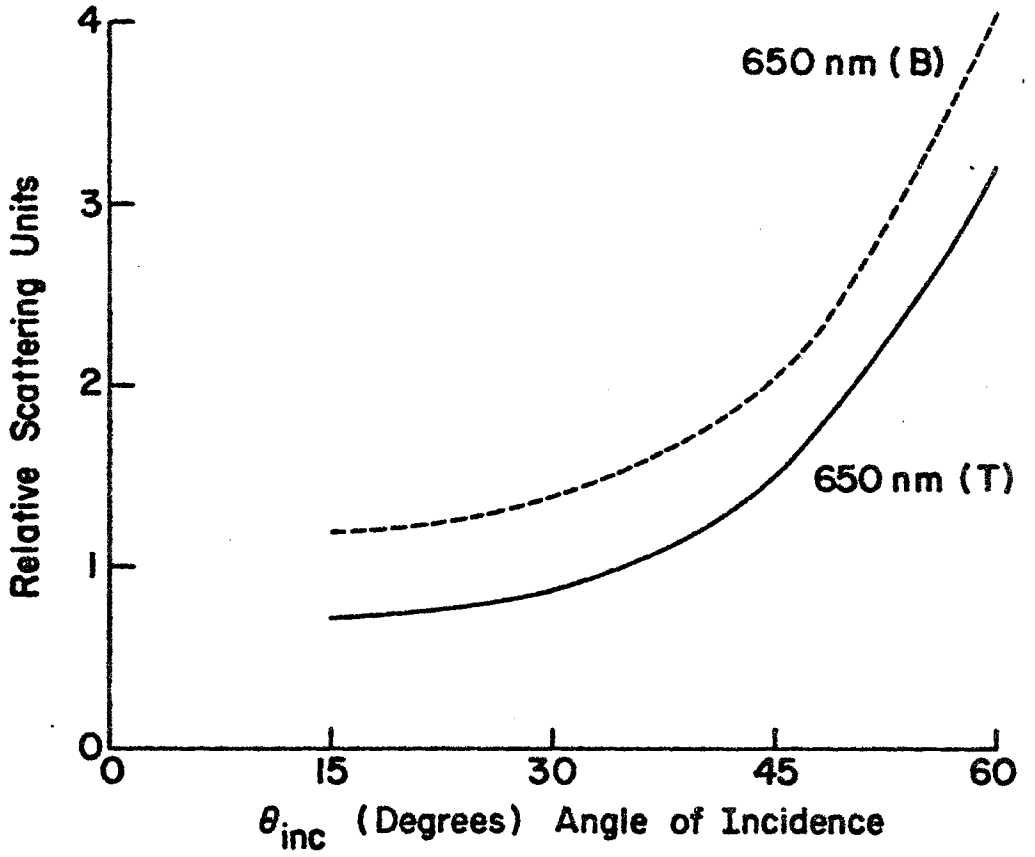

Figure 45. Soybean Leaf Relative $[\rho' \cos\theta_{coll}]$ at the specular collection angle versus θ_{inc} for Top Incidence (_____) and Bottom Incidence (– – –) at 650 nm.

scattering distribution function versus angle of incidence for reflection at the specular angle, for the representative wavelengths given above.

Figures 46 and 47 are the results for the scattering distribution function versus angle of incidence for transmission along a normal to the sample surface, for the representative wavelengths mentioned above.

The soybean leaf bi-directional scattering data were graphically analyzed to determine the angles for maximum reflection and transmission. It was difficult to make this graphical approximation of these angles since the polar plots are broad about these angles. Maximum reflection and transmission angles were determined from each of the polar plots given on the composite polar plot page for a particular angle of incidence. This was done for the range from 375 nm through 675 nm. The graph of Figure 48 gives the average of these points versus angle of incidence with the ideal mirror characteristic given for reference.

The transmission angles are measured counter-clockwise from a normal to the plane of the leaf sample so they can be plotted on the graph with the reflection angles.

Discussion of Results

A discussion of the experimental results is presented here with the major objective a classification of features for a bi-directional scattering model for a healthy, green soybean leaf.

Gross observations of the polar bi-directional scattering plots for soybean leaves show that the functional form of the scattering characteristics depends upon the angle of incidence. The reflection characteristic

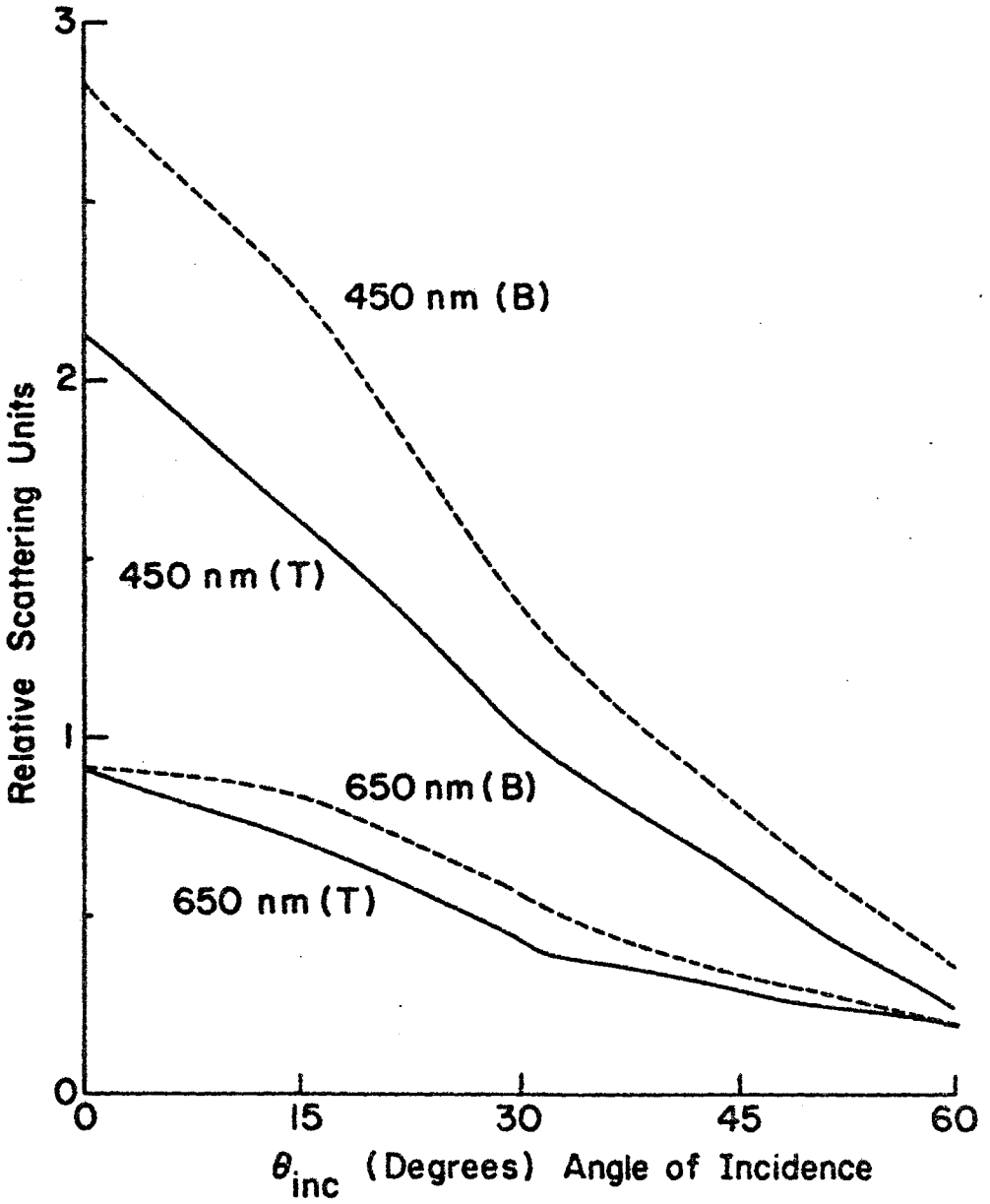

Figure 46. Soybean Leaf Relative $[\tau'\cos(\pi - \theta_{coll})]$ at $\theta_{coll} = 180^{\circ}$ versus θ_{inc} for Top Incidence (_____) and Bottom Incidence (– – – –) at 450 nm and 650 nm.

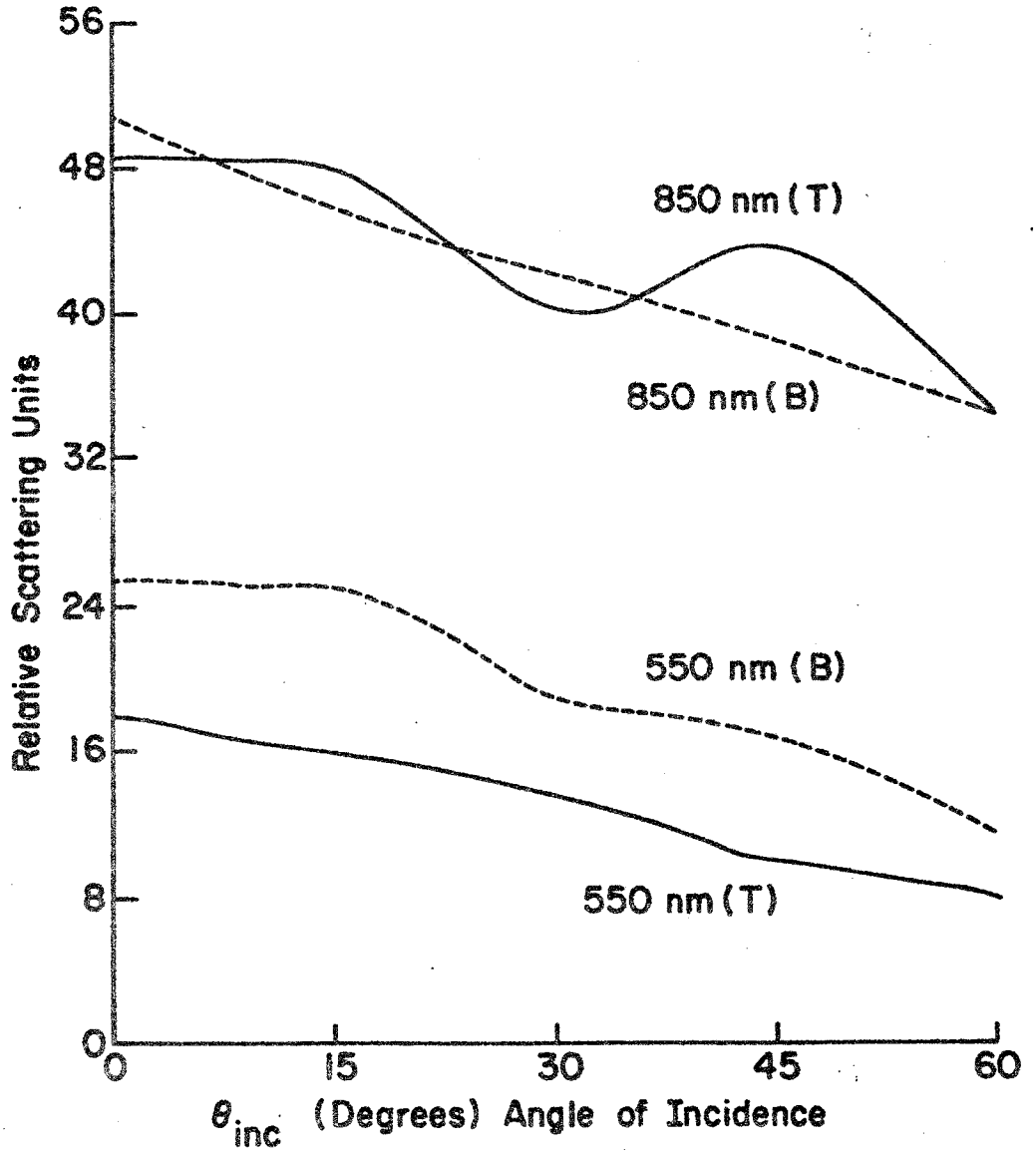

Figure 47. Soybean Leaf Relative $[\tau'\cos(\pi - \theta_{coll})]$ at $\theta_{coll} = 180^{\circ}$ versus θ_{inc} for Top Incidence (_____) and Bottom Incidence (———) at 550 nm and 850 nm.

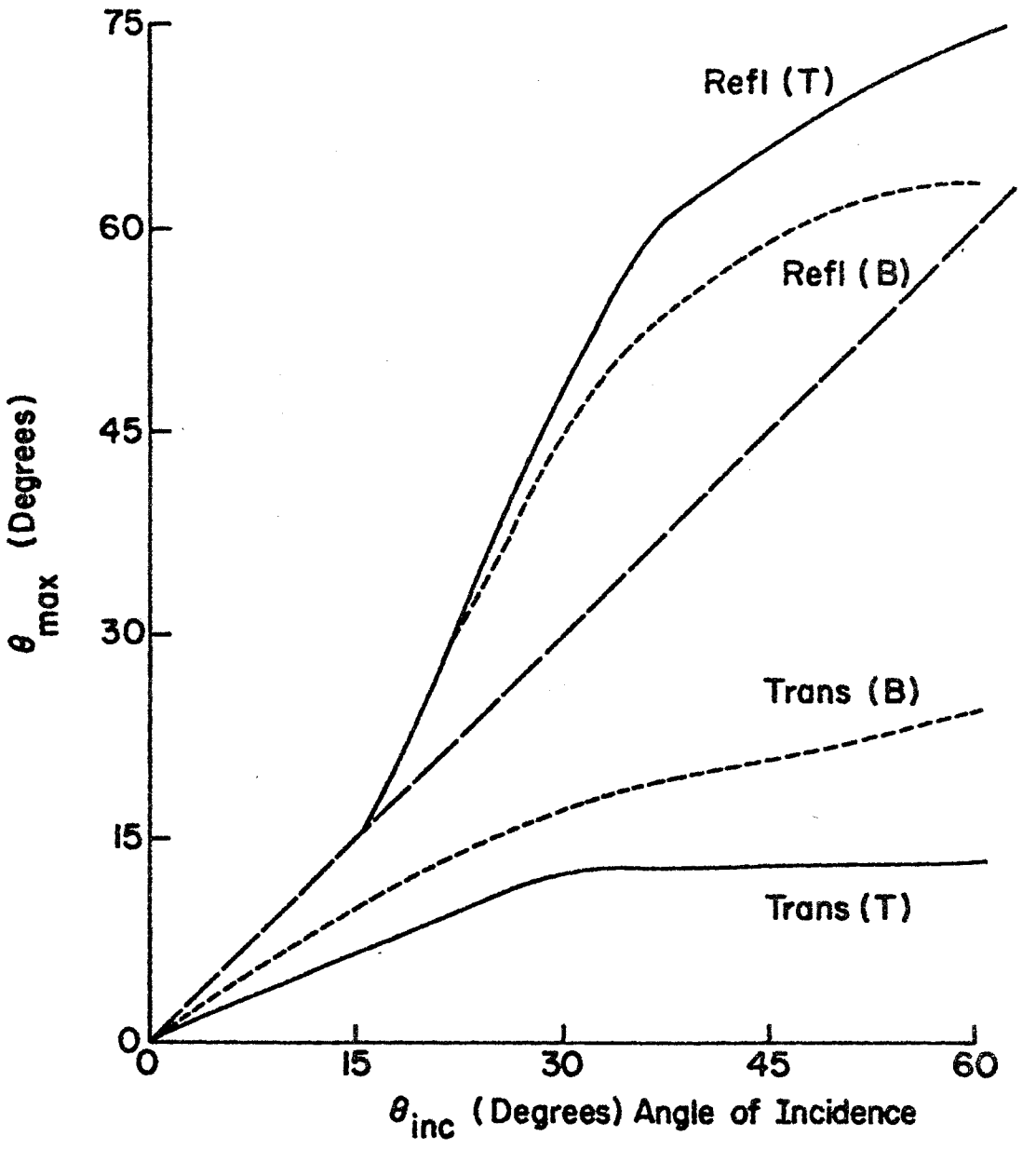

Figure 48. Soybean Leaf Average Collection Angle for Maximum Relative $[\rho'\cos\theta_{coll}]$ and Maximum Relative $[\tau'\cos(\pi - \theta_{coll})]$ versus θ_{inc} for Top Incidence (_____) and Bottom Incidence (– – – –) for the range of λ from 375 nm through 675 nm.

is apparently composed of both specular and diffuse components. Specular reflection is a familiar surface effect; however, diffuse reflection arises both from specular reflection on rough surfaces and from the radiation which enters the material and is scattered therein. The soybean transmission characteristic is apparently composed of a refracted component and a diffuse component.

The phrase "diffuse reflection" can have several connotations ranging from a theoretical development on a specific model, to a specific experimental definition (σ' = constant), to an empirical labelling of nonspecular reflected radiant power as a diffuse component.

There are two main theoretical developments of substance. In the first Chandrasekhar [2] presents the theoretical solution for diffuse reflection from plane-parallel atmospheres with Rayleigh scattering. Most of this theory is developed for isotropic scattering from atmospheres of a finite optical thickness with very little or no absorption. The result for this solution in polar form with intensity plotted versus collection angle for a given wavelength and incidence angle is an oblate ellipsoid. This reflection is due to radiation that penetrates into the interior of the sample and is scattered from small scatterers within.

Beckmann [1] presents a theory for diffuse reflection from rough surfaces but restricted almost entirely to perfectly conducting surfaces. He defines a factor called surface roughness in a statistical way as an indicator of the surface structure. For a very rough surface, the solution is a diffuse reflection. Although Beckmann restricts his efforts to the perfectly conducting surface, he does mention the finite conductivity problem occasionally.

On the experimental side, Wendlandt and Hecht [13] point out that no general theory is completely valid for the reflection from mat surfaces. The Lambert cosine law for diffuse reflection is phenomenologically formulated from the fact that a mat surface irradiated with constant intensity appears uniformly light at all angles of observation (ρ' = constant).

As was pointed out in the chapter on goniometry and plotted in Figure 5, the result in terms of a scattering distribution function for this case would be a cosine polar plot multiplied by the constant ρ'. On the basis of experimental evidence, Wendlandt and Hecht [13] report that the Lambert cosine law is strictly valid only for small values of θ_{inc} and θ_{coll}. Deviations occur for larger values, particularly in absorbing materials. In these cases of deviation, the polar plot of the scattering distribution function tends toward an oblate ellipsoid.

Specular reflection is a mirror effect where the scattered radiation is reflected at an angle equal to the angle of incidence in the principal plane, for an ideal plane mirror or a plane dielectric interface. For an uneven bumpy mirror surface and a reasonably large area incident beam the scattered radiation is spread somewhat about the specular reflection angle. The amount of the spread is a measure of the surface roughness or the extent to which it is uneven [1].

In his study of plane-parallel Rayleigh atmospheres, Chandrasekhar also deals with the case of diffuse transmission. The polar curve of the transmission part of the scattering distribution function versus collection angle for a given angle of incidence and wavelength has the form of an oblate ellipsoid. This solution is restricted to isotropic scattering with very little or no absorption.

Refractive transmission is biased in a particular direction and occurs in dielectric layers. In this case a pencil ray in medium 1 is incident upon medium 2 at a particular angle and is transmitted into medium 2 as a pencil ray in a direction determined by Snell's law of refraction [13].

$$n_1 \sin\theta_{inc} = n_2 \sin\theta_{trans}$$

The structure of the soybean leaf as shown in the cross-section of Figure 20 indicates that the conditions of both theoretical developments exist, though the rough surface is a dielectric, a case that Beckmann does not deal with though some of his techniques might be expected to apply. The surface has a thin waxy cuticle layer over a layer of guard cells. For the most part neither the cuticle nor the guard cells contain much chlorophyll [6]. The surface has a rough appearance suggesting the need for a dielectric form of the Beckmann rough surface theory. However, the surface appears transparent indicating a possibility for light to enter the leaf and be scattered as diffuse reflection if the inner cell layers have a Rayleigh-like scattering character similar to the plane-parallel Rayleigh atmosphere problem solved by Chandrasekhar.

The plane-parallel Rayleigh atmosphere consists of very small particles, relative to wavelength, uniformly distributed throughout a particular medium. While the Rayleigh law for molecular scattering is a possible beginning for the solution of this problem, the inner leaf structure is not homogeneous and is composed of structures of many different sizes relative to wavelength. There are many leaf structures smaller than the wavelength of light, however, Gates, et. al. [7] claim that scattering is in part caused by structures within the leaf which

are of the dimension of a wavelength of light, such as mitochondria, ribosomes, nuclei, starch grains and other plastids. Gates also mentions chloroplast and grana dimensions in this regard. Willslatter and Stoll [14] claim that light is critically reflected internally at the cell walls of the leaf where there is a change in the index of refraction from 1.33 for liquid water, to 1.00 for air in the intercellular spaces. These cell dimensions are on the order of 10μm to 50μm [7].

At this point it seems that scattering in leaves has many different causes. Thus the result is expected to be an integral result of each of these types of scattering.

An experimental approach similar to that of Wendlandt and Hecht [13] will be followed in the discussion of the experimental results for soybean leaf bi-directional scattering.

Gross observation indicates that there is less diffuse reflection relative to the total reflection for top incidence than for bottom incidence in the range from 375 nm to 675 nm. This is determined by using the relative magnitude of the scattering distribution function at $\theta_{coll} = 0^{\circ}$ as a feature to measure diffuse reflection at the specular angle. This value is called A. Another feature is the relative magnitude of the scattering distribution function at the specular collection angle. This value is called B.

The ratio A/B is qualitatively a measure of diffuse to total reflectance at the specular angle. For a perfect mirror, the ratio A/B would be zero except for $\theta_{inc} = 0^{\circ}$ where it would be unity. For a perfect Lambertian diffuser, the ratio A/B would be equal to $1/\cos\theta_{coll}$.

Referring to the actual soybean data for a given incidence angle and wavelength, the ratio A/B was formed for top incidence and then for

bottom incidence. These two ratios were compared for this given angle of incidence and wavelength. This was done at all of the incidence angles and wavelengths in order to determine the existence of a trend. For each particular angle of incidence and wavelength it was found that,

$$\frac{[A/B]^{Top}}{[A/B]^{Bottom}} < 1$$

This indicates that the top surface of the leaf is either not as rough as the bottom surface if the rough surface theory is applicable, or that the inner layers near the top surface have a higher absorption coefficient than the inner layers near the bottom surface if the plane-parallel Rayleigh atmosphere theory is applicable.

The soybean leaf structure shows that both explanations may be valid. The surfaces of the leaf definitely have a rough appearance, but it is difficult to compare top and bottom surface roughness upon visual examination. The inner cell layers of the soybean leaf have chlorophyll containing cells which account for absorption. The palisade cell layers near the top surface have a higher chlorophyll concentration than the spongy mesophyll cell layers near the bottom surface [7]. This would account for a higher absorption coefficient for the top cell layers than for the bottom cell layers.

If the plane-parallel Rayleigh atmosphere type theory is applicable, the diffuse reflection would be due to radiation that penetrated into the leaf sample, and it would be expected that the scattering distribution function for reflection at a particular collection angle for a given angle of incidence versus wavelength should have similar absorption characteristics to those for radiation transmitted through the leaf

sample. The experimental data contains spectra for both reflection at the specular angle and transmission along a normal to the leaf sample plane as shown in Figures 34 through 43. The transmission spectra show blue and red chlorophyll absorption, infrared water band absorption and strong transmission in the green and infrared ranges. The trends of the reflection spectra are different from the transmission spectra only in the blue region, where the reflection spectra indicate less blue absorption relative to the transmission spectra. This indicates that the diffuse reflection must be due at least in part to radiation which penetrates into the leaf sample since the reflection spectra so closely resemble those for transmission.

As the angle of incidence is increased, the reflection at the specular angle increases in the blue region relative to the green but does not increase as much in the red region relative to the green.

These results indicate that the diffuse reflection characteristic is probably due to both the rough surface and the radiation that penetrates into the leaf. The soybean leaf structure supports this since the surface is rough and the inner cell layers contain chlorophyll.

The transmission spectra remain nearly the same as the angle of incidence is changed. This indicates that the diffuse component of the transmission characteristic is predominant over the refractive component.

Plots of scattering distribution function relative magnitude for reflection at the specular angle versus angle of incidence are given in Figures 44 and 45 for 450 nm, 550 nm, 650 nm, and 850 nm. The data for both top and bottom incidence for each wavelength are presented on the same page for comparison.

The trend of the curves for 450 nm, 550 nm, and 650 nm is a small positive slope until about $\theta_{inc} = 45^{\circ}$ where the slope increases. This indicates a greater specular reflection component for $\theta_{inc} \geq 45^{\circ}$ at these wavelengths. Comparison of the curve for top incidence with the curve for bottom incidence for constant wavelength at 450 nm, 550 nm, and 650 nm indicates that the relative magnitude of the scattering distribution function for reflection at bottom incidence is equal to or greater than that for top incidence.

The trend of the reflection curves for 850 nm is a small negative slope until about $\theta_{inc} = 45^{\circ}$ where the slope for the top incidence curve becomes positive and increases and the bottom incidence curve continues with the small negative slope. The relative magnitude for the bottom incidence curve is nearly the same as that for the top incidence curve until $\theta_{inc} = 45^{\circ}$ where the bottom incidence curve becomes larger.

Plots of scattering distribution function relative magnitude for transmission along a normal versus angle of incidence are given in Figures 46 and 47 for 450 nm, 550 nm, 650 nm, and 850 nm. The data for both top and bottom incidence for each wavelength are presented on the same page for comparison.

The trend of the curves for 450 nm, 550 nm, 650 nm, and 850 nm is a negative slope. Comparison of the curve for top incidence with the curve for bottom incidence for constant wavelength at 450 nm, 550 nm, 650 nm, and 850 nm indicates that the relative magnitude of the scattering distribution function for transmission at bottom incidence is equal to or greater than that for top incidence.

The plot of angle for maximum reflected and transmitted scattering distribution function relative magnitudes is given in Figure 48 for the visible range. The trend of the reflection curves is a positive slope.

The bottom incidence curve for angle of maximum transmission versus angle of incidence has a greater maximum transmission angle than the top incidence curve indicating possibly a greater angle of refraction for bottom incidence. These transmission curves indicate that the index of refraction of the bottom layer of the soybean leaf model is probably greater than that for the top layer if there is a refractive transmission component. This would also be consistent with the possibly greater coefficient of reflection for the bottom surface than for the top layer.

Soybean Leaf Bi-Directional Scattering Model

An empirical model was formulated from the bi-directional scattering data.

Figure 49 is the diagram of a simple two-dimensional bi-directional scattering model for a healthy, green soybean leaf, suggested by the experimental results and the physical structure of the leaf. This is a four layer structure with isotropy relative to midvein orientation in the sample plane. The model does not include the midvein. The outer layers, layer 1 and layer 4, contribute refraction and specular reflection with no absorption. These layers have rough outer surfaces to give a component of diffuse reflection and a spread in the specular reflection characteristic. Layer 1 has a somewhat rougher surface than layer 4. The specular reflection characteristic is reduced somewhat in the

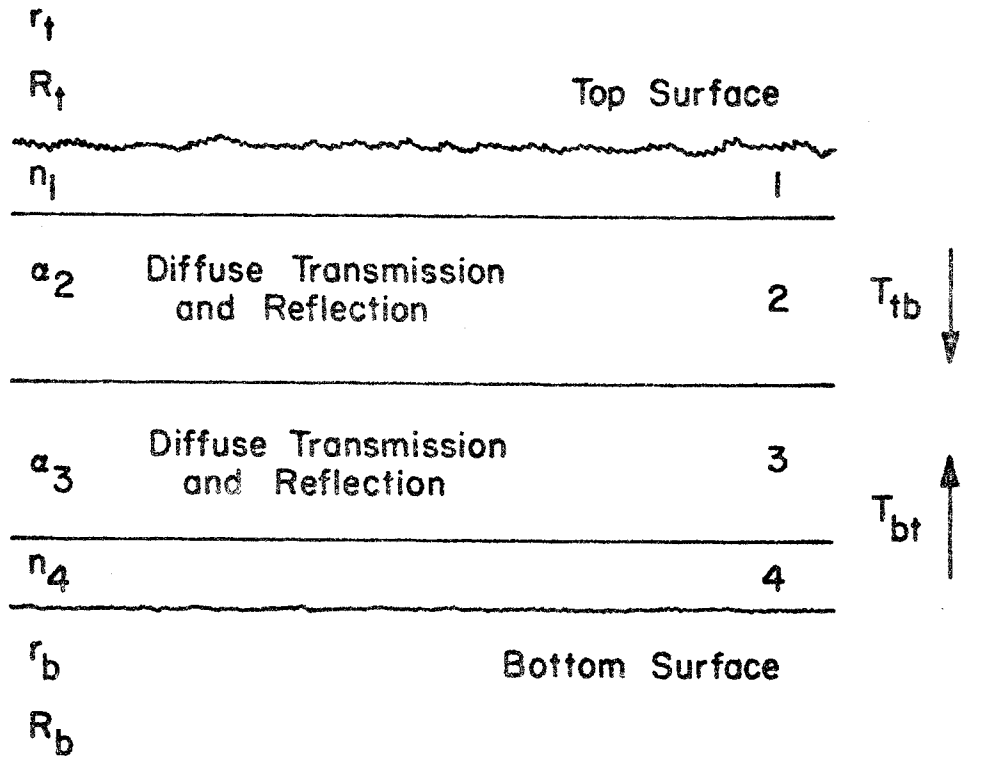

r – Roughness Coefficient $r_t > r_b$

n – Index of Refraction $n_4 > n_1$

α – Absorption Coefficient $\alpha_2 > \alpha_3$

R – Reflection Coefficient $R_b \geq R_t$

T – Transmission Coefficient $T_{bt} > T_{tb}$

Surface Isotropy Relative to Midvein Orientation

Figure 49. Soybean Leaf Bi-Directional Scattering Model.

infrared region for these epidermal layers in order to be consistent with the data.

The inner layers, layer 2 and layer 3, have refractive and diffuse transmission characteristics and a diffuse reflection characteristic together with a selective absorption characteristic. Layer 2 has a higher absorption coefficient than layer 3.

This is a general description of a simple soybean leaf scattering model. The experimental results give the approximate specifications for this empirical model.

The general result is a transmission characteristic which would have a diffuse cosine like scattering curve and a refracted narrow lobe like scattering curve. This could produce the transmission curve resembling an ellipse with its major axis along the direction of the angle of maximum transmission when these two components of transmission are added together. The reflection curve would have a diffuse cosine like component and a spread lobe like curve at the specular angle. This could produce the reflection curves shown in the experimental data when the components are added together. The light entering layers 2 and 3 encounters the selective absorption characteristic consistent with the experimental data.

CORN LEAF BI-DIRECTIONAL SCATTERING MEASUREMENTS

Procedure

Bi-directional scattering characteristic curves were taken on healthy, living, corn leaves over the range from 375 nm to 1000 nm; from 375 nm to 675 nm at 25 nm intervals and from 750 nm to 1000 nm at 50 nm intervals. Reflection and transmission spectra were taken at several fixed collection angles for use in determining the wavelengths for scattering study.

The data were taken on corn leaf sample areas not including the midvein. Both top and bottom incidence situations and both vertical and horizontal midvein orientation situations were studied.

The corn leaf is a monocotyledon with an internal structure having an undifferentiated mesophyll. The mesophyll contains large, irregular shaped cells. These cells are in a tight configuration leaving little volume for intercellular air spaces except for stomatal cavities. Corn has large bulliform cells interspersed in the ventral epidermis. Trichomes are present on corn leaves. Figure 50 is a photograph of a corn leaf cross-section.

Figure 51 is a photograph of several of the corn plants used in this scattering experiment. These plants were grown one plant to each six inch diameter pot in the greenhouse. The leaves used received adequate lighting and were not shaded. The corn leaves used had an average length of 31 inches and an average width of 3 1/2 inches. The average corn plant height was about 48 inches.

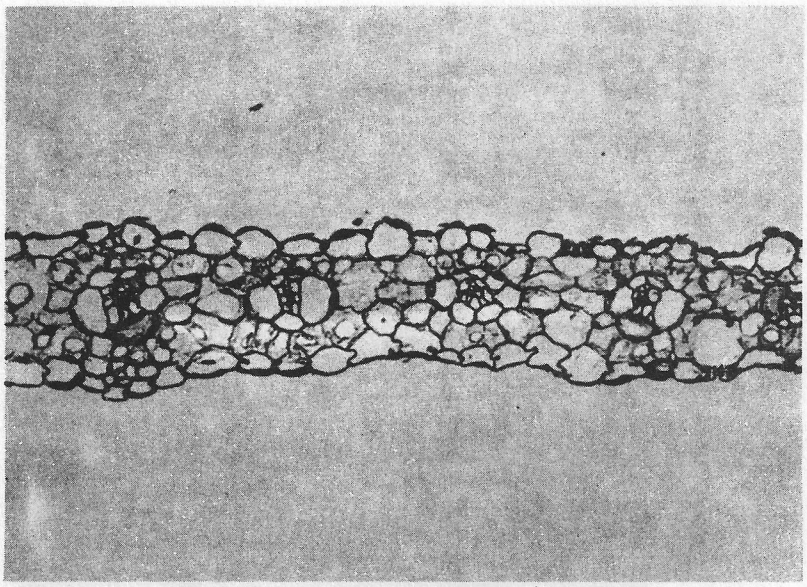

Figure 50. Corn Leaf Cross Section.

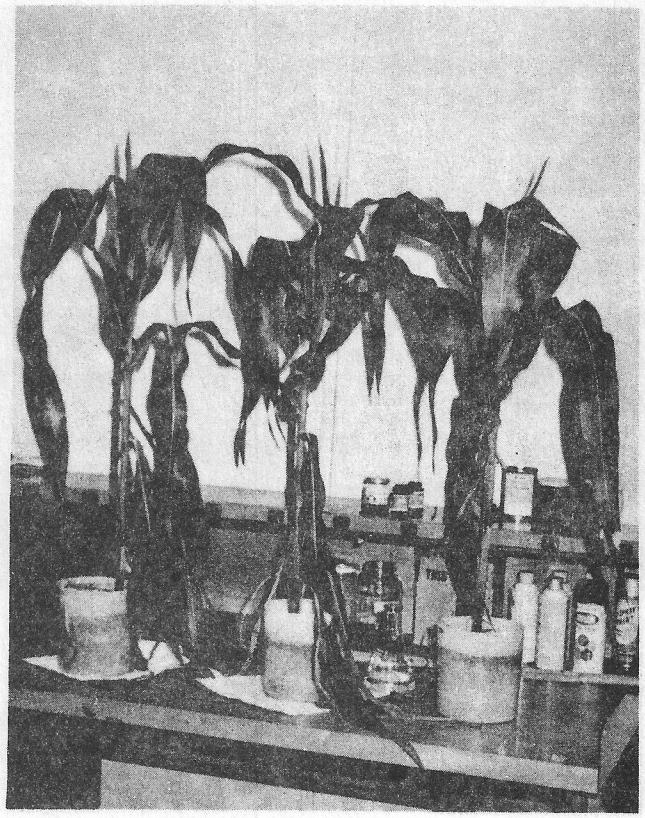

Figure 51. Corn Plants.

Figure 52 shows a corn plant with one of its leaves under study. The pot rests on the laboratory floor and the leaf stem extends up through the sample holder cylinder into the measurement chamber. This photograph shows the corn plant in an almost horizontal position resting on carefully positioned supports.

Figure 53 is a photograph of a corn leaf in the sample holder with vertical midvein orientation. The leaf remains whole which requires careful folding and support for the tip end of the corn leaf. Figure 54 is a photograph of a corn leaf in the sample holder with horizontal midvein orientation. This presents a greater problem for keeping the leaf whole. Portions nearer the tip portion are used because of flexibility.

In order to determine the necessary coordinates for a full set of two-dimensional bi-directional scattering measurements experiments were carried out to find the symmetry properties in the bi-directional scattering characteristics for corn leaves. This study compared results for top and bottom surfaces, positive and negative data collection angles and different orientations of the midvein in a given plane.

The midvein is parallel to the v axis of Figure 4 and is called horizontal orientation when the midvein is parallel to the h axis of Figure 4.

The bi-directional scattering results for the top and bottom leaf surfaces were different in magnitude and slightly different in functional form indicating that measurements must be carried out for both top and bottom corn leaf surfaces.

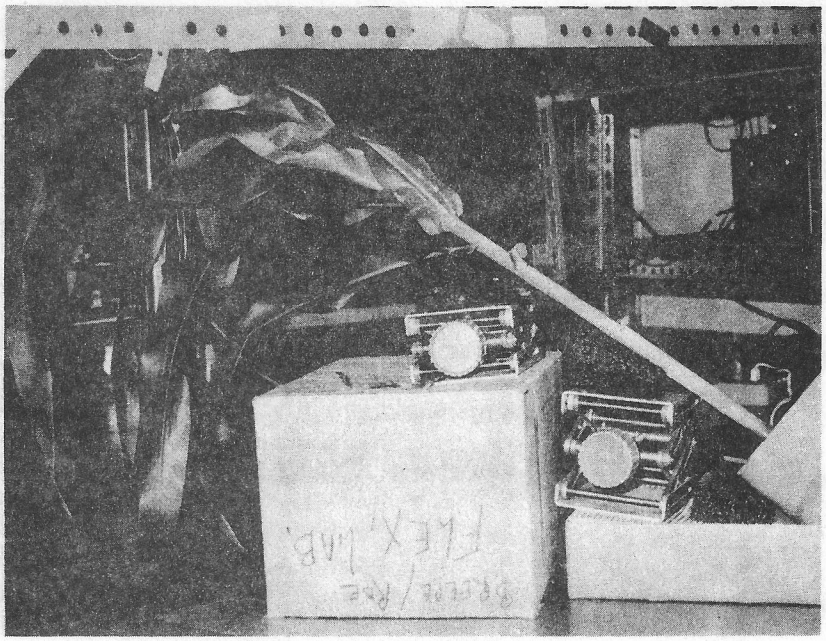

Figure 52. Corn Plant Positioned under Measurement Chamber.

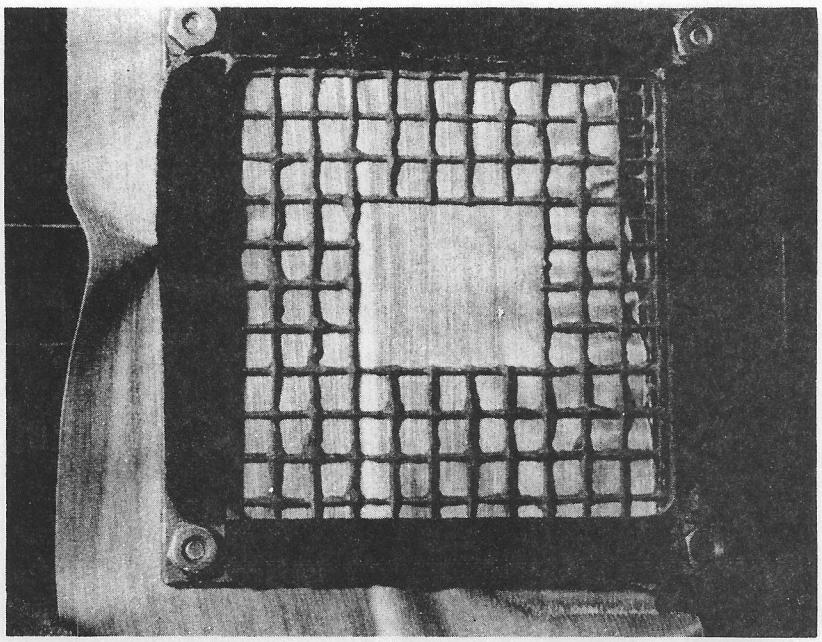

Figure 53. Corn Leaf in Sample Holder with Vertical Midvein Orientation.

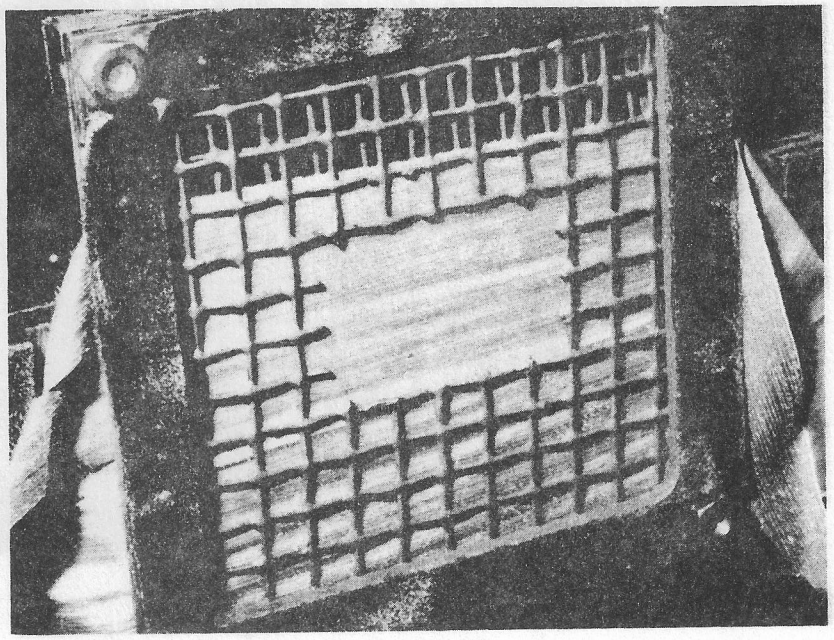

Figure 54. Corn Leaf in Sample Holder with Horizontal Midvein Orientation.

The results for $+\theta_{inc}$ and for $-\theta_{inc}$ have the same functional form and magnitudes within 5% of one another showing that measurements may be carried out at either $+\theta_{inc}$ or $-\theta_{inc}$.

A C_2 rotational symmetry for the sample plane about a normal to that plane is found to exist for both top and bottom corn leaf surfaces. Thus both vertical and horizontal midvein orientations must be used for the measurements.

Since a large amount of time was required to make the extensive full set of bi-directional scattering measurements it was not feasible to make the full set of measurements on one corn leaf. Thus some of the measurements were made at some of the conditions on one leaf and then at other conditions on another leaf, etc. until it had taken eight different leaves in order to take data for all of the different measurement conditions. The data were taken on three leaves each from two plants and two leaves from a third plant.

Since several leaves were used in order to make measurements at all of the conditions for a full set, an experiment was carried out on corn leaves to determine the consistency of bi-directional scattering measurements among several leaves for a particular fixed set of conditions. Two leaves on one plant and three leaves on a second plant were used for this consistency experiment.

In this consistency experiment polar bi-directional scattering plots were taken on both the top and bottom leaf surfaces. An incidence angle of 45° (with $\theta_{tilt} = 0^{\circ}$) was used with wavelengths of 500 nm and 550 nm. These wavelengths were selected in order to determine variation among polar plots for the highly absorbing blue region and for the highly reflecting green region for different leaves.

The polar plots for each set of measurement conditions had nearly the same functional form for both reflection and transmission. Thus one point on each curve was selected for comparison. The transmission curves were compared by using the magnitude of the radius vector for the transmission curve at $\theta_{coll} = 180^{o}$, which is along a normal to the leaf plane. The reflection curves were compared by using the magnitude of the radius vector for the reflection curve at $\theta_{coll} = 45^{o}$.

The mean value of the radius vectors for the five leaves was calculated for each particular set of conditions and coordinates. The standard deviation about each of these mean values was calculated and this information is presented in Table 4. The unit for measuring the radius vectors from the polar plots is consistent throughout, being 1 unit per 1/2 inch for a relative scattering unit scale of 20.

Using this information, the use of several different corn leaves to produce data for a composite scattering model was judged to be an acceptable plan.

The wavelength range of the experiment was divided into smaller ranges so that for a particular incident surface and midvein orientation an effort could be made to complete measurements at each incidence angle on the same leaf in the same data run. The polar plots have a leaf identification as outlined in the following scattering data section.

Corn data collection angles are measured clockwise from the normal to the surface of incidence while the incidence angles are measured counter-clockwise from this normal. The tilt angle is 0^{o} for this experiment so the source angle symbol is θ_{inc} as shown in Figure 4.

CORN LEAVES

VERTICAL MIDVEIN ORIENTATION

5 Samples

λ	θ_{inc}	θ_{coll}	Incident Surface	Mean Value of Radius Vector	Standard Deviation
500 nm	45°	180°	Top	1.697	0.266
550 nm	45°	180°	Top	10.72	1.007
500 nm	45°	45°	Top	10.5	1.208
550 nm	45°	45°	Top	11.515	1.240
550 nm	45°	180°	Bottom	1.692	0.306
550 nm	45°	180°	Bottom	11.38	0.920
500 nm	45°	45°	Bottom	11.61	2.150
550 nm	45°	45°	Bottom	12.90	2.290

TABLE 4. CORN LEAF CONSISTENCY EXPERIMENT

Corn Leaf Bi-Directional Scattering Data

The bi-directional scattering curves for healthy, green corn leaves are presented in two sections of ten curves each; the first section giving the results for vertical midvein orientation and the second giving the results for horizontal midvein orientation. This is a collection of 380 bi-directional scattering curves, representing 9120 individual data points.

The radial dimension of these directional scattering plots is given in relative scattering units. These are the values of the scattering distribution function for a given collection angle and wavelength. The data curves which were obtained as described in the data processing section of the chapter on apparatus and procedure were all multiplied by a constant scale factor in order that the scales for presentation be larger than unity. The use of these relative units allows the selection of any linear scale to study the results. For example, a scale of 20 could be 20 relative scattering units per centimeter if centimeters are used consistently for study and comparison. The scale is given on the plot along with its use for reflection or transmission. The symbol REFL 20 designates a reflection scale of 20 relative scattering units per unit length and the symbol TRANS 10 designates a transmission scale of 10 relative scattering units per unit length. This is used since for several wavelength bands it is necessary to use different scales for reflection and transmission for data presentation.

The corn leaf and plant designation is given for each scattering plot. For example, L1/P2 is used to designate leaf number 1 and plant number 2. A legend is given on each page to identify the wavelength at the data were taken.

It was difficult to restrain the corn leaf to a plane since it has a rough surface and a natural tendency to wrinkle, which caused several slight variations in the symmetry of the results. However, the effect is minor; for the most part the leaves could be fairly well restrained to a plane.

Vertical Midvein Orientation

The following ten figures present the bi-directional scattering data for healthy, green corn leaves with a vertical midvein orientation. Figures 55 through 59 are the results for top incidence and Figures 60 through 64 are the results for bottom incidence.

Scattering distribution functions versus wavelength for various collection angles are taken directly from the bi-directional polar scattering plots. Figures 65 through 69 give the spectra for top incidence and Figures 70 through 74 give the spectra for bottom incidence. The transmission curves are for a 180° collection angle which is along a normal to the leaf surface. This is a good measure of the transmission even though the functional forms vary for different incidence angles.

The reflection curves are plotted for the specular angle except for normal incidence where a 45° collection angle is used.

The unit is consistent throughout being 1 unit per 1/2 inch for a relative scattering unit scale of 20.

Results from several leaves are used to plot these spectra. The polar plots identify the leaf and the particular wavelength range.

Figure 55. Corn Leaf Relative $[\rho' \cos \theta_{coll}]$ and Relative $[\tau' \cos(\pi - \theta_{coll})]$ versus θ_{coll} for Top Incidence at $\theta_{inc} = 0^{\circ}$ (Vertical Midvein Orientation).

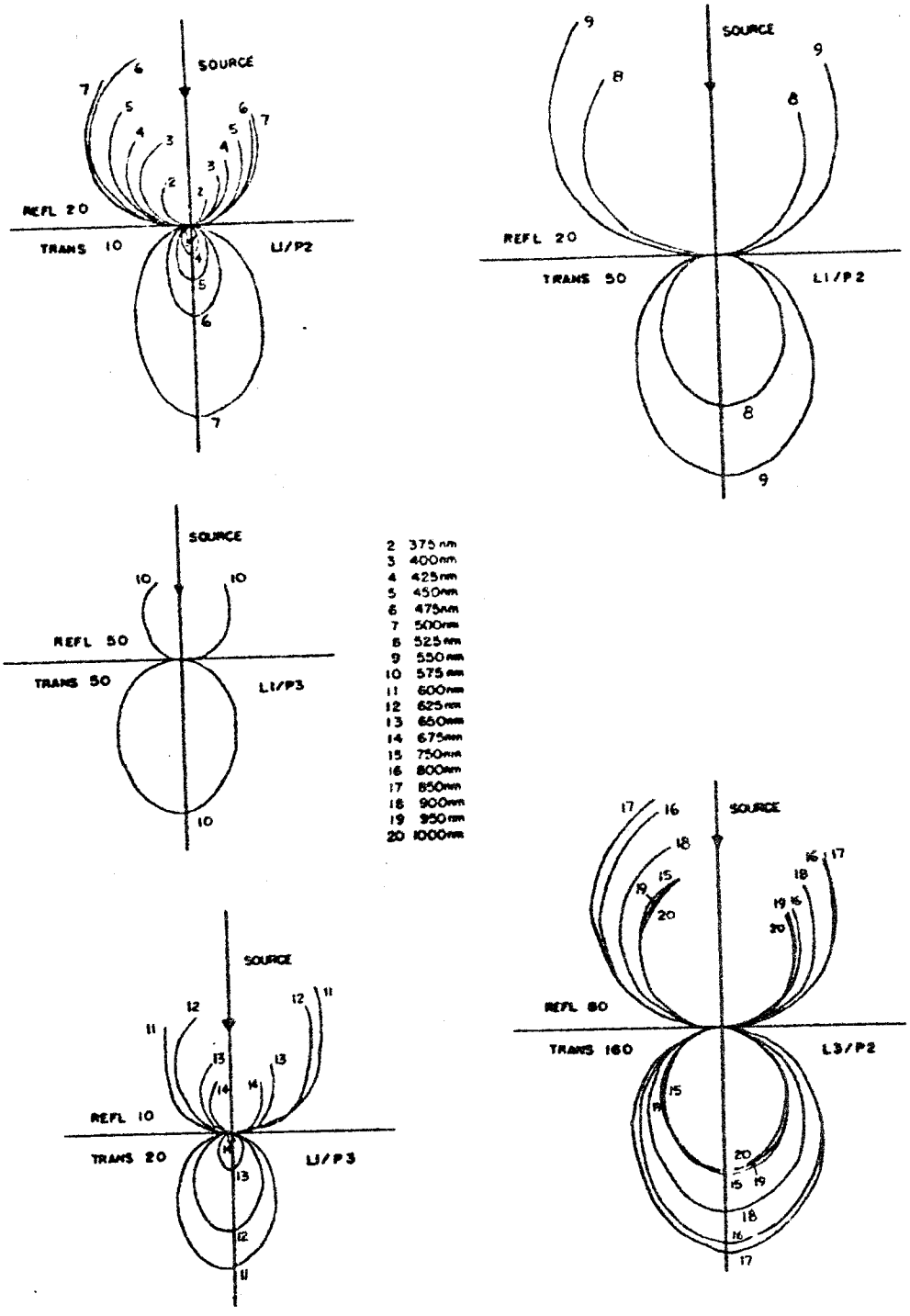
SOURCE
REFL 20
TRANS 10
L1/P2
SOURCE
REFL 20
TRANS 50
L1/P2
SOURCE
REFL 50
TRANS 50
L1/P3
2 375 nm
3 400nm
4 425nm
5 450nm
6 475nm
7 500nm
8 525nm
9 550nm
10 575nm
11 600nm
12 625nm
13 650nm
14 675nm
15 750nm
16 800nm
17 850nm
18 900nm
19 950nm
20 1000nm
SOURCE
REFL 10
TRANS 20
L1/P3
SOURCE
REFL 80
TRANS 160
L3/P2

Figure 55.

Figure 56. Corn Leaf Relative $[\rho'\cos\theta_{coll}]$ and Relative $[\tau'\cos(\pi - \theta_{coll})]$ versus θ_{coll} for Top Incidence at $\theta_{inc} = 15^{o}$ (Vertical Midvein Orientation).

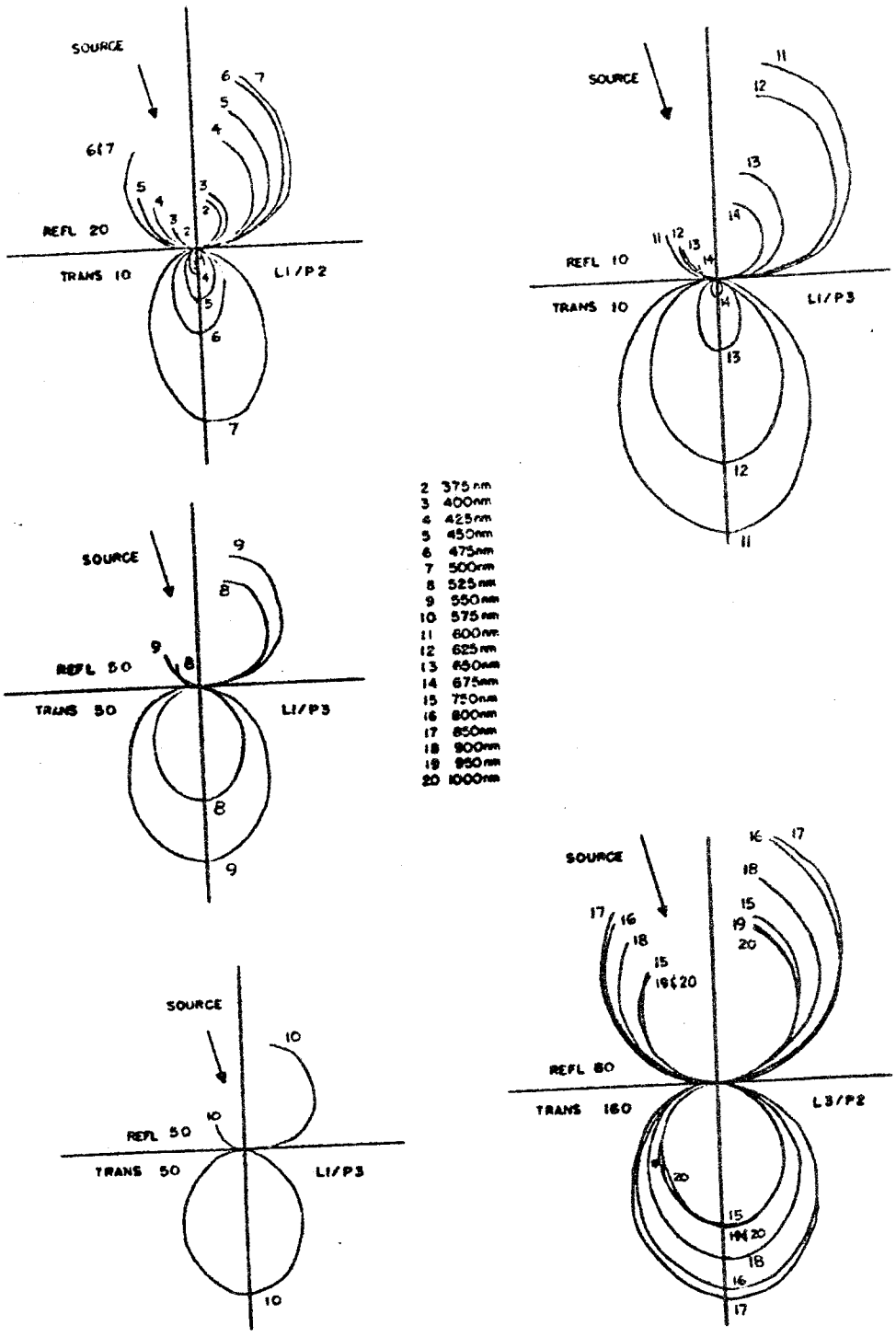
SOURCE
REFL 20
TRANS 10
LI/P2
SOURCE
REFL 10
TRANS 10
LI/P3
SOURCE
REFL 50
TRANS 50
LI/P3
SOURCE
REFL 50
TRANS 50
LI/P3
SOURCE
REFL 80
TRANS 160
L3/P2
2 375nm
3 400nm
4 425nm
5 450nm
6 475nm
7 500nm
8 525nm
9 550nm
10 575nm
11 600nm
12 625nm
13 650nm
14 675nm
15 750nm
16 800nm
17 850nm
18 900nm
19 950nm
20 1000nm

Figure 56.

Figure 57. Corn Leaf Relative $[\rho' \cos \theta_{coll}]$ and Relative $[\tau' \cos(\pi - \theta_{coll})]$ versus θ_{coll} for Top Incidence at $\theta_{inc} = 30^{\circ}$ (Vertical Midvein Orientation).

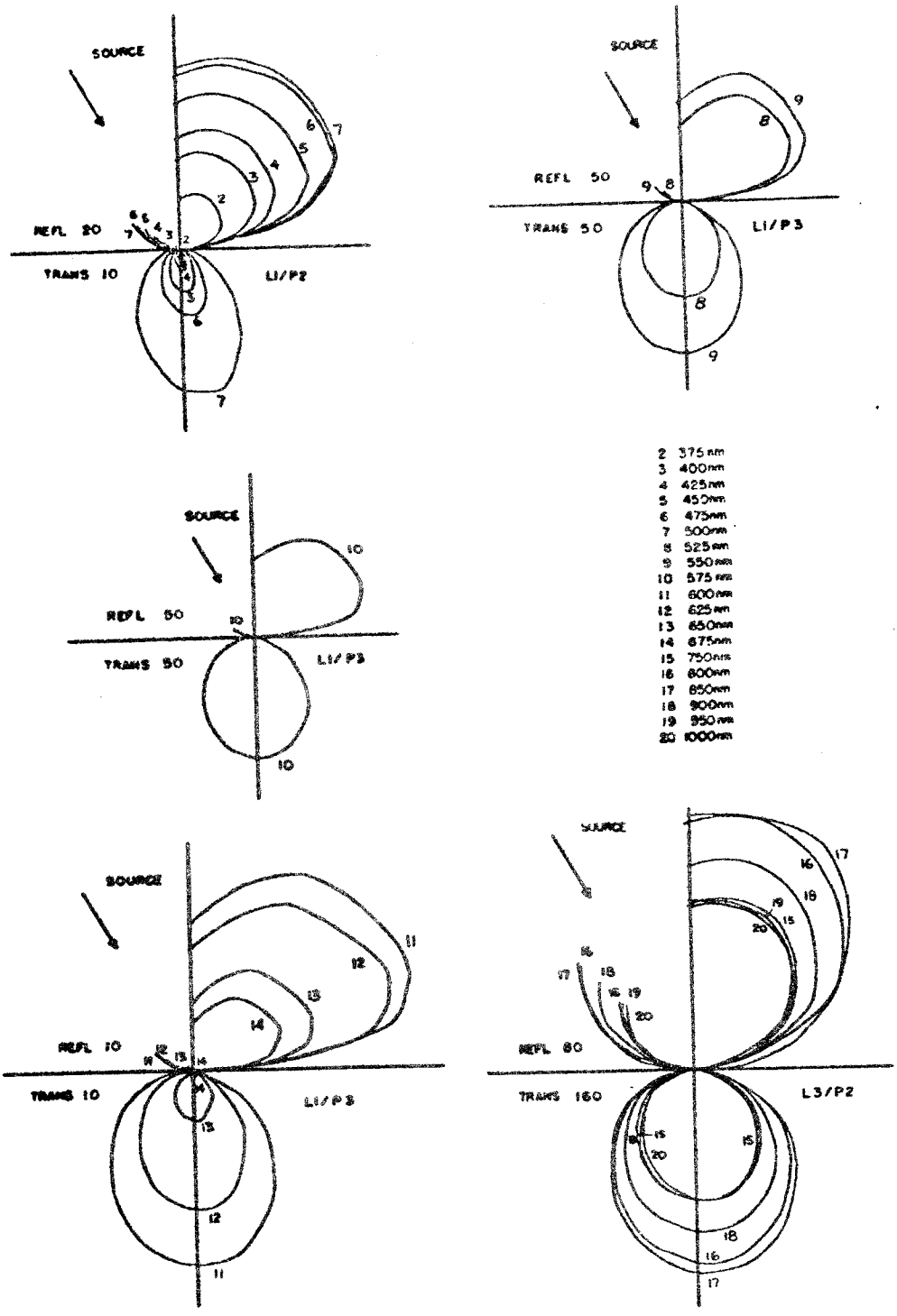
SOURCE
REFL 20
TRANS 10
L1/P2
SOURCE
REFL 50
TRANS 50
L1/P3
SOURCE
REFL 50
TRANS 50
L1/P3
2 375nm
3 400nm
4 425nm
5 450nm
6 475nm
7 500nm
8 525nm
9 550nm
10 575nm
11 600nm
12 625nm
13 650nm
14 675nm
15 750nm
16 800nm
17 850nm
18 900nm
19 950nm
20 1000nm
SOURCE
REFL 10
TRANS 10
L1/P3
SOURCE
REFL 80
TRANS 160
L3/P2

Figure 57.

Figure 58. Corn Leaf Relative $[\rho'\cos\theta_{coll}]$ and Relative $[\tau'\cos(\pi - \theta_{coll})]$ versus θ_{coll} for Top Incidence at $\theta_{inc} = 45^{\circ}$ (Vertical Midvein Orientation).

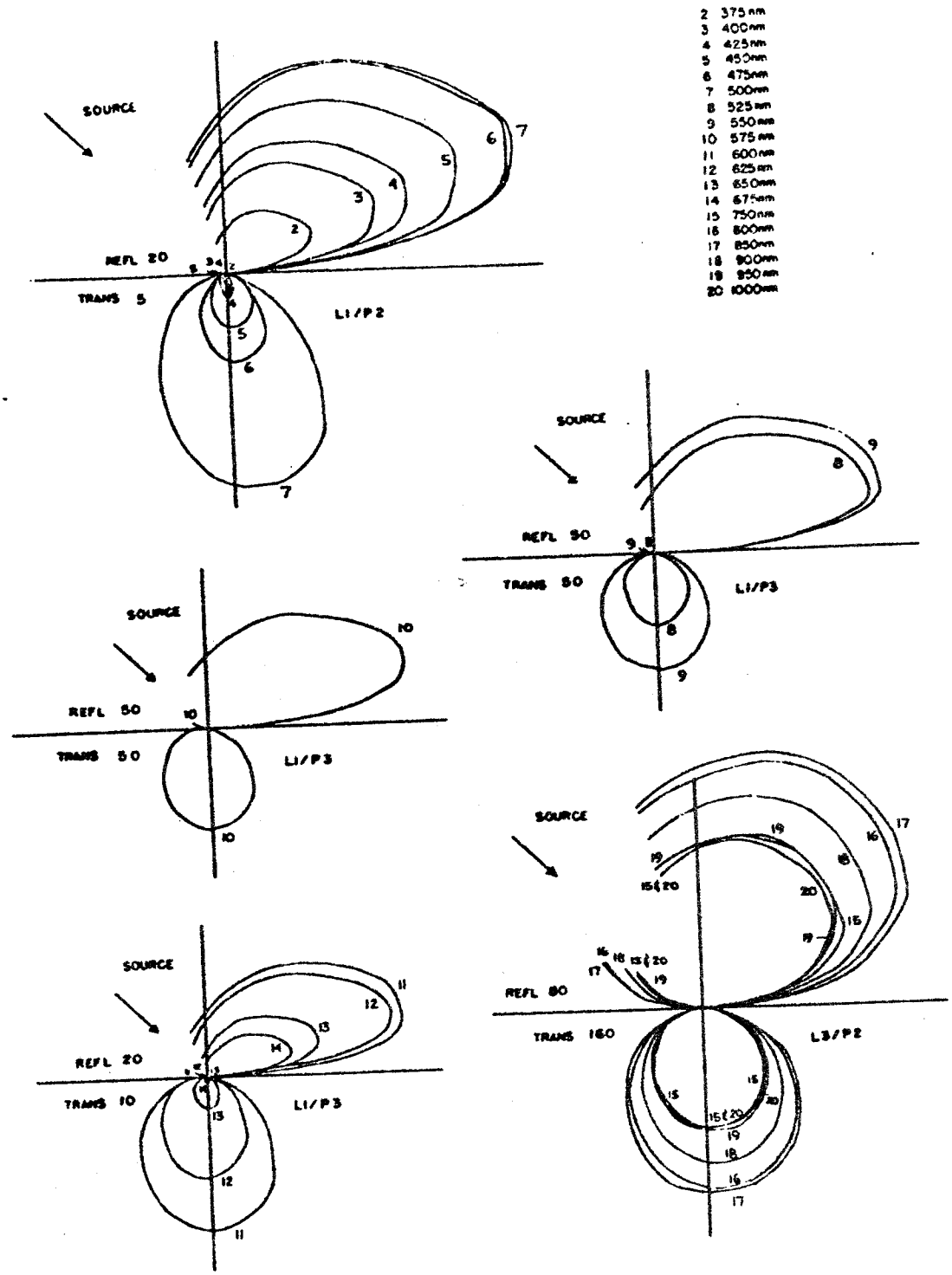
2 375nm
3 400nm
4 425nm
5 450nm
6 475nm
7 500nm
8 525nm
9 550nm
10 575nm
11 600nm
12 625nm
13 650nm
14 675nm
15 750nm
16 800nm
17 850nm
18 900nm
19 950nm
20 1000nm
SOURCE
REFL 20
TRANS 5
L1/P2
SOURCE
REFL 50
TRANS 50
L1/P3
SOURCE
REFL 50
TRANS 50
L1/P3
SOURCE
REFL 20
TRANS 10
L1/P3
SOURCE
REFL 80
TRANS 160
L3/P2

Figure 58.

Figure 59. Corn Leaf Relative $[\rho'\cos\theta_{coll}]$ and Relative $[\tau'\cos(\pi - \theta_{coll})]$ versus θ_{coll} for Top Incidence at $\theta_{inc} = 60^{\circ}$ (Vertical Midvein Orientation).

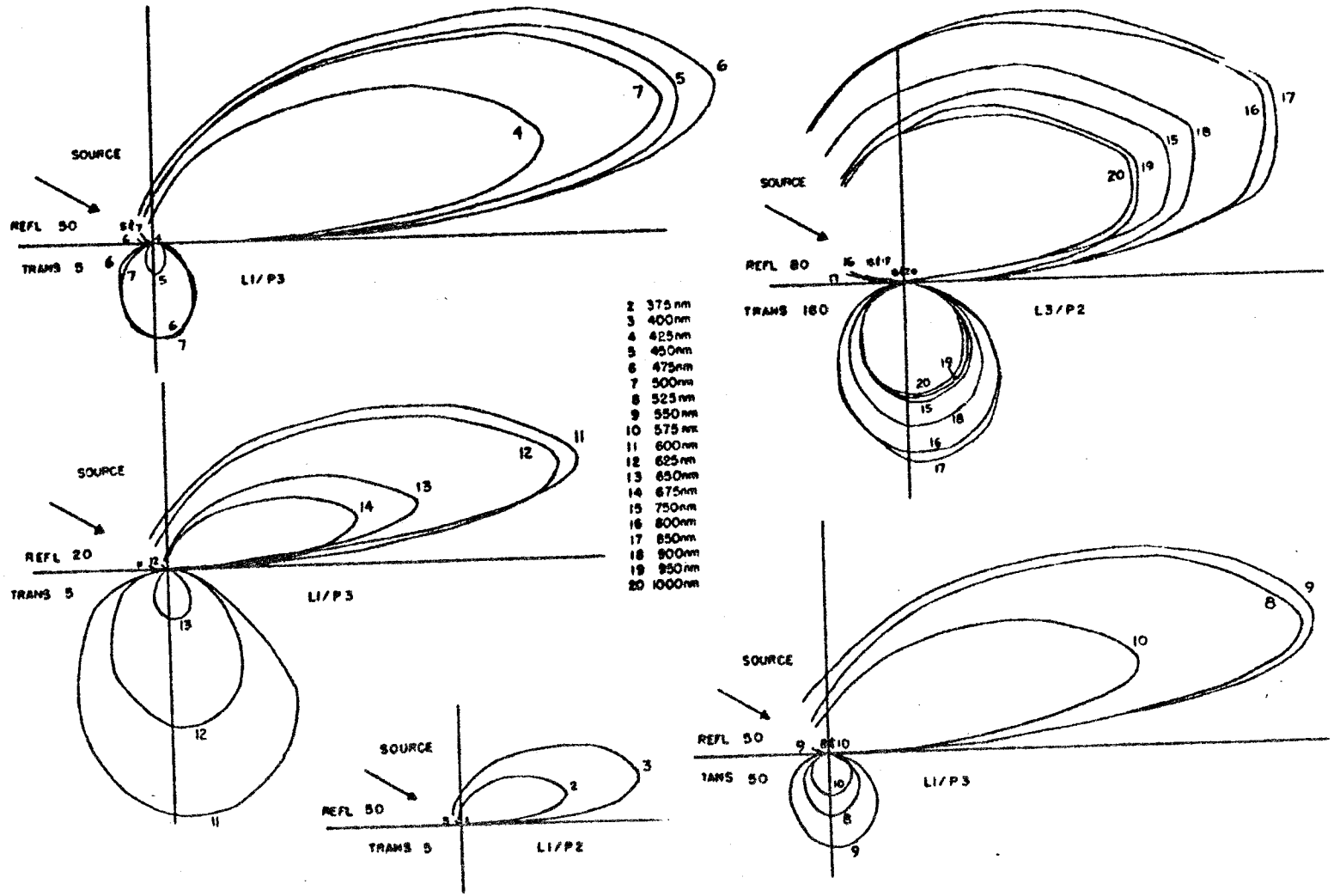
SOURCE
REFL 50
TRANS 5
LI/P3
SOURCE
REFL 20
TRANS 5
LI/P3
SOURCE
REFL 50
TRANS 5
LI/P2
SOURCE
REFL 80
TRANS 160
L3/P2
SOURCE
REFL 50
TANS 50
LI/P3
2 375nm
3 400nm
4 425nm
5 450nm
6 475nm
7 500nm
8 525nm
9 550nm
10 575nm
11 600nm
12 625nm
13 650nm
14 675nm
15 750nm
16 800nm
17 850nm
18 900nm
19 950nm
20 1000nm

Figure 59.

Figure 60. Corn Leaf Relative $[\rho'\cos\theta_{coll}]$ and Relative $[\tau'\cos(\pi - \theta_{coll})]$ versus θ_{coll} for Bottom Incidence at $\theta_{inc} = 0^{o}$ (Vertical Midvein Orientation).

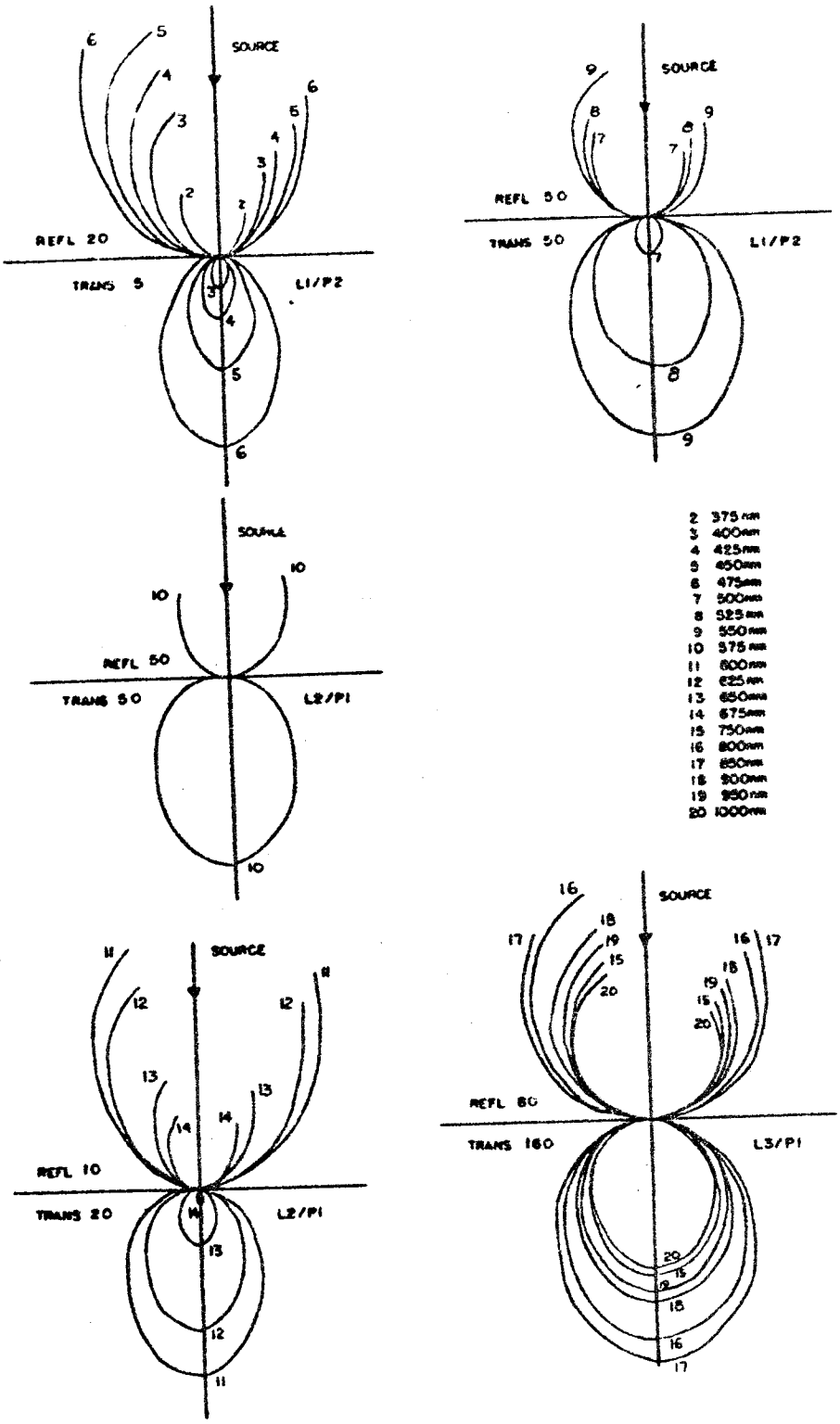
SOURCE
REFL 20
TRANS 5
L1/P2
SOURCE
REFL 50
TRANS 50
L1/P2
SOURCE
REFL 50
TRANS 50
L2/P1
2 375 nm
3 400nm
4 425nm
5 450nm
6 475nm
7 500nm
8 525nm
9 550nm
10 575nm
11 600nm
12 625nm
13 650nm
14 675nm
15 750nm
16 800nm
17 850nm
18 900nm
19 950nm
20 1000nm
SOURCE
REFL 10
TRANS 20
L2/P1
SOURCE
REFL 80
TRANS 160
L3/P1

Figure 60.

Figure 61. Corn Leaf Relative $[\rho' \cos\theta_{coll}]$ and Relative $[\tau' \cos(\pi - \theta_{coll})]$ versus θ_{coll} for Bottom Incidence at $\theta_{inc} = 15^{\circ}$ (Vertical Midvein Orientation).

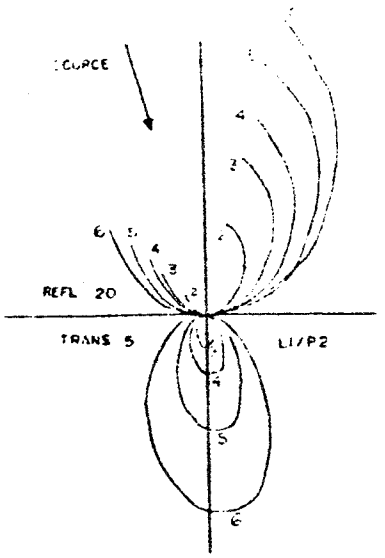

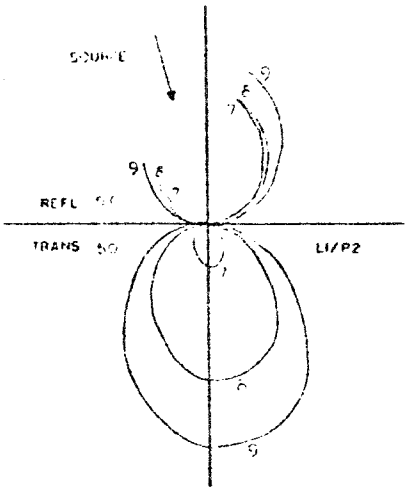

2 375nm
3 400nm
4 425nm
5 450nm
6 475nm
7 500nm
8 525nm
9 550nm
10 575nm
11 600nm
12 625nm
13 650nm
14 675nm
15 700nm
16 800nm
17 850nm
18 900nm
19 950nm
20 1000nm

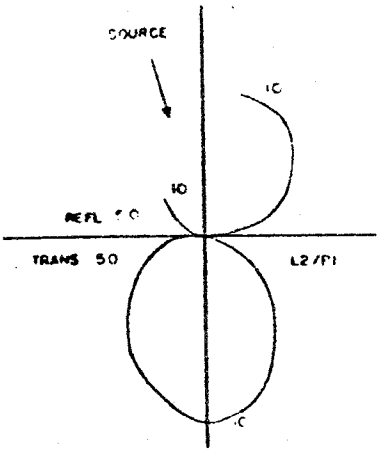

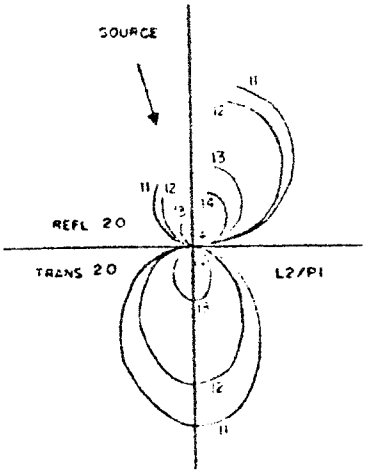

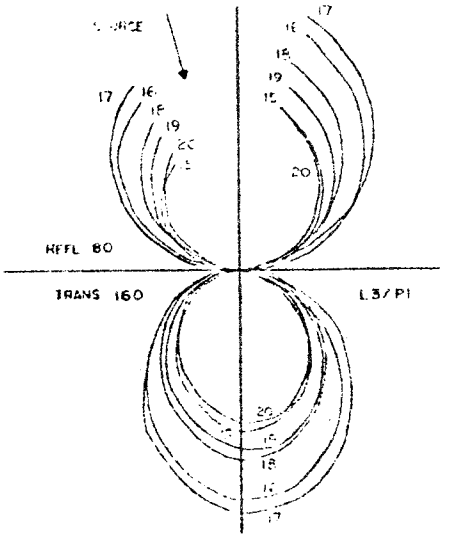

Figure 62.

Figure 62. Corn Leaf Relative $[\rho' \cos \theta_{coll}]$ and Relative $[\tau' \cos(\pi - \theta_{coll})]$ versus θ_{coll} for Bottom Incidence at $\theta_{inc} = 30^{o}$ (Vertical Midvein Orientation).

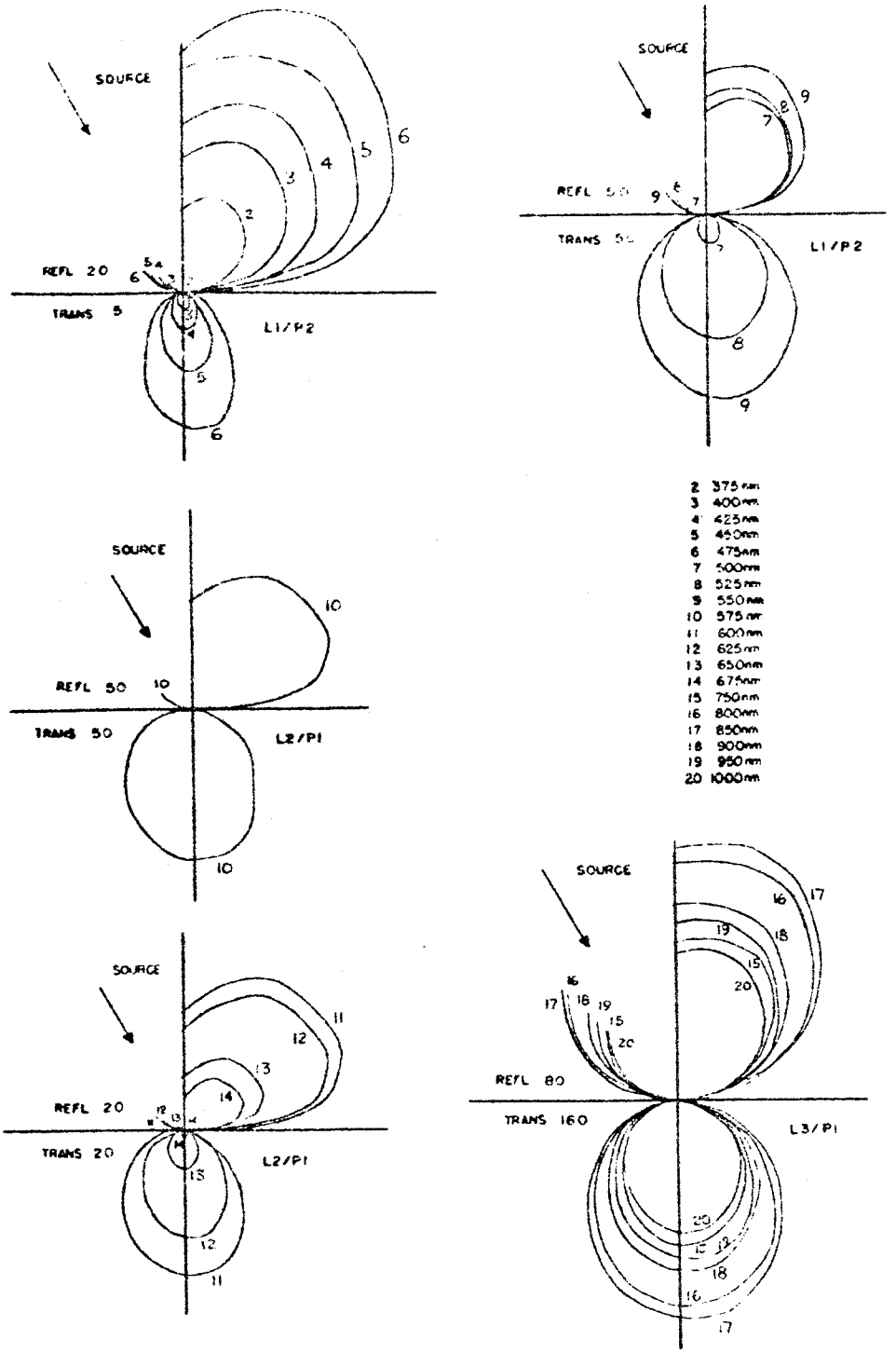
SOURCE
REFL 20
TRANS 5
L1/P2
SOURCE
REFL 50
TRANS 50
L1/P2
SOURCE
REFL 50
TRANS 50
L2/P1
2 375nm
3 400nm
4 425nm
5 450nm
6 475nm
7 500nm
8 525nm
9 550nm
10 575nm
11 600nm
12 625nm
13 650nm
14 675nm
15 750nm
16 800nm
17 850nm
18 900nm
19 950nm
20 1000nm
SOURCE
REFL 20
TRANS 20
L2/P1
SOURCE
REFL 80
TRANS 160
L3/P1

Figure 62.

Figure 63. Corn Leaf Relative $[\sigma'\cos\theta_{coll}]$ and Relative $[\tau'\cos(\pi - \theta_{coll})]$ versus θ_{coll} for Bottom Incidence at $\theta_{inc} = 45^{\circ}$ (Vertical Midvein Orientation).

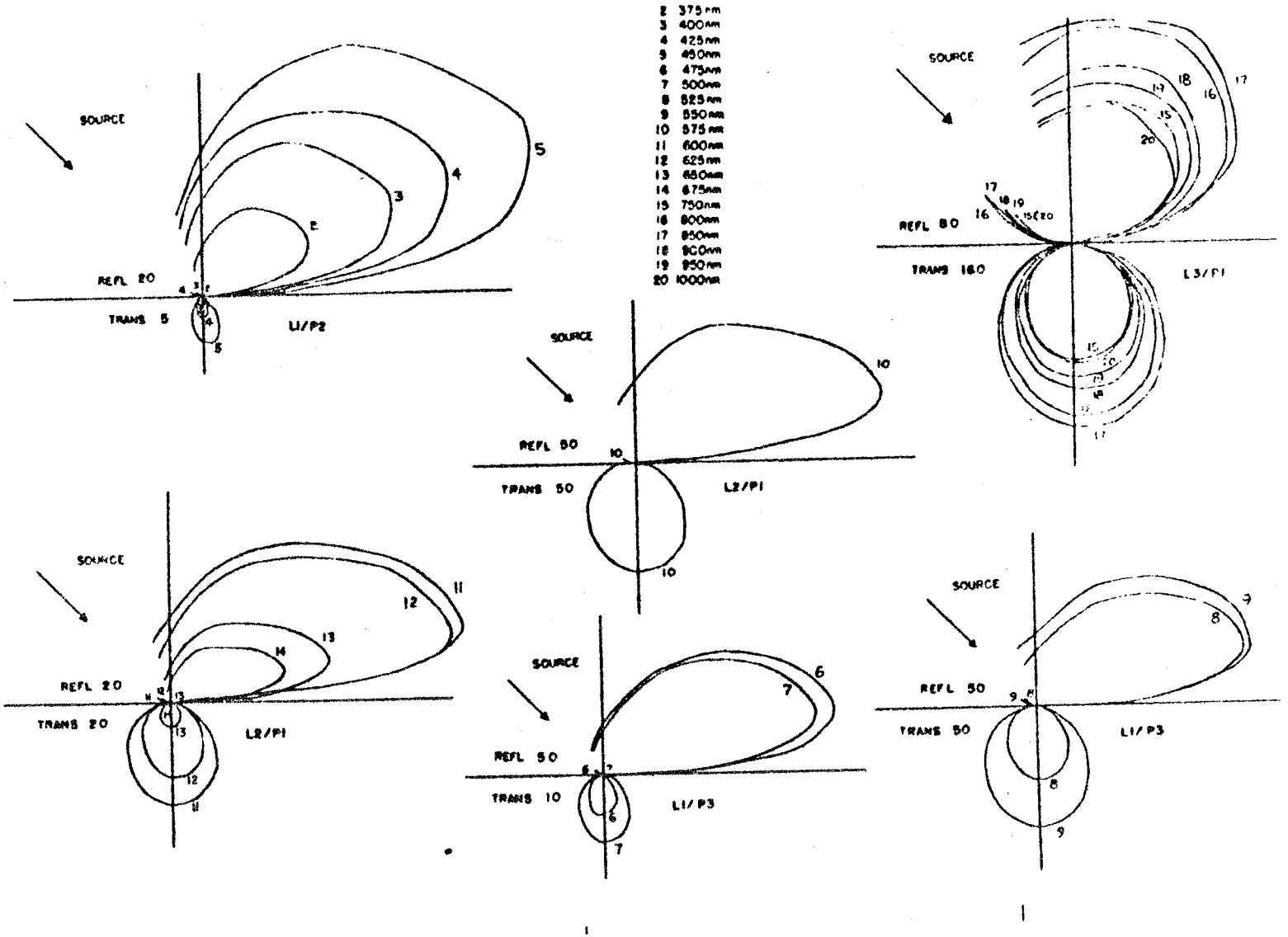
2 375nm
3 400nm
4 425nm
5 450nm
6 475nm
7 500nm
8 525nm
9 550nm
10 575nm
11 600nm
12 625nm
13 650nm
14 675nm
15 750nm
16 800nm
17 850nm
18 900nm
19 950nm
20 1000nm
SOURCE
REFL 20
TRANS 5
L1/P2
SOURCE
REFL 80
TRANS 160
L3/P1
SOURCE
REFL 50
TRANS 50
L2/P1
SOURCE
REFL 20
TRANS 20
L2/P1
SOURCE
REFL 50
TRANS 10
L1/P3
SOURCE
REFL 50
TRANS 50
L1/P3

Figure 63.

Figure 64. Corn Leaf Relative $[\sigma'\cos\theta_{coll}]$ and Relative $[\tau'\cos(\pi - \theta_{coll})]$ versus θ_{coll} for Bottom Incidence at $\theta_{inc} = 60^{o}$ (Vertical Midvein Orientation).

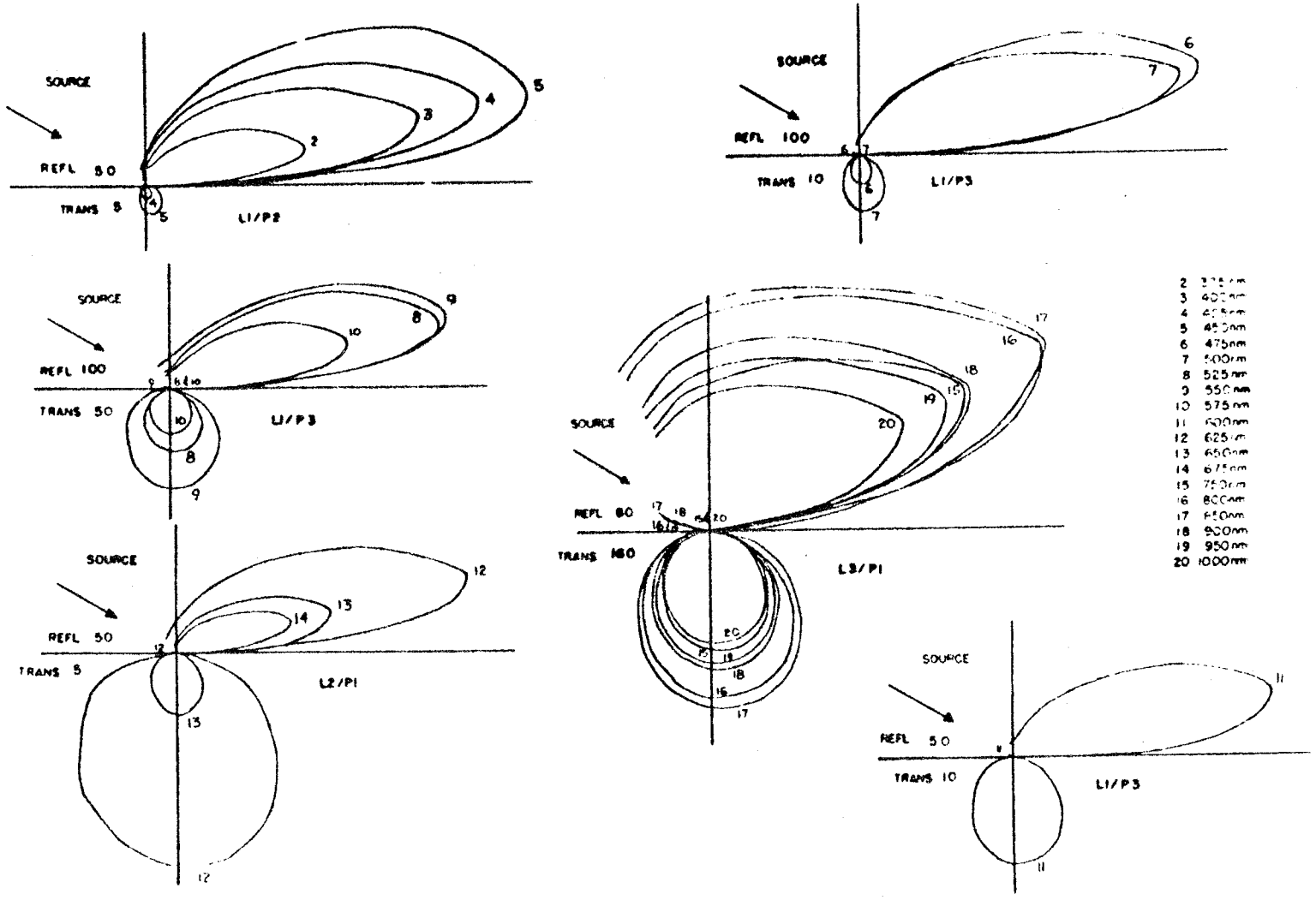
SOURCE
REFL 50
TRANS 5
L1/P2
SOURCE
REFL 100
TRANS 10
L1/P3
SOURCE
REFL 100
TRANS 50
L1/P3
SOURCE
REFL 50
TRANS 5
L2/P1
SOURCE
REFL 80
TRANS 160
L3/P1
SOURCE
REFL 50
TRANS 10
L1/P3
2 375nm
3 400nm
4 425nm
5 450nm
6 475nm
7 500nm
8 525nm
9 550nm
10 575nm
11 600nm
12 625nm
13 650nm
14 675nm
15 750nm
16 800nm
17 850nm
18 900nm
19 950nm
20 1000nm

Figure 64.

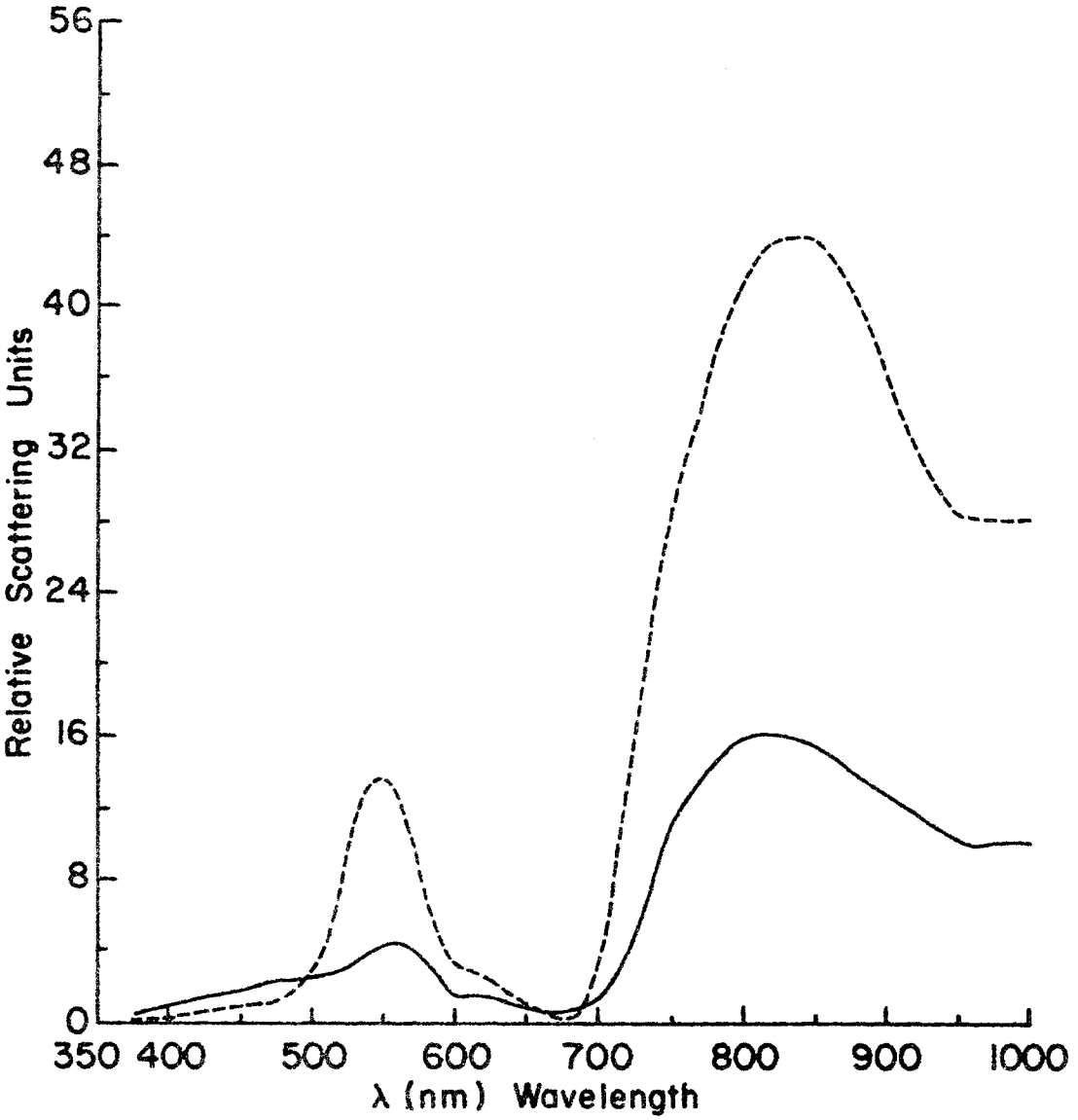

Figure 65. Corn Leaf Relative $[\sigma' \cos\theta_{coll}]$(_____) at $\theta_{coll} = 45^{\circ}$ and Relative $[\tau' \cos(\pi - \theta_{coll})]$(-----) at $\theta_{coll} = 180^{\circ}$ versus λ for Top Incidence at $\theta_{inc} = 0^{\circ}$ (Vertical Midvein Orientation).

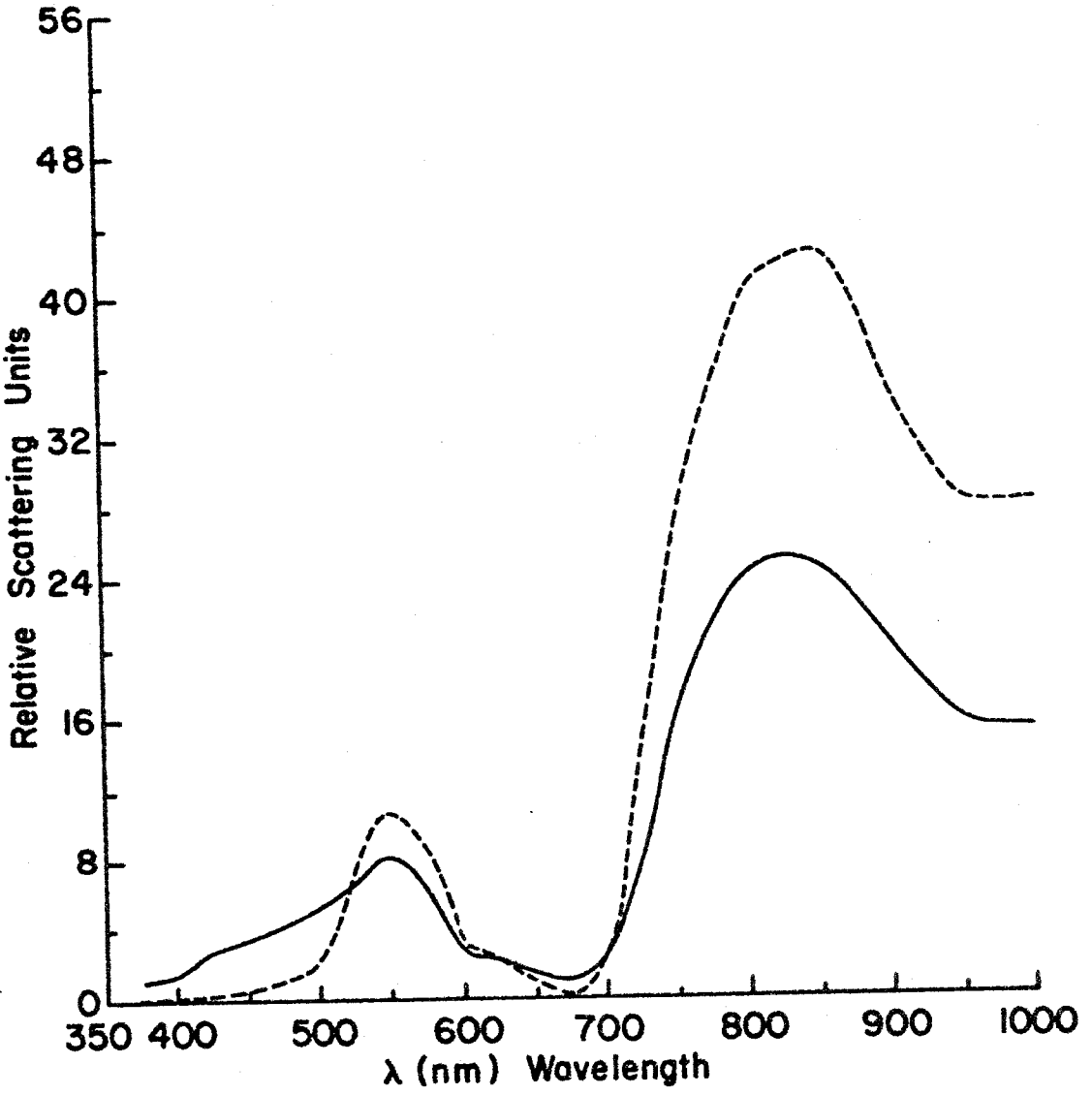

Figure 66. Corn Leaf Relative $[\sigma'\cos\theta_{coll}]$(_____) at $\theta_{coll} = 15^{\circ}$ and Relative $[\tau'\cos(\pi - \theta_{coll})]$(-----) at $\theta_{coll} = 180^{\circ}$ versus λ for Top Incidence at $\theta_{inc} = 15^{\circ}$ (Vertical Midvein Orientation).

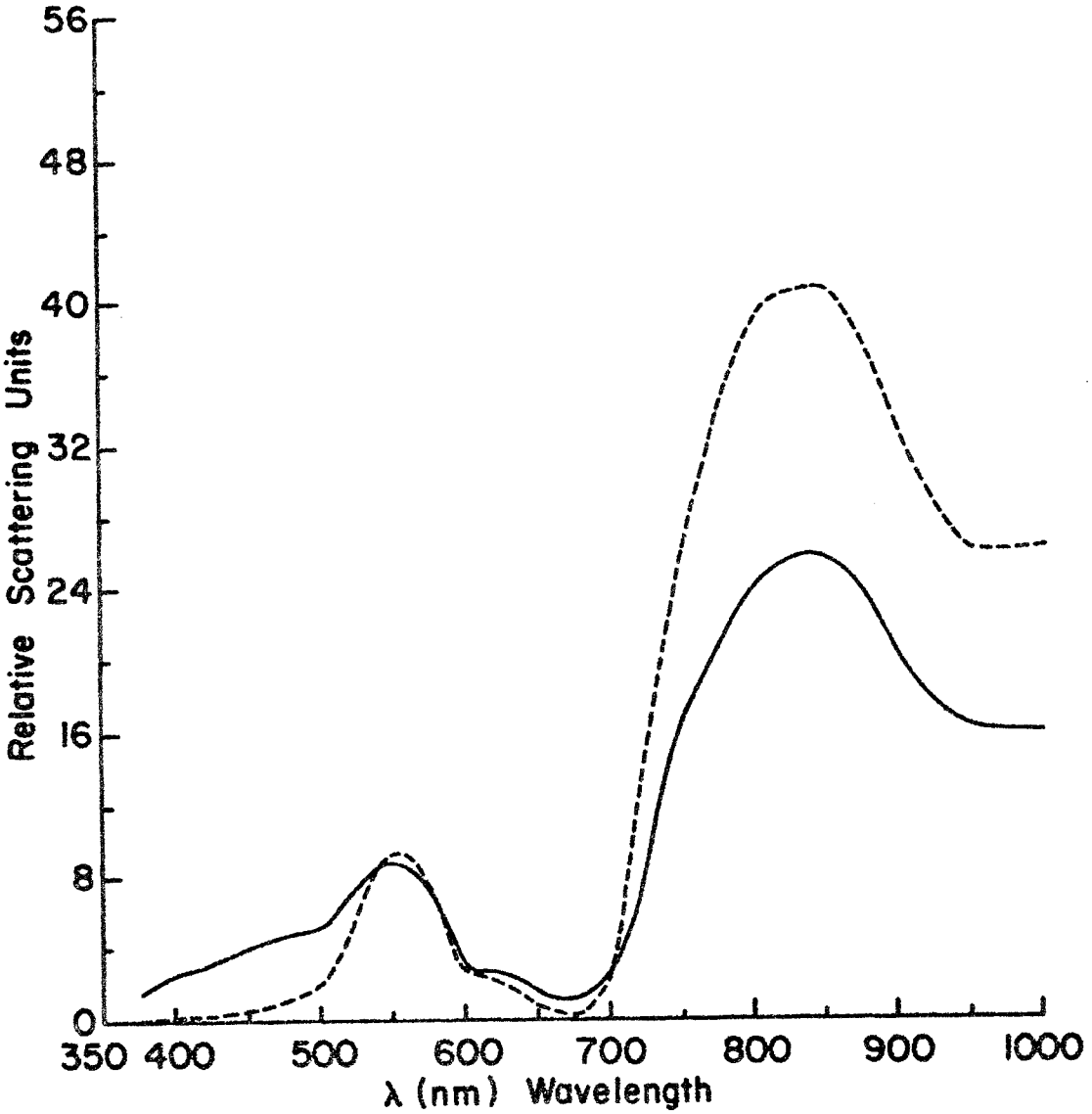

Figure 67. Corn Leaf Relative $[\sigma'\cos\theta_{coll}]$(_____) at $\theta_{coll} = 30^{\circ}$ and Relative $[\tau'\cos(\pi - \theta_{coll})]$(-----) at $\theta_{coll} = 180^{\circ}$ versus λ for Top Incidence at $\theta_{inc} = 30^{\circ}$ (Vertical Midvein Orientation).

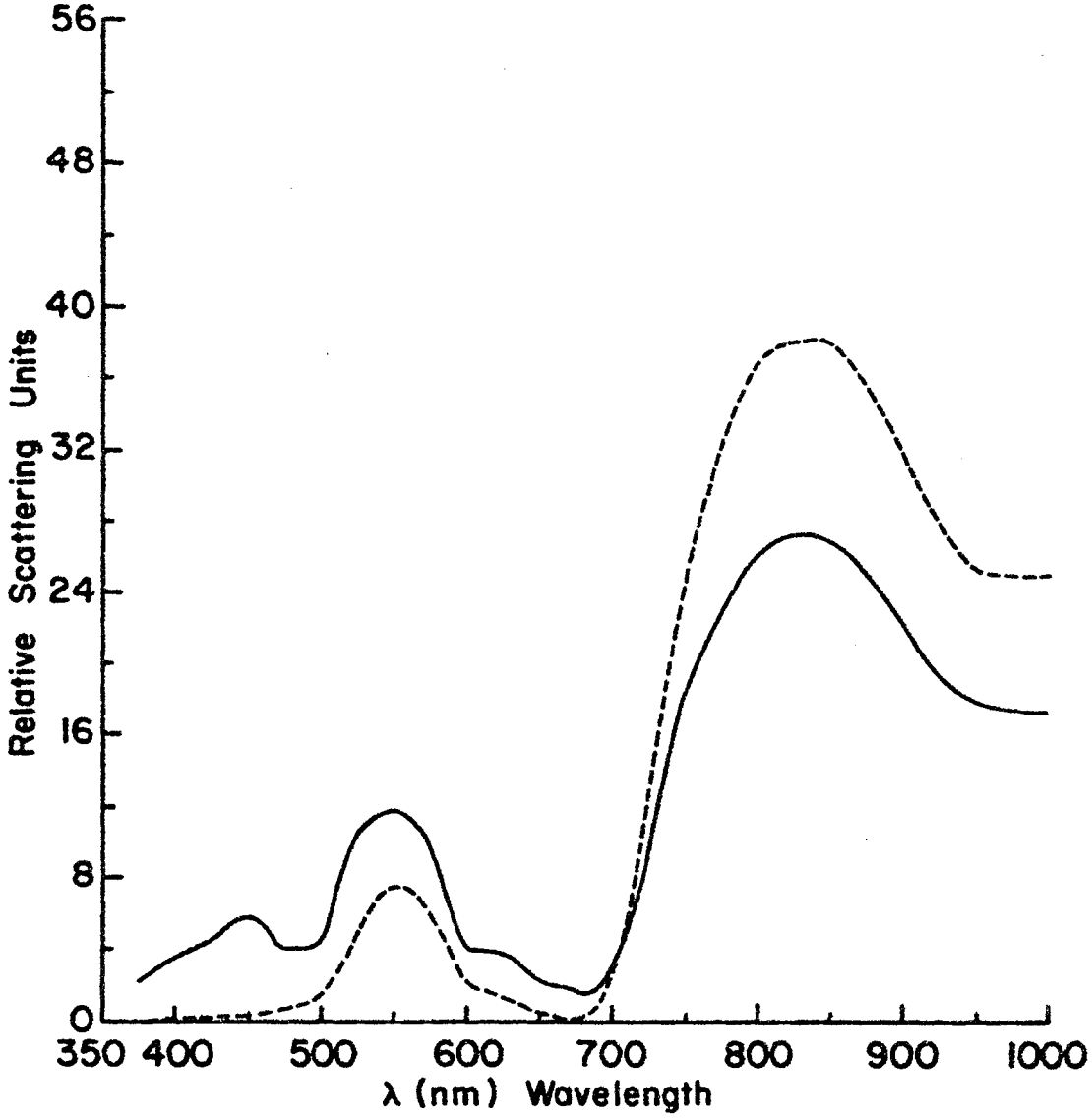

Figure 68. Corn Leaf Relative $[\rho'\cos\theta_{coll}]$(_____) at $\theta_{coll} = 45^{\circ}$ and Relative $[\tau'\cos(\pi - \theta_{coll})]$(– – – –) at $\theta_{coll} = 180^{\circ}$ versus λ for Top Incidence at $\theta_{inc} = 45^{\circ}$ (Vertical Midvein Orientation).

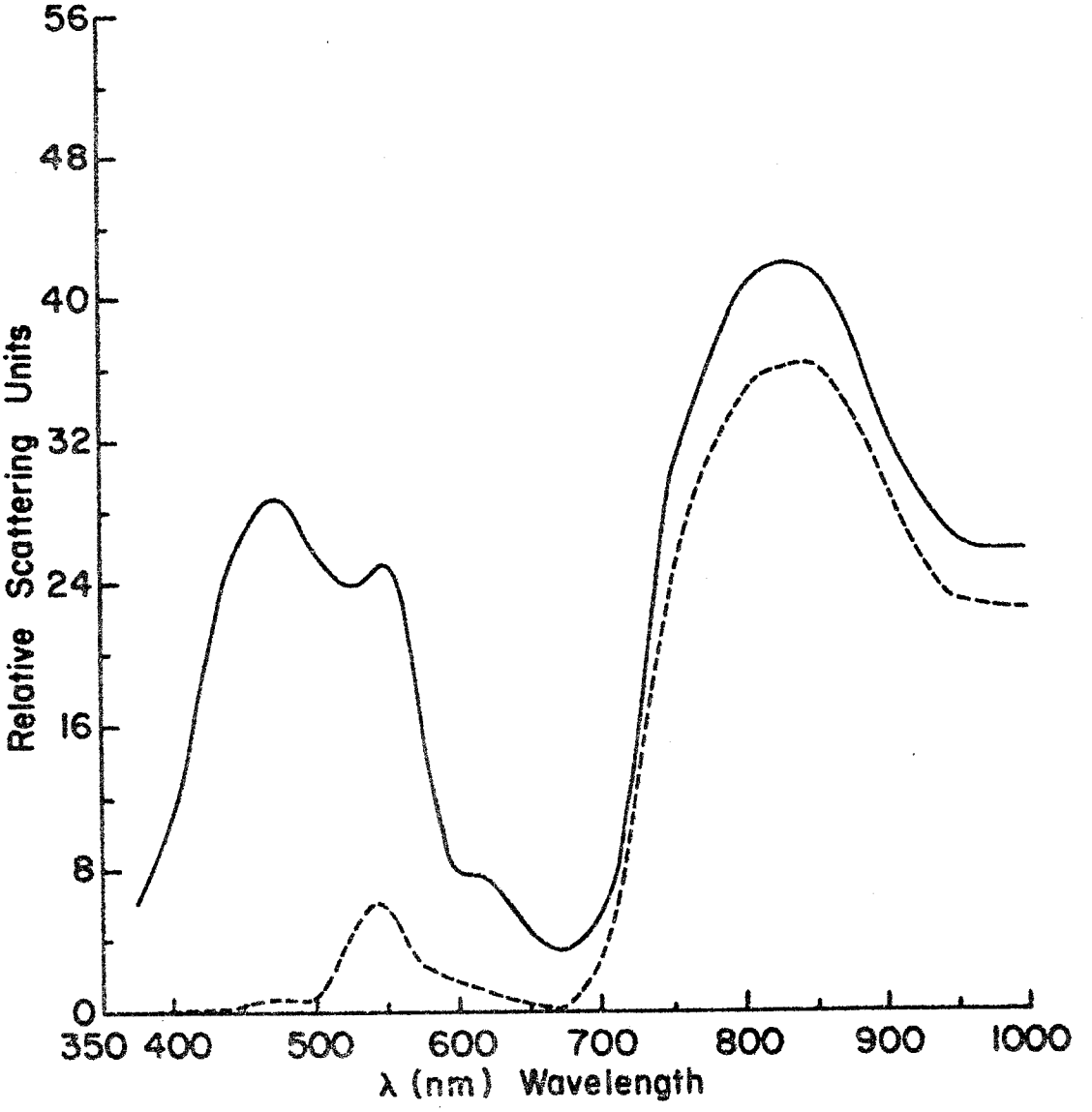

Figure 69. Corn Leaf Relative $[\rho'\cos\theta_{coll}]$(_____) at $\theta_{coll} = 60^{\circ}$ and Relative $[\tau'\cos(\pi - \theta_{coll})]$(– – – –) at $\theta_{coll} = 180^{\circ}$ versus λ for Top Incidence at $\theta_{inc} = 60^{\circ}$ (Vertical Midvein Orientation).

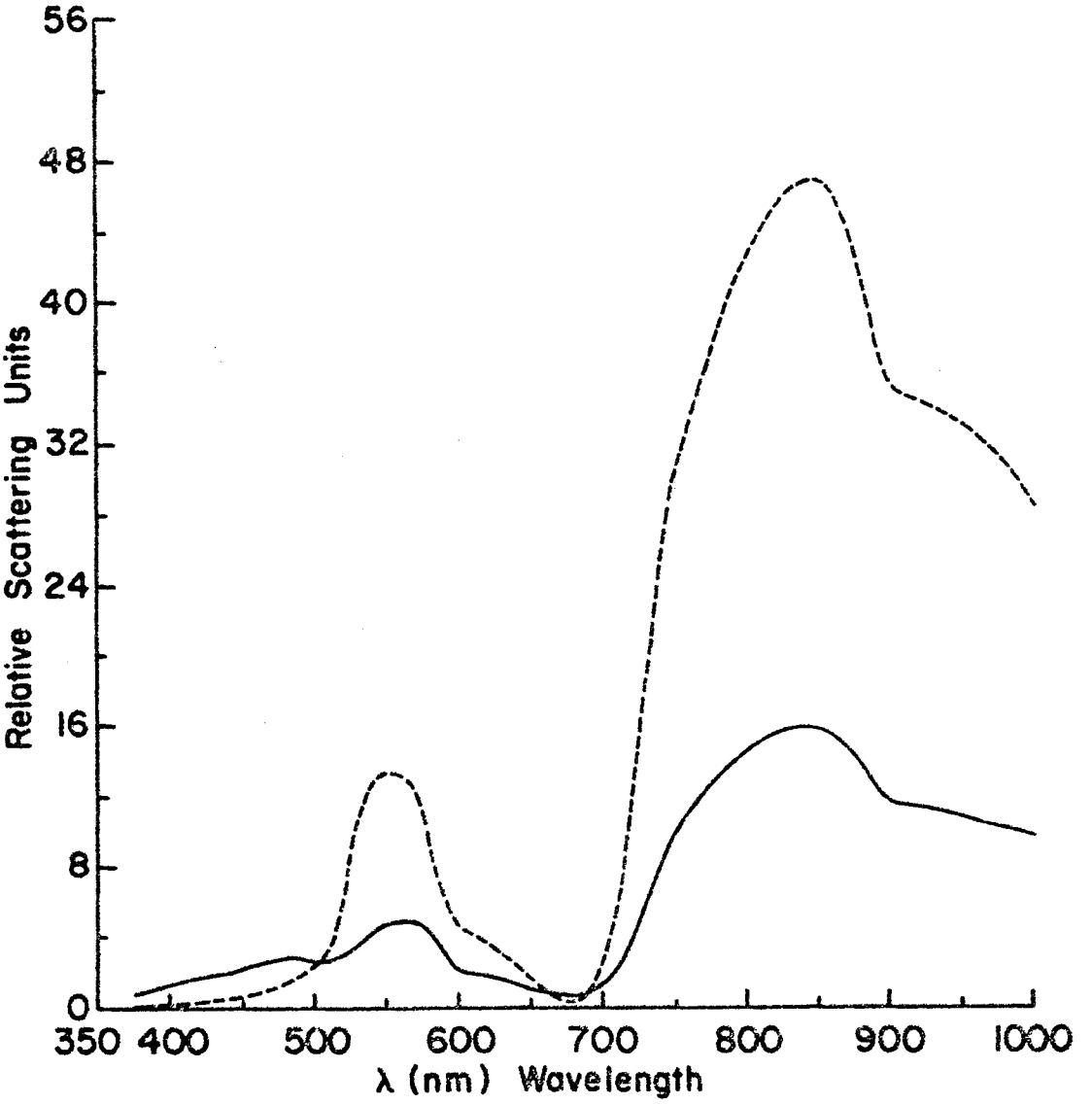

Figure 70. Corn Leaf Relative $[\sigma'\cos\theta_{coll}]$(_____) at $\theta_{coll} = 45^{\circ}$ and Relative $[\tau'\cos(\pi - \theta_{coll})]$(-----) at $\theta_{coll} = 180^{\circ}$ versus λ for Bottom Incidence at $\theta_{inc} = 0^{\circ}$ (Vertical Midvein Orientation).

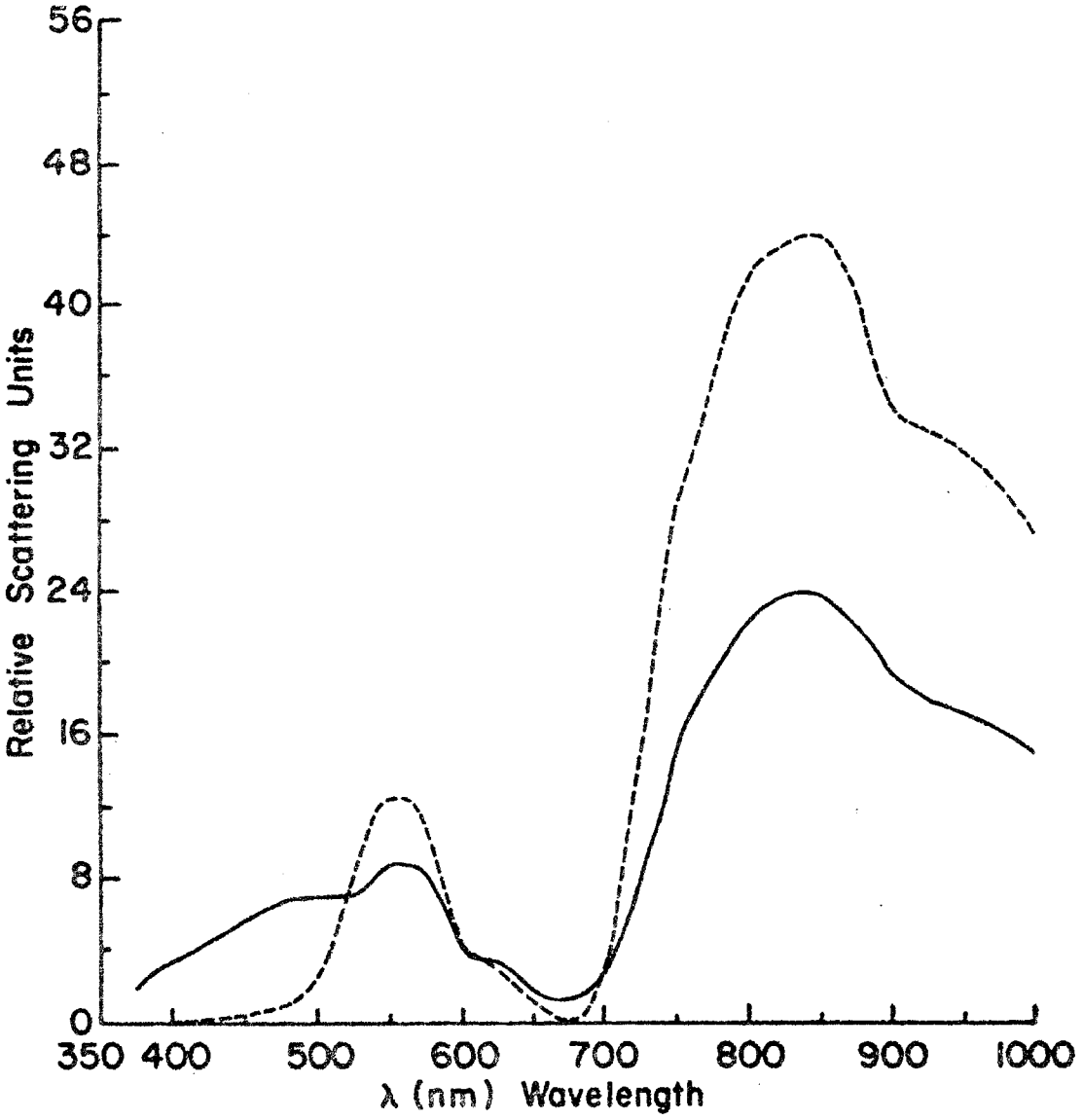

Figure 71. Corn Leaf Relative $[\rho'\cos\theta_{coll}]$(_____) at $\theta_{coll} = 15^{\circ}$ and Relative $[\tau'\cos(\pi - \theta_{coll})]$(-----) at $\theta_{coll} = 180^{\circ}$ versus λ for Bottom Incidence at $\theta_{inc} = 15^{\circ}$ (Vertical Midvein Orientation).

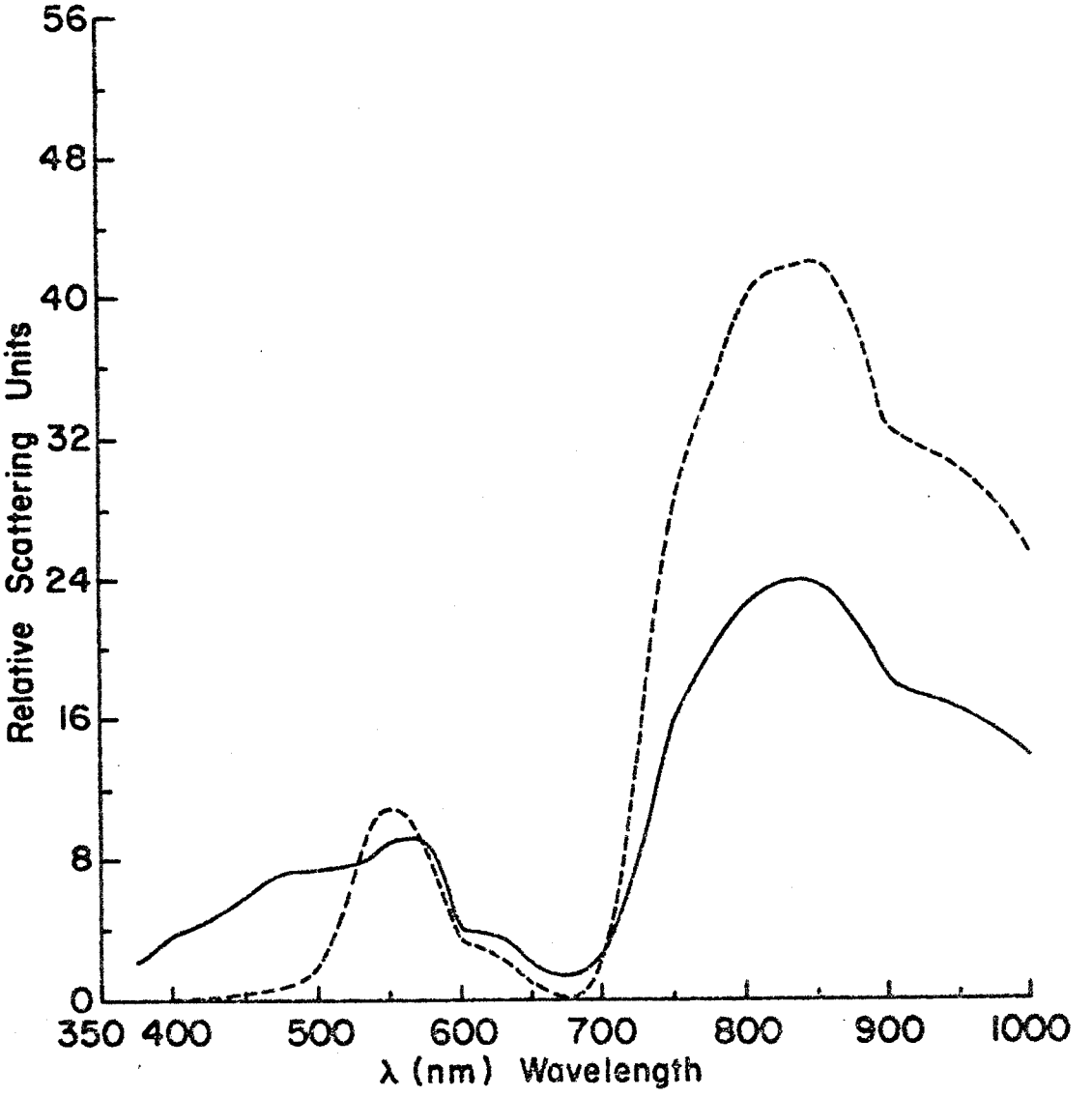

Figure 72. Corn Leaf Relative $[\rho'\cos\theta_{coll}]$(_____) at $\theta_{coll} = 30^{\circ}$ and Relative $[\tau'\cos(\pi - \theta_{coll})]$(-----) at $\theta_{coll} = 180^{\circ}$ versus λ for Bottom Incidence at $\theta_{inc} = 30^{\circ}$ (Vertical Midvein Orientation).

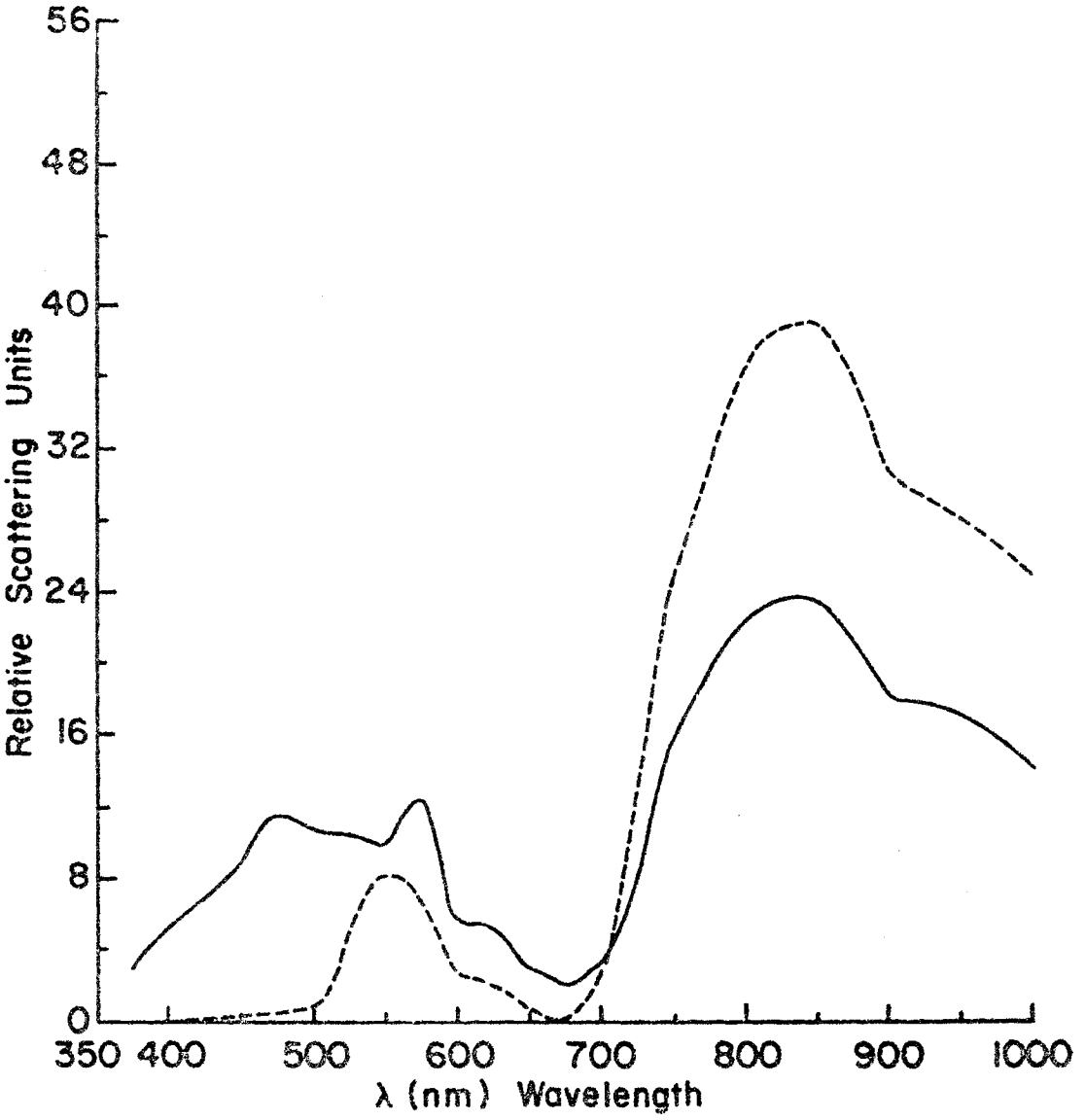

Figure 73. Corn Leaf Relative [$\rho'\cos\theta_{coll}$](_____) at $\theta_{coll} = 45^{\circ}$ and Relative [$\tau'\cos(\pi - \theta_{coll})$](-----) at $\theta_{coll} = 180^{\circ}$ versus λ for Bottom Incidence at $\theta_{inc} = 45^{\circ}$ (Vertical Midvein Orientation).

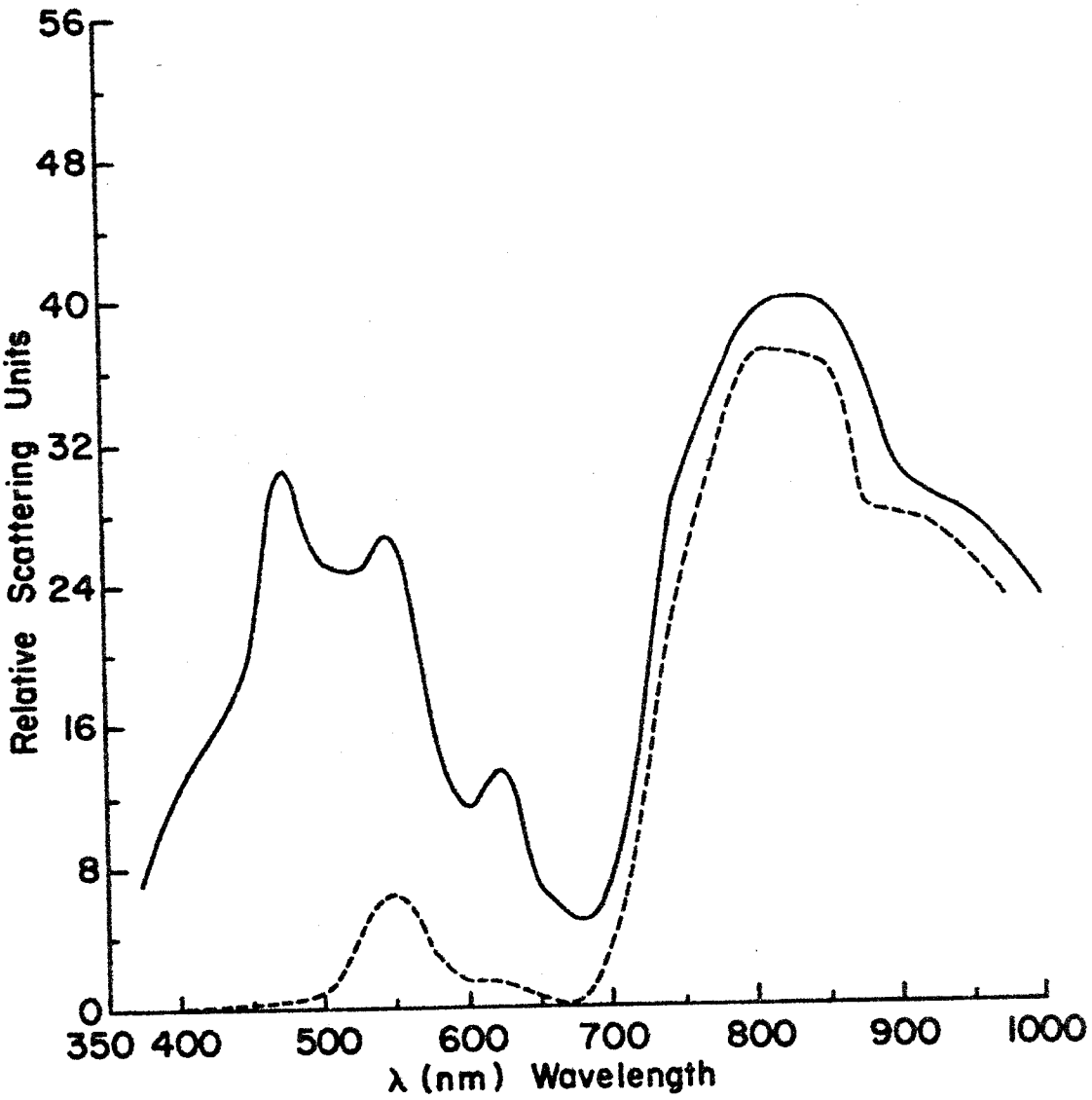

Figure 74. Corn Leaf Relative $[\sigma'\cos\theta_{coll}]$(_____) at $\theta_{coll} = 60^{\circ}$ and Relative $[\tau'\cos(\pi - \theta_{coll})]$(- - - - -) at $\theta_{coll} = 180^{\circ}$ versus λ for Bottom Incidence at $\theta_{inc} = 60^{\circ}$ (Vertical Midvein Orientation).

Plots of the scattering distribution functions versus angle of incidence were constructed from these spectra for 450 nm, 550 nm, 650 nm, and 850 nm. These representative wavelengths were chosen in order to show these results for highly absorbing regions as well as for highly reflecting and transmitting regions. The curves are for vertical midvein orientation and plots for top and bottom incidence are on the same graph for comparison. Different leaves are used for top and bottom curves and different leaves are sometimes used for each wavelength range. The polar plots identify the leaves used for each set of conditions. Figure 75 gives the scattering distribution function versus angle of incidence for reflection at the specular angle, for the representative wavelengths given above.

Figures 76 and 77 are the results for the scattering distribution function versus angle of incidence for transmission along a normal to the sample surface, for the representative wavelengths mentioned above.

The corn leaf bi-directional scattering data were graphically analyzed to determine the angles for maximum reflection and transmission. It was difficult to make this graphical approximation of these angles since the polar plots are broad about these angles. Maximum reflection and transmission angles were determined for each of the polar plots given on the composite polar plot page for a particular angle of incidence. This was done for the range from 375 nm through 675 nm and for the range from 750 nm through 1μm. Figure 78 gives the average of these points versus angle of incidence with the ideal mirror characteristic given for reference for the range from 375 nm through 675 nm and Figure 79 gives the average of these points versus angle of incidence for the range from 750 nm through 1μm.

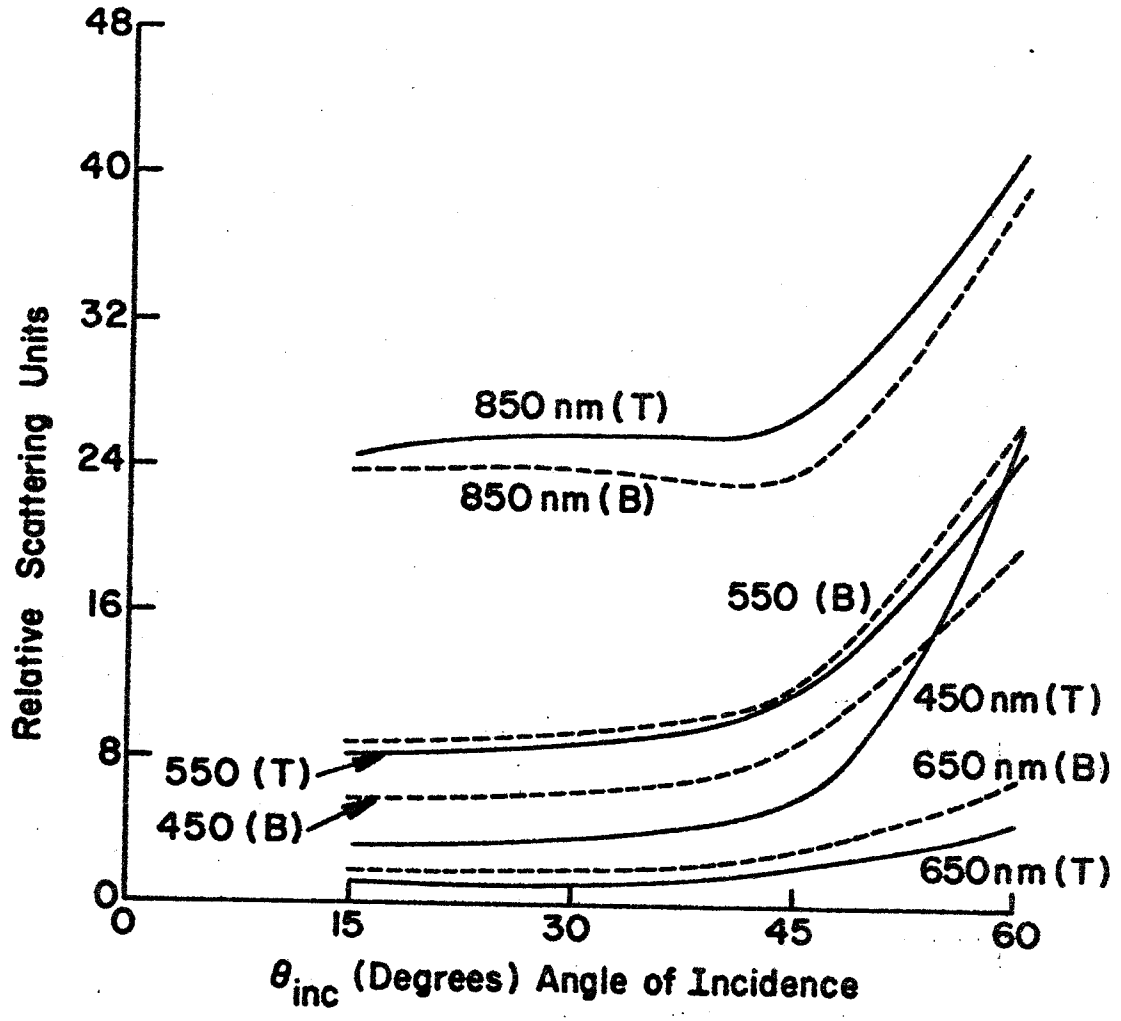

Figure 75. Corn Leaf Relative [$\rho' \cos\theta_{coll}$] at the specular collection angle versus θ_{inc} for Top Incidence (_____) and Bottom Incidence (– – – –) at 450 nm, 550 nm, 650 nm, and 850 nm (Vertical Midvein Orientation).

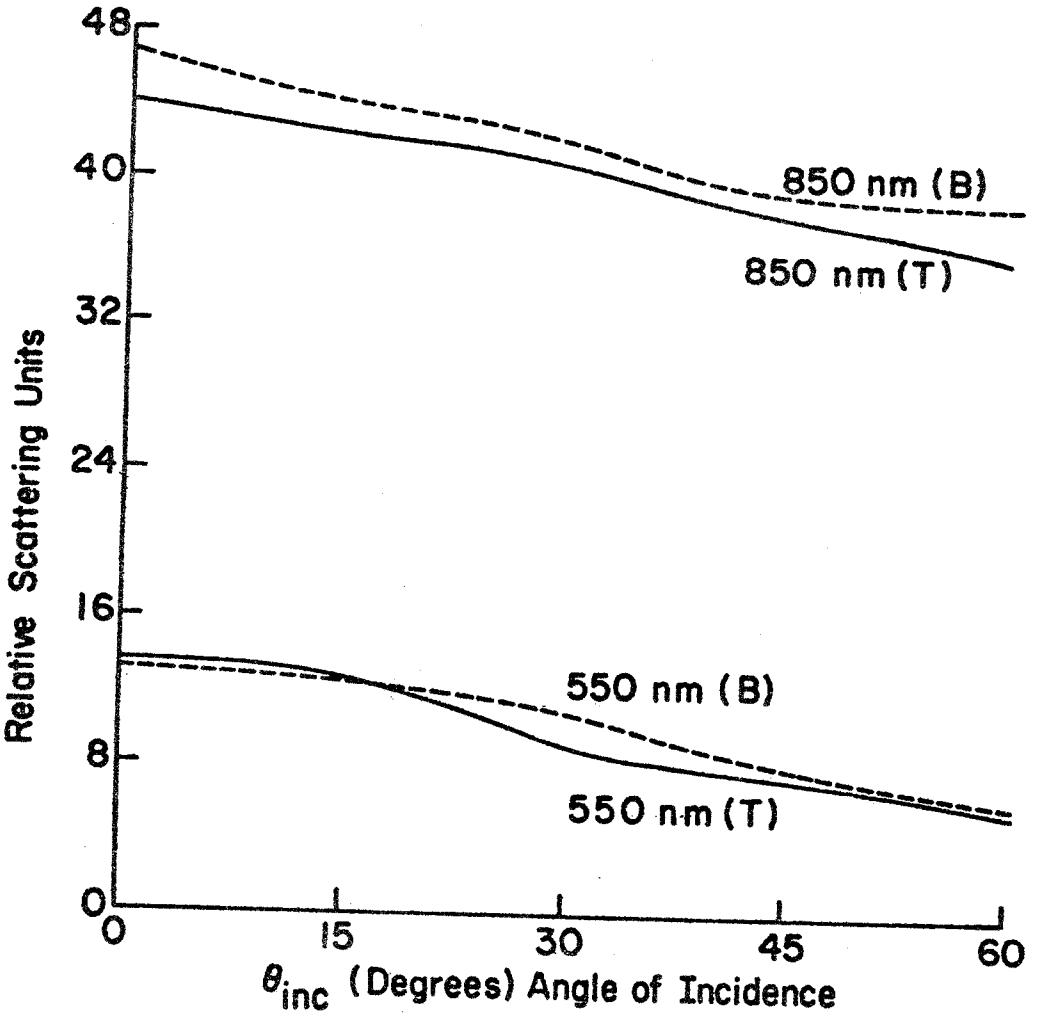

Figure 76. Corn Leaf Relative $[\tau'\cos(\pi - \theta_{coll})]$ at $\theta_{coll} = 180^{\circ}$ versus θ_{inc} for Top Incidence (_____) and Bottom Incidence (– – – –) at 550 nm and 850 nm (Vertical Midvein Orientation).

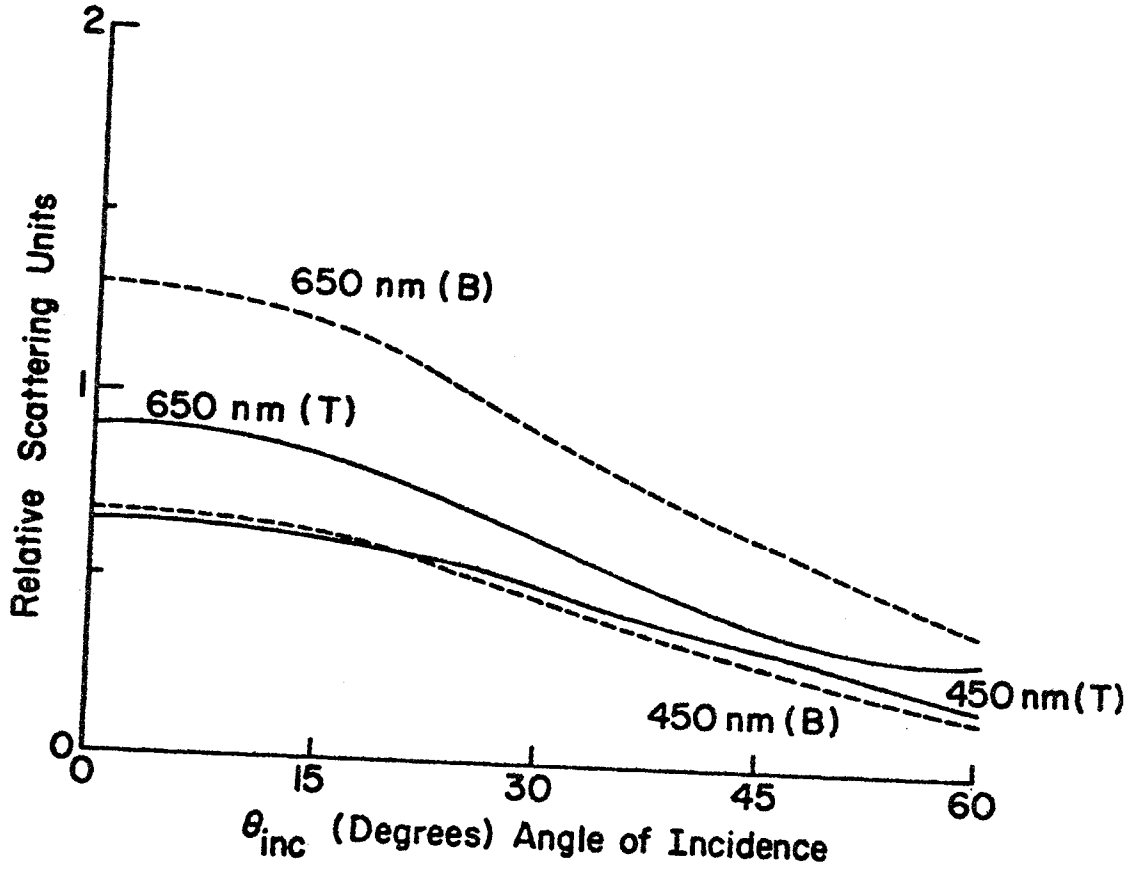

Figure 77. Corn Leaf Relative $[\tau' \cos(\pi - \theta_{coll})]$ at $\theta_{coll} = 180^{\circ}$ versus θ_{inc} for Top Incidence (_____) and Bottom Incidence (– – – –) at 450 nm and 650 nm (Vertical Midvein Orientation).

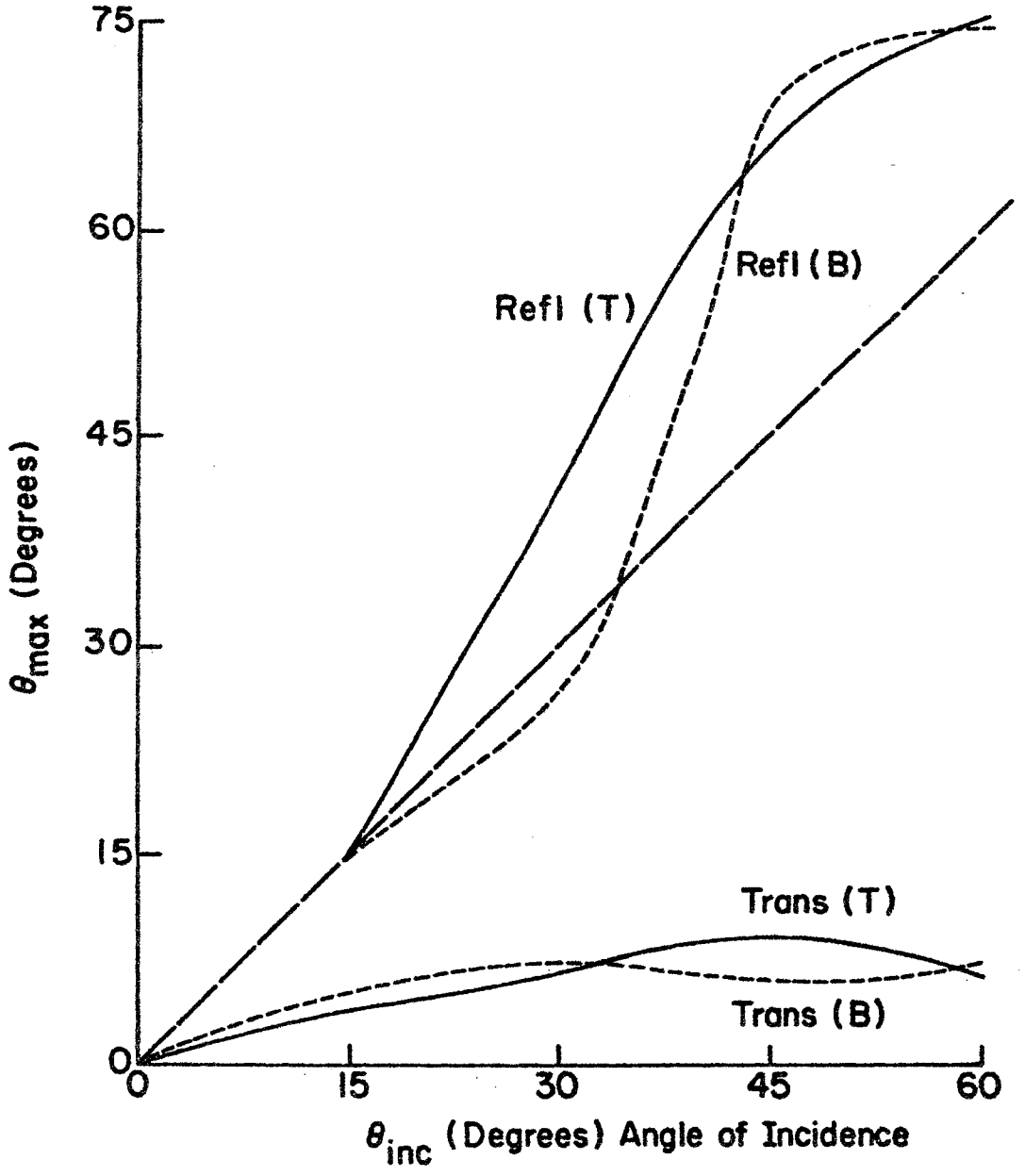

Figure 78. Corn Leaf Average Collection Angle for Maximum Relative $[\rho'\cos\theta_{coll}]$ and Maximum Relative $[\tau'\cos(\pi - \theta_{coll})]$ versus θ_{inc} for Top Incidence (_____) and Bottom Incidence (– – –) for the range of λ from 375 nm through 675 nm (Vertical Midvein Orientation).

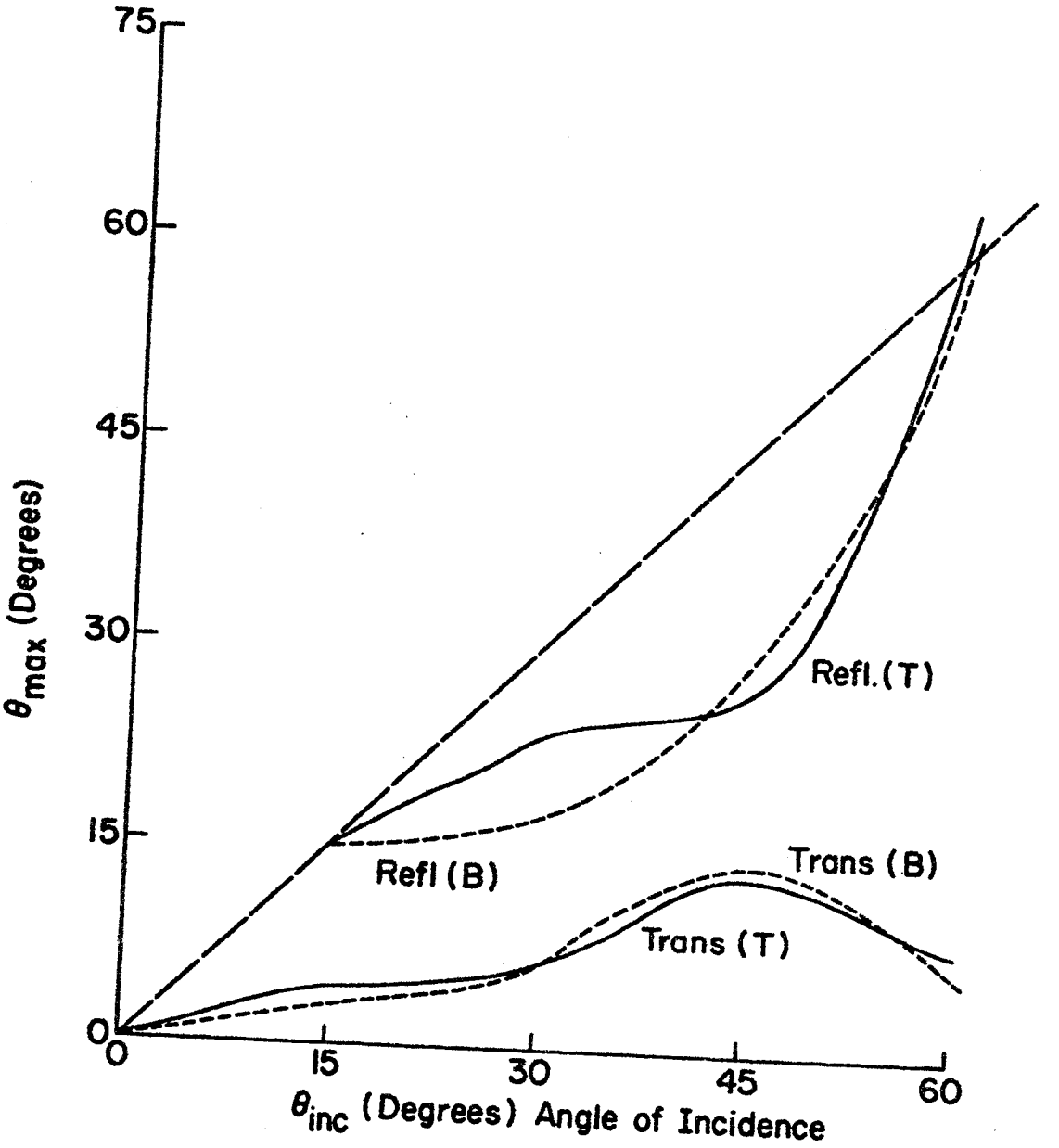

Figure 79. Corn Leaf Average Collection Angle for Maximum Relative $[\rho'\cos\theta_{coll}]$ and Maximum Relative $[\tau'\cos(\pi - \theta_{coll})]$ versus θ_{inc} for Top Incidence (_____) and Bottom Incidence (– – – –) for the range of λ from 750 nm through 1000 nm (Vertical Midvein Orientation).

The transmission angles are measured counter-clockwise from a normal to the plane of the leaf sample so they can be plotted on the graph with the reflection angles.

Horizontal Midvein Orientation

The following ten figures are the bi-directional scattering data for healthy, green corn leaves with a horizontal midvein orientation. Figures 80 through 84 are the results for top incidence and Figures 85 through 89 are the results for bottom incidence.

Scattering distribution functions versus wavelength for various collection angles are taken directly from the bi-directional polar scattering plots. Figures 90 through 94 give spectra for top incidence and Figures 95 through 99 give the spectra for bottom incidence. The transmission curves are for a 180° collection angle which is along a normal to the leaf surface. This is a good measure of the transmission even though the functional forms vary for different angles of incidence.

The reflection curves are plotted for the specular angle except for normal incidence where a 45° collection angle is used.

Results from several leaves were used to plot these spectra. The polar plots identify the leaf and the particular wavelength range.

Plots of the scattering distribution functions versus angle of incidence were constructed from these spectra for 450 nm, 550 nm, 650 nm, and 850 nm. These representative wavelengths were chosen in order to show these results for highly absorbing regions as well as for highly reflecting and transmitting regions. These curves are for horizontal midvein orientation and plots for top and bottom are on the same graph

Figure 80. Corn Leaf Relative $[\rho'\cos\theta_{coll}]$ and Relative $[\tau'\cos(\pi - \theta_{coll})]$ versus θ_{coll} for Top Incidence at $\theta_{inc} = 0^{\circ}$ (Horizontal Midvein Orientation).

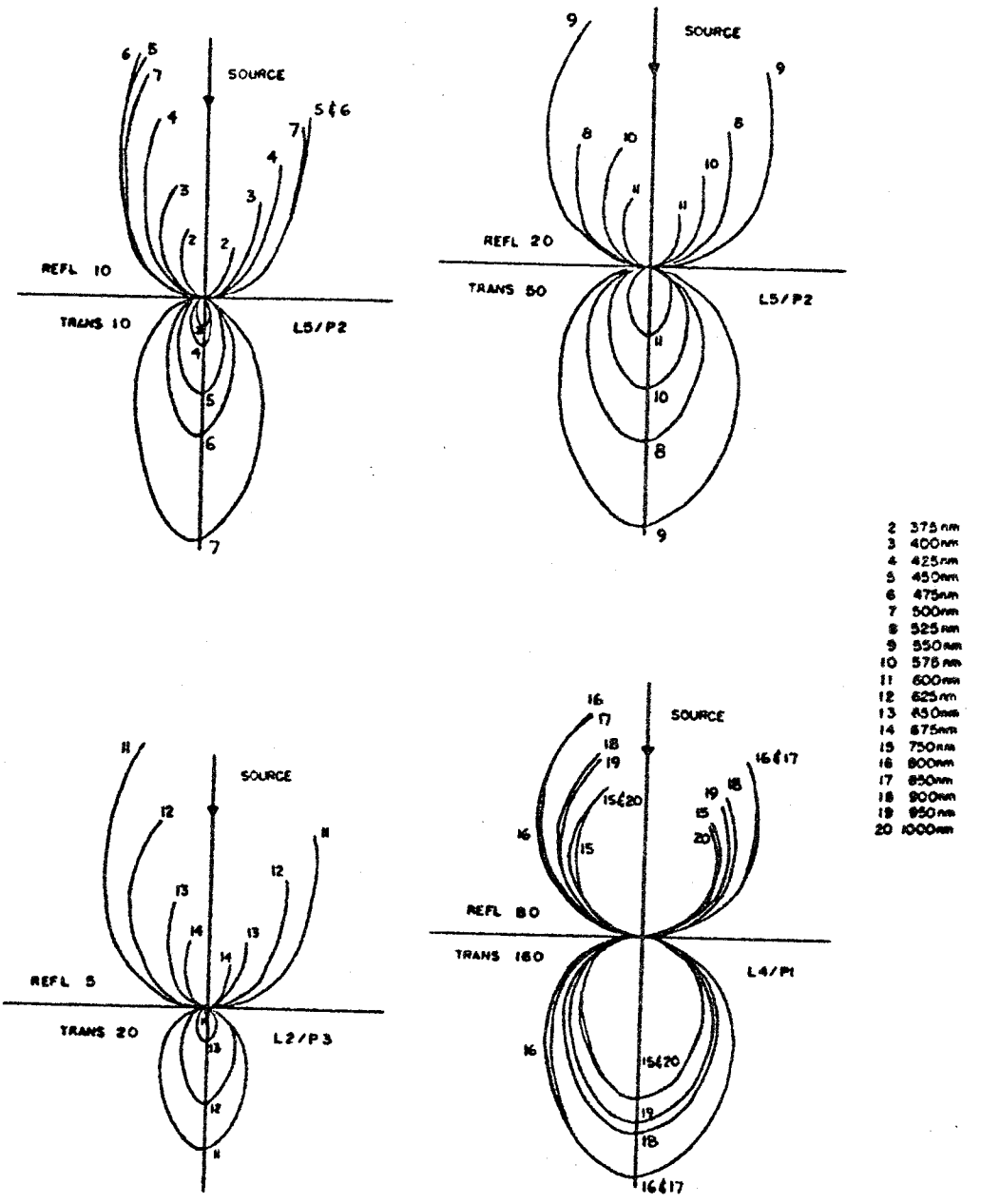
SOURCE
REFL 10
TRANS 10
L5/P2
SOURCE
REFL 20
TRANS 50
L5/P2
SOURCE
REFL 5
TRANS 20
L2/P3
SOURCE
REFL 80
TRANS 160
L4/P1
2 375nm
3 400nm
4 425nm
5 450nm
6 475nm
7 500nm
8 525nm
9 550nm
10 575nm
11 600nm
12 625nm
13 650nm
14 675nm
15 750nm
16 800nm
17 850nm
18 900nm
19 950nm
20 1000nm

Figure 80.

Figure 81. Corn Leaf Relative $[\rho'\cos\theta_{coll}]$ and Relative $[\tau'\cos(\pi - \theta_{coll})]$ versus θ_{coll} for Top Incidence at $\theta_{inc} = 15^{o}$ (Horizontal Midvein Orientation).

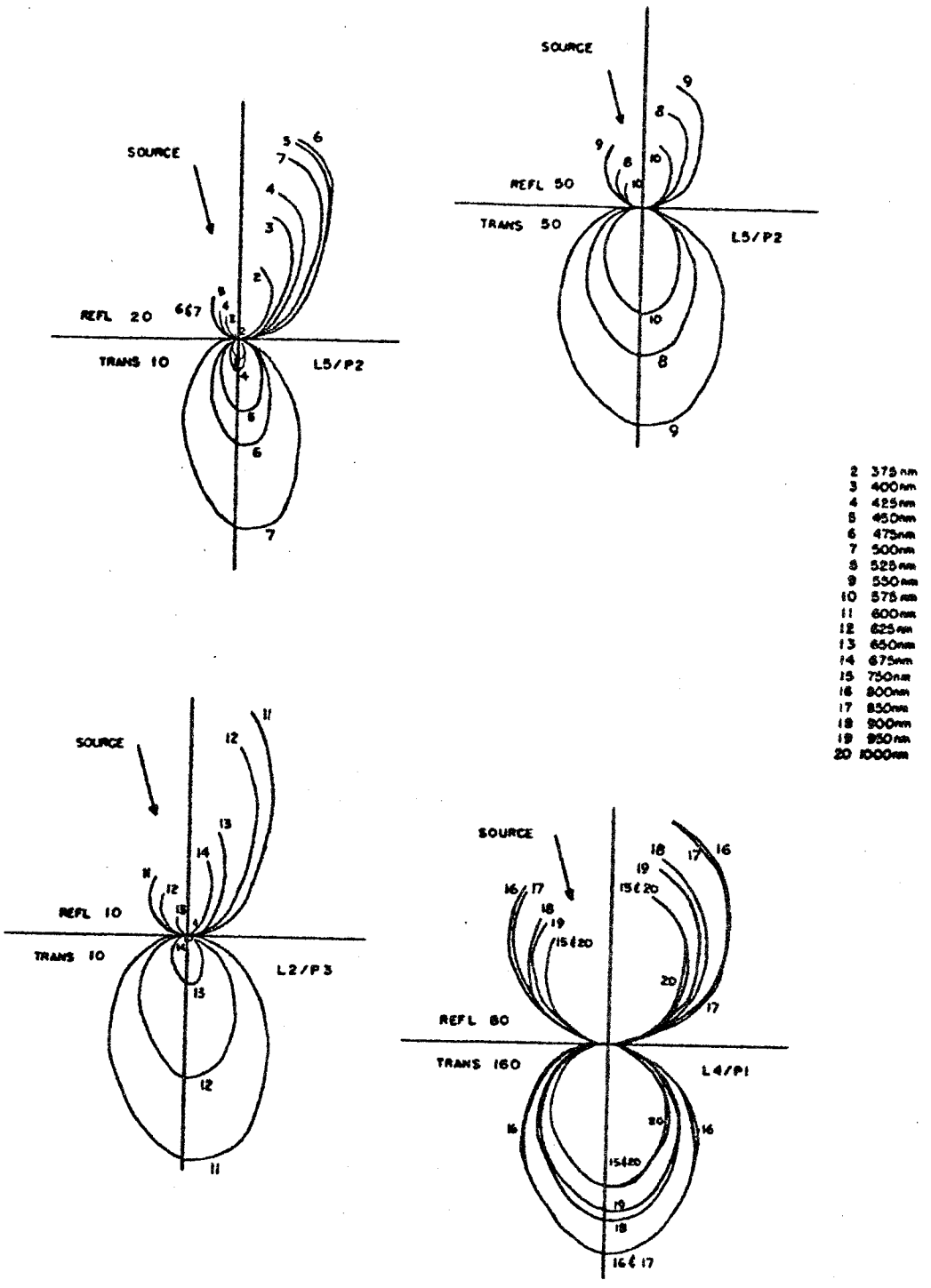
SOURCE
REFL 20
TRANS 10
L5/P2
SOURCE
REFL 50
TRANS 50
L5/P2
SOURCE
REFL 10
TRANS 10
L2/P3
SOURCE
REFL 80
TRANS 160
L4/P1
2 375 nm
3 400nm
4 425nm
5 450nm
6 475nm
7 500nm
8 525nm
9 550nm
10 575nm
11 600nm
12 625nm
13 650nm
14 675nm
15 750nm
16 800nm
17 850nm
18 900nm
19 950nm
20 1000nm

Figure 81.

Figure 82. Corn Leaf Relative $[\rho'\cos\theta_{coll}]$ and Relative $[\tau'\cos(\pi - \theta_{coll})]$ versus θ_{coll} for Top Incidence at $\theta_{inc} = 30^{\circ}$ (Horizontal Midvein Orientation).

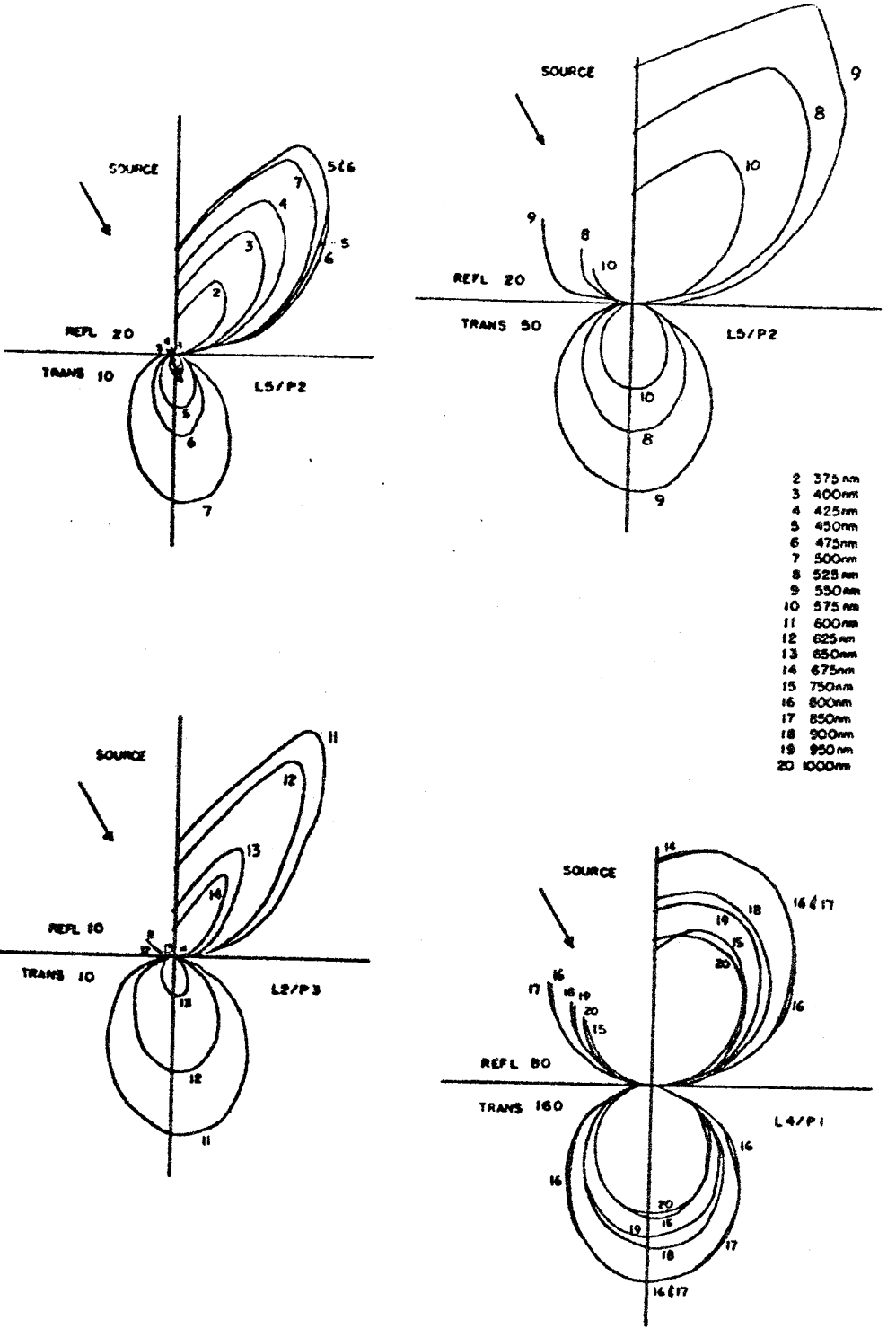
SOURCE
REFL 20
TRANS 10
L5/P2
SOURCE
REFL 20
TRANS 50
L5/P2
SOURCE
REFL 10
TRANS 10
L2/P3
SOURCE
REFL 80
TRANS 160
L4/P1
2 375 nm
3 400nm
4 425nm
5 450nm
6 475nm
7 500nm
8 525 nm
9 550nm
10 575 nm
11 600nm
12 625nm
13 650nm
14 675nm
15 750nm
16 800nm
17 850nm
18 900nm
19 950nm
20 1000nm

Figure 82.

Figure 83. Corn Leaf Relative $[\rho'\cos\theta_{coll}]$ and Relative $[\tau'\cos(\pi - \theta_{coll})]$ versus θ_{coll} for Top Incidence at $\theta_{inc} = 45^{o}$ (Horizontal Midvein Orientation).

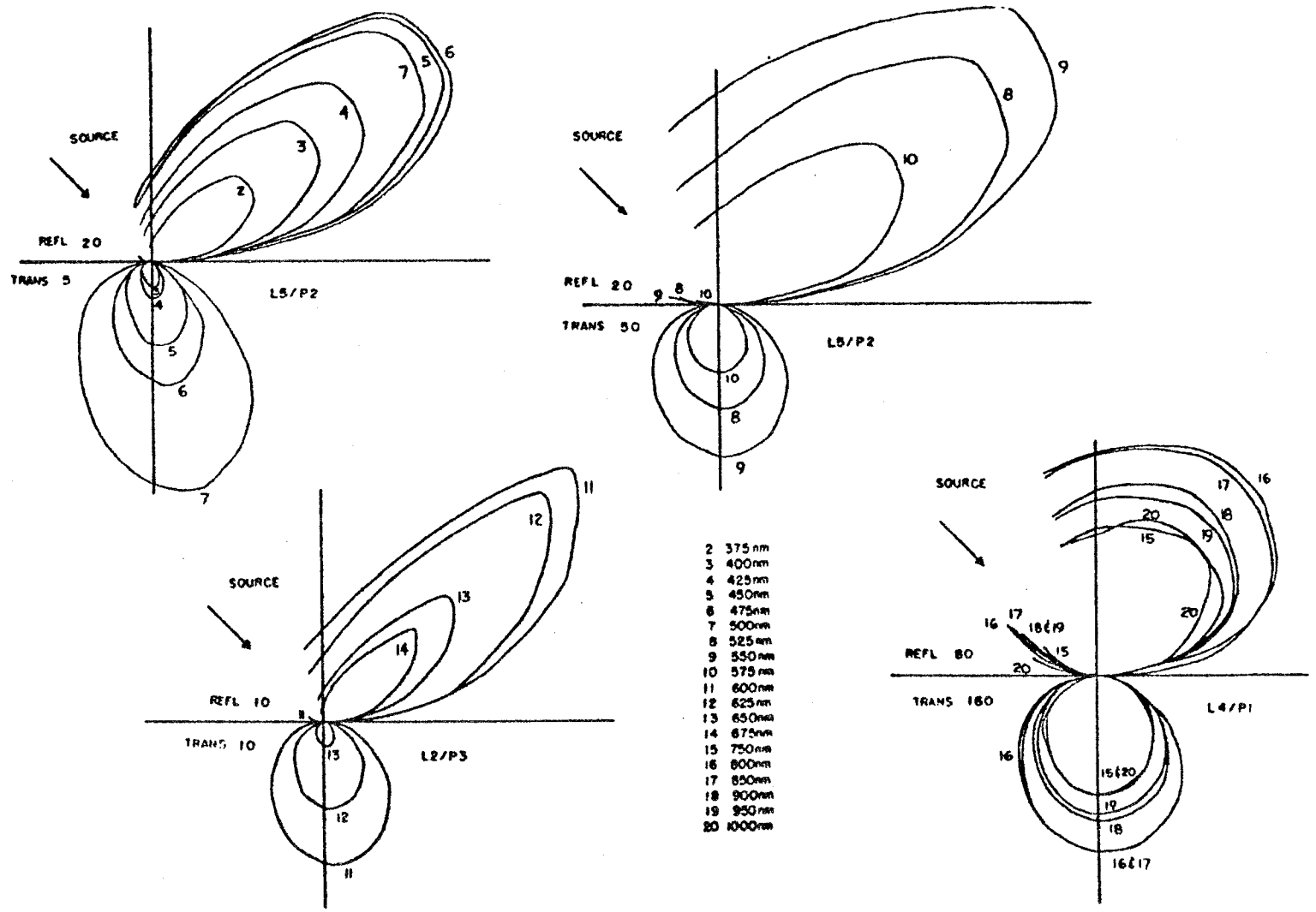
SOURCE
REFL 20
TRANS 5
L5/P2
SOURCE
REFL 20
TRANS 50
L5/P2
SOURCE
REFL 10
TRANS 10
L2/P3
SOURCE
REFL 80
TRANS 160
L4/P1
2 375nm
3 400nm
4 425nm
5 450nm
6 475nm
7 500nm
8 525nm
9 550nm
10 575nm
11 600nm
12 625nm
13 650nm
14 675nm
15 750nm
16 800nm
17 850nm
18 900nm
19 950nm
20 1000nm

Figure 83.

Figure 84. Corn Leaf Relative $[\rho'\cos\theta_{coll}]$ and Relative $[\tau'\cos(\pi - \theta_{coll})]$ versus θ_{coll} for Top Incidence at $\theta_{inc} = 60^{o}$ (Horizontal Midvein Orientation).

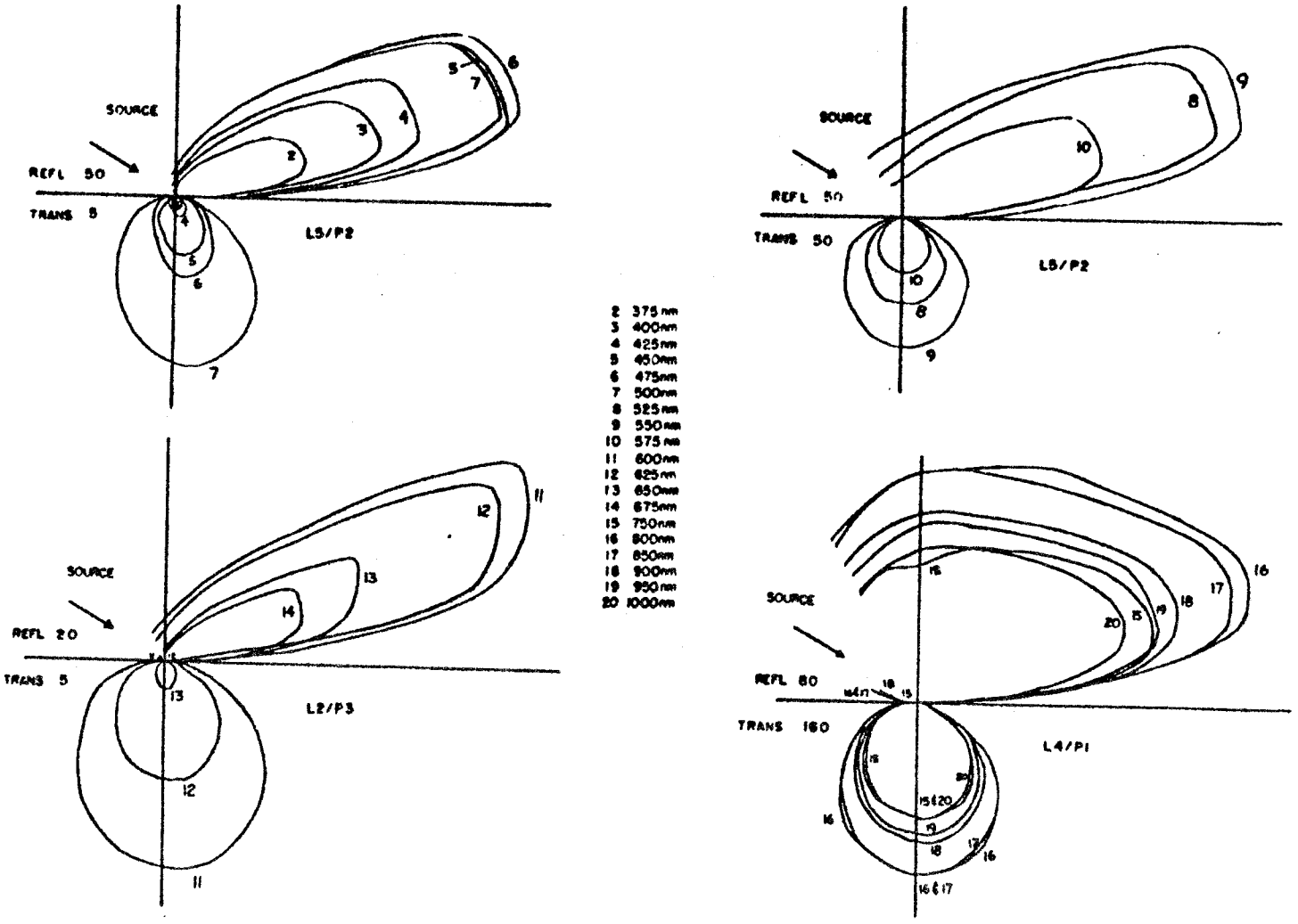
SOURCE
REFL 50
TRANS 8
L5/P2
SOURCE
REFL 50
TRANS 50
L5/P2
SOURCE
REFL 20
TRANS 5
L2/P3
SOURCE
REFL 80
TRANS 160
L4/P1
2 375nm
3 400nm
4 425nm
5 450nm
6 475nm
7 500nm
8 525nm
9 550nm
10 575nm
11 600nm
12 625nm
13 650nm
14 675nm
15 750nm
16 800nm
17 850nm
18 900nm
19 950nm
20 1000nm

Figure 84.

Figure 85. Corn Leaf Relative $[\rho' \cos \theta_{coll}]$ and Relative $[\tau' \cos(\pi - \theta_{coll})]$ versus θ_{coll} for Bottom Incidence at $\theta_{inc} = 0^{o}$ (Horizontal Midvein Orientation).

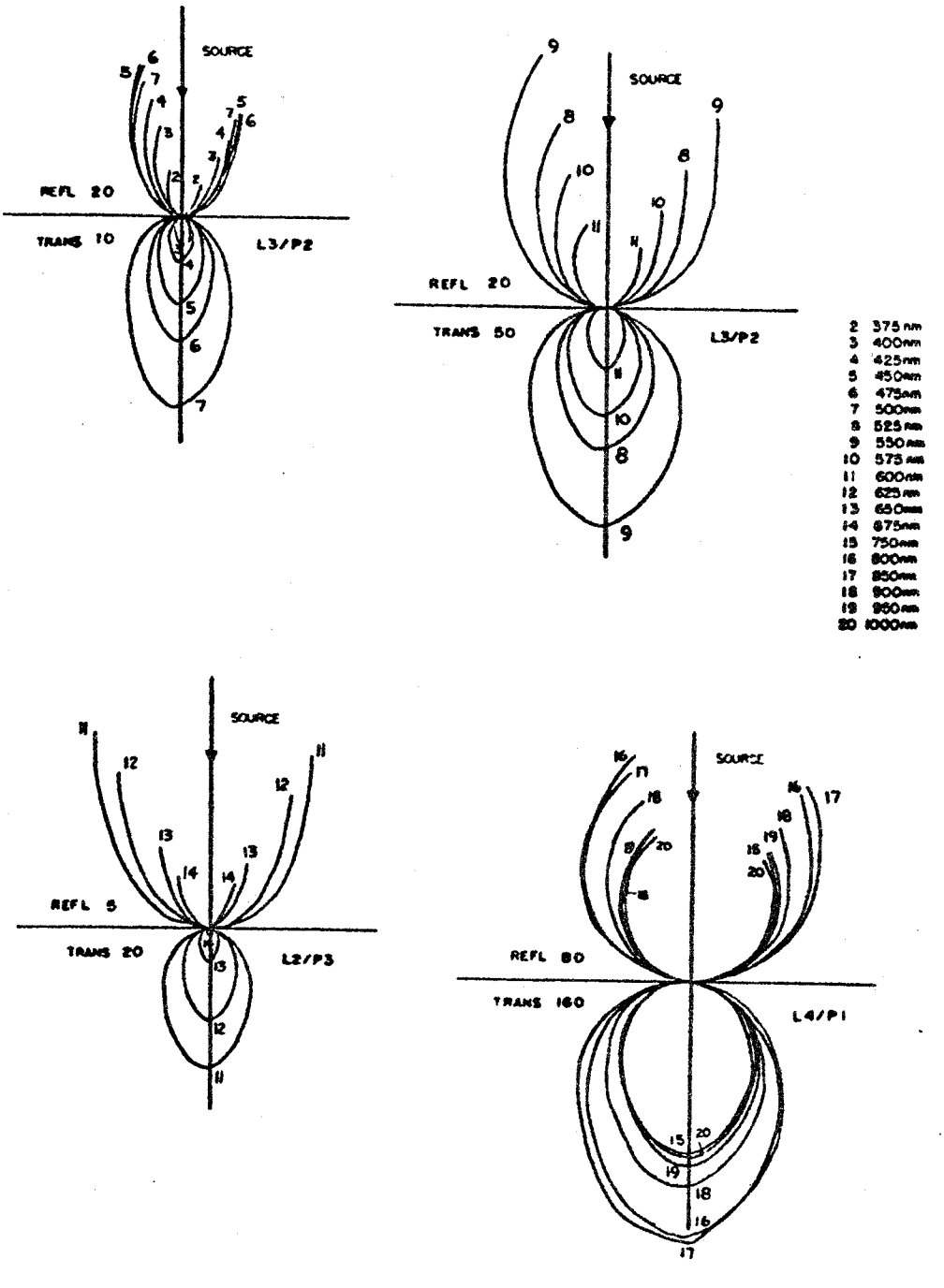
SOURCE
REFL 20
TRANS 10
L3/P2
SOURCE
REFL 20
TRANS 50
L3/P2
2 375nm
3 400nm
4 425nm
5 450nm
6 475nm
7 500nm
8 525nm
9 550nm
10 575nm
11 600nm
12 625nm
13 650nm
14 675nm
15 700nm
16 800nm
17 850nm
18 900nm
19 950nm
20 1000nm
SOURCE
REFL 5
TRANS 20
L2/P3
SOURCE
REFL 80
TRANS 160
L4/P1

Figure 85.

Figure 86. Corn Leaf Relative [$\rho'\cos\theta_{coll}$] and Relative [$\tau'\cos(\pi - \theta_{coll})$] versus θ_{coll} for Bottom Incidence at $\theta_{inc} = 15^{o}$ (Horizontal Midvein Orientation).

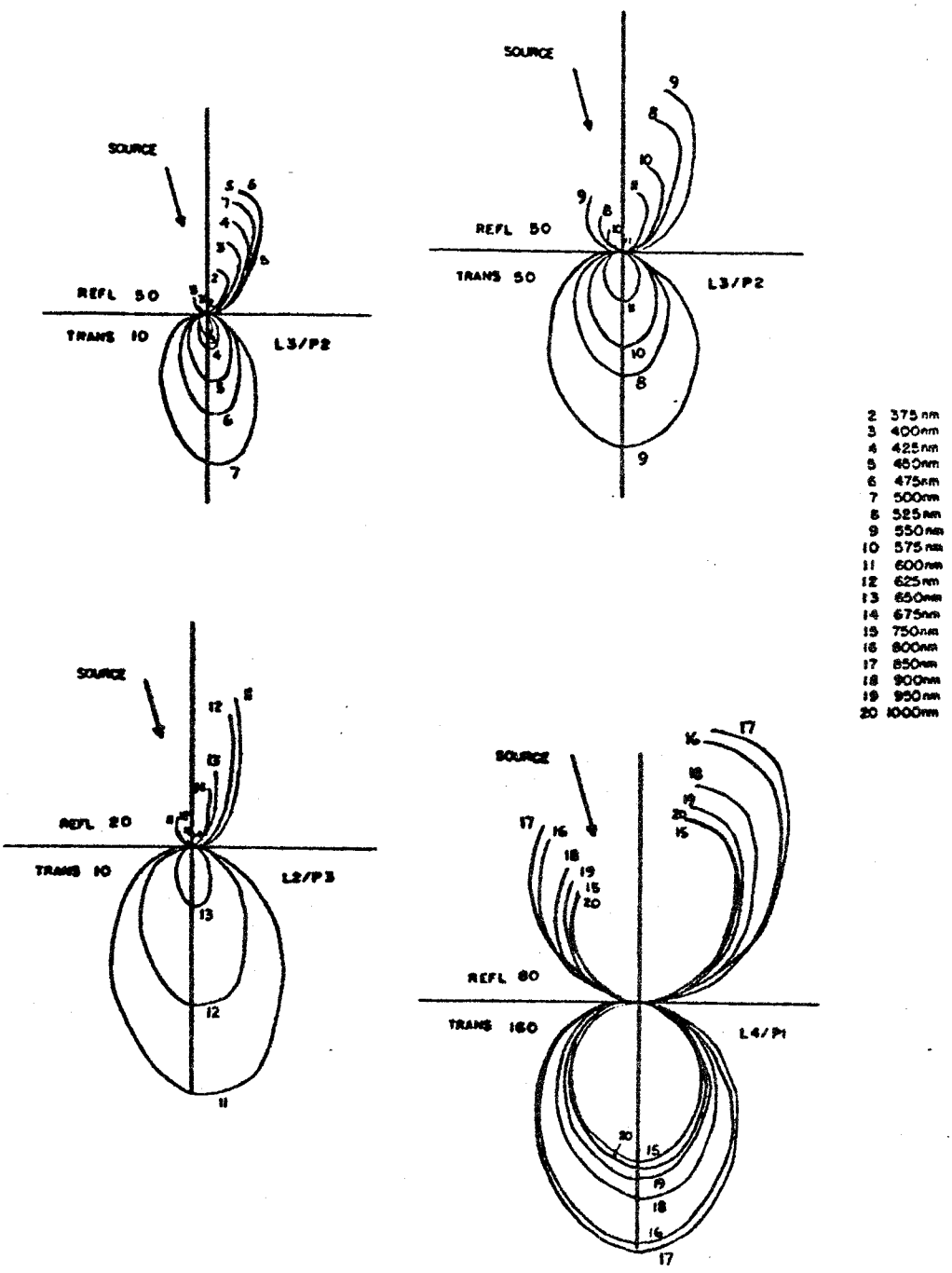
SOURCE
REFL 50
TRANS 10
L3/P2
SOURCE
REFL 50
TRANS 50
L3/P2
SOURCE
REFL 20
TRANS 10
L2/P3
SOURCE
REFL 80
TRANS 160
L4/P1
2 375 nm
3 400nm
4 425nm
5 450nm
6 475nm
7 500nm
8 525nm
9 550nm
10 575nm
11 600nm
12 625nm
13 650nm
14 675nm
15 750nm
16 800nm
17 850nm
18 900nm
19 950nm
20 1000nm

Figure 86.

Figure 87. Corn Leaf Relative $[\rho' \cos \theta_{coll}]$ and Relative $[\tau' \cos(\pi - \theta_{coll})]$ versus θ_{coll} for Bottom Incidence at $\theta_{inc} = 30^{\circ}$ (Horizontal Midvein Orientation).

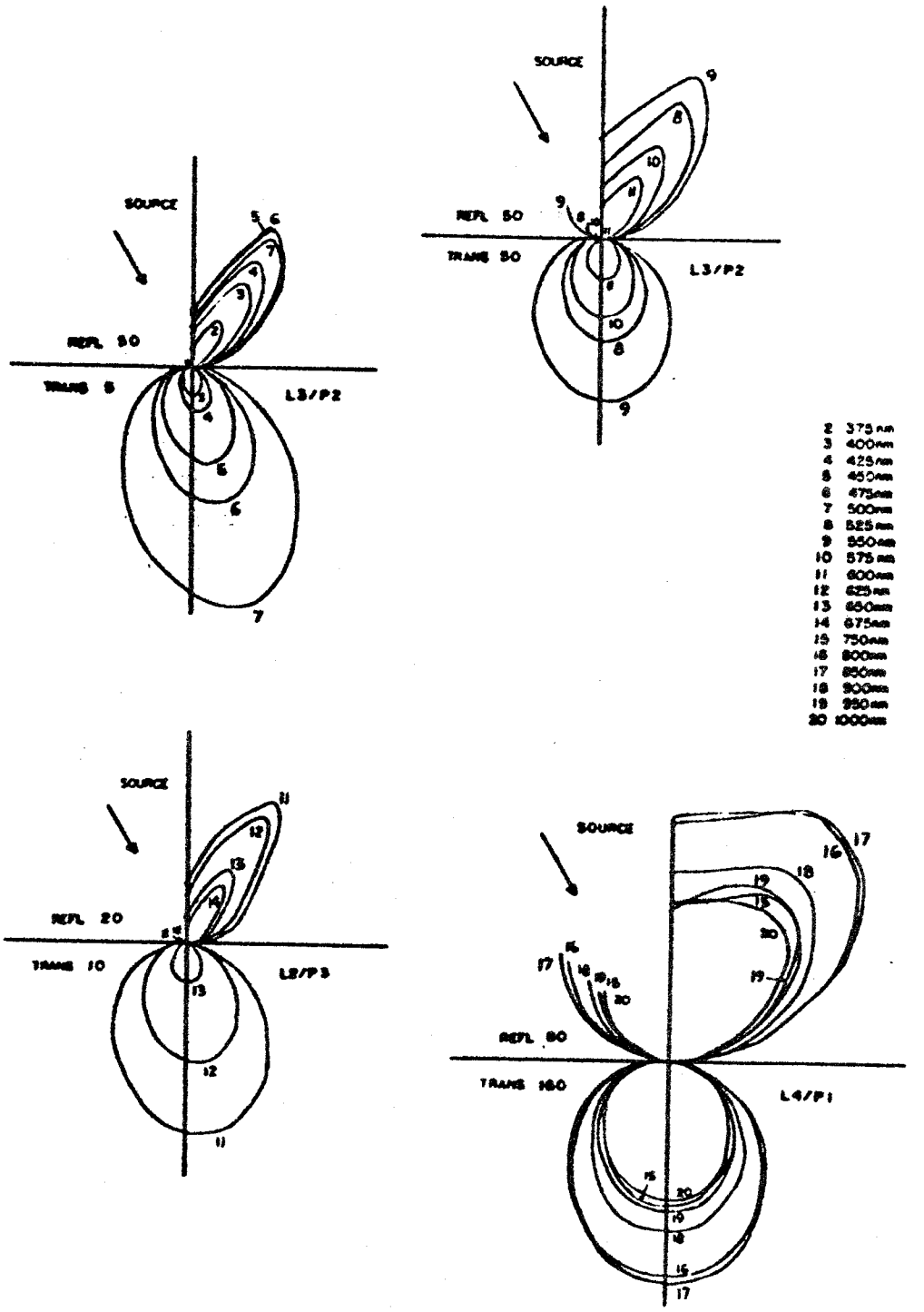
SOURCE
REFL 50
TRANS 5
L3/P2
SOURCE
REFL 50
TRANS 50
L3/P2
SOURCE
REFL 20
TRANS 10
L2/P3
SOURCE
REFL 80
TRANS 180
L4/P1
2 375 nm
3 400nm
4 425nm
5 450nm
6 475nm
7 500nm
8 525nm
9 550nm
10 575nm
11 600nm
12 625nm
13 650nm
14 675nm
15 750nm
16 800nm
17 850nm
18 900nm
19 950nm
20 1000nm

Figure 87.

Figure 88. Corn Leaf Relative $[\rho' \cos\theta_{coll}]$ and Relative $[\tau' \cos(\pi - \theta_{coll})]$ versus θ_{coll} for Bottom Incidence at $\theta_{inc} = 45^{\circ}$ (Horizontal Midvein Orientation).

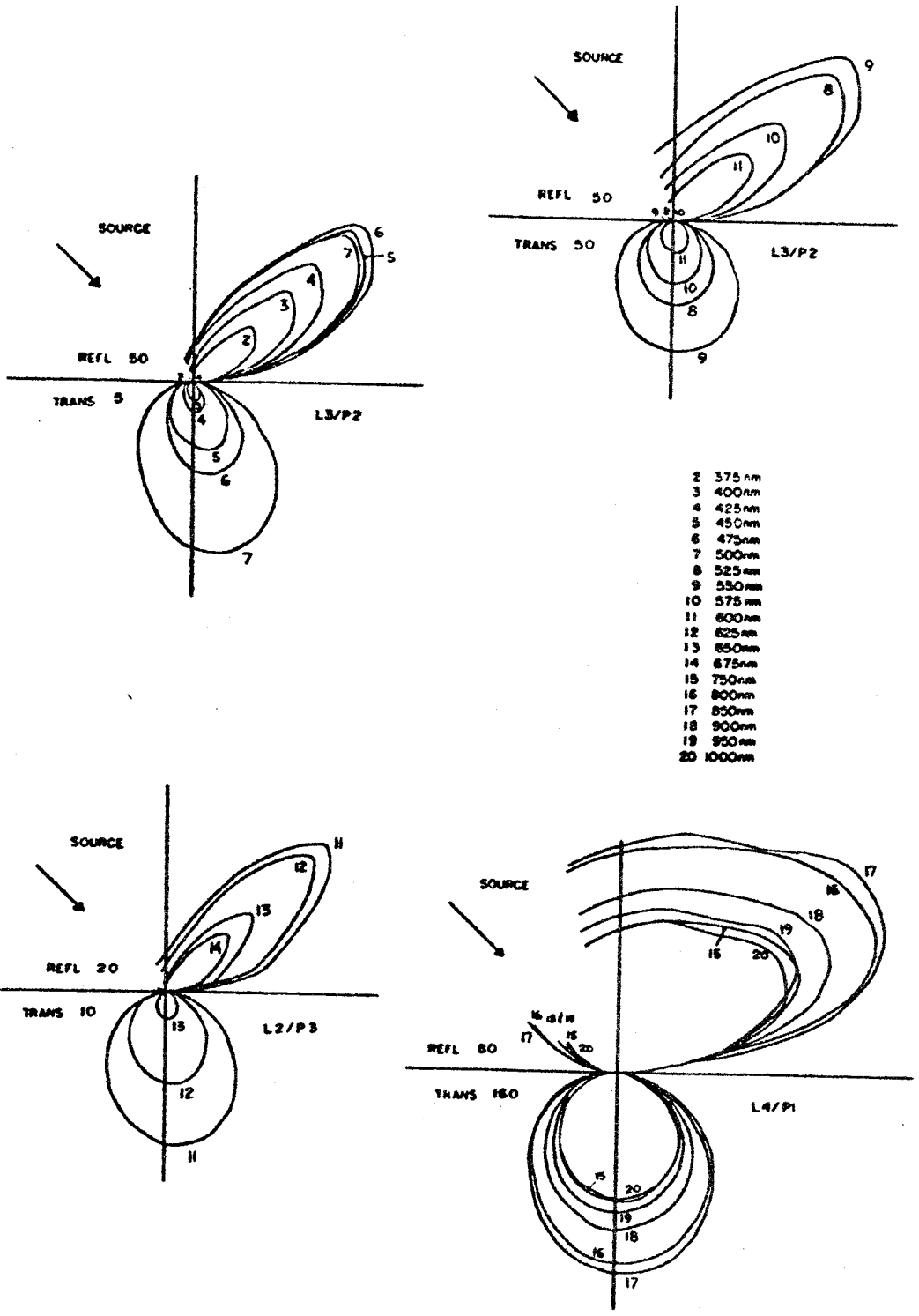
SOURCE
REFL 50
TRANS 5
L3/P2
SOURCE
REFL 50
TRANS 50
L3/P2
2 375nm
3 400nm
4 425nm
5 450nm
6 475nm
7 500nm
8 525nm
9 550nm
10 575nm
11 600nm
12 625nm
13 650nm
14 675nm
15 750nm
16 800nm
17 850nm
18 900nm
19 950nm
20 1000nm
SOURCE
REFL 20
TRANS 10
L2/P3
SOURCE
REFL 80
TRANS 180
L4/P1

Figure 88.

Figure 89. Corn Leaf Relative [$\rho'\cos\theta_{coll}$] and Relative [$\tau'\cos(\pi - \theta_{coll})$] versus θ_{coll} for Bottom Incidence at $\theta_{inc} = 60^{\circ}$ (Horizontal Midvein Orientation).

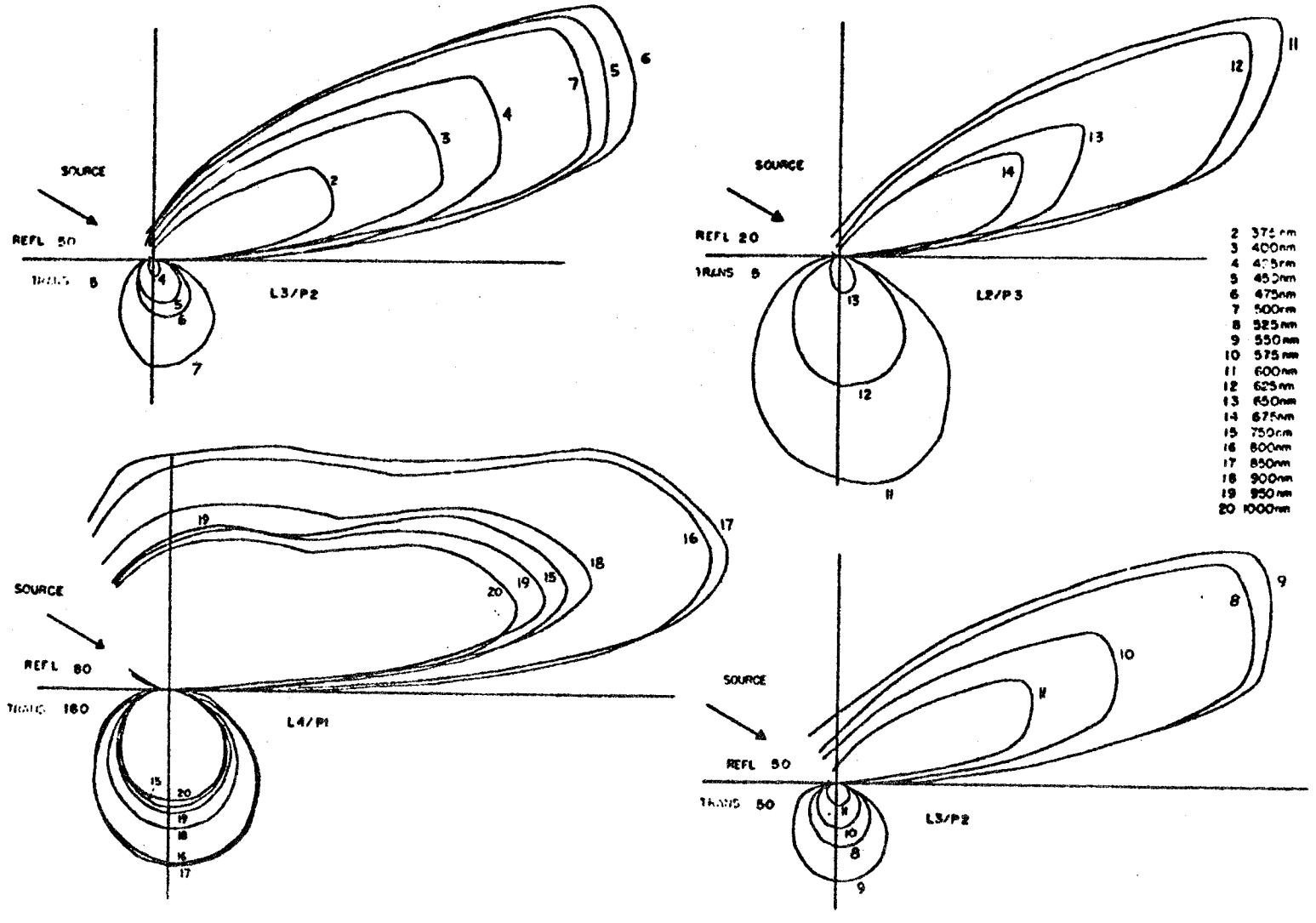
SOURCE
REFL 50
TRANS 5
L3/P2
SOURCE
REFL 20
TRANS 5
L2/P3
SOURCE
REFL 80
TRANS 160
L4/P1
SOURCE
REFL 50
TRANS 50
L3/P2
2 375nm
3 400nm
4 425nm
5 450nm
6 475nm
7 500nm
8 525nm
9 550nm
10 575nm
11 600nm
12 625nm
13 650nm
14 675nm
15 750nm
16 800nm
17 850nm
18 900nm
19 950nm
20 1000nm

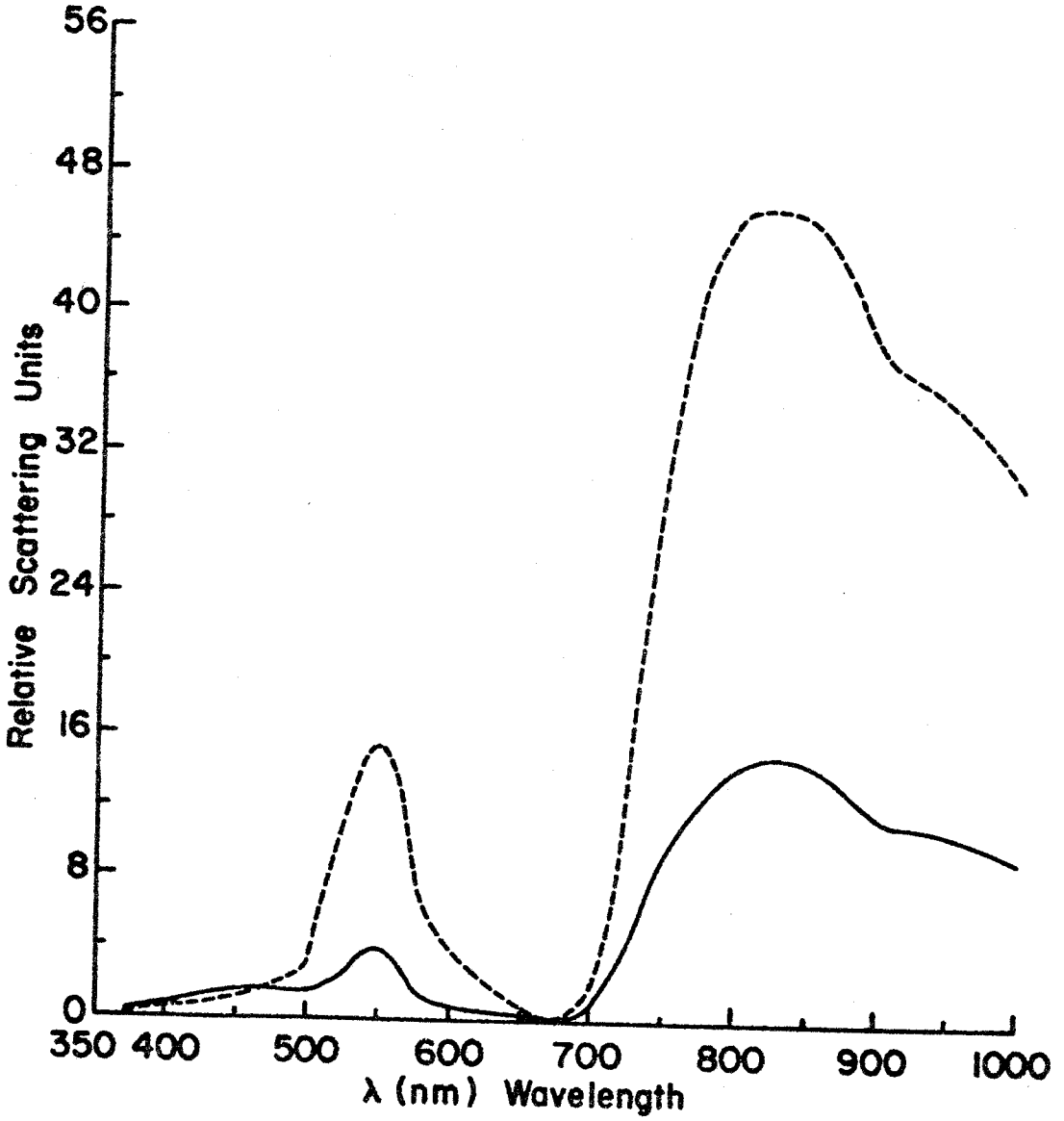

Figure 90. Corn Leaf Relative $[\rho'\cos\theta_{coll}]$(_____) at $\theta_{coll} = 45°$ and Relative $[\tau'\cos(\pi - \theta_{coll})]$(——) at $\theta_{coll} = 180°$ versus λ for Top Incidence at $\theta_{inc} = 0°$ (Horizontal Midvein Orientation).

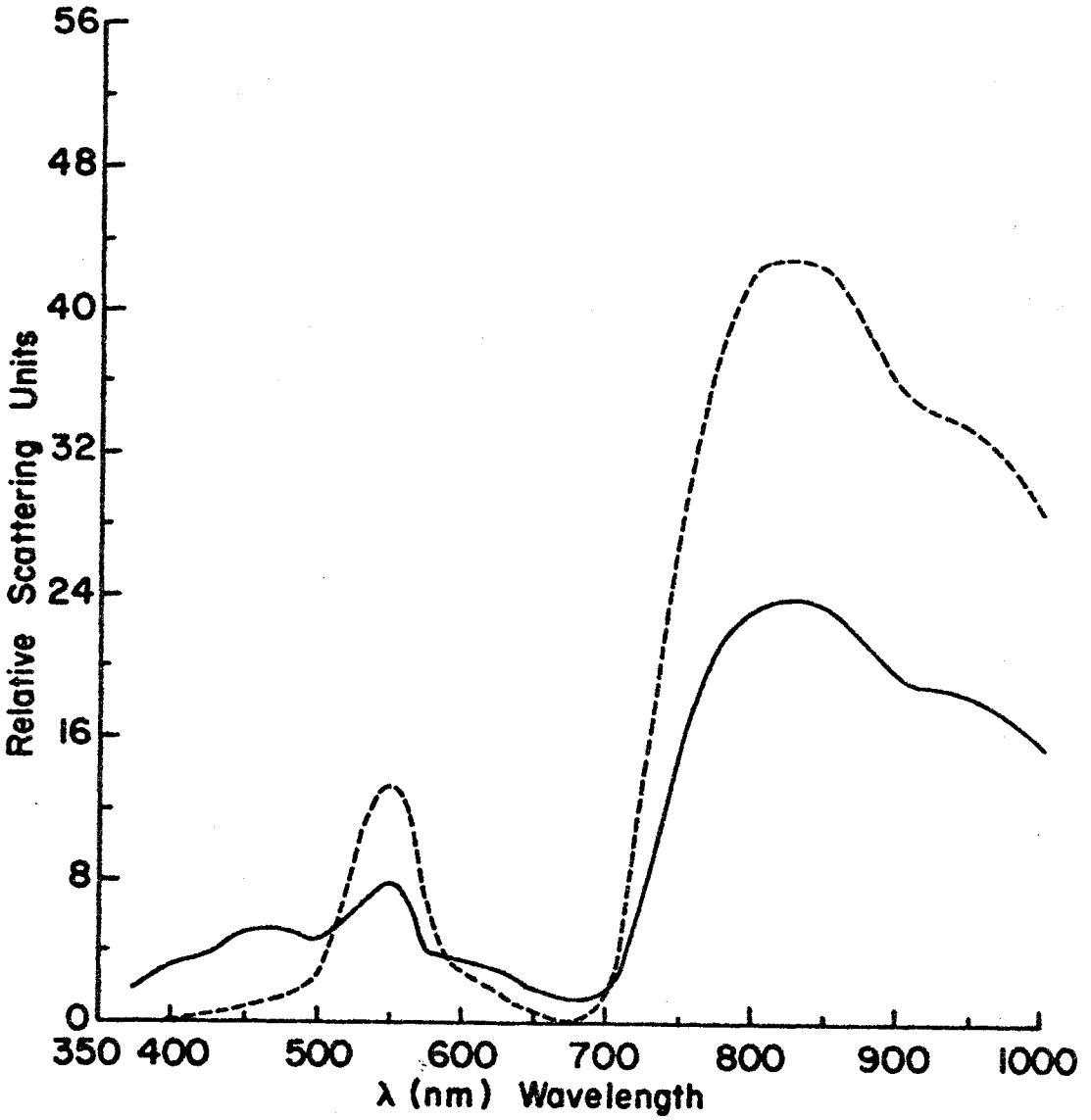

Figure 91. Corn Leaf Relative $[\rho'\cos\theta_{coll}]$(_____) at $\theta_{coll} = 15^{\circ}$ and Relative $[\tau'\cos(\pi - \theta_{coll})]$(——–) at $\theta_{coll} = 180^{\circ}$ versus λ for Top Incidence at $\theta_{inc} = 15^{\circ}$ (Horizontal Midvein Orientation).

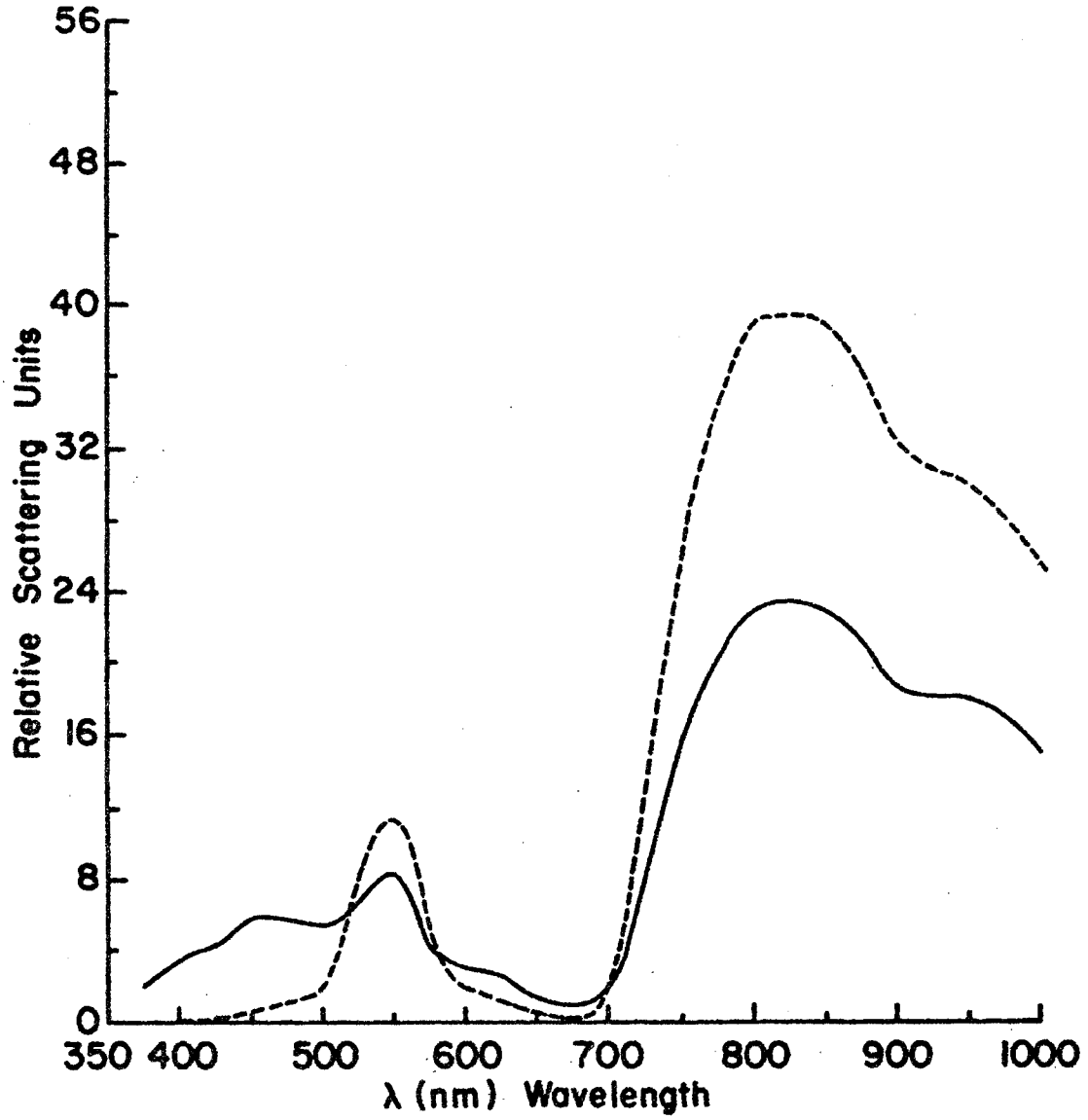

Figure 92. Corn Leaf Relative $[\rho'\cos\theta_{coll}]$(_____) at $\theta_{coll} = 30^{\circ}$ and Relative $[\tau'\cos(\pi - \theta_{coll})]$(——) at $\theta_{coll} = 180^{\circ}$ versus λ for Top Incidence at $\theta_{inc} = 30^{\circ}$ (Horizontal Midvein Orientation).

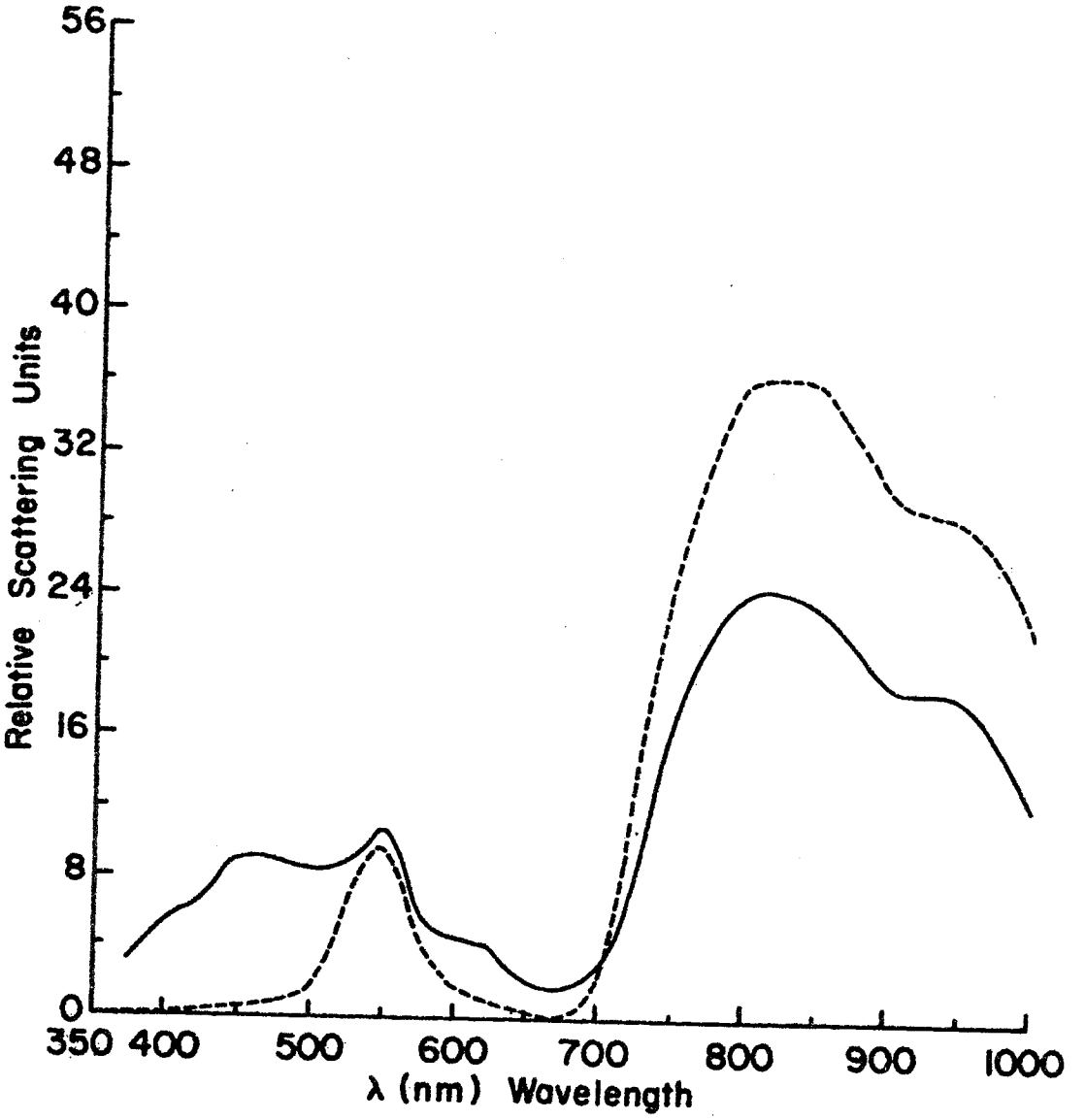

Figure 93. Corn Leaf Relative $[\rho'\cos\theta_{coll}]$(_____) at $\theta_{coll} = 45^{\circ}$ and Relative $[\tau'\cos(\pi - \theta_{coll})]$(——) at $\theta_{coll} = 180^{\circ}$ versus λ for Top Incidence at $\theta_{inc} = 45^{\circ}$ (Horizontal Midvein Orientation).

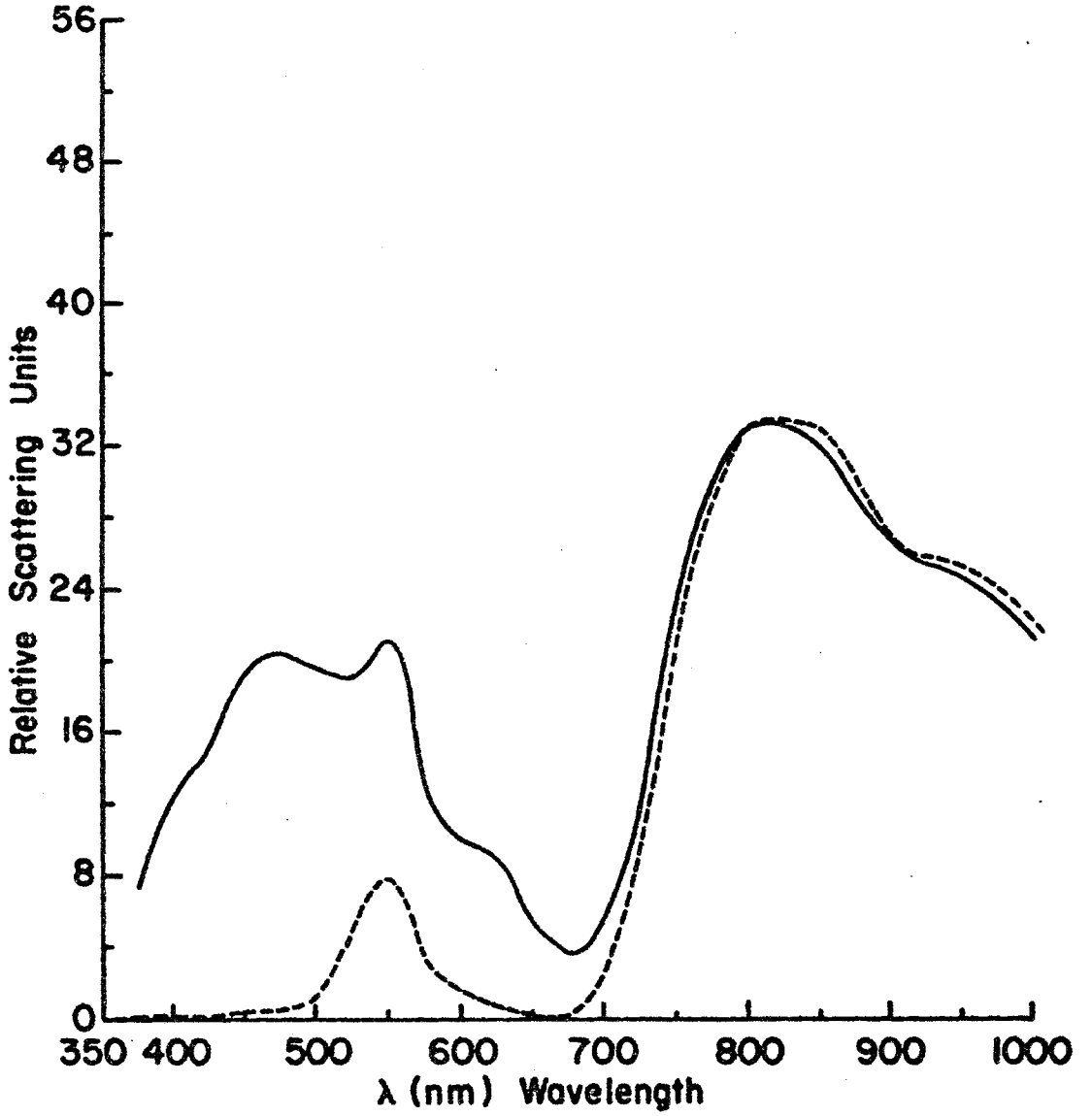

Figure 94. Corn Leaf Relative $[\rho'\cos\theta_{coll}]$(_____) at $\theta_{coll} = 60^{\circ}$ and Relative $[\tau'\cos(\pi - \theta_{coll})]$(———) at $\theta_{coll} = 180^{\circ}$ versus λ for Top Incidence at $\theta_{inc} = 60^{\circ}$ (Horizontal Midvein Orientation).

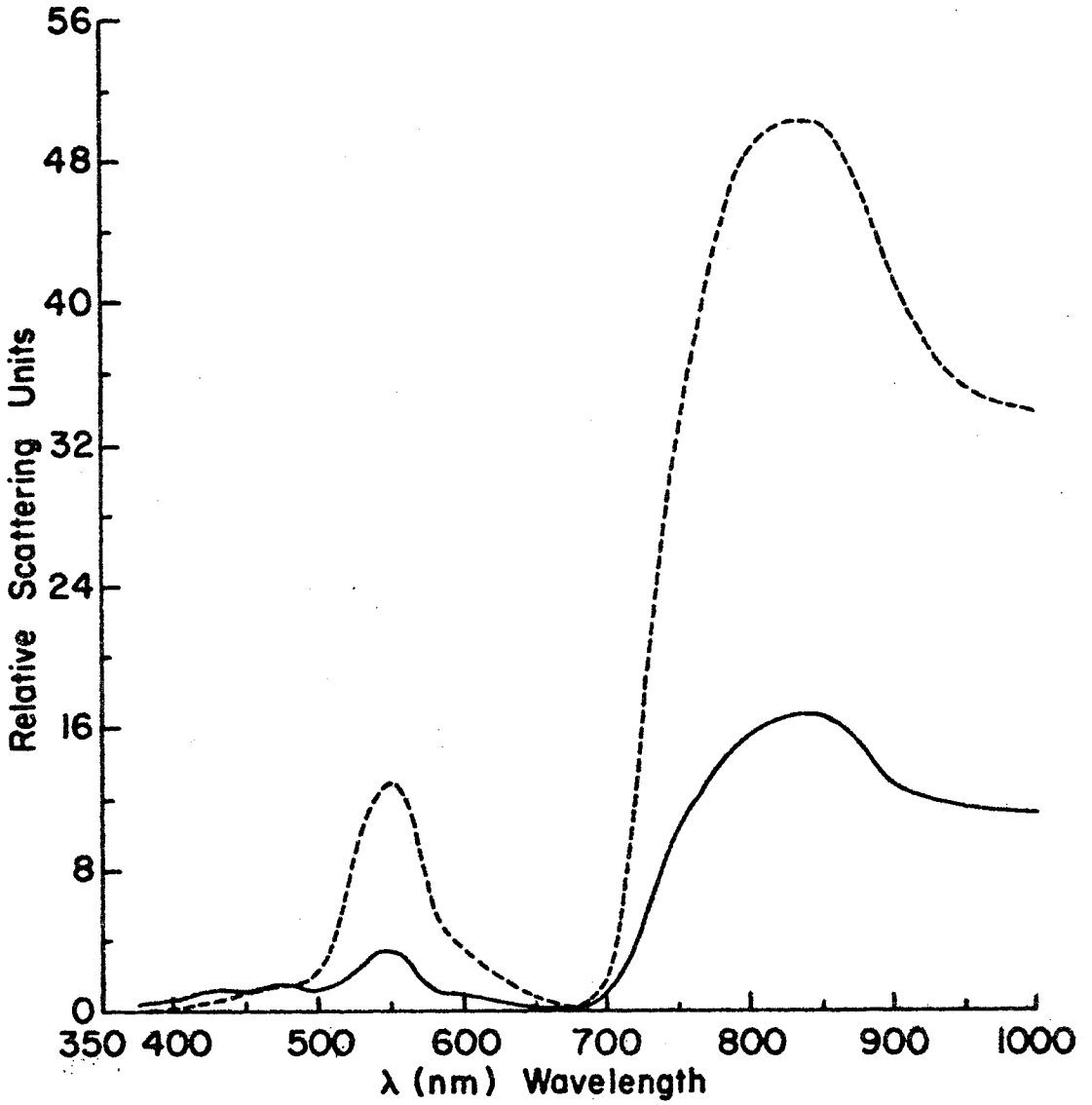

Figure 95. Corn Leaf Relative $[\rho'\cos\theta_{coll}]$(_____) at $\theta_{coll} = 45^{o}$ and Relative $[\tau'\cos(\pi - \theta_{coll})]$(-----) at $\theta_{coll} = 180^{o}$ versus λ for Bottom Incidence at $\theta_{inc} = 0^{o}$ (Horizontal Midvein Orientation).

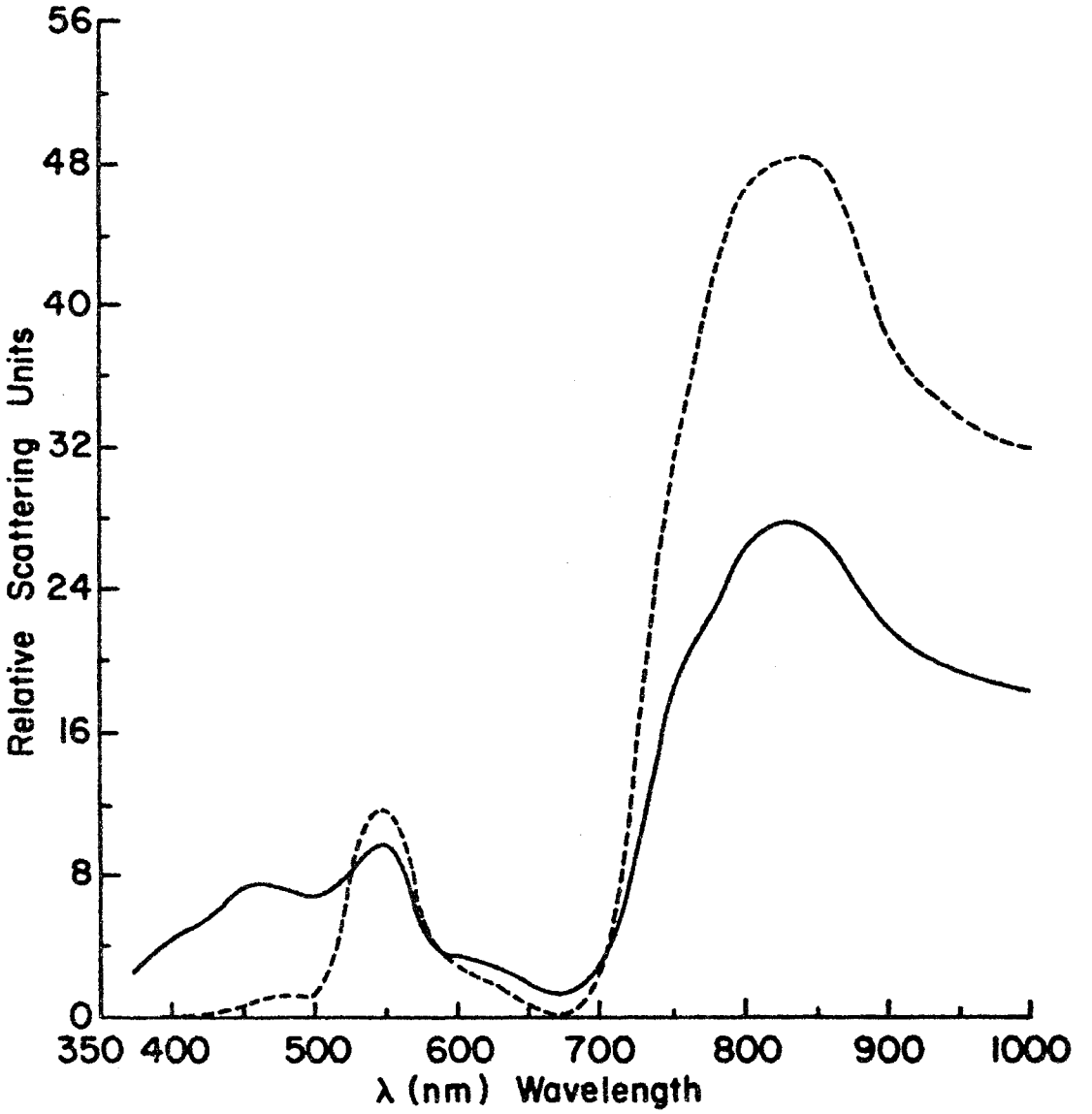

Figure 96. Corn Leaf Relative $[\rho'\cos\theta_{coll}]$(_____) at $\theta_{coll} = 15^{\circ}$ and Relative $[\tau'\cos(\pi - \theta_{coll})]$(– – – –) at $\theta_{coll} = 180^{\circ}$ versus λ for Bottom Incidence at $\theta_{inc} = 15^{\circ}$ (Horizontal Midvein Orientation).

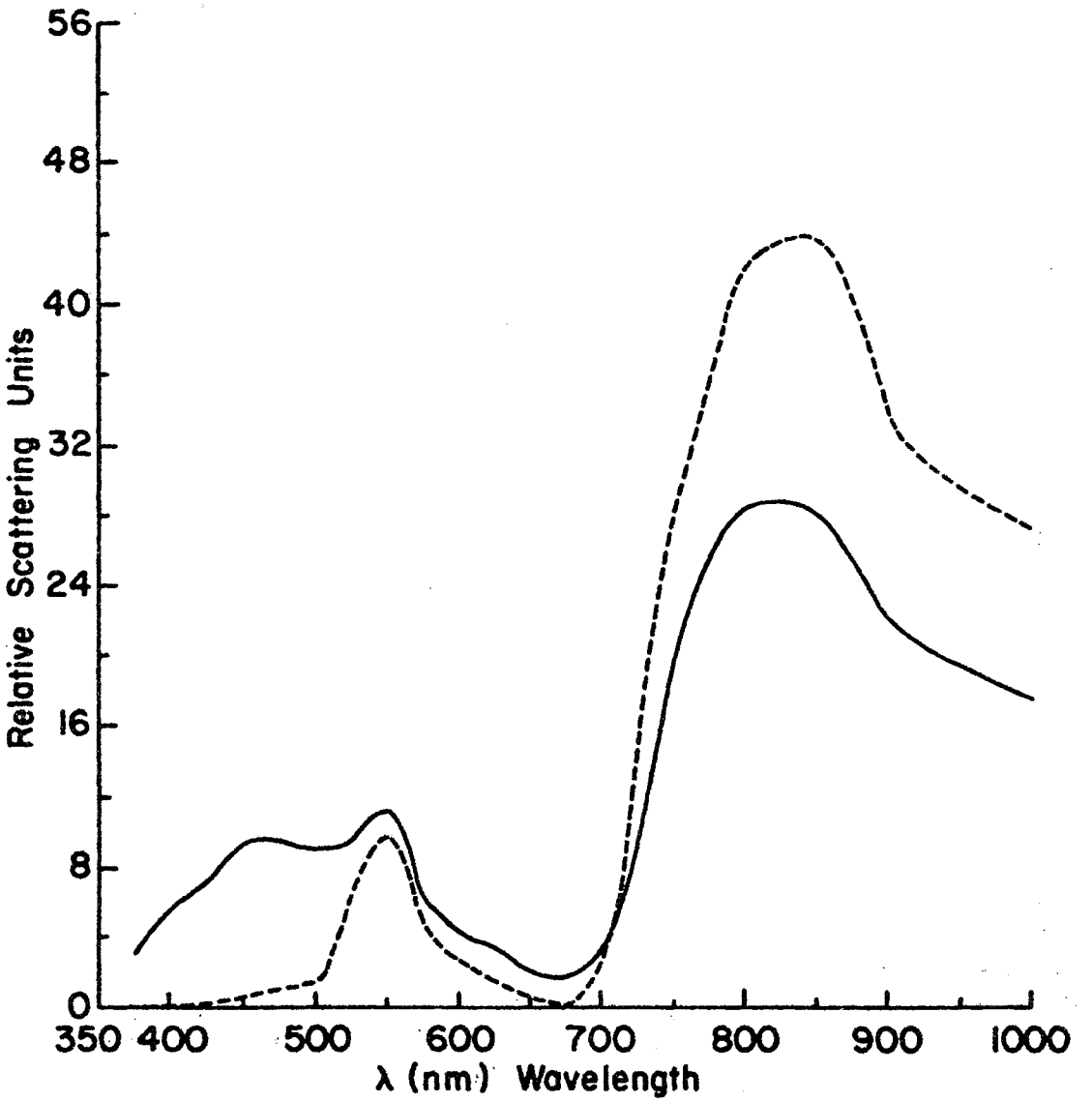

Figure 97. Corn Leaf Relative $[\rho'\cos\theta_{coll}]$(_____) at $\theta_{coll} = 30^{\circ}$ and Relative $[\tau'\cos(\pi - \theta_{coll})]$(-----) at $\theta_{coll} = 180^{\circ}$ versus λ for Bottom Incidence at $\theta_{inc} = 30^{\circ}$ (Horizontal Midvein Orientation).

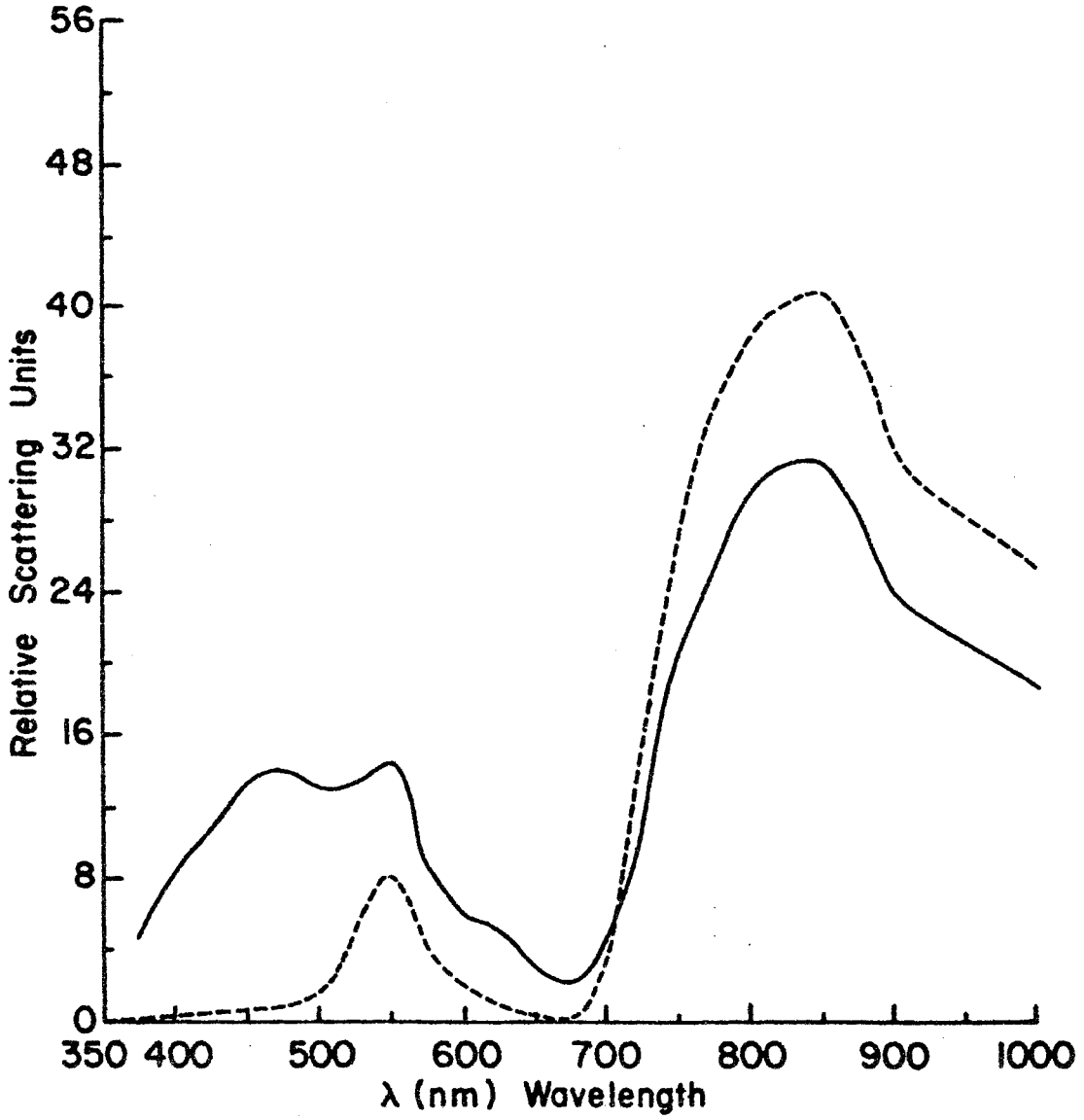

Figure 98. Corn Leaf Relative $[\rho'\cos\theta_{coll}]$(_____) at $\theta_{coll} = 45^{\circ}$ and Relative $[\tau'\cos(\pi - \theta_{coll})]$(– – – –) at $\theta_{coll} = 180^{\circ}$ versus λ for Bottom Incidence at $\theta_{inc} = 45^{\circ}$ (Horizontal Midvein Orientation).

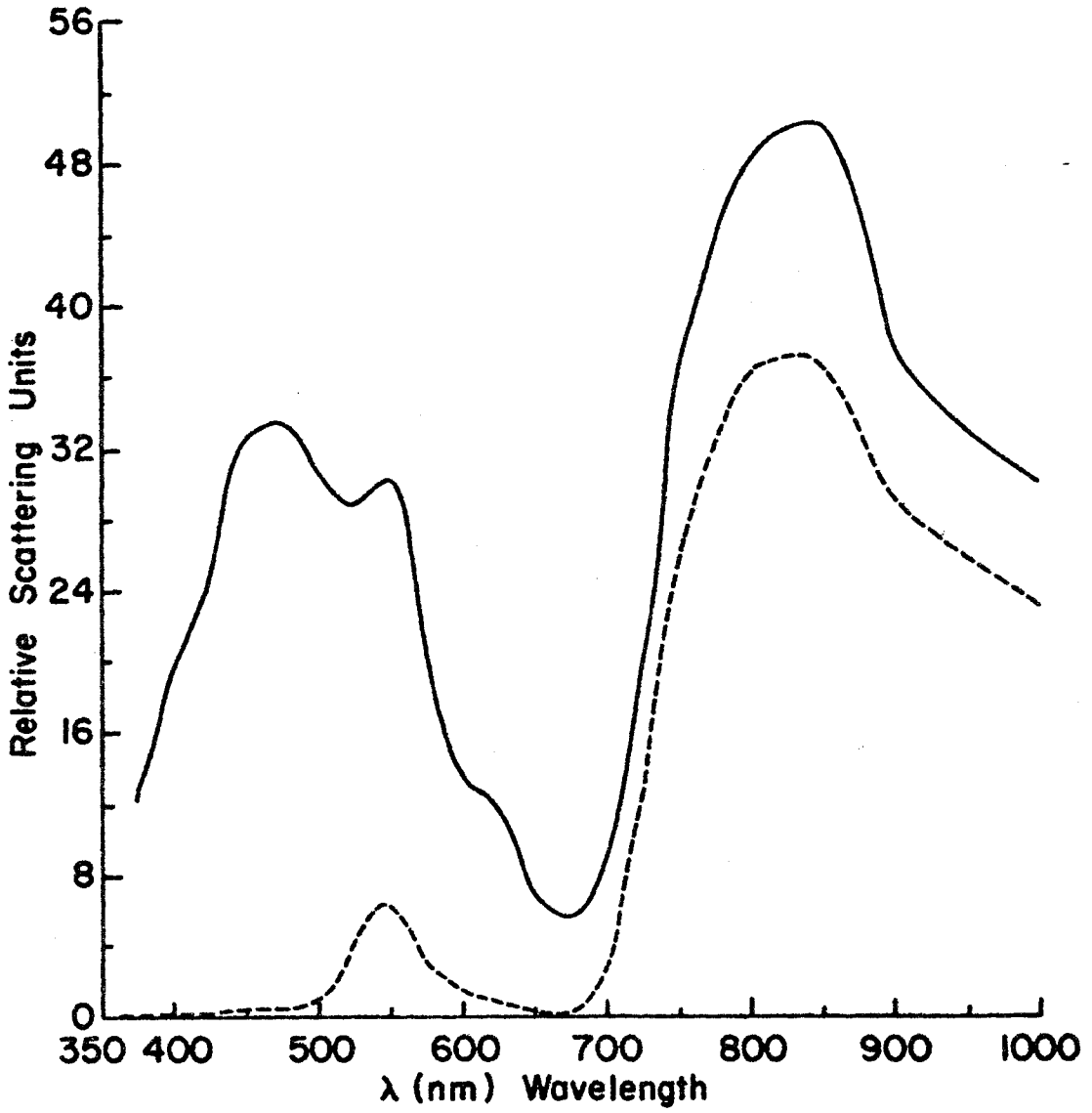

Figure 99. Corn Leaf Relative $[\rho'\cos\theta_{coll}]$(_____) at $\theta_{coll} = 60^{\circ}$ and Relative $[\tau'\cos(\pi - \theta_{coll})]$(– – –) at $\theta_{coll} = 180^{\circ}$ versus λ for Bottom Incidence at $\theta_{inc} = 60^{\circ}$ (Horizontal Midvein Orientation).

for comparison. Different leaves were used for top and bottom curves and different leaves were sometimes used for each wavelength range. The polar plots identify the leaves used for each set of conditions. Figure 100 gives the scattering distribution function versus angle of incidence for reflection at the specular angle, for the representative wavelengths given above.

Figures 101 and 102 present the results for the scattering distribution function versus angle of incidence for transmission along a normal to the sample surface, for the representative wavelengths mentioned above.

The corn leaf bi-directional scattering data were graphically analyzed to determine the angles for maximum reflection and transmission. It was difficult to make this graphical approximation of these angles since the polar plots are broad about these angles. Maximum reflection and transmission angles were determined for each of the polar plots given on the composite polar plot page for a particular angle of incidence. This was done for the range from 375 nm through 675 nm and for the range from 750 nm through 1μm. Figure 103 gives the average of these points versus angle of incidence with the ideal mirror characteristic given for reference for the range from 375 nm through 675 nm and Figure 104 gives the average of these points versus angle of incidence for the range from 750 nm through 1μm.

These transmission angles are measured counter-clockwise from a normal to the plane of the leaf sample so they can be plotted on the graph with the reflection angles.

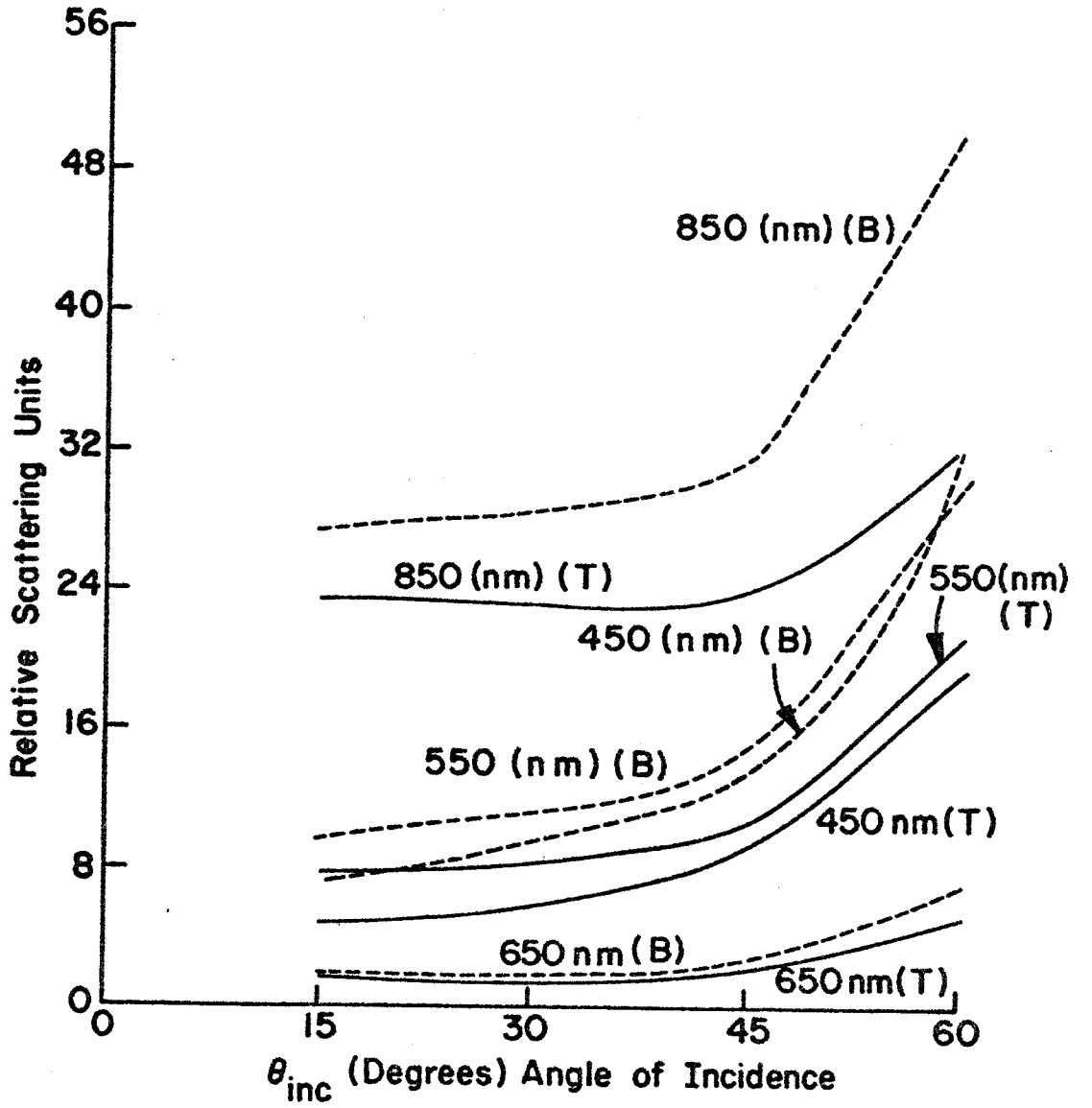

Figure 100. Corn Leaf Relative [$\rho' \cos\theta_{coll}$] at the specular collection angle versus θ_{inc} for Top Incidence (_____) and Bottom Incidence (– – – –) at 450 nm, 550 nm, 650 nm, and 850 nm (Horizontal Midvein Orientation).

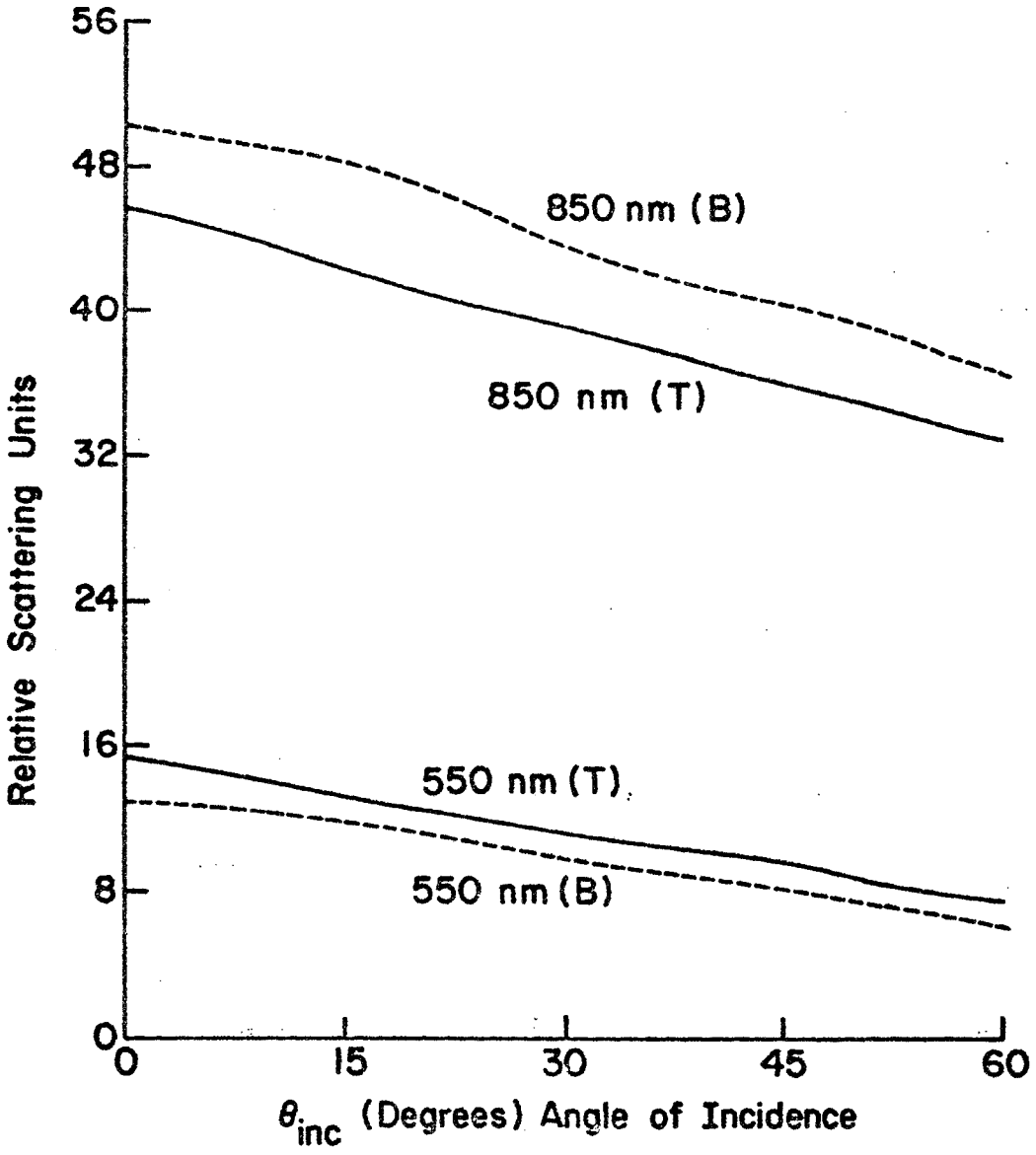

Figure 101. Corn Leaf Relative $[\tau'\cos(\pi - \theta_{coll})]$ at $\theta_{coll} = 180^{o}$ versus θ_{inc} for Top Incidence (_____) and Bottom Incidence (– – – –) at 550 nm and 850 nm (Horizontal Midvein Orientation).

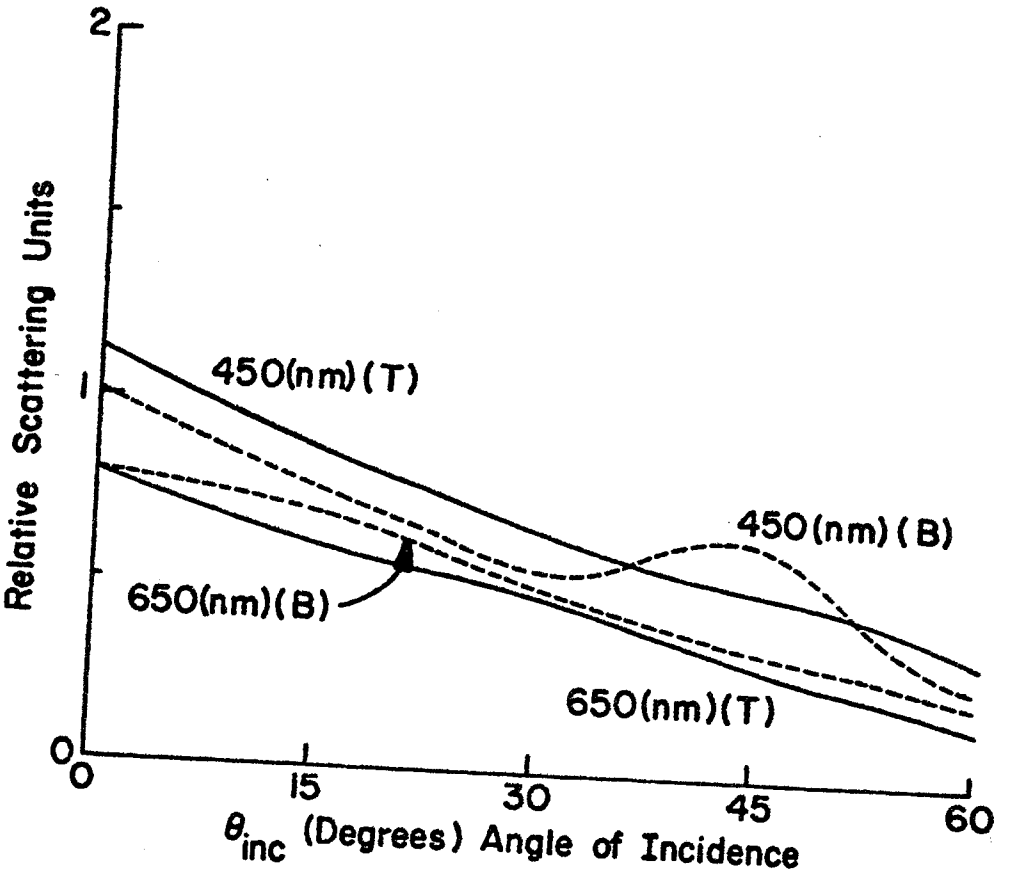

Figure 102. Corn Leaf Relative $[\tau'\cos(\pi - \theta_{coll})]$ at $\theta_{coll} = 180^{\circ}$ versus θ_{inc} for Top Incidence (_____) and Bottom Incidence (— — —) at 450 nm and 650 nm (Horizontal Midvein Orientation).

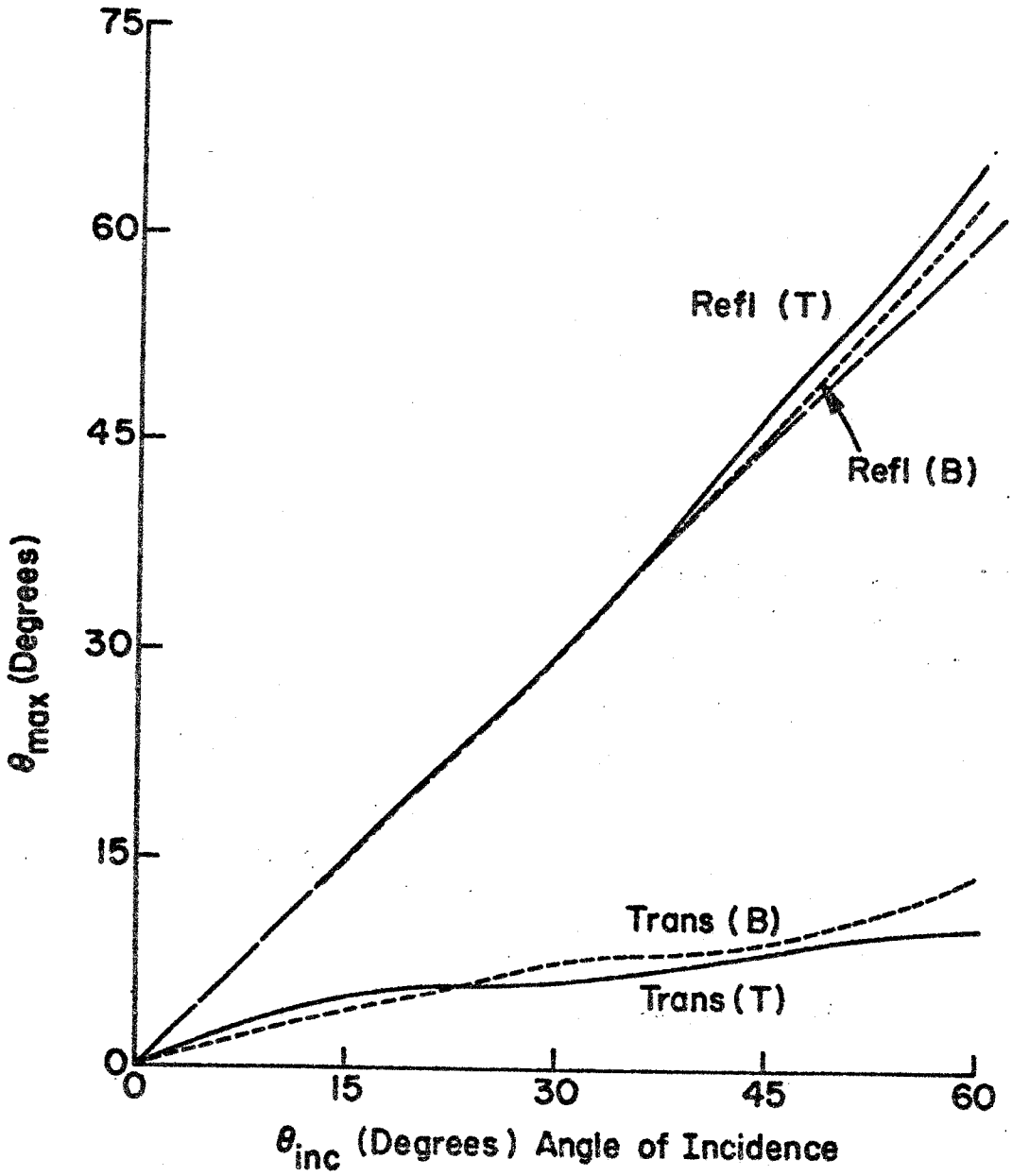

Figure 103. Corn Leaf Average Collection Angle for Maximum Relative $[\rho' \cos \theta_{coll}]$ and Maximum Relative $[\tau' \cos(\pi - \theta_{coll})]$ versus θ_{inc} for Top Incidence (_____) and Bottom Incidence (——) for the range of λ from 375 nm through 675 nm (Horizontal Midvein Orientation).

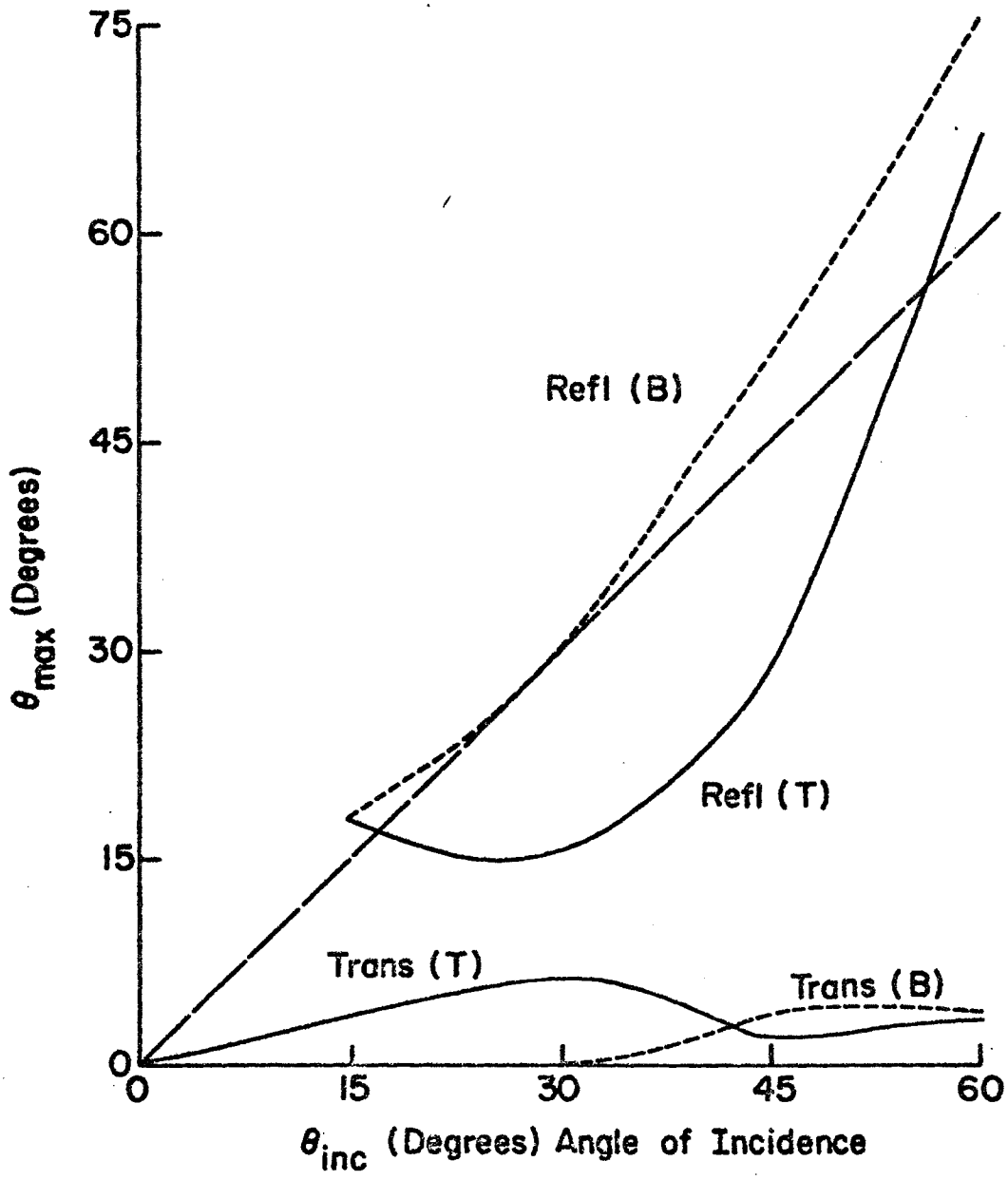

Figure 104. Corn Leaf Average Collection Angle for Maximum Relative $[\rho'\cos\theta_{coll}]$ and Maximum Relative $[\tau'\cos(\pi - \theta_{coll})]$ versus θ_{inc} for Top Incidence (_____) and Bottom Incidence (– – – –) for the range of λ from 750 nm through 1000 nm (Horizontal Midvein Orientation).

Discussion of Results

A discussion of the experimental results is presented here with the major objective being a classification of features for a bi-directional scattering model for a healthy, green corn leaf. The discussion is divided into three sub-sections, the first dealing with results for vertical midvein orientation, the second dealing with results for horizontal midvein orientation and the third comparing results from both vertical and horizontal midvein orientations.

Vertical Midvein Orientation

Gross observations of the polar bi-directional scattering plots for corn leaves with vertical midvein orientation show that the functional form of the scattering characteristic depends upon the angle of incidence. The reflection characteristic is apparently composed of both specular and diffuse components. The corn leaf transmission characteristic is apparently composed of a refracted or slightly scattered component and a diffuse component.

The polar curves for the infrared range appear diffuse for both reflection and transmission except for an angle of incidence of 60°. At 60° a definite specular characteristic is measured with the specular reflection being slightly sharper for the bottom incidence than for the top incidence.

The polar curves for the visible range exhibit both diffuse and specular reflection components. The reflection curves are spread at the specular angle for both top and bottom incidence indicating a rough surface for both top and bottom. The spread for the reflection at the

specular angle is nearly the same for both top and bottom incidence. This indicates that the top and bottom surfaces have nearly the same roughness coefficient.

The corn leaf cross-section of Figure 50 shows that the corn leaf has a rough surface, a cuticle layer over a layer of guard cells. This surface is rough in a regular way, consisting of grooves which are all parallel to the midvein. This would give the roughness for this midvein orientation a regular peaked roof or sawtooth appearance. The inner cell layers are mesophyll cells which contain chlorophyll. This is a homogeneous inner structure with the same structure for cell layers near the top and for cell layers near the bottom. This leaf structure, like the soybean leaf, can have both rough surface diffuse reflection and diffuse reflection due to radiation that penetrates into the interior of the leaf to be scattered within.

Spectra for both reflection at the specular angle and transmission along a normal to the leaf sample plane as shown in Figures 65 through 74 show the dependence of these two characteristics on wavelength. The transmission spectra show blue and red chlorophyll absorption, infrared water band absorption and strong transmission in the green and infrared ranges. The trends of the reflection spectra are different from the transmission spectra only in the blue region, where the reflection spectra indicate less blue absorption relative to the transmission spectra. This indicates that the diffuse reflection may be due in part to radiation which penetrates into the corn leaf sample since the reflection spectra so closely resemble those for transmission. As the angle of incidence is increased, the reflection at the specular angle increases

in the blue region relative to the green but does not increase as much in the red region relative to the green.

These results indicate that the diffuse reflection characteristic is probably due to both the rough surface and the radiation that penetrates into the leaf.

The transmission spectra remain nearly the same as the angle of incidence is changed. This indicates that the diffuse component of the transmission characteristic is predominant over the refractive or direct beam component.

Plots of scattering distribution function relative magnitude for reflection at the specular angle versus angle of incidence are given in Figure 75 for 450 nm, 550 nm, 650 nm, and 850 nm. The data for both top and bottom incidence are presented on the same page for comparison.

The trend of the curves for 450 nm, 550 nm, 650 nm, and 850 nm is a very small positive slope until about $\theta_{inc} = 45^{\circ}$ where the slope increases. This indicates a greater specular reflection component for $\theta_{inc} \geq 45^{\circ}$ at these wavelengths. Comparison of the curve for top incidence with the curve for bottom incidence for constant wavelength at 450 nm, 550 nm, 650 nm, and 850 nm indicates that the relative magnitude for reflection at bottom incidence is nearly the same as that for top incidence.

Plots of scattering distribution function relative magnitude for transmission along a normal versus angle of incidence are given in Figures 76 and 77 for 450 nm, 550 nm, 650 nm, and 850 nm. The data for both top and bottom incidence for each wavelength are presented on the same page for comparison.

The trend of the curves for 450 nm, 550 nm, 650 nm, and 850 nm is a negative slope. Comparison of the curve for top incidence with the curve for bottom incidence for constant wavelength at 450 nm, 550 nm, and 850 nm indicates that the relative magnitude of the scattering distribution function for transmission at bottom incidence is nearly the same as to that for top incidence. For the 650 nm curve the bottom incidence curve has a slightly larger relative magnitude than the top incidence curve.

The plot of angle for maximum reflected and transmitted scattering distribution function relative magnitudes is given in Figure 78 for the visible range. The trend of the reflection curves is a positive slope. The transmission and reflection curves indicate approximately the same result for top incidence or bottom incidence. These transmission curves indicate that the index of refraction is the same for the top and bottom layers of the corn leaf, assuming refractive transmission.

The plot of angle for maximum reflected and transmitted scattering distribution function relative magnitudes is given in Figure 79 for the low infrared range. The trend of the reflection curves is a positive slope. The bottom and top incidence transmission curves are nearly the same.

Horizontal Midvein Orientation

Gross observations of the polar bi-directional scattering plots for corn leaves with horizontal midvein orientation show that the functional form of the scattering characteristic depends upon the angle of incidence. The reflection characteristic is composed of both specular and

diffuse components. The corn leaf transmission characteristic is composed of a refracted component and a diffuse component.

The polar curves for bottom incidence in the infrared range have the appearance of having a definite specular reflection characteristic component even for $\theta_{inc} = 15^{\circ}$ while the top incidence curves have a diffuse reflection characteristic appearance for incidence angles of 15° and 30° and a specular component for angles of 45° and 60°. In each case the bottom incidence curves have a greater value for the scattering distribution function at the specular angle than the top incidence curves.

The polar curves for the visible range have a definite lobe-like characteristic oriented along the specular angle for both top and bottom incidence.

The lobe character of some of the reflection curves at the specular angle indicates a fairly smooth surface for both top and bottom.

The transmission characteristic has both refraction or direct beam scattering and diffuse transmission present for both top and bottom incidence at all of the wavelengths studied.

The corn leaf appears fairly smooth for horizontal midvein orientation since the view is one which does not cross the peaked roof or sawtooth structure but which runs along on one of the peaks or groove bottoms.

Spectra for both reflection at the specular angle and transmission along a normal to the leaf sample plane as shown in Figures 90 through 99 show the dependence of these two characteristics on wavelength. The transmission spectra show blue and red chlorophyll absorption, infrared water band absorption and strong transmission in the green and infrared

ranges. The trends of the reflection spectra are different from the transmission spectra only in the blue region, where the reflection spectra indicate less blue absorption relative to the transmission spectra. This indicates that the diffuse reflection is probably due in part to radiation which penetrates into the corn leaf sample since the reflection spectra so closely resemble those for transmission. As the angle of incidence is increased the reflection at the specular angle increases in the blue region relative to the green but does not increase as much in the red region relative to the green.

It seems possible that the diffuse reflection characteristic could be due to both a slightly rough surface and to radiation that penetrates into the leaf. The lobe-like appearance of the polar curve at the specular angle indicates the smooth or only slightly rough surface for this orientation.

The transmission spectra remain nearly the same as the angle of incidence is changed. This indicates that the diffuse component of the transmission characteristic is predominant over the refractive or direct beam scattering component.

Plots of scattering distribution function relative magnitude for reflection at the specular angle versus angle of incidence is given in Figure 100 for 450 nm, 550 nm, 650 nm, and 850 nm. The data for both top and bottom incidence for each wavelength are presented on the same page for comparison.

The trend of the curves for 450 nm, 550 nm, and 650 nm is a very small positive slope until about $\theta_{inc} = 45^{\circ}$ where the slope increases. This indicates a greater specular reflection component for $\theta_{inc} \geq 45^{\circ}$ at these wavelengths. Comparison of the curve for top incidence with

the curve for bottom incidence for constant wavelength at 450 nm, 550 nm, and 650 nm indicates that the relative magnitude for reflection at bottom incidence is equal to or slightly greater than that for top incidence.

The trend of the reflection curves for 850 nm shows a very small negative slope for top incidence until about $\theta_{inc} = 45^{\circ}$ where the slope becomes positive and increases. The bottom incidence curve for 850 nm shows a very small positive slope until about $\theta_{inc} = 45^{\circ}$ where the slope increases. The relative magnitude for the bottom incidence curve is larger than the top incidence curve.

Plots of scattering distribution function relative magnitude for transmission along a normal versus angle of incidence are given in Figures 101 and 102 for 450 nm, 550 nm, 650 nm, and 850 nm. The data for both top and bottom incidence for each wavelength are presented on the same page for comparison.

The trend of the curves for 450 nm, 550 nm, 650 nm, and 850 nm is a negative slope. Comparison of the curve for top incidence with the curve for bottom incidence for constant wavelength at 450 nm, 550 nm, 650 nm, and 850 nm indicates that the relative magnitude of the scattering distribution function for transmission at bottom incidence is nearly the same as that for top incidence.

The plot of angle for maximum reflected and transmitted scattering distribution function relative magnitudes is given in Figure 103 for the visible range. The trend of the reflection curves is a positive slope almost equal to the plane mirror reference line. The transmission and reflection curves indicate essentially the same result for top and bottom incidence. The transmission curves indicate that the index of

refraction is the same for the top and bottom layers of the corn leaf, assuming refractive transmission.

The plot of angle for maximum reflected and transmitted scattering distribution function relative magnitudes is given in Figure 104 for the low infrared range. The trend of the bottom incidence curve is a positive slope while the trend of the top incidence curve is a negative slope from $\theta_{inc} = 15^{o}$ to $\theta_{inc} = 30^{o}$ and a positive slope for $\theta_{inc} > 30^{o}$. The bottom and top incidence transmission curves are, however, nearly the same.

Composite Results

This sub-section is a discussion of the corn leaf bi-directional scattering with regard to comparison of results for vertical midvein orientation with results for horizontal midvein orientation.

The experimental results show a rougher surface for the vertical midvein orientation than for the horizontal midvein orientation.

Comparison of scattering distribution function relative magnitudes for the reflection curves indicate that the reflection coefficients are nearly the same for the two orientations even though the shapes of the polar curves for the two orientations are different. Comparison of scattering distribution function relative magnitudes for the transmission curves indicate that the transmission coefficients are nearly the same for the two orientations. Here again, the polar transmission curves do not have the same shape for the two orientations.

The spectra have the same trends for the two orientations.

Corn Leaf Bi-Directional Scattering Model

A simple empirical bi-directional scattering model for a healthy, green corn leaf is presented in three stages. The first stage will present the empirical model for vertical midvein orientation, the second stage will present the empirical model for horizontal midvein orientation and the third stage will present the composite empirical corn leaf scattering model.

Vertical Midvein Orientation

Figure 105 is the diagram of a simple two dimensional bi-directional scattering model for a healthy, green corn leaf with vertical midvein orientation suggested by the experimental results and the physical leaf structure. This model does not include the midvein. This is a three layer structure with outer layers 1 and 3 contributing refraction and specular reflection but having no selective absorption characteristic. These epidermal layers are effective for specular reflection at all angles of incidence in the visible range and for a 60° angle of incidence in the infrared range. These layers have rough surfaces which could cause diffuse reflection and a spread in the specular reflection characteristic.

The inner layer, layer 2, has both refractive and diffuse transmission characteristics and a diffuse reflection characteristic together with a selective absorption characteristic.

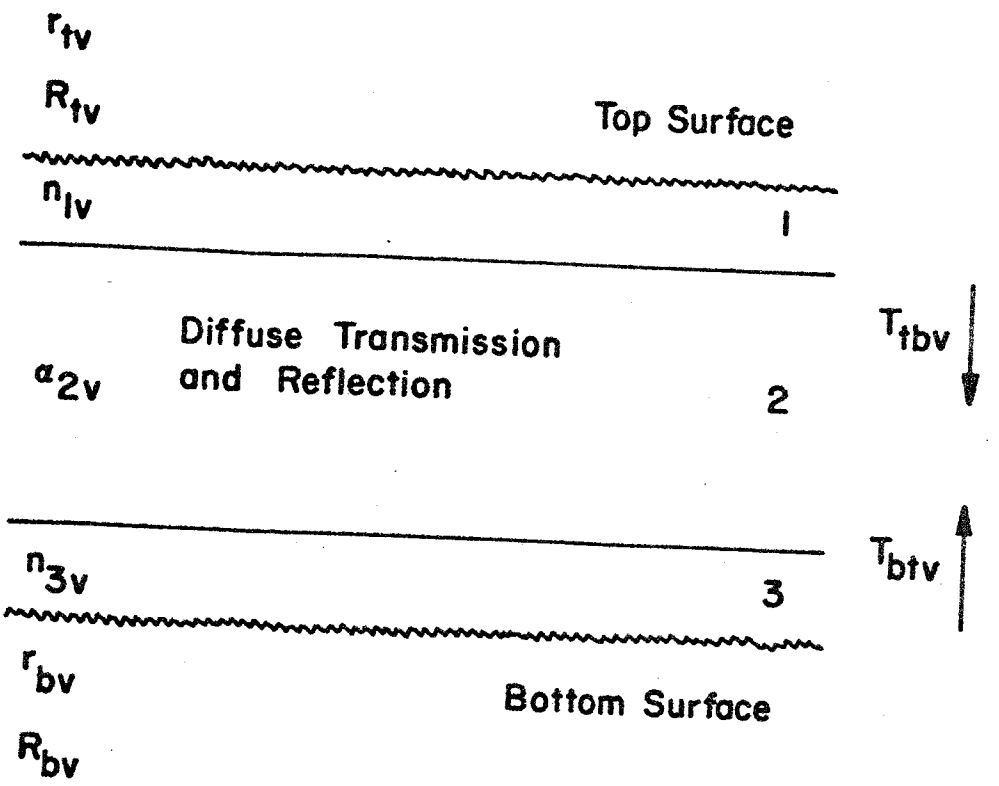

r – Roughness Coefficient

n – Index of Refraction

α – Absorption Coefficient

R – Reflection Coefficient

T – Transmission Coefficient

$r_{tv} \approx r_{bv}$

$n_{1v} \approx n_{3v}$

Figure 105. Corn Leaf Bi-Directional Scattering Model (Vertical Midvein Orientation).

Horizontal Midvein Orientation

Figure 106 is the diagram of a simple two dimensional bi-directional scattering model for a healthy, green corn leaf with horizontal midvein orientation, suggested by these experimental results and the physical leaf structure. This model does not include the midvein. This is a three layer structure with outer layers 1 and 3 contributing refraction and specular reflection but having no selective absorption characteristic. These epidermal layers are effective for specular reflection in both the infrared and visible ranges. The inner layer, layer 2, has both refractive and diffuse transmission characteristics and a diffuse reflection characteristic together with a selective absorption characteristic.

The surfaces are smooth giving rise to fairly sharp reflection at the specular angle.

Composite Model

Figure 107 is the diagram of a simple bi-directional scattering model for a healthy, green corn leaf suggested by the results of this experiment and the physical leaf structure. This is a three layer structure with outer layers 1 and 3 contributing refraction and specular and diffuse reflection but having no selective absorption characteristic. The inner layer, layer 2, has both refractive and diffuse transmission characteristics and a diffuse reflection characteristic together with a selective absorption characteristic.

The experimental results are the specifications for the bi-directional scattering model. The composite parameters are given by the

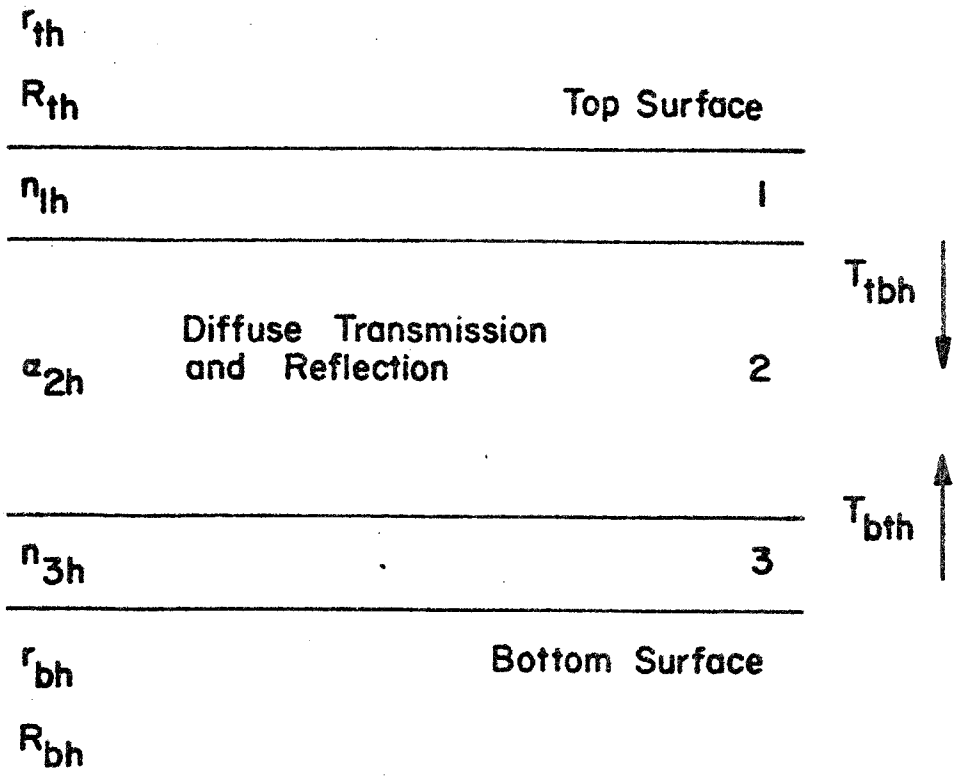

r – Roughness Coefficient $r_{th} \approx r_{bh}$

n – Index of Refraction $n_{1h} \approx n_{3h}$

α – Absorption Coefficient

R – Reflection Coefficient

T – Transmission Coefficient

Figure 106. Corn Leaf Bi-Directional Scattering Model (Horizontal Midvein Orientation).

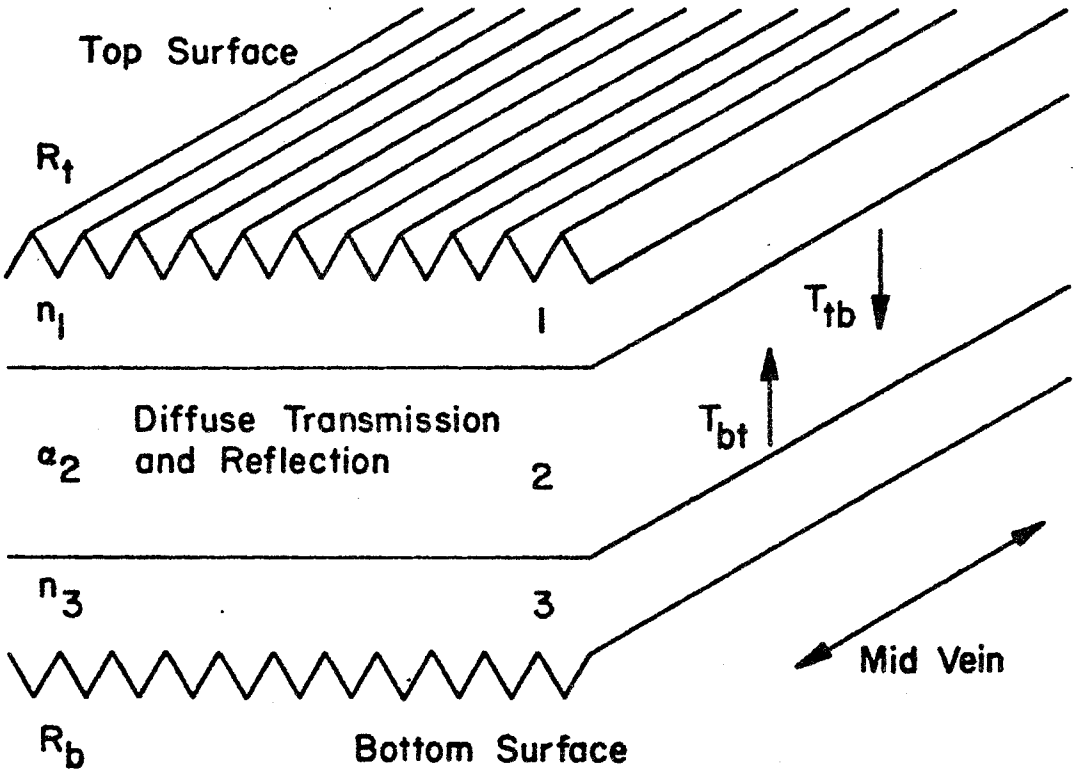

n – Index of Refraction $n_1 \approx n_3$

α – Absorption Coefficient

R – Reflection Coefficient

T – Transmission Coefficient

Figure 107. Composite Corn Leaf Bi-Directional Scattering Model.

individual vertical and horizontal midvein orientation models. The composite model does not include the midvein.

$$
\begin{aligned}
n_1 &\approx n_{1v} \approx n_{1h} \\
n_3 &\approx n_{3v} \approx n_{3h} \\
\alpha_2 &\approx \alpha_{2v} \approx \alpha_{2h} \\
R_t &\approx R_{tv} \approx R_{th} \\
R_b &\approx R_{bv} \approx R_{bh} \\
T_{tb} &\approx T_{tbv} \approx T_{tbh} \\
T_{bt} &\approx T_{btv} \approx T_{bth}
\end{aligned}
$$

Each of these parameters is a function of wavelength, incidence angle and collection angle as shown by the data.

The model surface is designed from the actual physical leaf structure using a peaked roof design for both the bottom and top surfaces. Each peak runs along the direction of the midvein so that for vertical orientation the surface appears rough and for horizontal orientation the surface appears smooth.

CONCLUSIONS

This experiment has resulted in two-dimensional bi-directional scattering curves for healthy, green soybean leaves and healthy, green corn leaves in the range from 375 nm to 1000 nm. These results suggest a simple model for soybean bi-directional leaf scattering and a simple model for corn bi-directional leaf scattering.

The results show a large specular reflection component along with diffuse reflection and both refractive and diffuse transmission. A selective absorption characteristic is evident along with definite surface effects. The leaf scattering mechanism is very complex having many possible integral components. The specular reflection spreading can be due to a rough surface yet the rough surface also appears to contribute diffuse reflection, and only an arbitrary boundary between the two can be established by an observer. Diffuse reflection is also due to scattering within inner leaf layers. The diffuse transmission is due to scattering within the inner leaf layers and also can be due to the rough surface. Refractive transmission can be expected to occur within the inner leaf layers.

Further study could use a polarized beam as a possible means of separating the diffuse and specular reflection components. The effect of the sample scattering upon the source polarization can be measured and used to study the leaf. The problem of separating the diffuse and specular reflection components is still unsolved particularly with respect to rough surface scattering. The source used in this experiment did not have sufficient intensity for a polarized beam study. A new monochromator design is needed to provide the necessary increase in

intensity. The results of this scattering experiment serve as a guide to the selection of wavelengths and conditions for this further investigation.

Future work at the Laboratory for Agricultural Remote Sensing should include bi-directional scattering measurements on the leaves of plants other than corn and soybean plants. Other plants having a high agricultural economic value in the midwest are wheat, oats, and sorghum. The small size of the wheat and oat leaves makes a higher intensity source necessary for some of these future experiments.

Again in the interest of the basic mission of the Laboratory for Agricultural Remote Sensing, experiments should be carried out to measure bi-directional scattering characteristics for leaves under stress conditions and for various times in the growing season. This work will be involved since the leaves naturally begin to curl and wrinkle under several stress conditions including moisture stress. If, for instance, in a moisture stress experiment the normal leaf is constrained to a plane in the sample holder and later subjected to moisture stress while in the sample holder, the leaf curling action would not be allowed to occur in the natural way. However, it would be difficult to uncurl a dry leaf in order to fit a plane without breaking and destroying the leaf.

Future work could be concerned with the extension of bi-directional scattering data for leaves to three dimensions. Experiments involving non-zero tilt angles carried out as a part of this corn and soybean leaf project suggest a trend for the three-dimensional data. These tilt studies showed that the two-dimensional data plots are good indicators of the actual three-dimensional scattering surfaces.

In this experiment the leaf sample was tilted in the sample holder using the protractor to measure the angle of tilt. Effectively this considered situations where the normal to the sample surface was not parallel to the plane of the source and detector. This began to give an indication of the three-dimensional result.

The results indicate that rotation of the two-dimensional curves about certain axes will produce a good approximation to the actual scattering surfaces. For normal incidence both the reflection and transmission curves are rotated about the surface normal axes to produce the scattering surface which correlates best with the results from the tilt experiment. For the 15°, 30°, 45°, and 60° incidence angle experiments, if the two-dimensional reflection data polar curves were rotated about an axis constructed along the line of the specular angle in each case, the resultant three-dimensional scattering distribution function correlated well with measurements from the tilt experiment. For the 15°, 30°, 45°, and 60° incidence angle experiments, if the two-dimensional transmission data polar curves were rotated about an axis constructed along the line of the angle of maximum transmission in each case, the resultant three-dimensional scattering distribution function correlated well with measurements from the tilt experiment. This technique gave approximate predictions of the three-dimensional scattering surfaces.

Bi-directional scattering studies on leaves can be continued with several different approaches. Three possible approaches to the problem will be suggested here with some concern being given to application of the results. The first approach is a purely theoretical scattering study of the leaf structure. This could use the plane-parallel Rayleigh

atmosphere model as given by Chandrasekhar or possibly a rough surface model similar to the theory outlined by Beckmann. In order to use either of these theories the leaf structure must be greatly idealized. Therefore it is necessary to develop significant additional theory for a selectively absorbing and highly inhomogeneous medium with a pseudo-random rough dielectric surface. A numerical approach would be to carry out a large scale ray tracing problem on a leaf cross-section with assumed optical parameters for the leaf components.

The basic difficulties inherent in the theoretical treatment of the bi-directional scattering problem for leaves make it necessarily important only for long range contribution. This treatment should be carried on at a modest level for its long range value.

The second approach to the bi-directional scattering problem for leaves is for the physical scientist or engineer to continue to collect valid measurements on more leaf samples. Work could be done on more varieties and possibly work using polarization and other experiments could be carried out. This work would be done with modest guidance from the life scientist in the care and selection of samples. This approach would result in enormous amounts of data which must be put into convenient form for analysis or statistical compilation. Not many life scientists would try to look at these data and make conclusions, particularly on normal leaves with which the engineer would of necessity be working.

This treatment of the problem, while contributing to the further development of the instrumentation and data handling system design, would result in a data production rate far in excess of user demand.

The third approach to the bi-directional scattering problem for leaves is for the life scientist to use the apparatus with sufficient engineering support to study optical scattering from leaves subject to various physiological changes or stress conditions. The leaf is a photo-chemical structure and should be sensitive to optical measurement. The life scientist is the only one qualified to develop the various stress situations for the plant.

This approach appears to have the most immediate short range and potential long range value for optical sensing of plant conditions.

BIBLIOGRAPHY

1. Beckmann, Petr and Andre Spizzichino. The Scattering of Electromagnetic Waves from Rough Surfaces. New York: The Macmillan Co., 1963.

2. Chandrasekhar, S. Radiative Transfer. New York: Dover Publications, Inc., 1960.

3. Christensen, R. L. and I. Ames. "Absolute Calibration of a Light Detector", Journal of the Optical Society of America, Vol. 51, No. 2, pp. 224-236, February, 1961.

4. Coulson, K. L. "Effects of Reflection of Natural Surfaces in Aerial Reconnaissance", Applied Optics, Vol. 5, No. 6, pp. 905-917, June, 1966.

5. Dinger, Jacob E. "The Absorption of Radiant Energy in Plants", Unpublished Ph.D. Thesis, Iowa State College, 1941.

6. Esau, Katherine. Plant Anatomy. New York: John Wiley and Sons, Inc., 1953.

7. Gates, David M., Harry J. Keegan, John C. Schleter and Victor R. Weidner. "Spectral Properties of Plants", Applied Optics, Vol. 4, No. 1, pp. 11-20, January, 1965.

8. Nicodemus, F. E. "Emissivity of Isothermal Spherical Cavity with Gray Lambertian Walls", Applied Optics, Vol. 7, No. 7, pp. 1359-1362, July, 1968.

9. Remote Multispectral Sensing in Agriculture, Vol. 3, The Laboratory for Agricultural Remote Sensing, Purdue University, 1968.

10. Seybold, A. "Uber Die Optischen Eigenschaften Der Laubblatter. III", Planta - Archiv Fur Wissenschaftliche Botanik, Vol. 20, pp. 577-601, 1933.

11. Shul'gin, I.A., V. S. Khazanov and A. F. Kleshnin. "On the Reflection of Light as Related to Leaf Structure", Doklady Botanical Sciences Sections - Plant Morphology, Vol. 134, No. 2, pp. 197-199, September, 1960.

12. Shul'gin, I. A. and V. S. Khazanov. "On the Problem of Light Conditions in Plant Associations", Doklady Botanical Sciences Sections - Plant Ecology, Vol. 141, No. 6, pp. 210-212, December, 1961.

13. Wendlandt, W. W. and H. G. Hecht. Reflectance Spectroscopy. New York: Interscience Publishers, 1966.

14. Willstatter, R. and A. Stoll. Investigations on Chlorophyll. Lancaster: The Science Press Printing Company, 1928.

General References

Agnew, John T. and Richmond B. McQuistan. "Experiments Concerning Infrared Diffuse Reflectance Standards in the Range 0.8 to 20.0 Microns", Journal of the Optical Society of America, Vol. 43, No. 11, pp. 999-1007, November, 1953.

American Institute of Physics Handbook, Second Edition. New York: McGraw Hill Book Company, 1963.

Arnon, Daniel I. "The Role of Light in Photosynthesis", Scientific American, pp. 105-118, June, 1960.

Bassham, J. A. "The Path of Carbon in Photosynthesis", Scientific American, pp. 89-100, 1962.

Blau, Henry H., Ronald P. Espinola, and Edward C. Reifenstein, III. "Near Infrared Scattering by Sunlit Terrestrial Clouds", Applied Optics, Vol. 5, No. 4, April, 1966.

Boast, W. B. Illumination Engineering. New York: McGraw-Hill Book Co., 1953.

Boileau, Almerian R. and Jacqueline I. Gordon. "Atmospheric Properties and Reflectances of Ocean Water and Other Surfaces for a Low Sun", Applied Optics, Vol. 5, No. 5, May, 1966.

Born, Max and Emil Wolf. Principles of Optics. New York: The Macmillan Company, 1964.

Brand, Kolman W. and Frank A. Spagnolo. "Lambert Diffuse Reflection from General Quadric Surfaces", Journal of the Optical Society of America, Vol. 57, No 4, pp. 452-458, April, 1957.

Brown, Earle B. Modern Optics. New York: Reinhold Publishing Corp., 1965.

Chandrasekhar, S. and Donna D. Elbert. "The Illumination and Polarization of the Sunlit Sky on Rayleigh Scattering", Transactions of the American Philosophical Society New Series, Vol. 44, Part 6, pp. 643-728, 1954.

Christensen, R. L. and Robert J. Potter. "Double Monochromator Systems", Applied Optics, Vol. 2, No. 10, pp. 1049-1054, October, 1963.

Clark, Carl, Ralph Vinegar, and James P. Hardy. "Goniometric Spectrometer for the Measurement of Diffuse Reflectance and Transmittance of Skin in the Infrared Spectral Region", Journal of the Optical Society of America, Vol. 43, No. 11, pp. 993-998, November, 1953.

Clark, Walter. Photography by Infrared. New York: John Wiley and Sons, Inc., 1939.

Clayton, Roderick K. "The Biophysical Problems of Photosynthesis", Science, Vol. 149, pp. 1346-1354, September 17, 1965.

Clayton, Roderick K. Molecular Physics in Photosynthesis. New York: Blaisdell Publishing Company, 1965.

Colwell, Robert N. "Determining the Prevalence of Certain Cereal Crop Diseases by Means of Aerial Photography", Hilgardia, Vol. 26, No. 5, pp. 223-286, 1956.

Coulson, K. L. "Characteristics of the Radiation Emerging from the Top of a Rayleigh Atmosphere I", Planetary and Space Science, Vol. 1, pp. 265-276, 1959.

Coulson, K. L. "Characteristics of the Radiation Emerging from the Top of a Rayleigh Atmosphere II", Planetary and Space Science, Vol. 1, pp. 277-284, 1959.

Coulson, K. L., J. V. Dave and Z. Sekera. Tables Related to Radiation Emerging from a Planetary Atmosphere with Rayleigh Scattering. Los Angeles: University of California Press, 1960.

Dave, J. V. and P. M. Furukawa. "Intensity and Polarization of the Radiation Emerging from an Optically Thick Rayleigh Atmosphere", Journal of the Optical Society of America, Vol. 56, No. 3, pp. 394-400, March, 1966.

Davis, Raymond, Kasson S. Gibson, and Geraldine Walker Haupt. "Spectral Energy Distribution of the International Commission on Illumination Light Sources A, B, and C", Journal of Research of the National Bureau of Standards, Vol. 50, No. 1, pp. 31-37, January, 1953.

Drude, Paul. The Theory of Optics. New York: Longmans, Green, and Company, 1913.

Duncan, W. G., R. S. Loomis, W. A. Williams, and R. Hanau. "A Model for Simulating Photosynthesis in Plant Communities", Hilgardia, Vol. 38, No. 4, pp. 181-205, March, 1967.

Egan, W. G., J. Grusauskas, and H. B. Hallock. "Optical Depolarization Properties of Surfaces Illuminated by Coherent Light", Applied Optics, Vol. 7, No. 8, August, 1968.

Eldridge, Ralph G. "Water Vapor Absorption of Visible and Near Infrared Radiation", Applied Optics, Vol. 6, No. 4, pp. 709-713, April, 1967.

Engelsrath, Amos and Ernest V. Loewenstein. "Uncertainties in Optical Constants Determined from Isoreflectance Curves", Applied Optics, Vol. 5, No. 4, April, 1966.

Fredrickson, W. R. and N. Ginsberg. "Infrared Spectral Emissivity of Terrain", Department of Physics, Syracuse University, ASTIA Document 132839.

French, C. S. "The Chlorophylls in Vivo and in Vitro", Encyclopedia of Plant Physiology, W. Ruhland, Ed., Vol. 5, Part 1, pp. 252-297. Berlin: Springer-Verlag, 1960.

Gates, David M. "Heat Transfer in Plants", Scientific American, Vol. 3, pp. 76-84, 1964.

Gates, David M. and Wirojana Tantraporn. "The Reflectivity of Deciduous Trees and Herbaceous Plants in the Infrared to 25 Microns", Science, Vol. 115, pp. 613-661, June 6, 1952.

Gordon, Jacqueline I. and Peggy V. Church. "Sky Luminances and the Directional Luminous Reflectances of Objects and Backgrounds for a Moderately High Sun", Applied Optics, Vol. 5, No. 5, May, 1966.

Hartman, Robert J. Colloid Chemistry. New York: Houghton Mifflin Company, 1947.

Haupt, Geraldine W. "An Alkaline Solution of Potassium Chromate as a Transmittancy Standard in the Ultraviolet", Journal of Research of the National Bureau of Standards, Vol. 48, No. 12, pp. 414-423, June, 1952.

Hauser, Ernst A. and J. Edward Lynn. Experiments in Colloid Chemistry. New York: McGraw-Hill Book Company, Inc., 1940.

Hayward, Herman E. The Structure of Economic Plants. New York: The Macmillan Company, 1948.

Hovis, W. A., Jr. "Infrared Spectral Reflectance of Some Common Minerals", Applied Optics, Vol. 5, No. 2, pp. 245-248, February, 1966.

Hovis, W. A., Jr. "Optimum Wavelength Intervals for Surface Temperature Radiometry", Applied Optics, Vol. 5, p. 815, 1966.

Jenkins, Francis A. and Harvey E. White. Fundamentals of Optics. New York: McGraw-Hill Book Company, Inc., 1957.

Jirgensons, B. and M. E. Straumanis. A Short Textbook of Colloid Chemistry. New York: The Macmillan Company, 1962.

Jones, R. Clark. "On the Relation Between the Speed of Response and the Detectivity of Lead Sulfide Photoconductive Cells", Journal of the Optical Society of America, Vol. 43, No. 11, pp. 1008-1013, November, 1953.

Judd, Deane B. "Terms, Definitions, and Symbols in Reflectometry", Journal of the Optical Society of America, Vol. 57, No. 4, pp. 445-452, April, 1967.

Keegan, Harry J., Marion A. Belknap, and Dorothy J. Cordrey. "Spectral Transmissive Properties of Five Selected Optical Glasses", Journal of Research of the National Bureau of Standards, Vol. 52, No. 6, pp. 305-308, June, 1954.

Keegan, Harry J., John C. Schleter, and Marion A. Belknap. "Recalibration of the NBS Glass Standards of Spectral Transmittance", Journal of the Optical Society of America, Vol. 54, No. 1, pp. 69-74, January, 1964.

Keegan, Harry J., John C. Schleter, Wiley A. Hall, Jr., and Gladys M. Haas. "Spectrophotometric and Colorimetric Study of Foliage Stored in Covered Metal Containers", U. S. Dept. of Commerce, National Bureau of Standards Rep. 4370, (AD 84923), November, 1955.

Knipling, Edward B. "Physical and Physiological Basis for Differences in Reflectance of Healthy and Diseased Plants", Workshop on Infrared Color Photography in Plant Sciences, Florida Department of Agriculture, Winter Haven, Florida, March, 1967.

Kondratiev, K. Ya., G. A. Nicolsky, I. Ya. Badinov, and S. D. Andreev. "Direct Solar Radiation up to 30 km and Stratification of Attenuation Components in the Stratosphere", Applied Optics, Vol. 6, No. 2, pp. 197-207, February, 1967.

Kronstein, Max, Robert J. Kraushaar, and Robert E. Deacle. "Sulfur as a Standard of Reflectance in the Infrared", Journal of the Optical Society of America, Vol. 53, No. 4, pp. 458-465, April, 1963.

Lathrop, Arthur L. "Absorption of Radiation in a Diffusely Scattering Medium", Journal of the Optical Society of America, Vol. 56, No. 7, pp. 926-931, July, 1966.

Latimer, Paul. "Apparent Shifts of Absorption Bands of Cell Suspensions and Selective Light Scattering", Science, Vol. 127, pp. 29-30, 1958.

Lowe, Donald S. and John G. Braithwaite. "A Spectrum Matching Technique for Enhancing Image Contrast", Applied Optics, Vol. 5, No. 6, June, 1966.

McDougal, D. T. The Green Leaf. New York: D. Appleton and Company, 1930.

Mestre, Harold. "The Absorption of Radiation by Leaves and Algae", Cold Spring Harbor Symposia, Quantitative Biology, Vol. 3, pp. 191-209, 1935.

Monteith, J. L. "Radiation and Crops", Experimental Agriculture Review I, pp. 241-251, 1965.

Moss, R. A. "The Absorption Spectra of Leaves", Ph.D. Thesis, Iowa State College, 1951.

Moss, R. A. and W. E. Loomis. "Absorption Spectra of Leaves, I. The Visible Spectrum", Plant Physiology, pp. 370-391, 1951.

Nicodemus, F. E. Applied Optics and Optical Engineering. R. Kingslake, Ed., Vol. 4, Part 1. New York: Academic Press, 1967.

Plumb, Robert C. "Analysis of Elliptically Polarized Light", Journal of the Optical Society of America, Vol. 50, No. 9, September, 1960.

Plyler, Earle K., L. R. Blaine, and Matthew Nowak. "Reference Wavelengths for Calibrating Prism Spectrometers", Journal of Research of the National Bureau of Standards, Vol. 58, No. 4, pp. 195-200, April, 1957.

Plyler, Earle K., Norman M. Gailar, and Thomas A. Wiggins. "Some Accurately Measured Infrared Wavelengths for Calibration of Grating Spectrometers", Journal of Research of the National Bureau of Standards, Vol. 48, No. 3, pp. 221-227, March, 1952.

Plyler, Earle K. and C. Wilbur Peters. "Wavelengths for Calibration of Prism Spectrometers", Journal of Research of the National Bureau of Standards, Vol. 45, No. 6, pp. 462-467, December, 1950.

Rabinowitch, Eugene I. and Govindjee. "The Role of Chlorophyll in Photosynthesis", Scientific American, pp. 74-83, 1965.

Rayleigh. "On the Light from the Sky, Its Polarization and Colour", Philosophical Magazine, Vol. 41, pp. 107-120, pp. 274-279, 1871.

Rayleigh. "On the Scattering of Light by Small Particles", Philosophical Magazine, Vol. 41, pp. 447-454, 1871.

Rayleigh. "On the Transmission of Light Through an Atmosphere Containing Small Particles in Suspension, and on the Origin of the Blue of the Sky", Philosophical Magazine, Vol. 47, pp. 375-384, 1899.

Renau, Cheo, and Cooper. "Depolarization of Linearly Polarized E. M. Waves Backscattered from Rough Metals and Inhomogeneous Dielectrics", Journal of the Optical Society of America, Vol. 57, No. 4, pp. 459-466, April, 1967.

Rossi, Bruno. Optics. Reading, Massachusetts: Addison-Wesley Publishing Company, Inc., 1957.

Rutgers, G. A. W. "Temperature Radiation of Solids", Handbuch der Physik, Vol. 26, p. 129, Springer-Verlag, Berlin, 1958.

Sanders, C. L. and E. Knowles Middleton. "The Absolute Spectral Diffuse Reflectance of Magnesium Oxide in the Near Infrared", Journal of the Optical Society of America, Vol. 43, No. 1, p. 58, January, 1953.

Schanderl, Hugo and Wolfgang Kaempfert. "Uber die Strahlungsdurchlassigkeit von Blattern und Blattgeweben", Planta - Archiv Fur Wissenschaftliche Botanik, Vol. 18, pp. 700-750, 1933.

Sears, F. W. and M. W. Zemansky. University Physics. Reading Massachusetts: Addison-Wesley Publishing Company, Inc., 1955.

Seybold, A. "Uber die Optischen Eigenschaften der Laubblatter. I", Planta - Archiv Fur Wissenschaftliche Botanik, Vol. 16, pp. 195-226, 1932.

Seybold, A. "Uber die Optischen Eigenschaften der Laubblatter. II", Planta - Archiv Fur Wissenschaftliche Botanik, Vol. 18, pp. 479-508, 1933.

Seybold, V. A. and A. Weissweiler. "Specktrophotometrische Messungen an grunen Pflanzen und an Chlorophyll-Losungen", Botanisches Archiv, Vol. 43, pp. 252-290, 1942.

Seybold, V. A. and A. Weissweiler. "Weitere Spektrophotometrische Messungen an Laubblattern und an Chlorophyll-Losungen sowie an Meeresalgen", Botanisches Archiv, Vol. 44, pp. 102-153, 1943.

Seybold, V. A. and A. Weissweiler. "Zur Klarung einiger Elementarer Optischer Fragen der Photophysiologie", Botanisches Archiv, Vol. 44, pp. 456-520, 1943.

Shurcliff, William A. Polarized Light, Production and Use. Cambridge, Massachusetts: Harvard University Press, 1962.

Shurcliff, William A. and Stanley S. Ballard. Polarized Light. Princeton, New Jersey: D. Van Nostrand Co., Inc., 1964.

Sinclair, T. R. "Pathway of Solar Radiation Through Leaves", M. S. Thesis, Purdue University, 1968.

Sobolev, V. V. A Treatise on Radiative Transfer. New York: D. Van Nostrand Co., Inc., 1963.

Sogo, Rower B., Ning G. Pon, and Melvin Calvin. "Photo Spin Resonance in Chlorophyll-Containing Plant Material", Biochemistry, Vol. 43, 1957.

Stair, Ralph. "Ultraviolet Spectral Distribution of Radiant Energy from the Sun", Journal of Research of the National Bureau of Standards, Vol. 46, No. 5, pp. 353-357, May, 1951.

Stair, Ralph, William E.Schneider, and John K. Jackson. "A New Standard of Spectral Irradiance", Applied Optics, Vol. 2, No. 11, pp. 1151-1154, November, 1963.

"Standards for Checking the Calibration of Spectrophotometers (200 to 100 milli-microns)", National Bureau of Standards, Letter Circular, LC-1017, January, 1955.

Stephens, Robert E. and William S. Rooney. "Refractive Indices of Five Selected Optical Glasses", Journal of Research of the National Bureau of Standards, Vol. 52, No. 6, pp. 303-304, June, 1954.

Stone, John M. Radiation and Optics. New York: McGraw-Hill Book Company, Inc., 1963.

Streete, John L. "Infrared Measurements of Atmospheric Transmission at Sea Level", Applied Optics, Vol. 7, No. 8, August, 1968.

The Science of Color, Committee on Colorimetry Optical Society of America. New York: Thomas Y. Crowell Company, 1953.

Tollin, Gordon and Melvin Calvin. "The Luminescence of Chlorophyll-Containing Plant Material", Chemistry, Vol. 43, 1957.

Van De Hulst, H. C. Light Scattering by Small Particles. New York: John Wiley and Sons, Inc., 1957.

Wilson, Ralph A. "The Remote Surveillance of Forest Fires", Applied Optics, Vol. 5, No. 6, June, 1966.

Winsor, D. E. "A Permanent Standard for Reflectance Spectra Over the Range 0.3-2.6 Microns", Journal of Scientific Instruments, Vol. 43, pp. 108-109, 1966.

Wolfe, William E. (ed.). Handbook of Military Infrared Technology, Office of Naval Research, Department of the Navy, Washington, D.C., 1965.

Wright, W. D. The Measurement of Colour. New York: The Macmillian Company, 1958.

Zipin, Richard B. "A Preliminary Investigation of the Bidirectional Spectral Reflectance of V-grooved Surfaces", Applied Optics, Vol. 5, No. 12, pp. 1954-1957, December, 1966.

APPENDIX A

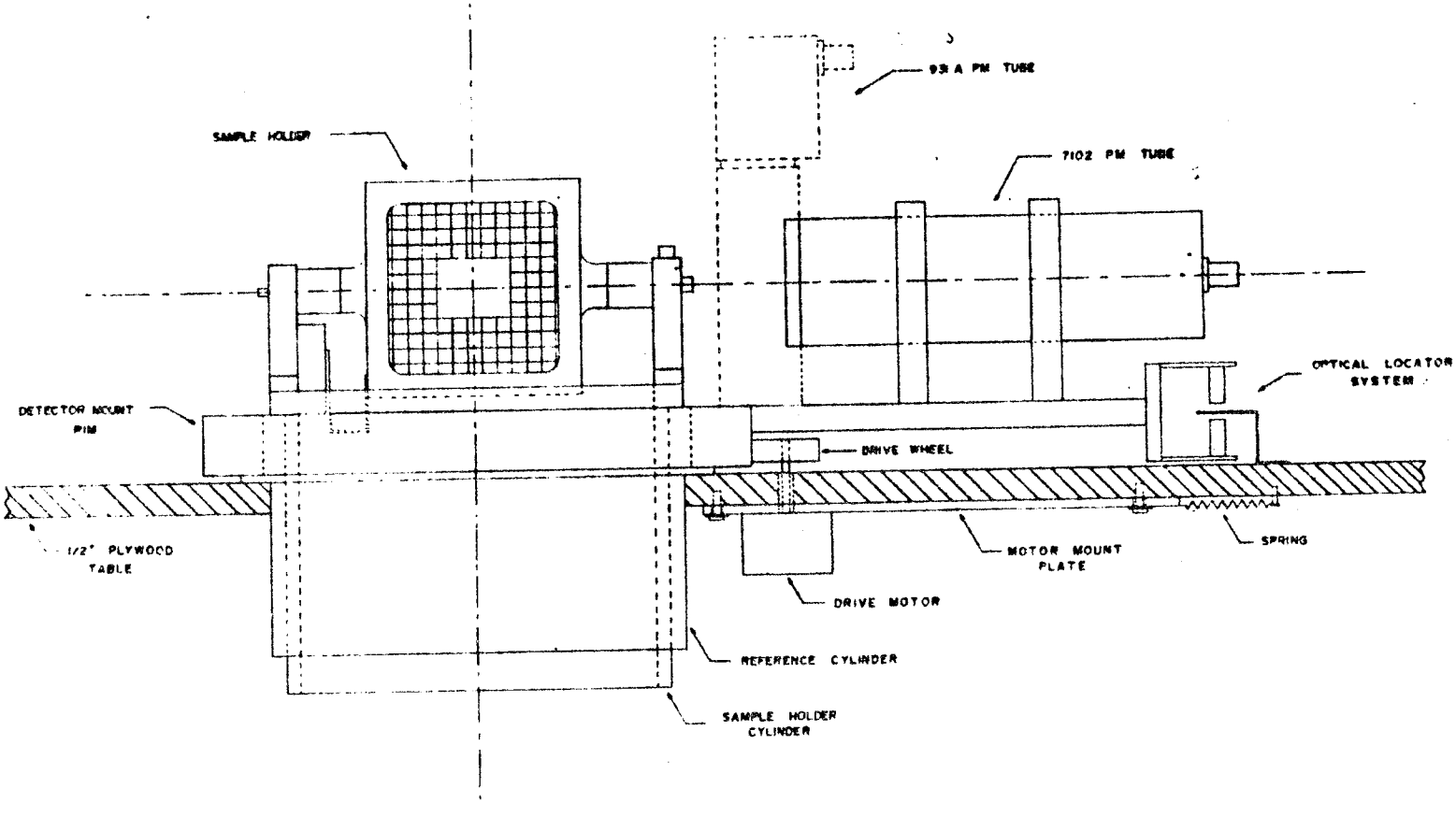

Figure 108. Apparatus Assembly Drawing.

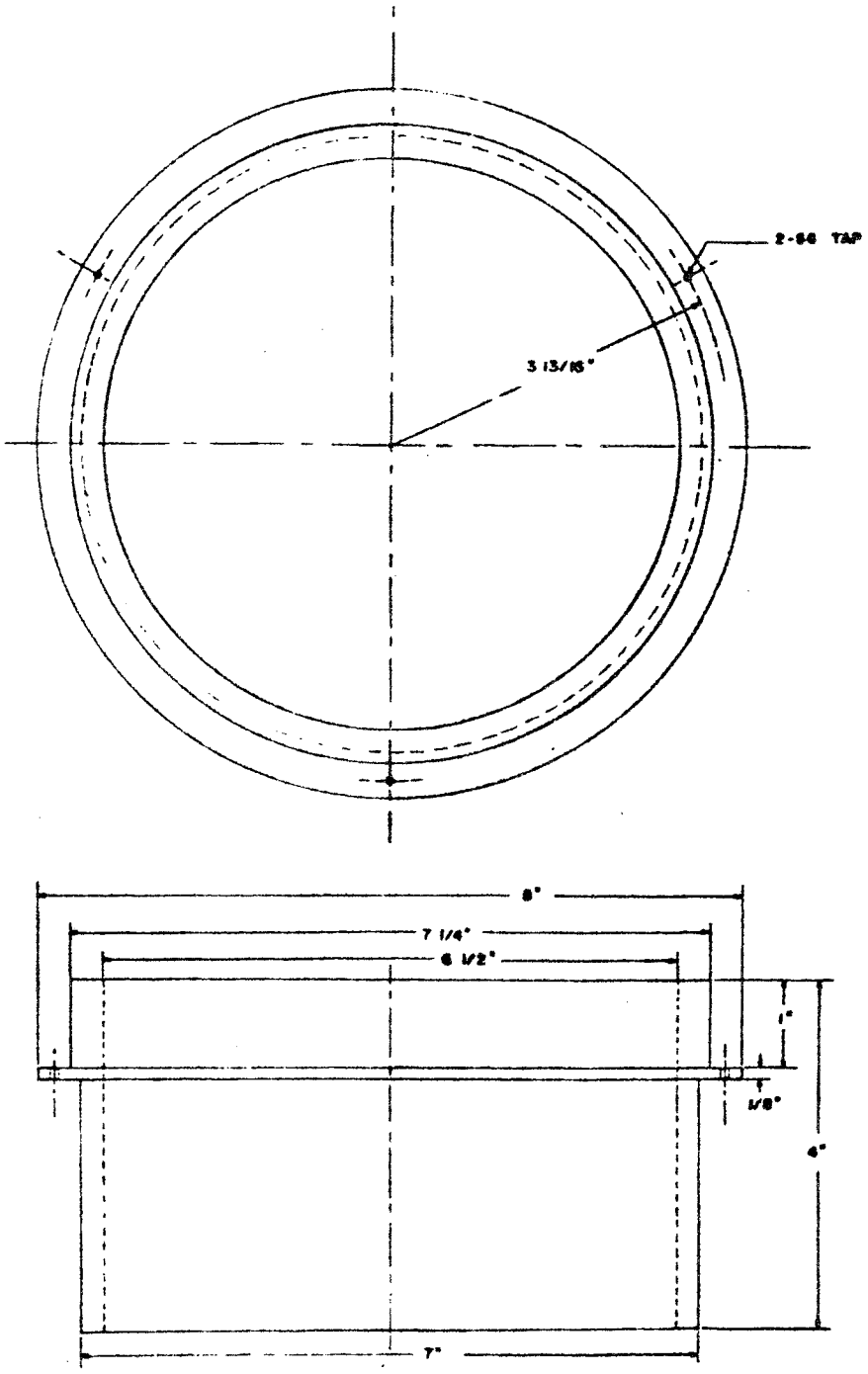

Figure 109. Reference Cylinder.

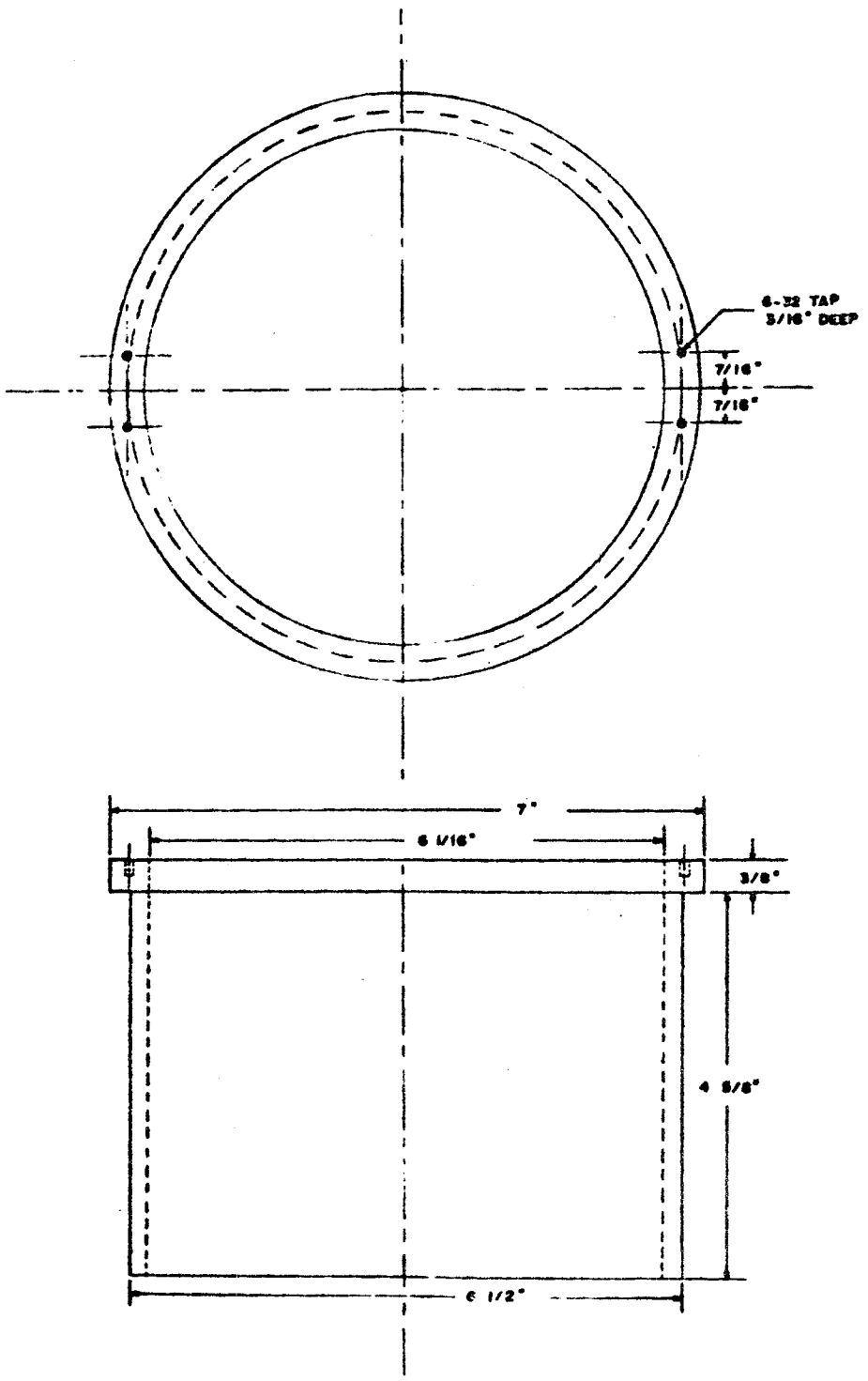

Figure 110. Sample Holder Cylinder.

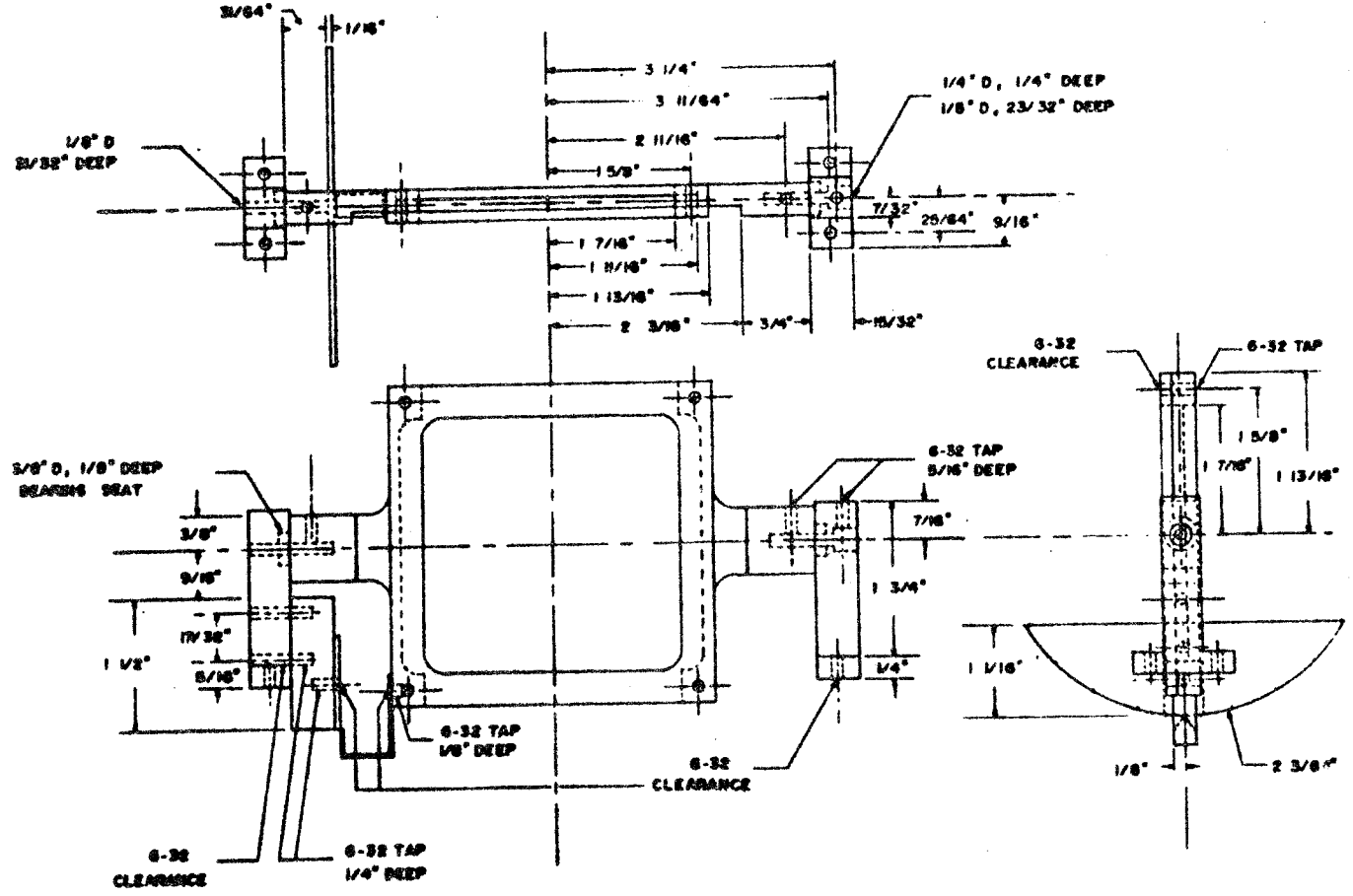

Figure 111. Sample Holder.

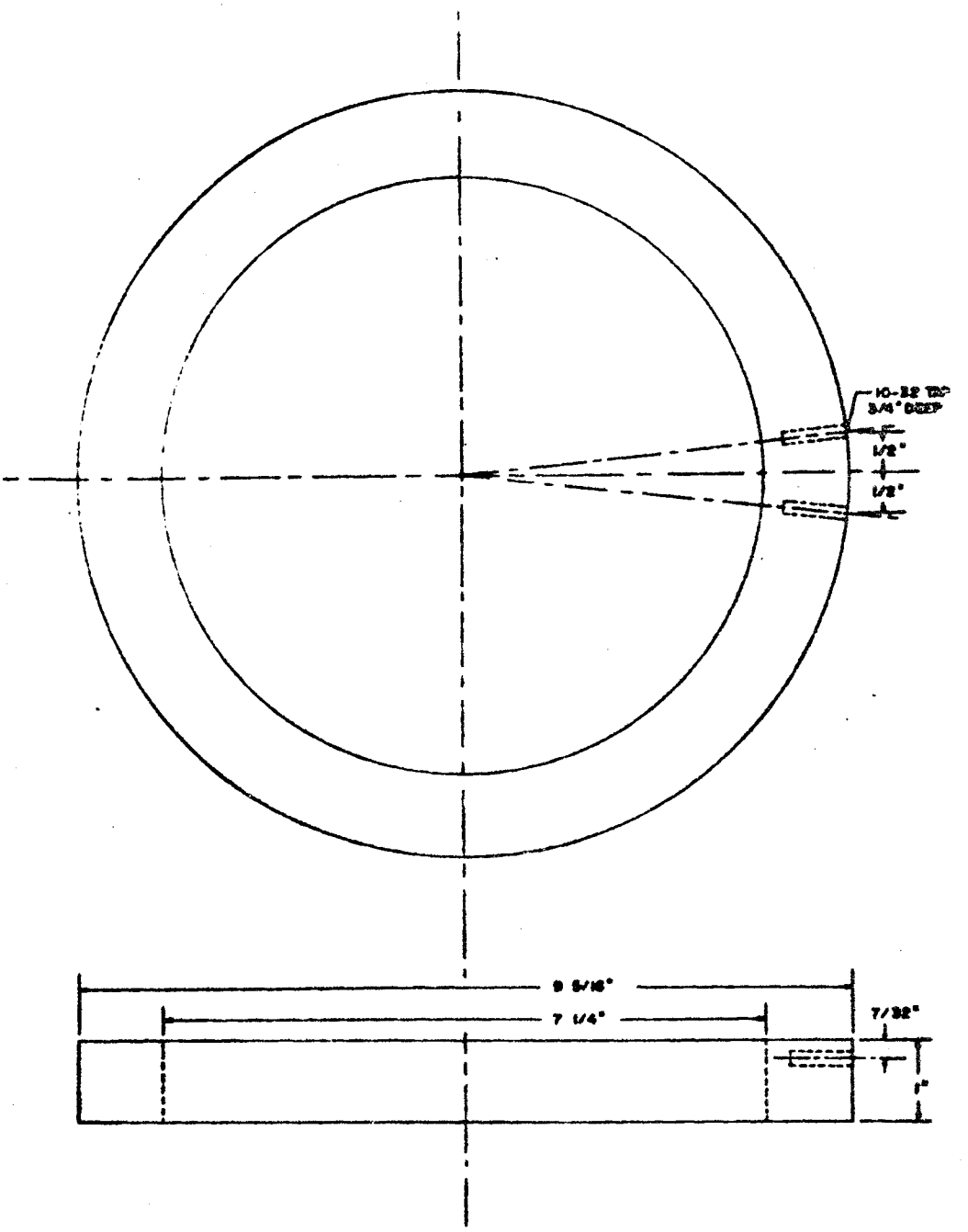

Figure 112. Detector Rim.

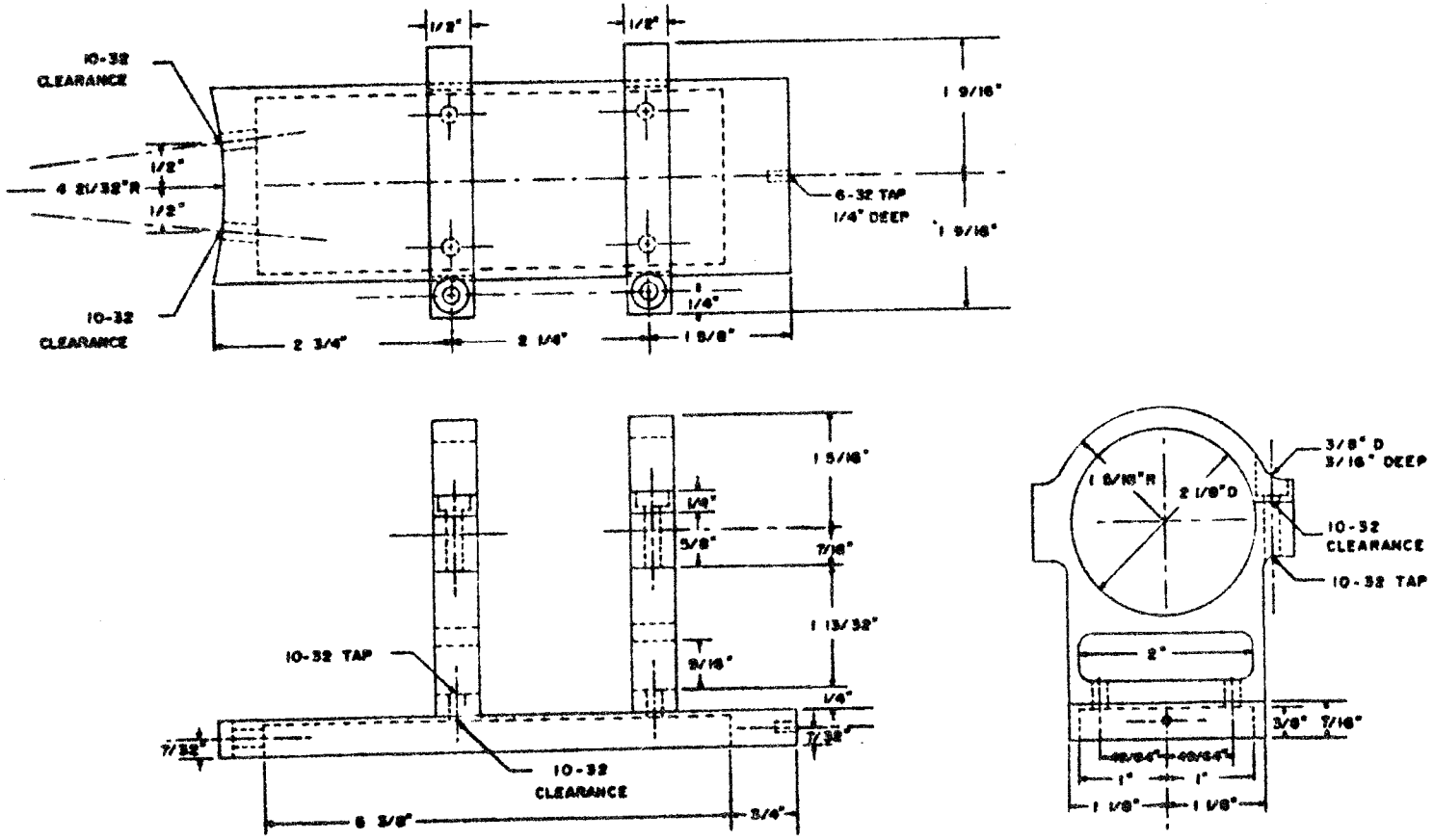

Figure 113. Detector Rim Arm.

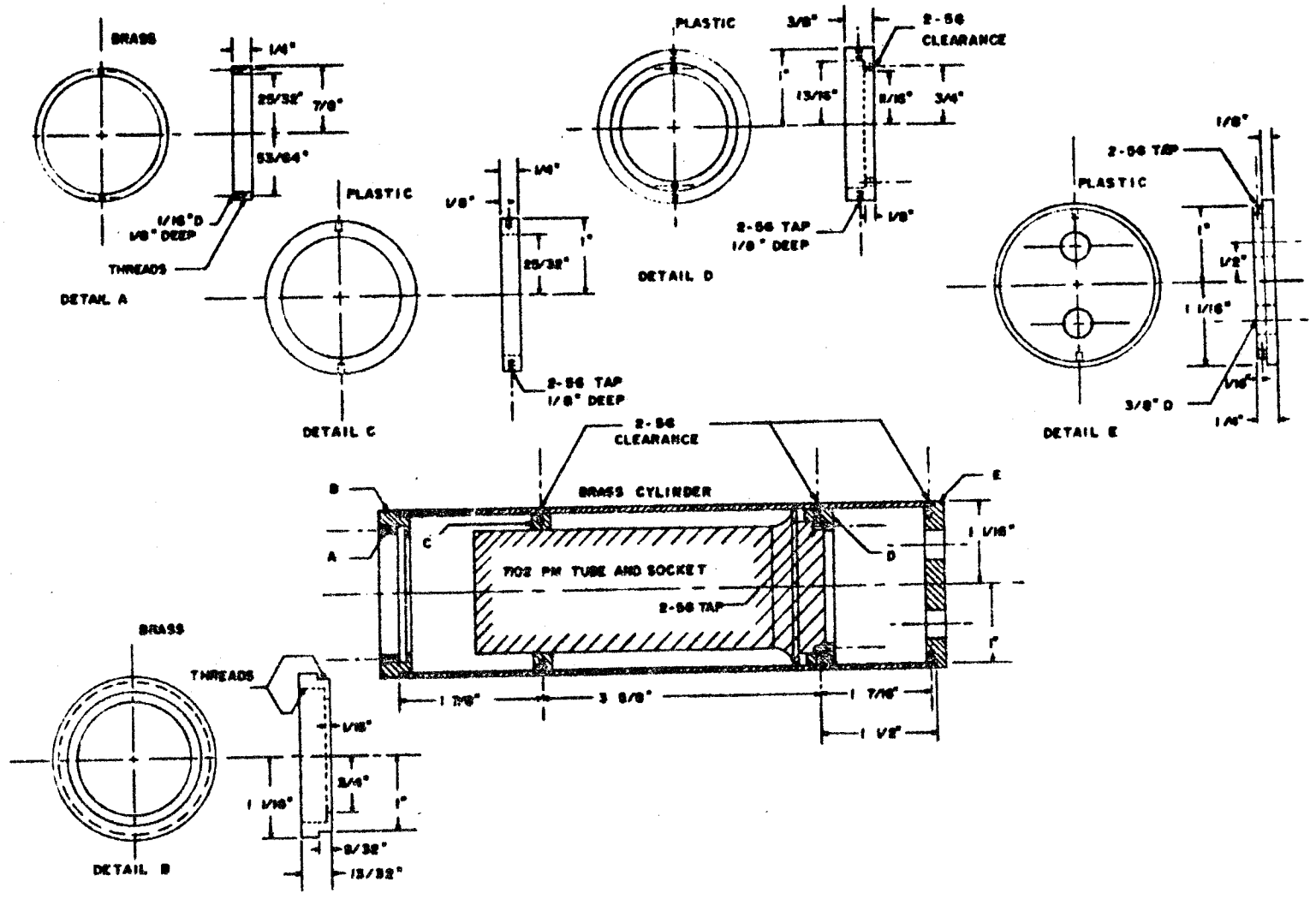

Figure 114. 7102 PM Tube Mount.

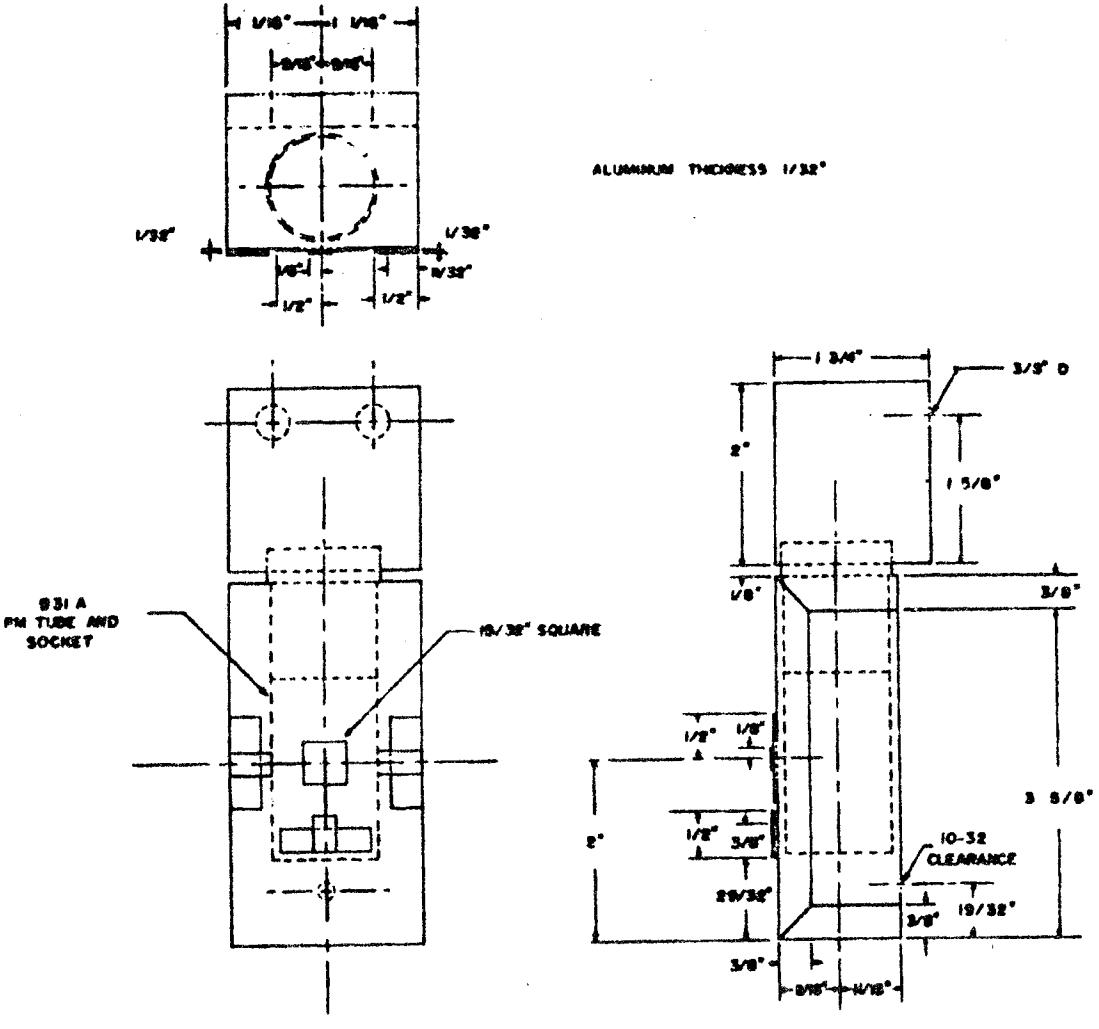

Figure 115. 931A PM Tube Mount.

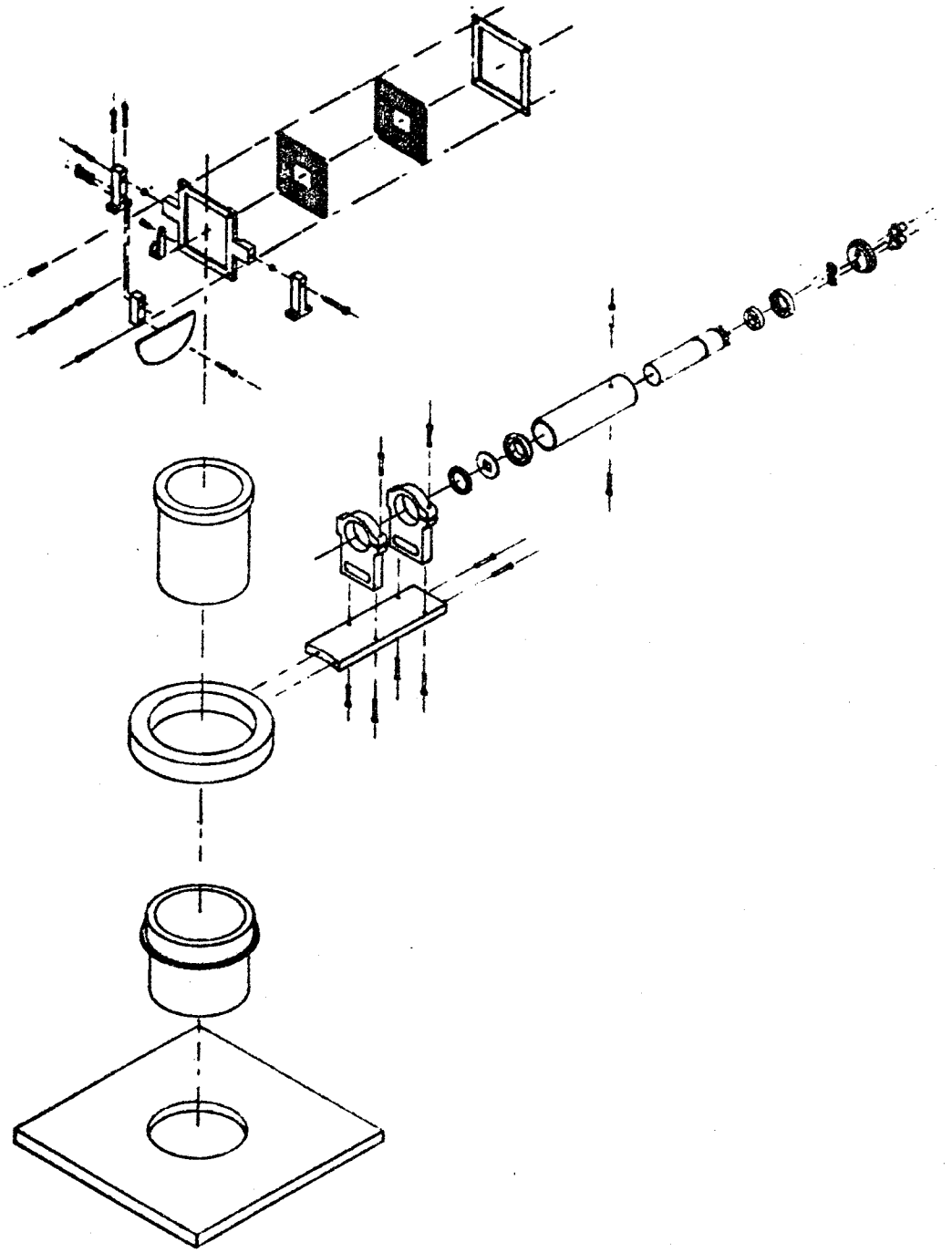

Figure 116. Exploded Isometric Apparatus Drawing.

APPENDIX B

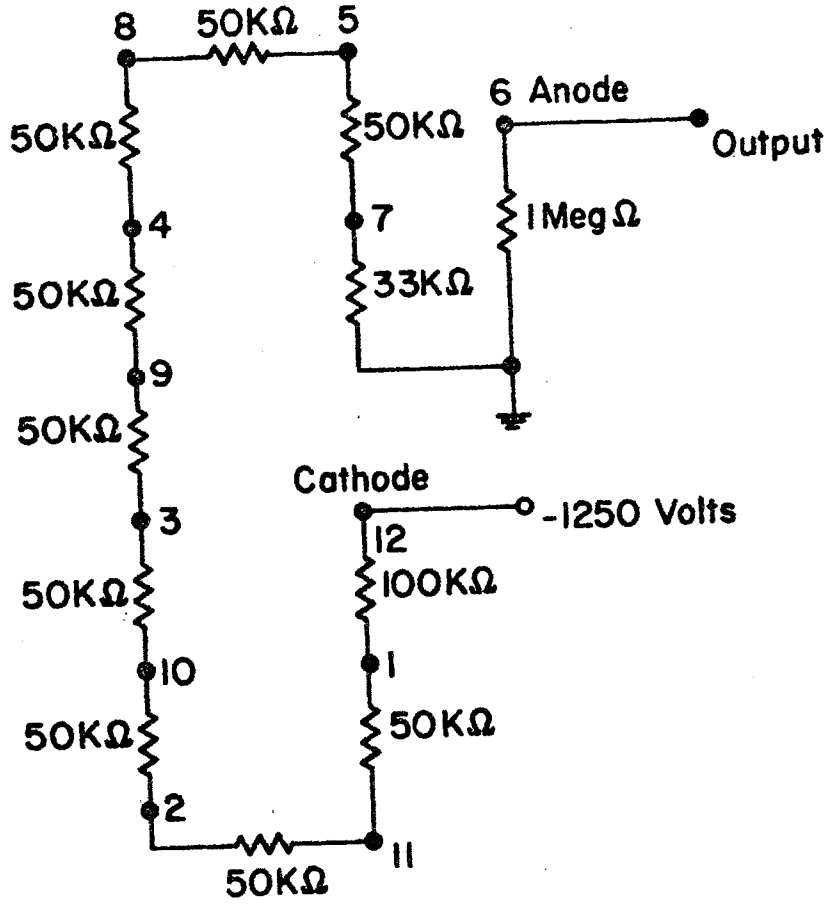

Figure 117. 7102 Photomultiplier Tube Voltage Divider Circuit.

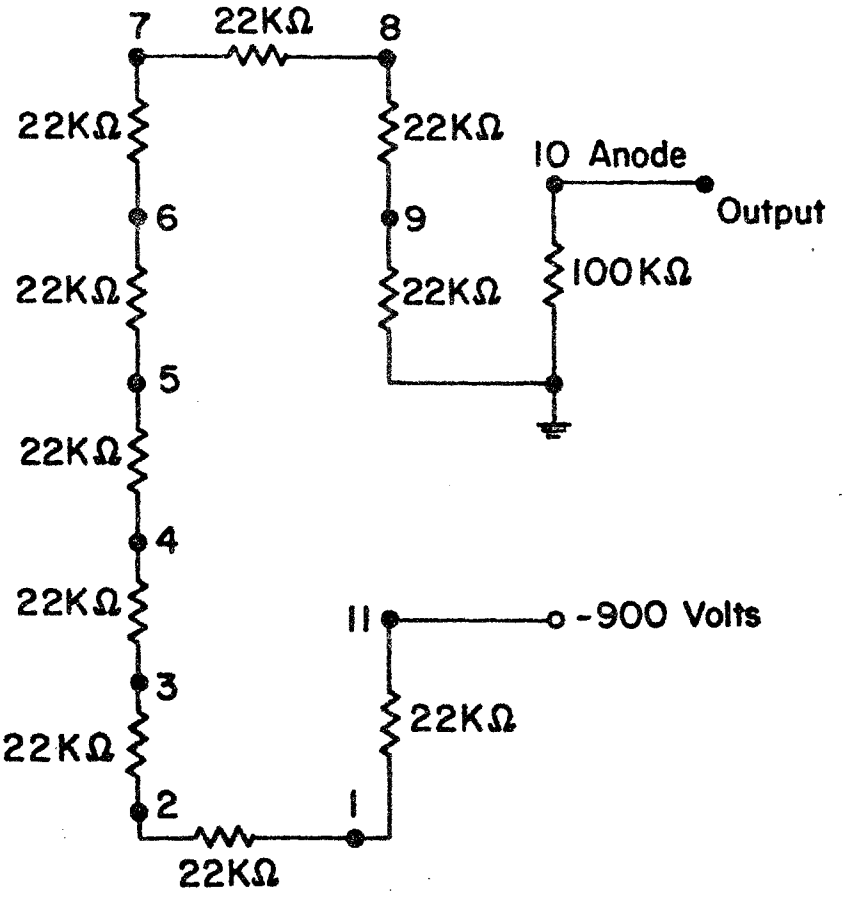

Figure 118. 931A Photomultiplier Tube Voltage Divider Circuit.

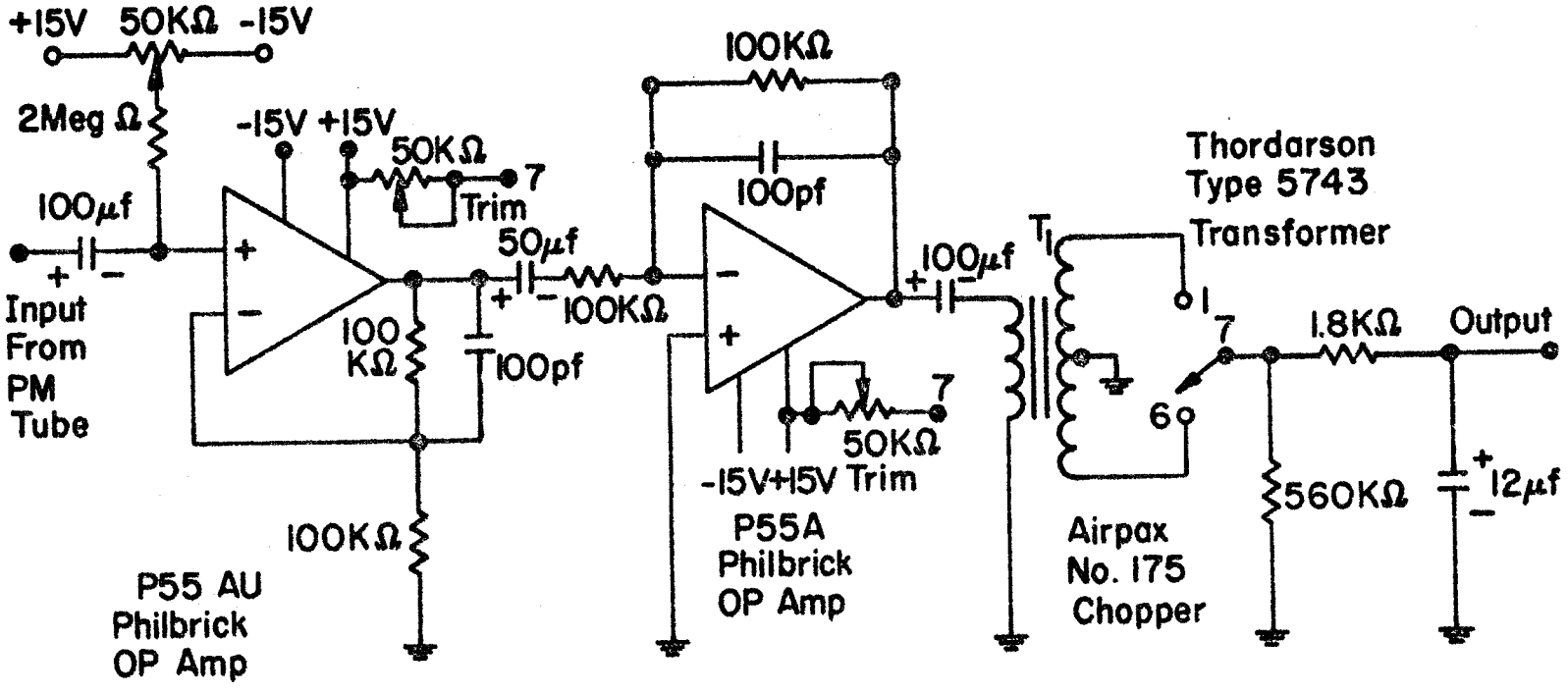

Figure 119. Synchronous Demodulator Circuit.

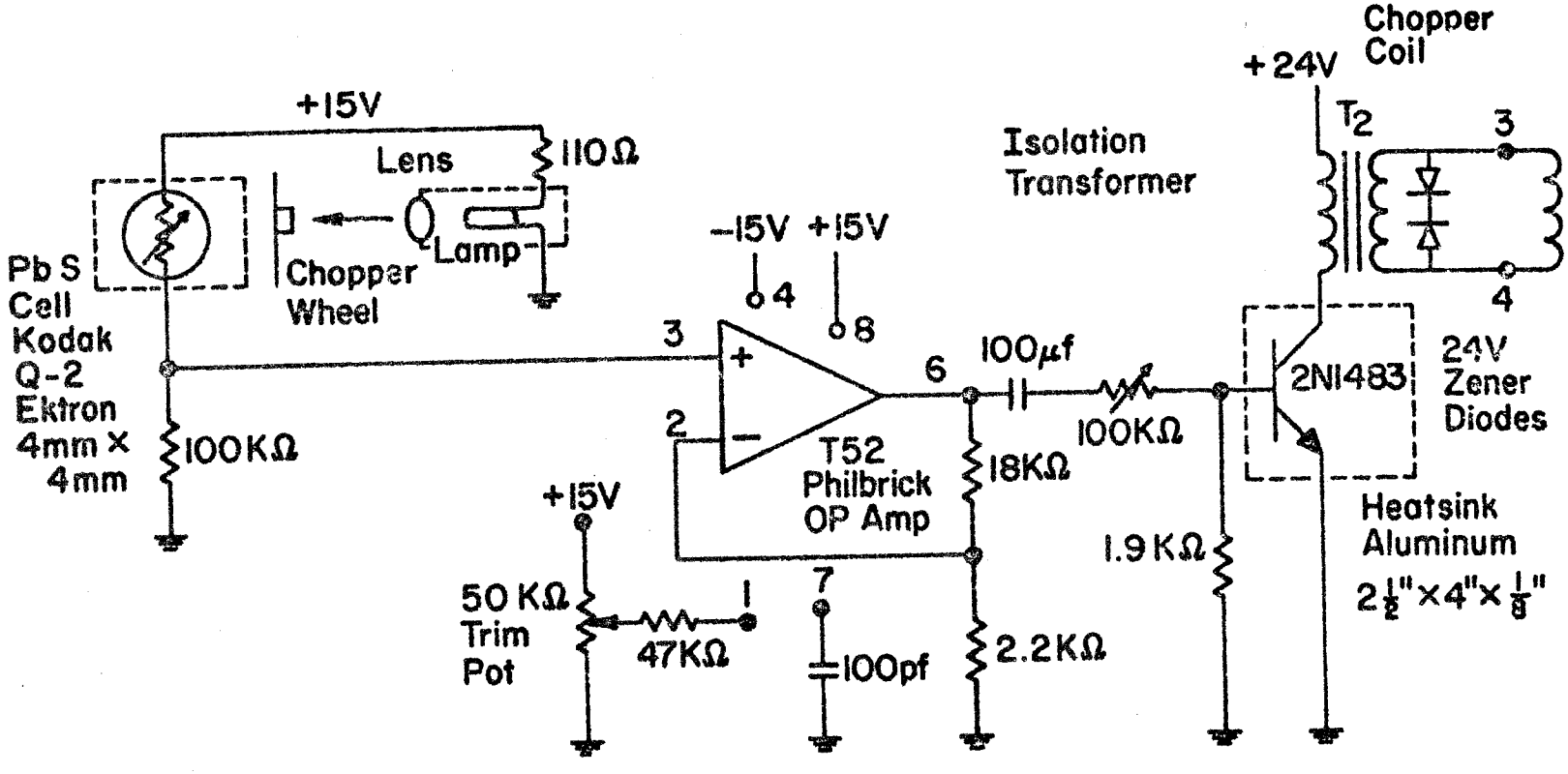

Figure 120. Chopper Driver Circuit.

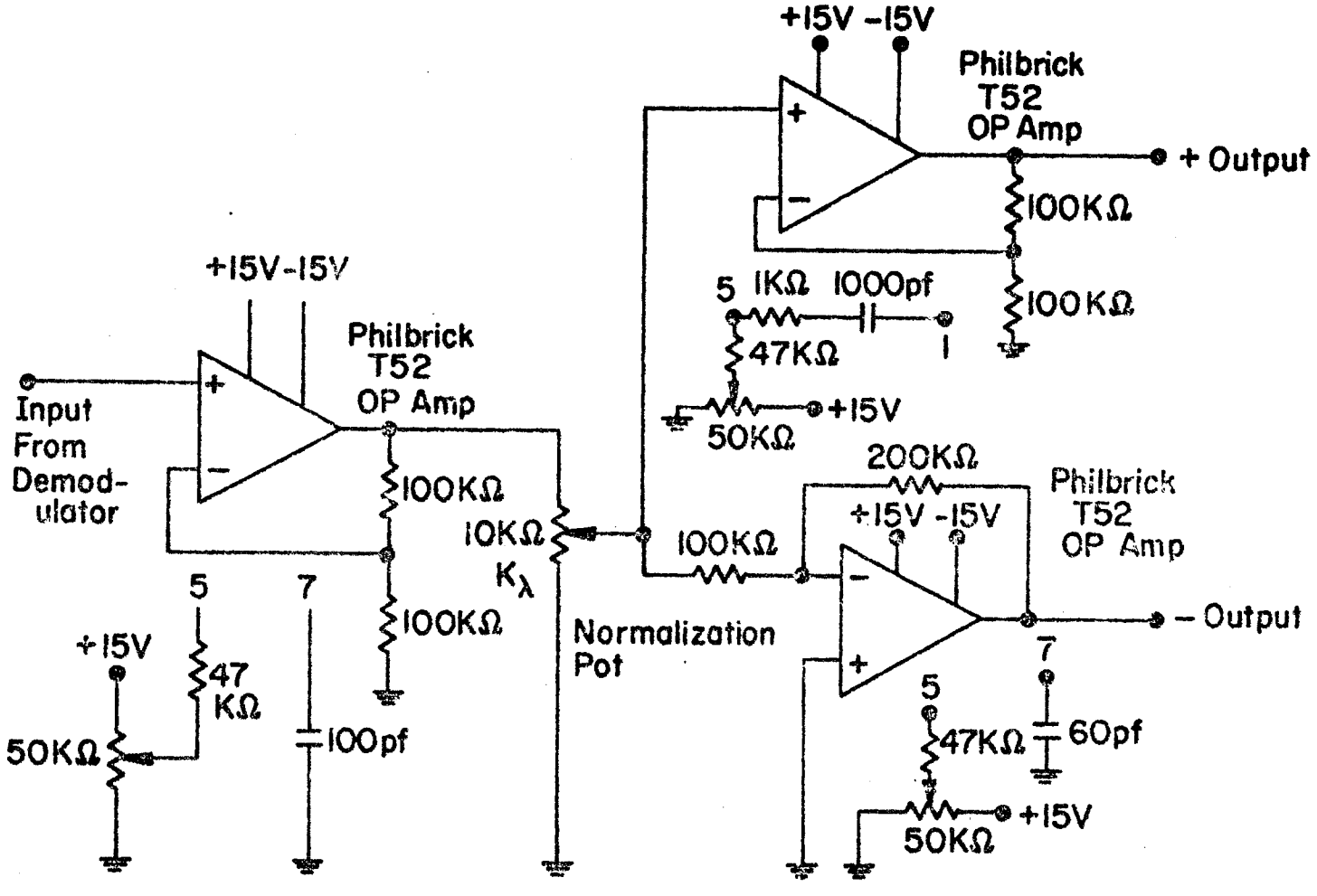

Figure 121. Output Normalization Amplifier Circuit.

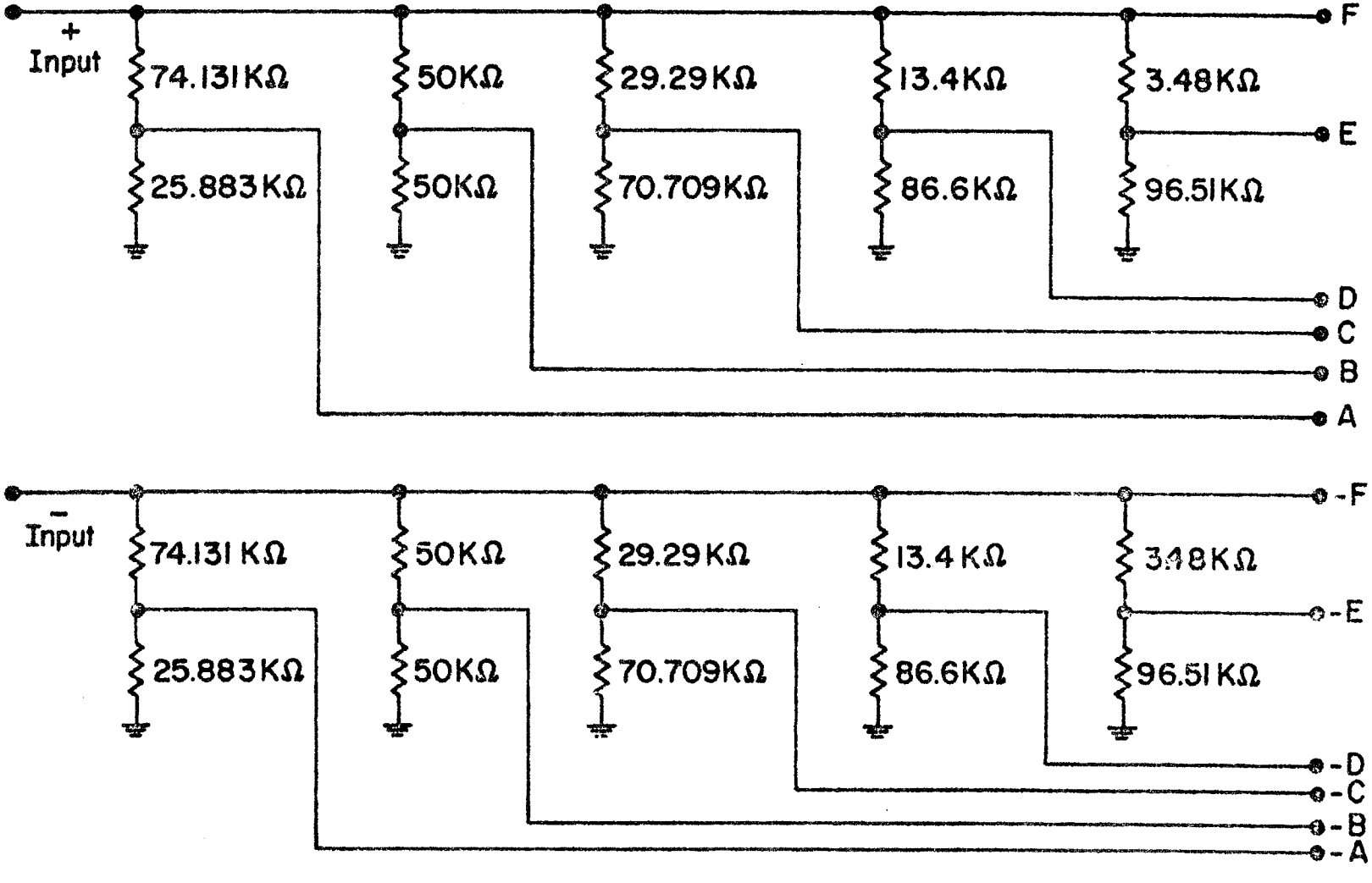

Figure 122. Coordinate Converter Circuit.

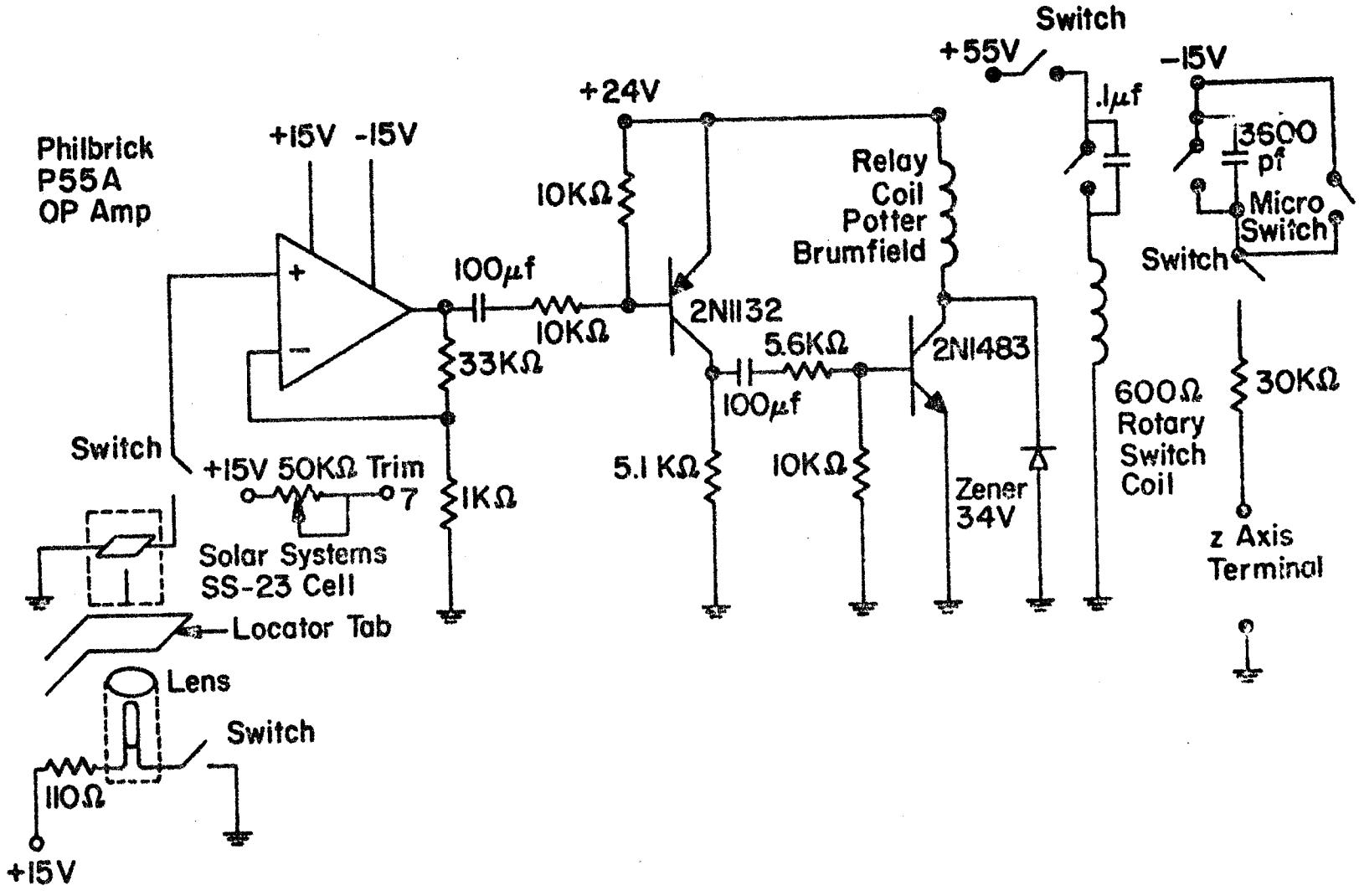

Figure 123. Optical Interrupt Relay Driver Circuit.

UNCLASSIFIED
Security Classification

DOCUMENT CONTROL DATA - R & D

(Security classification of title, body of abstract and indexing annotation must be entered when the overall report is classified)

1. ORIGINATING ACTIVITY (Corporate author)

School of Electrical Engineering
Purdue University, Lafayette, Indiana 47907

2a. REPORT SECURITY CLASSIFICATION

Unclassified

2b. GROUP

3. REPORT TITLE

BI-DIRECTIONAL SCATTERING CHARACTERISTICS OF HEALTHY, GREEN SOYBEAN AND CORN LEAVES IN VIVO

4. DESCRIPTIVE NOTES (Type of report and inclusive dates)

Scientific

5. AUTHOR(S) (First name, middle initial, last name)

Harry T. Breece, III

Roger A. Holmes

6. REPORT DATE	7a. TOTAL NO. OF PAGES	7b. NO. OF REFS
April, 1969	244 + 20	14 + 95

8a. CONTRACT OR GRANT NO.	9a. ORIGINATOR'S REPORT NUMBER(S)
JSEP N00014-67-A-0226	TR-EE 69-11
b. PROJECT NO.	
c.	9b. OTHER REPORT NO(S) (Any other numbers that may be assigned this report)
d.	LARS Information Note 033169

10. DISTRIBUTION STATEMENT

Unlimited

11. SUPPLEMENTARY NOTES	12. SPONSORING MILITARY ACTIVITY
	Joint Services Electronics Program

13. ABSTRACT

Measurements were made to determine the bi-directional scattering characteristics of living, green soybean and corn leaves in the range from 375 mm to 1μm.

A goniometer was constructed to study bi-directional scattering on the leaves of potted soybean and corn plants. The leaf sample was held in a plane and light of a selected wavelength was incident at a given angle. A detector was then moved around the sample at a constant radius resulting in a polar plot of scattered radiant power as a function of observation angle for a given angle of incidence and wavelength.

The results show strong specular components of reflection in addition to diffuse components for both soybean and corn leaves. Both soybean and corn leaves have a diffuse transmission component along with a definite refractive component.

The results describe a simple four layer bi-directional scattering model for a soybean leaf. This model has a rough surface with isotropy relative to the midvein.

The results for a corn leaf describe a simple three layer bi-directional scattering model. This model has a rough surface with a definite anisotropy relative to the midvein.

The results are two-dimensional polar graphs. Measurements were carried out which indicate the extension of these results to three dimensions.

DD FORM 1473 (PAGE 1)